SEMMELWEIS EGYETEM

DOKTORI ISKOLA

Ph.D. értekezések

3373.

VATTAY BORBÁLA

Szív- és érrendszeri betegségek élettana és klinikuma

című program

Programvezető: Dr. Merkely Béla, egyetemi tanár

Témavezetők: Dr. Szilveszter Bálint, egyetemi adjunktus

ANATOMICAL AND FUNCTIONAL ASSESSMENT OF CORONARY ARTERY DISEASE USING COMPUTED TOMOGRAPHY ANGIOGRAPHY

PhD thesis

Borbála Vattay, MD

Doctoral School of Theoretical and Translational Medicine

Semmelweis University

Supervisor:	Bálint Szilveszter, MD, PhD
Official reviewers:	Katalin Keltai, MD, PhD
	Eszter Végh, MD, PhD

Head of the Complex Examination Committee:
István Karádi, MD, PhD, DSc
Members of the Complex Examination Committee:
Henriette Farkas, MD, PhD, DSc
Hassan Charaf, PhD, DSc
Miklós Kellermayer, MD, PhD, DSc

Budapest
2025

TABLE OF CONTENTS

LIST OF ABBREVIATIONS

ASCVD: Atherosclerotic cardiovascular disease

BMI: Body mass index

CAD: Coronary artery disease

CAD-RADS: Coronary artery disease - reporting and data system

CCS: Chronic coronary syndrome

CI: Confidence interval

CNR: Contrast-to-noise ratio

CP: Calcified plaque

CT: Computed tomography

CTA: Computed tomography angiography

CTP: Computed tomography perfusion

CVD: Cardiovascular disease

DPCT: Dynamic perfusion computed tomography

ECG: Electrocardiogram

EID: Energy-integrating detector

HU: Hounsfield unit

HRP: High-risk plaque

ICA: Invasive coronary angiography

MACE: Major adverse cardiovascular events

MI: Myocardial infarction

NCP: Non-calcified plaque

LAD: Left anterior descending

LAP: Low-attenuation non-calcified plaque

LCX: Left circumflex

LM: Left main

LV: Left ventricle

PCI: Percutaneous coronary intervention

PCCT: Photon-counting computer tomography

RCA: Right coronary artery

ROI: Region of interest

RV: Right ventricle

SCCT:	Society of Cardiovascular Computed Tomography
SD:	Standard deviation
SIS:	Segment involvement score
SPECT:	Single-photon emission computed tomography
SSS:	Segment stenosis score
TPV:	Total plaque volume
VMI:	Virtual monoenergetic image

1. INTRODUCTION

Cardiovascular diseases are consistently one of the leading causes of mortality globally, including coronary artery disease (CAD), heart failure, stroke, hypertension, and other cardiovascular disorders (1, 2). As a major global health concern, it is responsible for a significant proportion of deaths in both developed and developing countries. Also, CAD imposes a substantial economic burden on healthcare systems worldwide, driving up treatment costs, hospital admissions, and long-term care expenditures. Over the past 15 years, there has been a significant reduction in deaths from acute myocardial infarction and cerebrovascular diseases in Hungary. However, mortality due to other ischemic heart diseases has not improved; in fact, it has doubled. This further draws our attention to the importance of preventive cardiology and the crucial role of imaging modalities in the diagnosis and management of ischemic heart disease (3-5).

Several risk factors contribute to the development of cardiovascular diseases, including hypertension, hyperlipidemia, serum cholesterol levels, ethnicity, smoking, obesity, diabetes, lack of physical activity and family history of CAD (6, 7). These risk factors were incorporated into cardiovascular risk scores such as the Framingham Risk Score, the SCORE2/SCORE2-OP (Systematic COronary Risk Evaluation - Older Persons) score, ASSIGN score, Reynold risk score, QRISK score or the atherosclerotic cardiovascular disease (ASCVD) score (8) and these were designed to estimate the 10-year risk of cardiovascular events. Despite substantial efforts, CAD remains the primary cause of mortality among cardiovascular diseases that is responsible for approximately 1 in 4 deaths in the United States of America (9). Addressing this challenge requires a comprehensive approach that includes prevention, early detection by healthcare screening programs, equitable healthcare access, and ongoing research into more effective treatments and interventions (10, 11). Risk prediction models are based on retrospective population-level data, which may not fully reflect the current prevalence of diseases and risk factors due to ongoing changes in public health trends, such as reduced smoking and cholesterol levels but increasing obesity and diabetes rates that drives current research (e.g. use of GLP-1 Receptor Agonists and SGLT-2-inhibitors) (12). Cardiovascular risk is not a static parameter but rather exists on a continuous spectrum that dynamically evolves over time, making accurate risk assessment challenging. As a result, these models require continuous calibration to ensure they accurately identify individuals at risk, as

traditional scores may fail to pinpoint high-risk patients who would benefit from further testing and preventive treatment (13).

Moreover, CAD is a chronic process characterized by dynamic morphological changes over time, including size and composition. Significant portion of patients remain asymptomatic throughout the development of the disease, with initial manifestation as acute coronary syndrome (ACS) or sudden cardiac death (14). This underlines the importance of early recognition of CAD, where noninvasive imaging has an increasingly central role. The forthcoming studies (e.g. The DANE-HEART Trial - Computed Tomography Coronary Angiography for Primary Prevention or SCOT-HEART 2) will explore asymptomatic patients to delineate subclinical CAD and establish treatment thresholds for pharmacotherapy (12). Notably, a more personalized risk assessment has been proposed recently to prevent ASCVD events involving CAD phenotypes obtained by computed tomography (CT) imaging (15).

Currently, invasive coronary angiography (ICA) is the gold standard diagnostic tool for CAD (16). However, due to its invasive nature and associated periprocedural complication risks, other non-invasive imaging modalities have come to the forefront, capable of detecting CAD and/or consistent ischemia (17). CT, through developments in recent decades, has become capable of imaging rapidly moving coronary arteries with sub-millimeter spatial resolution (18-21). Therefore, non-invasive imaging modalities such as coronary CT angiography (CTA), suitable for examining the coronaries are gaining greater importance in the examination of CAD and therapy monitoring including changes in plaque composition and volume (18) (**Figure 1**).
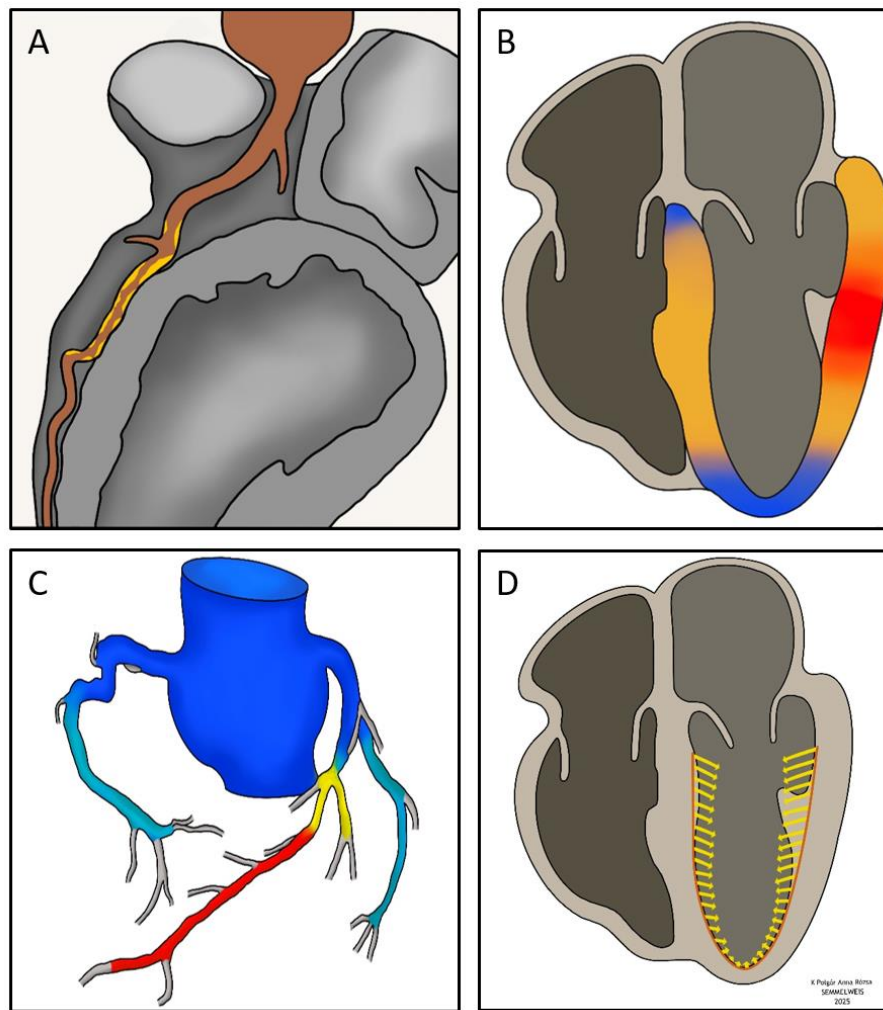
Figure 1. Assessment of CAD using coronary CTA.

CTA enables comprehensive evaluation of CAD through advanced techniques: (A) Quantification of total coronary atherosclerotic plaque burden; (B) CT perfusion imaging, which combines anatomical visualization with functional assessment of myocardial perfusion and identifies ischemic/necrotic myocardium; (C) CT-derived fractional flow reserve to estimate lesion-specific ischemia; (D) CT-based myocardial strain analysis to assess regional myocardial deformation and function. (Own material, credit: K. Polgár Anna Róza.)

CAD: coronary artery disease, CTA: computed tomography angiography

Coronary CTA has emerged as class I diagnostic test, serving as the first-line test to assess patients with symptoms of chronic coronary syndrome (CCS) in the latest European and American guidelines (22, 23). With a high negative predictive value in diagnosing obstructive CAD compared to ICA, its primary indication is to exclude anatomically and also functionally relevant CAD across patients with a broad spectrum of pre-test probability (24). From merely being a tool to exclude coronary obstruction, technical advancements - such as increased spatial resolution and temporal resolution - have transformed CT into a powerful tool for cardiovascular prevention in the last 8 to 10 years. Coronary CTA offers reliable evaluation of the severity, extent and vulnerability of CAD enabling further risk stratification and guiding treatment decision (e.g. bypass surgery planning, CT guided coronary intervention) (25, 26). Coronary CTA can detect significantly larger number of atherosclerotic lesions as compared with ICA and enables compositional analysis of the total coronary plaque burden (27). This has revolutionized prevention efforts and guides secondary prevention therapies (28-31). Approximately half of the plaque ruptures leading to severe cardiovascular events occur in lesions causing less than 50% luminal stenosis (32). CT has been increasingly used to assess plaque progression, and in recent years, it has also been applied to monitor and tailor the effects of medical therapies. The progression of CAD may serve as a prognostic indicator for adverse cardiac events, regardless of the severity of stenosis identified by CTA (31). However, various clinical definitions and metrics have been proposed to identify coronary plaque progression, leading to a lack of consensus in the field. Moreover, data are scarce regarding the clinical predictors of CAD progression using different definitions of plaque progression as assessed by CTA (26). Current thesis aims to assess whether different clinical definitions of CAD affect which patients are considered to progress and which risk factors affect progression.

Traditionally, the assessment of luminal stenosis is pivotal in the management of CAD (33). However, emerging data suggests that total coronary plaque burden is the strongest predictor of events independently from stenosis severity and therefore should be considered as a therapeutic target for personalized prevention (34). This challenges the current concept which prioritizes therapy based on the presence of luminal stenosis or myocardial ischemia. Integrating CTA based quantitative plaque analysis to identify adverse plaque characteristics and total plaque burden could refine patient management

strategies (27). Total coronary plaque volume may also be associated with myocardial ischemia; however, data on this relationship remain limited, and anatomical coregistration of a given plaque to a specific myocardial territory is challenging.

Recent guidelines emphasize the combined use of anatomical and functional evaluation of CAD in patients with CCS and intermedier stenoses to optimize post-test probability and improve clinical decision-making (22). CTA could serve as a one-stop solution for detecting both ischemia and anatomical stenosis (**Figure 2**). Nonetheless, the correlation between stenosis severity, coronary plaque volume and corresponding myocardial ischemia remains a subject of ongoing debate (35).

Severe LAD stenosis on CTA Myocardial ischemia detected on stress CTP images
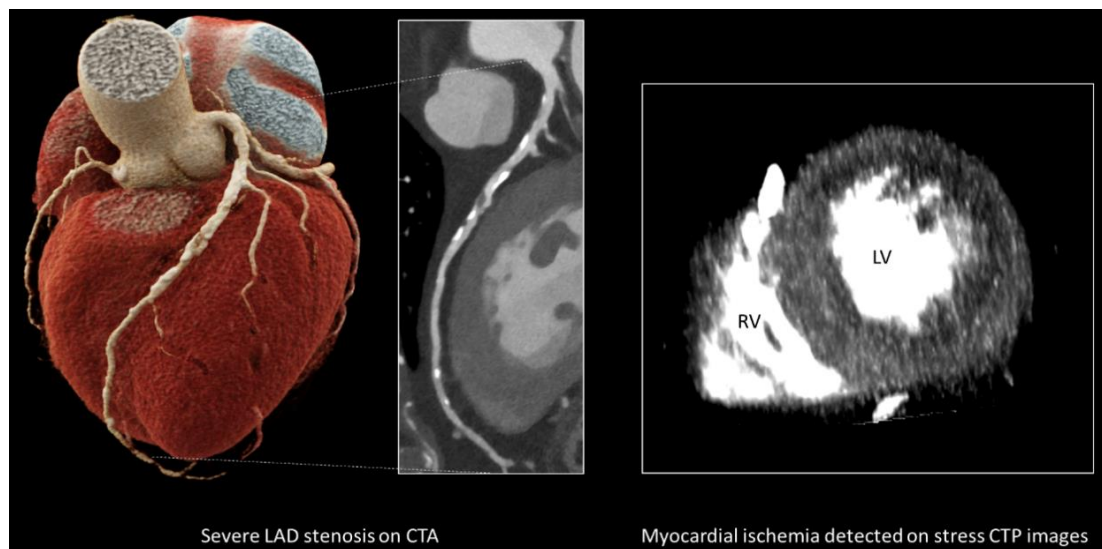
Figure 2. Combined anatomical and functional assessment of CAD by CTA.
Severe stenosis of the LAD was detected on the rest coronary CTA images with corresponding perfusion deficit in the anterior and lateral wall of the left ventricle on stress CT perfusion imaging. (Own material.)

CAD: coronary artery disease; CTA: computed tomography angiography; CTP: computed tomography perfusion; LAD: left anterior descending; LV: left ventricle; RV: right ventricle

Despite its advantages, coronary CTA has limitations, particularly in its specificity and positive predictive value, often overestimating stenosis severity, especially in cases of moderate to severe luminal narrowing, multi-vessel disease and extensive calcification (35). To address these shortcomings, CT perfusion (CTP) imaging has emerged as a robust complement to traditional anatomical assessment with CTA by verifying functional relevance of CAD based on alterations in the myocardium (20, 36, 37). Unlike

other imaging techniques, CTA is uniquely versatile, capable of simultaneously evaluating plaque characteristics and myocardial ischemia. CTP imaging not only enhances diagnostic accuracy especially in patients at higher risk of CAD or microvascular disease but could also detect residual ischemia following percutaneous coronary intervention (PCI). Dynamic myocardial perfusion CT (DPCT) versus static CTP can quantitatively assess myocardial perfusion under pharmacological stress that is associated with higher reproducibility of findings and better diagnostic performance for detecting ischemia as compared with invasive fractional flow reverse (FFR) or single-photon emission computed tomography (SPECT) (20). This methodology also provided us with segmental myocardial analysis and facilitated the assessment of plaque and ischemia.

Previous observational studies have investigated the relationship between coronary plaque burden and global myocardial ischemia using qualitative or visual assessments with modalities like static CTP, stress echocardiography, or SPECT. However, uncertainties persist regarding whether stenosis severity, adverse plaque features, or overall coronary plaque burden reliably predict ischemia. Additionally, it remains unclear whether quantitative plaque characterization can effectively predict segmental ischemia as evaluated by quantitative DPCT imaging. Therefore, our second aim is to assess whether quantitative plaque characterization can effectively predict segmental ischemia, as evaluated by quantitative DPCT imaging using combined rest and stress CT imaging.

Developments in CT technology have resulted in significant advancements in the imaging of the heart (38). A significant leap was the introduction of photon-counting detector technology in 2021, which holds the potential to improve image quality while reducing radiation dose. As the use of coronary CTA expands, concerns about radiation exposure have become more prominent. Implementing new dose-reducing strategies such as prospective-ECG triggering and iterative image reconstruction algorithms not only enhance image quality but also facilitate accurate diagnosis and the identification of high-risk plaque (HRP) features, all while lowering radiation dose (39-41). Dual-source CT technology has led to reduced motion artifacts by improved temporal resolution and reduced acquisition times, enabling good image quality even at higher heart rate (42). Photon-counting CT (PCCT) represents an innovative technology for coronary artery assessment, offering superior spatial and temporal resolution compared to conventional

energy-integrating detector (EID) scanners (38). Unlike traditional detectors, photon-counting detectors directly capture the energy of each photon, leading to improved spatial resolution, reduced noise, and enhanced soft tissue contrast. Moreover, PCCT technology enables the creation of virtual monoenergetic images (VMI), which can mitigate blooming artifacts and enhance the contrast-to-noise ratio (CNR) in coronary CTA (40). Therefore, employing different VMI reconstructions has the potential to enhance coronary plaque detection by modifying intraluminal contrast attenuation and CNR (**Figure 3**). However, it is important to acknowledge that VMIs may alter the Hounsfield unit (HU) values of voxels related to the plaque, which could potentially influence estimates of plaque volume during quantitative plaque assessment. Thus, current thesis also aims to assess how different VMI levels affect quantitative plaque components using novel PCCT system.
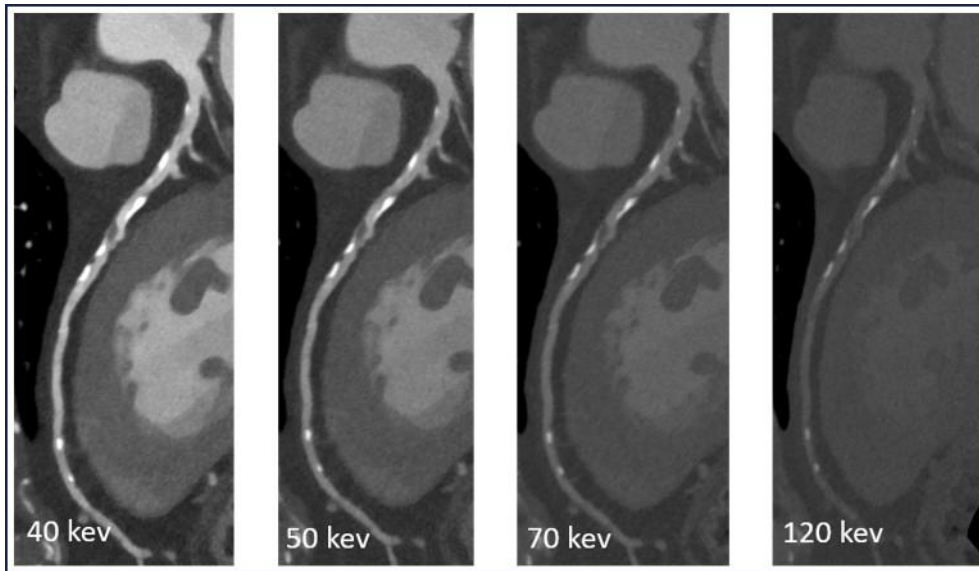
Figure 3. Representative image of different VMI energy levels using PCCT.
Coronary CTA images reconstructed at different keV levels (40, 50, 70 and 120 keV) are depicted. Using higher energy levels decrease blooming blooming artifacts caused by heavy calcification in the LAD. (Own material.)

CTA: computed tomography angiography; LAD: left anterior descending; PCCT: photon-counting computed tomography; VMI: virtual monoenergetic image

1.1 Anatomical assessment of coronary artery disease using CT angiography

Assessing symptomatic patients suspected of CCS poses a fundamental task in clinical practice. The advent of anatomical evaluation through coronary CTA offers a reliable and precise diagnostic approach for CAD (43, 44). The spatial resolution of current multidetector EID CT reaches 400 μm, allowing for the examination of coronary segments ranging from 2 to 5 mm. Using modern model based iterative reconstruction techniques, CT images can be analyzed in excellent quality, enabling the precise detection of coronary plaques and adjacent structures. Importantly, coronary CTA demonstrated excellent intra- and inter-observer reproducibility in the detection of luminal stenosis or plaque volumes (45, 46). In addition to the volumetric plaque analysis, CTA allows accurate assessment composition of atherosclerotic plaques including HRP features. The coronary artery system is analyzed based on the 18-segment model established by the American Heart Association (AHA) and the Society of Cardiovascular Computed Tomography (SCCT) (**Figure 4**) (47). The main aspects of analyzing coronary atherosclerosis based on CTA are described below.

1.1.1 Stenosis assessment

The determination of luminal stenosis follows the guidelines of the SCCT. Stenosis severity can thus be classified into five categories based on the degree of luminal stenosis: < 25% as minimal, 25% - 49% as mild, 50% - 69% as moderate, 70% - 99% as severe and 100% as occluded (**Figure 5**). Additional semi-quantitative methods are available for assessing the severity of the disease. When calculating the segment stenosis score (SSS), a score of 0 - 5 is assigned based on the degree of stenosis observed in the segment. According to the stenosis classification described above, the scores are as follows: no stenosis - 0, minimal - 1, mild - 2, moderate - 3, severe - 4, occluded - 5. Eventually the points are summed up characterizing the severity of CAD. Using quantitative coronary angiography as the reference standard, latest scanner technology demonstrated a vessel-

level diagnostic accuracy of 97.2% for detecting more than 50% diameter stenosis using CTA (48).
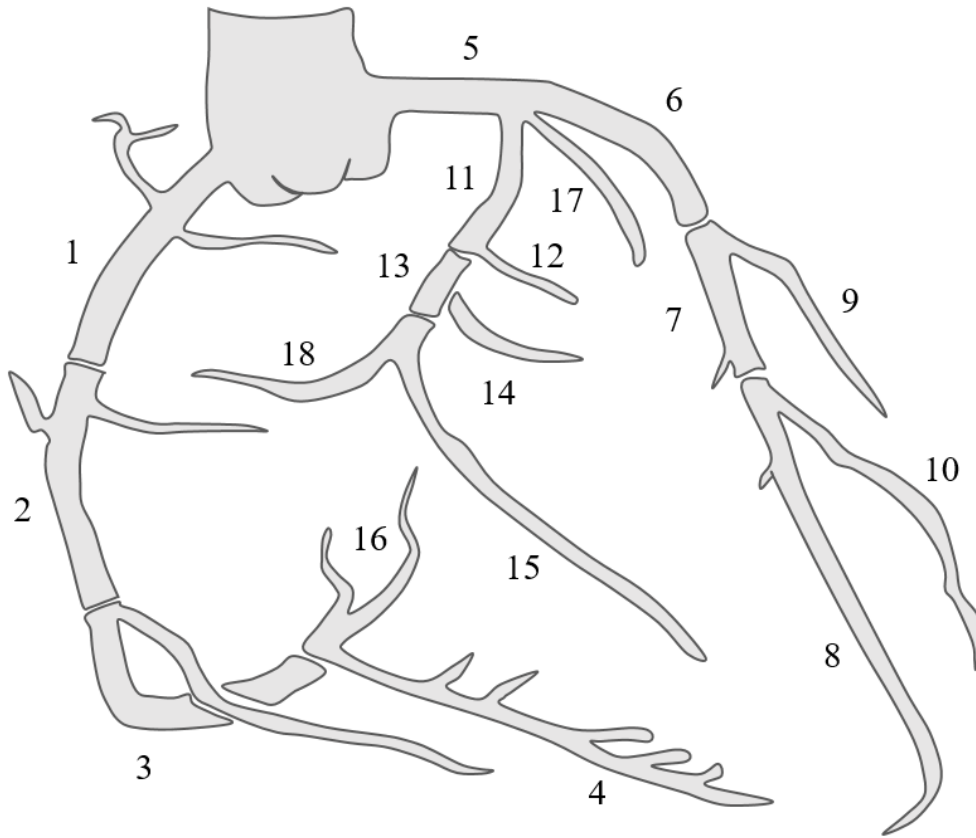
Figure 4. Coronary artery segments evaluated by CTA.

The 18-segment American Heart Association (AHA) segmentation scheme is recommended for defining segmental involvement by CAD using CTA. By utilizing this scheme, we can compare findings with invasive angiography without anatomical mismatch and assign the Segment Involvement Score (SIS) to describe the extent of CAD. (Own material.)

CAD: coronary artery disease; CTA: coronary computed tomography angiography
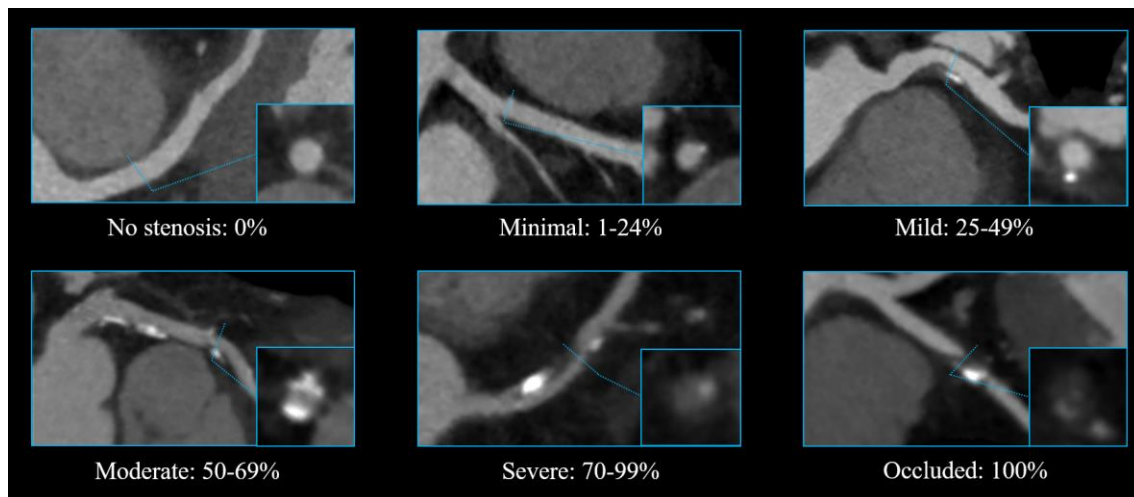
Figure 5. Coronary stenosis grading using CTA.

In clinical routine, stenosis is categorized according to the above classifications, which serve as the basis for formulating patient management recommendations. (Own material.)

CTA: computed tomography angiography

1.1.2 Extent of coronary atherosclerosis

Coronary artery calcium score (CACS) calculated based on the Agatston method using non-enhanced CT images is a surrogate of total coronary plaque burden. The calculation of CACS can be used for cardiovascular risk prediction in asymptomatic patients. The risk of future major adverse cardiovascular events (MACE) is increasing with higher scores and based on total CACS, four risk levels are defined: 0; 1 - 99; 100 - 399 and $\geq$ 400 (**Figure 6**) (49). A score of 0 represents an extremely low risk in asymptomatic individuals, while score of $\geq$ 1000 indicates 12 times higher risk (50). Utilizing CACS in asymptomatic patients improves risk estimation in individuals at intermediate risk and increase statin eligibility, as shown by the MESA (Multi-Ethnic Study of Atherosclerosis) trial (51). Importantly, statin therapy for prevention in patients without detectable coronary calcification does not seem to improve clinical outcomes (52). The SCCT consensus statement proposed a CACS threshold of 100 for initiating statin therapy in patients with 5-20% ASCVD risk. The "Power of Zero" concept highlights that a CACS of zero is one of the strongest protective factors against cardiovascular events (53, 54). Statin therapy can increase CACS due to the conversion of non-calcified plaques into more stable, calcified plaques. This process does not necessarily indicate worsening

disease but rather a change in plaque composition (55). Therefore, CACS is not recommended as a biomarker to monitor the effects of statin therapy.

CACS	Risk
0	Extremely low
1-10	Minimal
11-100	Mild
101-400	Moderate
>400	High
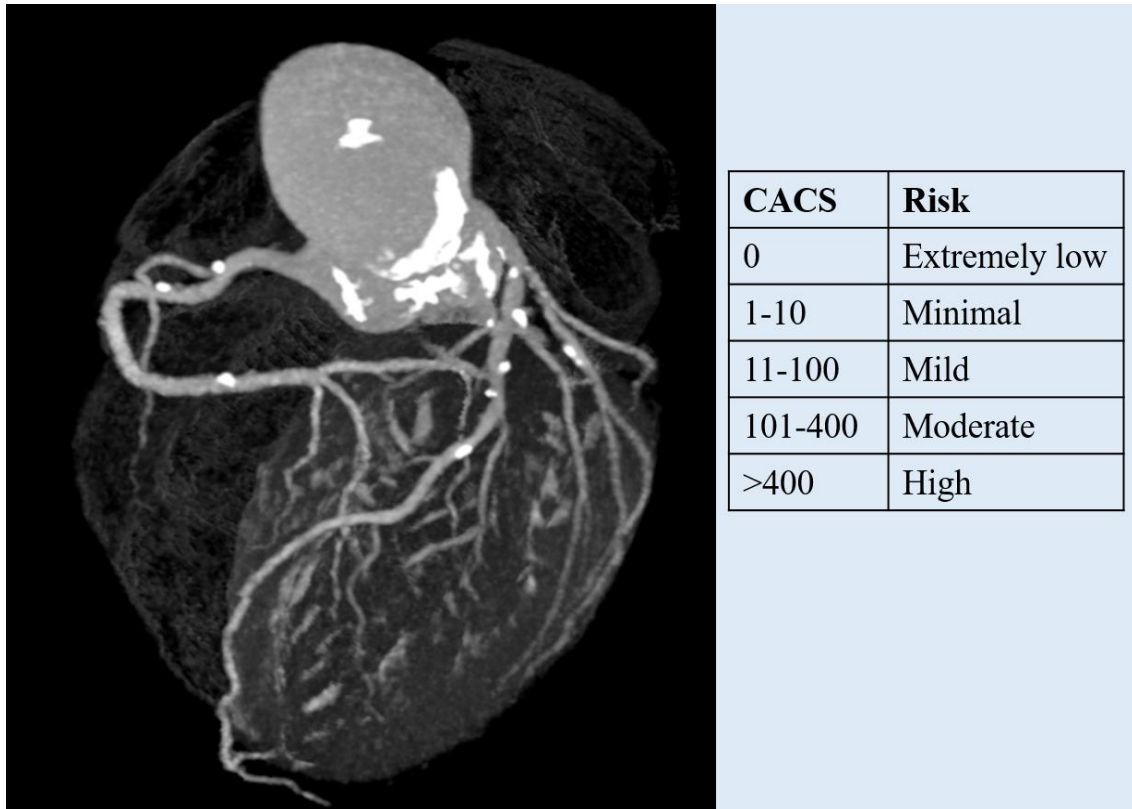
Figure 6. Coronary calcium score based on non-contrast CT images.

Current image depicts a representative case of diffuse calcification on non-contrast CT images, and the associated risk categories based on CACS. (Own material.)

CACS: coronary artery calcium score; CT: computed tomography

Analyzing coronary plaques on contrast-enhanced CT images allows for the determination of a semi-quantitative score proposed by Min et al. known as the segment involvement score (SIS). SIS is a measure of the extent of coronary atherosclerosis and can be calculated by summing up the number of coronary segments with atherosclerotic plaque. SIS is increasingly used in both the research and clinical settings and was found predictive for MACE in both obstructive and non-obstructive CAD (56, 57).

1.1.3 Plaque composition

Different tissues are characterized by their attenuation on CT scans that can be quantified using HU values, allowing for their identification, differentiation and even precise quantification of a given structure. In terms of composition, three main plaque types can be distinguished based on CTA: calcified plaques (CP), partially calcified plaques and non-calcified plaques (NCP). Recent guidelines also distinguish partially calcified plaques based on the amount of calcification into predominantly calcified ($\geq$75% calcified component) and predominantly non-calcified ($\geq$75% non-calcified component) plaques. Within non-calcified lesions, homogeneous and heterogeneous plaques can be differentiated based on attenuation, with further categorization including napkin-ring sign plaque, which will be discussed in more detail later (58). NCPs are characterized by lower density, while CPs are characterized by higher density values (>350 HU) (27). Analyzing composition provides important information about plaque calcium content, calcium density and allows for the differentiation of plaques containing fatty and fibrotic elements.

During morphological assessment of coronary plaques, certain HRP features can be determined by qualitative or semiquantitative characteristics that demonstrated prognostic value in prior studies (59). Traditional HRP features detected by CTA are the following: low-attenuation, positive remodeling, spotty calcification and napkin-ring sign (**Table 1; Figure 7**).

a.   Low-attenuation plaque

Plaques rich in lipid present as low-density areas on CT images supported by data comparing coronary CTA and intravascular ultrasound (IVUS) that characterized lipid-rich plaques with low CT density (18). Culprit lesions tend to have larger lipid-rich core than non-culprit lesions of ACS (60). Therefore, it is important to distinguish high-risk, prone to rupture, lipid-rich lesions for predicting ACS. Motoyama et al. reported that low-attenuation plaques (LAP) of < 30 HU were significantly more prevalent in patients presenting with ACS (79% vs. 9%, $p < 0.001$) (61). Similarly, further studies have also reported attenuation value < 30 HU as a threshold for identifying lipid-rich plaques and found a higher proportion of LAP in patients presenting with ACS compared to those with stable angina (88% vs. 18%, $p < 0.001$) (62).

Table 1. Key CT trials on high-risk coronary plaque features and outcomes.

Trial	Year	Study population	High-risk plaque features	Primary outcomes	Key findings
SCOT-HEART	2019	1,778 stable chest pain patients	positive remodeling, low-attenuation plaque, spotty calcification, napkin ring sign	coronary heart disease death or nonfatal MI	Identification of HRP features on CTA was associated with a higher rate of events.
PROMISE	2018	4,415 stable chest pain patients	positive remodeling, low-attenuation plaque, napkin-ring sign	MACE (death, MI, or unstable angina pectoris)	Presence of HRP features carried a 70% increased risk of future MACE over a median follow-up of 25 months.
ROMICAT-II	2014	472 acute chest pain patients with suspected ACS	positive remodeling, low-attenuation plaque, spotty calcification, napkin ring sign	ACS (acute MI or unstable angina pectoris)	HRP was associated with ACS independently and incrementally to the presence of significant CAD and clinical risk assessment.
Motoyama et al.	2015	449 stable patients with known or suspected CAD	positive remodeling and/or low-density plaque	ACS	HRP was an independent predictor of ACS.

ACS: acute coronary syndrome; CAD: coronary artery disease; CTA: coronary computed tomography angiography; HRP: high-risk plaque; MACE: major adverse cardiovascular events; MI: myocardial infarction

b.   Positive remodeling

Atherosclerotic plaques often grow outward to the coronary lumen without causing relevant stenosis. This phenomenon is known as positive remodeling, which can be characterized by the remodeling index (RI). The calculation of the RI is as follows: the largest luminal diameter containing the coronary plaque is divided by the average of the

proximal and distal luminal diameters from the lesion (60). A coronary plaque is considered to have positive remodeling if the RI is ≥ 1.1. Studies have shown that lesions characterized by positive remodeling have a larger lipid core and contain more macrophages. Furthermore, validation of its vulnerability is evident in studies comparing lesions causing ACS and stable angina, where positive remodeling was more common in plaques causing ACS (61).

c.   Spotty calcification

Spotty calcification in coronary CTA is defined as a small, dense (> 130 HU) lesion surrounded by NCP components. By definition, the size of spotty calcification is less than 3 mm, but further classifications distinguish between small (< 1 mm), medium (1 - 3 mm), and large (> 3 mm) calcifications. The extent of calcification detected by CT correlates with the overall plaque burden, which is associated with poor prognosis (63). However, studies using IVUS to assess the vulnerability of calcified plaques have yielded conflicting results. While plaques containing extensive calcification typically remain clinically silent, those with small calcifications have been associated with disease progression (64). Additionally, lesions causing ACS typically contain spotty calcification (65). Compared to stable angina patients, lesions causing ACS also exhibited a higher prevalence of spotty calcification (66).

d.   Napkin-ring sign

The napkin-ring sign corresponds to the cross-sectional CT image of thin-cap fibroatheroma (TCFA) (67). As a qualitative imaging marker distinct from other vulnerability features, it is characterized by a low-density central region in contact with the vessel lumen, surrounded by a higher-density ring-shaped layer (68). The low-density central area corresponds to the necrotic core of TCFA, while the higher attenuation layer represents the CT image of the fibrous ring-like structure around the core. Based on ex-vivo studies, Maurovich-Horvat et al described napkin-ring sign with excellent specificity (98.9%) and low sensitivity (24.4%) for recognizing plaques containing large necrotic cores on histology (58). Thus, coronary CTA might enable the identification of TCFA containing large necrotic cores associated with increased risk of cardiovascular events. Otzuka et al during 1-year follow-up of 895 patients who underwent coronary CTA found that several HRP features identified by CT, including napkin-ring sign, were independent predictors of ACS (69).
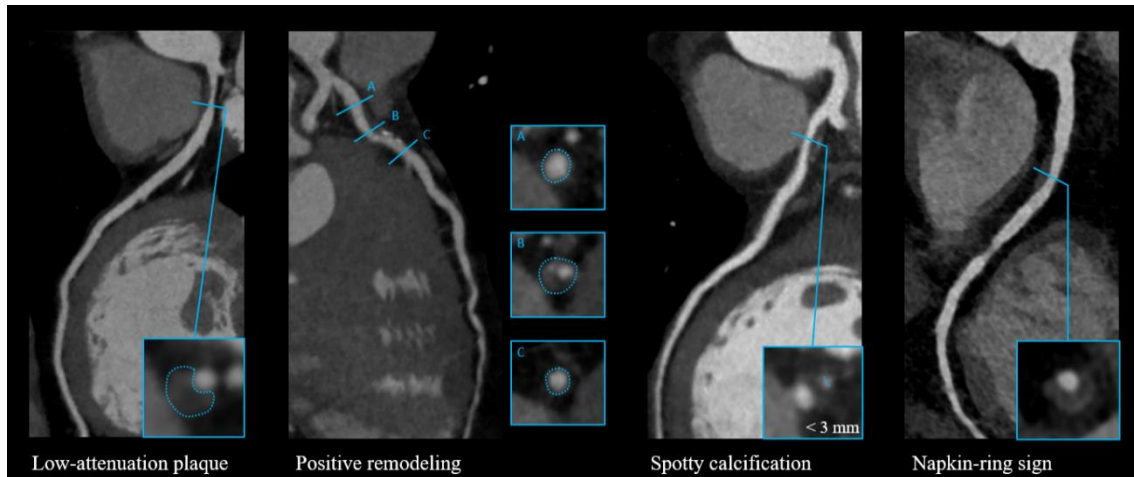
Figure 7. Representative images of CT derived HRP features associated with adverse outcomes.

CT-based HRP features shown in this figure include low attenuation plaque, positive remodeling, napkin-ring sign and spotty calcification, all of which have been associated with major adverse events. (Own material.)

CT: computed tomography; HRP: high-risk plaque

1.1.4 Quantitative plaque assessment

Quantifying coronary plaque burden and identifying adverse plaque characteristics have the potential to enhance risk prediction of MACE (70). Particularly, the burden of LAP has been identified as an independent predictor of myocardial infarction (71). Dedicated software tools allow quantitative evaluation of coronary atherosclerosis by determining lumen and vessel wall borders and by characterizing plaque composition based on CT attenuation values (72) (**Figure 8**). Therefore, plaque volumes, composition, and diameter stenosis can be quantified. Currently utilized softwares have been validated against gold standard methods such as IVUS, optical coherence tomography (OCT) or histology (73). Clinical trials investigating the effect of lipid-lowering pharmacological therapies have been utilized quantitative metrics to monitor coronary atherosclerosis progression (55, 74). As growing body of evidence supports the importance of plaque burden and plaque characterization, plaque quantification is expected to be more commonly used in clinical practice as well. This requires its seamless incorporation into the reporting softwares.
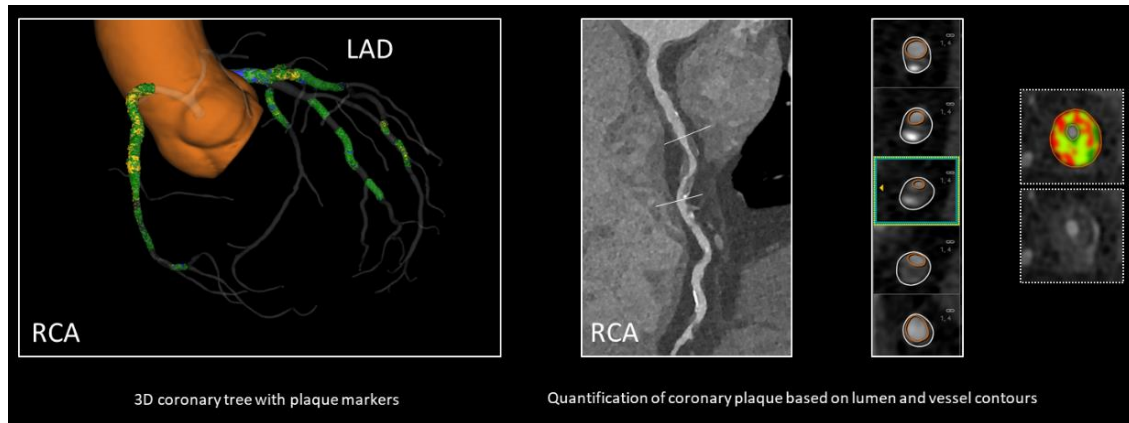
Figure 8. Quantitative coronary plaque assessment using CTA.

Current software tools provide 3-dimensional models of the coronary tree for better visualization of plaque burden and composition. The color coding is based on the HU values. This approach is increasingly applied in PCI planning and monitoring medical therapy (e.g. statin). (Own material.)

CAD: coronary artery disease; CTA: computed tomography angiography; HU: Hounsfield unit; LAD: left anterior descending; PCI: percutaneous coronary intervention; RCA: right coronary artery

However, some limitations hinder its widespread utilization in everyday practice that need to be addressed. Particularly, quantitative plaque analysis requires excellent image quality. Coronary plaque segmentation is relatively time consuming and need substantial manual corrections, although developments aim for automated quantification methods creating it more convenient. Also, consistent methods for plaque quantification are lacking including plaque composition thresholds and plaque burden definition (27). For plaque characterization fixed or adaptive thresholds are also in use. Fixed thresholds are commonly used with predefined HU values for NCP components including necrotic core, fibrotic, and fibrofatty tissues and for CP components. Plaque attenuation is influenced by luminal contrast density as well. To overcome this limitation, adaptive thresholds are used correcting for lumen density to achieve more accurate results, however data are scarce on the use of such approaches. Further standardization is needed for plaque quantification, as contrast media protocols, body size, acquisition protocols including tube current and voltage and reconstruction settings also effect attenuation values, hence influencing plaque quantification. Furthermore, with the advent of photon-counting

21

technology, several additional imaging parameters including novel set of kernels, iterative reconstruction algorithms, VMIs or different slice thickness settings introduced even more variability in plaque assessment (21, 75, 76).

1.1.5 CAD-RADS classification

The Coronary Artery Disease Reporting and Data System (CAD-RADS) facilitates a uniform and standardized reporting structure of coronary CTA and guidance of patient management with further examinations and therapeutic suggestions (**Table 2**). CAD-RADS 2.0 was introduced in 2022 with the implementation of technological developments and novel clinical trials (77). It incorporates stenosis severity, extent, vulnerability and the presence of ischemia, as well as previous revascularization. Based on the degree of the most severe atherosclerotic lesion, the stenosis category ranges from 0 - 5 (CAD-RADS 0 - 5), where 0 means no plaque or stenosis and 5 indicates occlusion in the coronary system. The use of additional modifiers allows for a more detailed description of CAD: describing plaque burden "P1 - P4" is added; in the presence of at least 2 HRP features "V" as vulnerable modifier is used; "I" modifier can be added based on proven ischemia; "G" stands for bypass grafts; "S" indicates coronary stents; "N" represents non-diagnostic segments; and "E" stands for exceptions (coronary dissection, vasculitis, fistula etc.) (**Figure 9**).

Table 2. CAD-RADS classification for the interpretation and reporting of coronary CTA.

Category	Degree of maximal coronary stenosis	Interpretation	Further cardiac investigation	Management considerations
CAD-RADS 0	0% (No plaque or stenosis)	Absence of CAD	None	Reassurance. Consider non-atherosclerotic causes of symptoms.
CAD-RADS 1	1-24% (Minimal stenosis or plaque with no stenosis)	Minimal non-obstructive CAD	None	Consider non-atherosclerotic causes of symptoms.
CAD-RADS 2	25-49% (Mild stenosis)	Mild non-obstructive CAD	None	Consider non-atherosclerotic causes of symptoms.
CAD-RADS 3	50-69% (Moderate stenosis)	Moderate stenosis	Consider functional assessment	Aggressive risk factor modification and preventive pharmacotherapy.
CAD-RADS 4	A - 70-99% or B - Left main ≥50% or 3-vessel obstructive (≥70%) disease	Severe stenosis	A: Consider ICA or functional assessment B: ICA is recommended	Aggressive risk factor modification and preventive pharmacotherapy.
CAD-RADS 5	100% (Total occlusion)	Total coronary occlusion or sub-total occlusion	Consider ICA, functional and/or viability assessment	Aggressive risk factor modification and preventive pharmacotherapy.
CAD-RADS N	Non-diagnostic study	Obstructive CAD cannot be excluded	Additional/alternative evaluation may be needed	

CAD-RADS: coronary artery disease reporting and data system; CTA: computed tomography angiography; ICA: invasive coronary angiography
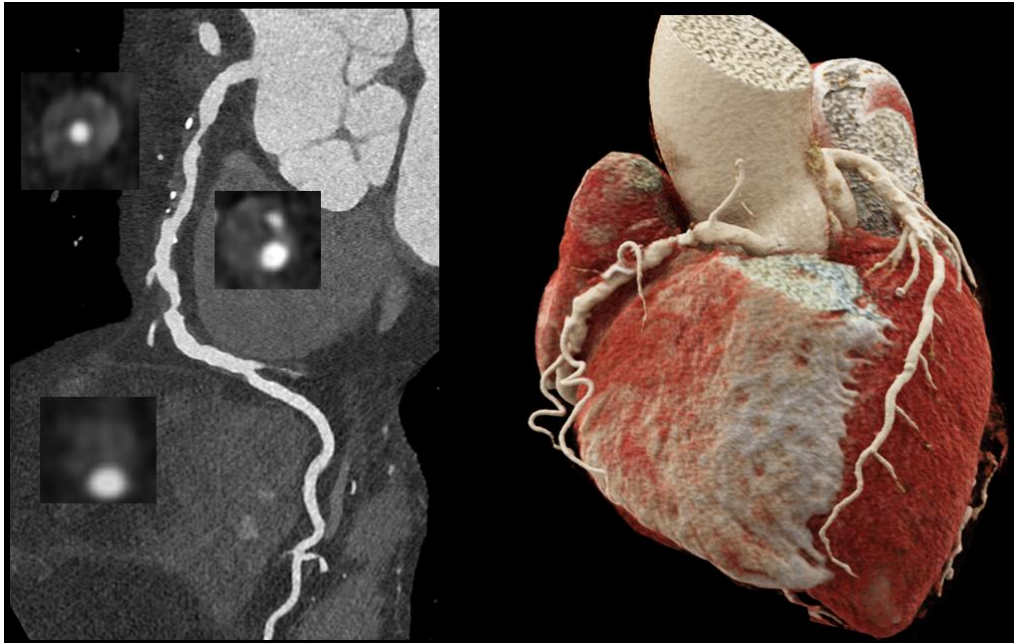
Figure 9. Discrepancy between CAD-RADS classification and SIS.

While CAD-RADS severity is based on the most significant stenosis - in this case, a moderate narrowing - the overall extent of disease also has important prognostic value. The segment involvement score can help reclassify the risk for adverse events. The left panel displays an RCA with high-risk plaque and a borderline stenosis; however, the total plaque burden (SIS of 5) suggests a significantly higher risk than what would be inferred from the most severe stenosis alone. Additionally, multiple HRP features are present including positive remodeling and low plaque attenuation. (Own material.)

CAD-RADS: coronary artery disease reporting and data system; RCA: right coronary artery; SIS: segment involvement score

1.2 Functional assessment of coronary artery disease using CT angiography

In the recent years, functional assessment of CAD has become available using CTA. Addressing the limitations of anatomical assessment by coronary CTA, additional functional evaluation improves specificity and positive predictive value for the detection of hemodynamically significant coronary lesions (78). These methods include myocardial CTP imaging and CT-based fractional flow reserve (CT-FFR) (79). Becoming a true one-stop-shop, cardiac CTA uniquely offers anatomical and functional information of coronary atherosclerosis using one modality (80).

In the management of patients presenting with CCS, ischemia driven revascularization has potential benefit regarding symptom relief and prognosis, as revascularization does not improve symptoms or outcome in patients lacking detectable ischemia (81-83). Nevertheless, evidence suggest that more than 10% ischemia may correlate with improved prognosis after revascularization (84). Notably, a significant discordance between the severity of luminal stenosis by imaging and the presence of detectable ischemia as demonstrated by previous studies utilizing SPECT or invasive FFR (85, 86). Myocardial CTP imaging has emerged as a promising modality for ischemia detection, capable of identifying hypoattenuated areas corresponding to myocardial injury in the left ventricle during the first-pass uptake of contrast agent. Wider heart volume coverage by modern CT detector technology facilitated the application of CTP in clinical practice. However, standardization remains challenging due to variability in imaging protocols and perfusion parameter cut-off values. The SCCT released a consensus document on myocardial perfusion imaging in 2020, delineating technical principles, diagnostic utility, patient selection criteria and reporting guidelines (87). Importantly, the document advocates for the utilization of CTP in patients with a high likelihood of ischemic heart disease, known CAD, prior coronary intervention or extensive calcification.

Perfusion imaging by CTA is performed during ischemia provocation using vasodilator stressor agents (88). Different stressors are in use to provoke ischemia, predominantly adenosine and regadenoson, a selective adenosine A(2A) receptor agonist. Latter has the advantage of safe utilization without dose modulation for patients' size or comorbidities used as a single 10 second bolus, and provides adequate long and effective vasodilator stress for CTP based on recent investigations (89). Regarding the sequence of rest and stress CTA imaging, different approaches are available. Rest images could be performed either initially to rule out CAD with subsequent stress imaging or after perfusion imaging to avoid pre-enhancement of the myocardium by the contrast agent. No guidelines are available on the exact order of rest and stress imaging, however there are recommendations based on patients' pre-test probability by traditional risk scores or coronary calcium scoring (90). Generally, in patients with lower risk an initial rest CTA is suggested, while in patients with higher risk an initial stress perfusion imaging should be performed.

CTP can be performed using static or dynamic acquisitions, each offering distinct advantages. While static CTP provides qualitative and semi-quantitative analysis of peak myocardial blood flow (MBF) in one specific time point, hence the timing for static CTP is crucial (90, 91). On the other hand, dynamic CTP allows for precise quantitative assessment of MBF, by characterizing contrast agent distribution in the left ventricular myocardium during several cardiac cycles (92). Obtaining time attenuation curves (TAC) and arterial input function curves using the upslope method, MBF is calculated and can be measured in the myocardium globally or segment-based. Despite growing body of evidence suggesting improved diagnostic accuracy of quantitative assessment using dynamic perfusion protocols, it is associated with higher radiation dose exposure (approximately 4 - 15 mSv) (90, 93).

TAC curves differ significantly for normal and ischemic myocardium. Therefore, enabling the detection of semi-quantitative and quantitative parameters of myocardial perfusion including: the upslope, peak enhancement, time to peak (TTP), area under the curve, absolute and relative MBF values and myocardial blood volume (MBV) (80). Notably, in case of multivessel disease, dynamic CTP allows more precise and reproducible assessment of ischemia as compared to static CTP. Importantly, standardization regarding imaging protocols and thresholds for ischemia detection are lacking. A wide range of MBF cut-off values for the detection of myocardial ischemia are reported in the literature from 75 to even 103 ml/100 ml/min (93-101).

Excellent diagnostic performance of CTP has previously been reported in single center studies compared to SPECT, cardiac magnetic resonance imaging (MRI), positron emission tomography (PET), ICA and invasive FFR (102-105). The CORE320 (Combined Non-invasive Coronary Angiography and Myocardial Perfusion Imaging Using 320 Detector Computed Tomography) multicenter study found higher diagnostic performance for static CTP compared to SPECT for the detection of significant CAD in patients with known obstructive disease detected by ICA (106). Also, using ICA and FFR as reference standard, CTP had excellent sensitivity and specificity based on a meta-analysis by Takx et al (107). Compared to different non-invasive modalities, CTP yielded similar diagnostic performance to PET and stress MRI, while higher diagnostic performance compared to SPECT and echocardiography. Also based on a meta-analysis,

the addition of CTP to coronary CTA improved specificity from 62% to 84% compared to coronary CTA alone using ICA as reference standard (108).

In conclusion, CTP is a promising and accessible diagnostic approach for the evaluation of myocardial ischemia with superior spatial resolution compared to SPECT allowing for the detection of smaller ischemic territories. Notably, CT is the only non-invasive modality for the combined anatomical and functional assessments of CAD allowing more precise patient management.

1.3 Prognostic value of coronary CT angiography in chronic coronary syndrome

In recent years, coronary CTA became a first-line diagnostic tool for the diagnosis of CCS in patients presenting with stable angina at low- to intermediate risk for obstructive CAD in both European and American guidelines (23, 109). Several randomized trials have demonstrated the prognostic value of coronary CTA compared to standard-care including functional testing or ICA. The PROMISE (Prognostic Value of Noninvasive Cardiovascular Testing in Patients With Stable Chest Pain) trial showed that non-obstructive CAD detected on coronary CTA provides prognostic information contributing to improved risk stratification and preventive therapy (110). Importantly, in the CT arm more than half of the events occurred in cases with non-obstructive disease, defined as < 70% stenosis. While one-third of the events occurred in patients with < 50% luminal stenosis detected on CTA. In the SCOT-HEART (Scottish Computed Tomography of the Heart) trial, at 5-year follow-up no difference between the incidence of ICA or revascularization was found between the CTA and standard-care group (111). In addition, lower event rate was found in patients referred to CTA, predominantly driven by lower rate of nonfatal myocardial infarction. In the DISCHARGE trial similar MACE rate was associated with coronary CTA and ICA, while less procedure-related complication occurred in the CTA group demonstrating a safer alternative to ICA, further reinforcing the use of CTA as a safe first-line test in stable angina (17).

Supporting the additional value of CTA in the management of CCS, in the CONFIRM registry coronary plaque burden based on SIS was an independent predictor for major adverse outcomes (112). Similarly, Bittencourt et al. demonstrated that extensive (SIS>4) but non-obstructive CAD showed similar hazard ratio for predicting major adverse events

as compared to obstructive, non-extensive (SIS≤4) CAD, underlining the importance of coronary plaque burden assessment (57).

Coronary CTA allows accurate visualization of the vessel wall and plaque morphology, enabling the assessment of CT surrogates of HRP. HRP features including positive remodeling, low plaque attenuation and napkin-ring sign demonstrated significant association with MACE in several single-center, observational studies (113). In the SCOT-HEART trial, the presence of HRP features including positive remodeling and low plaque attenuation and obstructive CAD showed the highest rate of cardiovascular events compared to normal coronaries (114). A substudy of the trial also found that quantitatively assessed LAP burden was an independent predictor of myocardial infarction (71). In a substudy of the PROMISE trial, HRP (defined as having either positive remodeling, low plaque attenuation or napkin-ring sign) was found to be an independent predictor of major adverse events over traditional cardiovascular risk factors and obstructive CAD (115).

Serial coronary CTA imaging allows for the detection of CAD progression. Motoyama et al assessed plaque progression during serial scanning with a median 1 year between the two exams. Their study demonstrated that plaque progression defined as increase in stenosis grade or increase in RI was an independent predictor of ACS over cardiovascular risk factors and HRP features detected on CTA (31).

Currently, data of the prognostic value of myocardial CTP are scarce. In the CORE320 trial, during a 5-year follow-up, a combined CTA and CTP approach compared to the combination of ICA and SPECT for the detection of CCS showed similar prognostic value of MACE (116). This indicated that utilizing a non-invasive strategy using CTA and CTP for the detection of CAD could further reduce invasive procedures.

1.4 Photon-counting CT for the evaluation of coronary artery disease

The first photon-counting detector CT has been introduced to clinical practice in 2021. Its novelty lies in the innovative detector technology that allows more detailed assessment of the heart as compared to conventional CT scanners (117). Compared to the EID technology, photon-counting detectors directly convert each x-ray photons to electric signal without converting them to light, improving detector efficacy (118). Captured photons generate electric charge with the amplitude proportional to the photon's energy,

enabling spectral imaging. The novel detector technology does not require reflecting septa dividing the detector, allowing for smaller detector pixels. These features contribute to improved spatial resolution, noise reduction, and better tissue characterization. In addition, as a dual-source scanner, the first clinically available PCCT also has improved temporal resolution (66 ms). Furthermore, by generating VMI images, blooming artifacts can be reduced further improving stenosis assessment in calcified lesions and improving CNR for further enhancement in image quality (119). Previous studies have shown that spectral data from a PCCT system can accurately differentiate between different plaque components and the vessel lumen, as observed in histological atherosclerotic plaque samples (120). Moreover, PCCT provides sharper delineation of structures such as calcifications due to its superior spatial resolution and reduced blooming. With the above-mentioned advantages, novel dual-source PCCT is a promising tool for the assessment of the coronaries by reducing motion artifacts at even higher heart rates, improving plaque characterization and stenosis assessment (**Figure 10**).

Due to the novelty of the technique, currently only a limited amount of data is available evaluating the role of PCCT in CAD. Nevertheless, early evidence from recent studies suggests several potential advantages of PCCT over conventional EID-CT. Compared with EID-CT, ultra-high-resolution PCCT has been shown to provide more accurate stenosis assessment in calcified coronary plaques, leading to a CAD-RADS reclassification in approximately 49% of patients (121). In addition, PCCT enabled improved reproducibility of LAP quantification compared to conventional CT (122). Studies have also reported a lower rate of subsequent ICA referrals among patients undergoing coronary CT angiography with PCCT, particularly in those with extensive coronary calcification (123). Moreover, while fewer patients were referred to ICA after PCCT compared to EID-CT, those who were referred were more likely to undergo revascularization, indicating improved diagnostic performance (48). Finally, PCCT holds promise for reducing both the financial burden on healthcare systems and the rate of procedure-related complications in patients with CCS compared with conventional CT technologies (124).
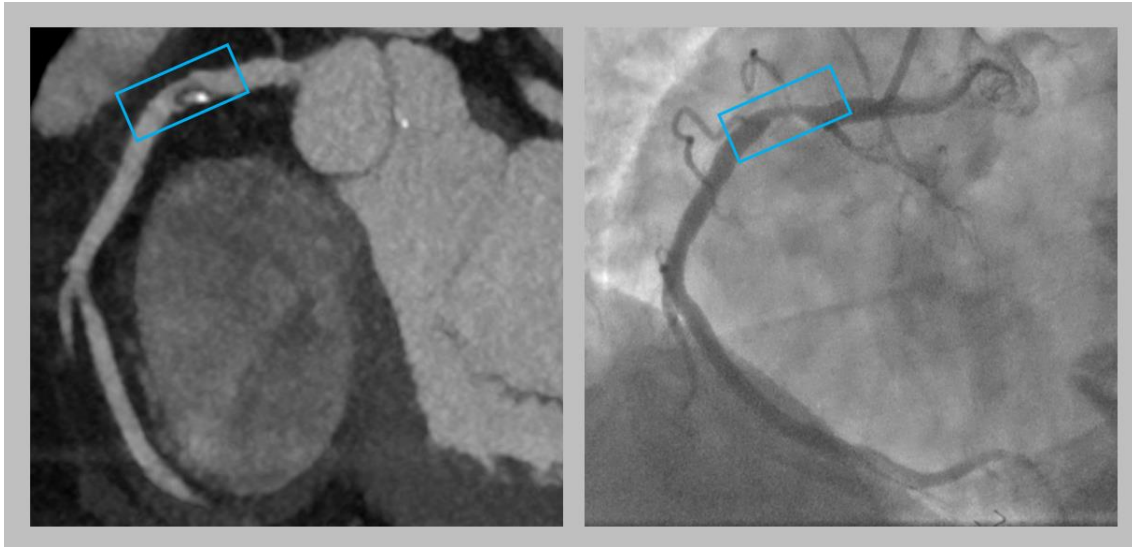
Figure 10. Excellent correlation in stenosis severity between CTA and ICA was detected using novel PCCT technology. Representative image of a stenosis in the proximal RCA detected on coronary CTA (left) and ICA (right). (Own material.)

CTA: computed tomography angiography; ICA: invasive coronary angiography; PCCT: photon-counting computed tomography; RCA: right coronary artery

2. OBJECTIVES

The objective of this thesis was to establish the following aims:

2.1 Defining coronary plaque progression using different definitions of coronary artery disease assessed by coronary CTA

The aim of the study was to identify predictors of CAD progression using various clinical definitions of plaque burden based on serial coronary CTA imaging.

In addition, we aimed to compare the detection of plaque progression using three distinct semi-quantitative definitions of CAD, including the stenosis classification outlined in the CAD-RADS classification.

2.2 Defining the association between quantitative coronary plaque metrics and myocardial ischemia using CTA

The aim of the study was to elucidate the association between quantitative atherosclerotic plaque metrics derived from coronary CTA and segmental myocardial ischemia based on MBF detected by DPCT imaging.

2.3 Defining the changes in quantitative coronary plaque characteristics using spectral CTA imaging

The aim of the study was to investigate how the quantification of individual plaque components changes concerning different monoenergetic levels obtained using novel PCCT system.

Also, our aim was to assess quantitative image quality of different VMI reconstructions.

3. METHODS

3.1 Study design for plaque progression assessment

3.1.1 Patient population

For the analysis of plaque progression based on coronary CTA, patients were retrospectively included from the cardiac CT registry of the Heart and Vascular Center, Semmelweis University. Inclusion criteria was serial coronary CTA imaging - with at least 1-year interval between the two examinations - using the same 256-slice CT scanner (Philips Brilliance iCT, Best, The Netherlands). Exclusion criteria were prior myocardial infarction, percutaneous coronary intervention, heart transplantation, coronary bypass graft surgery, or non-diagnostic CT image quality. A total of 115 patients were included in our final database for analysis. Indication for serial coronary CTA were planning of pulmonary vein isolation due to paroxysmal atrial fibrillation (23.4%) or recurrent stable angina after initial CTA (76.6%).

Comprehensive demographic data, comorbidities and medication histories were collected from patients at both baseline and follow-up CT scans. Hyperlipidemia was recorded by elevated plasma cholesterol levels (total cholesterol >200 mg/dl) or the use of lipid-lowering therapy. Hypertension was marked in case of a systolic blood pressure >140 mmHg and/or a diastolic blood pressure >90 mmHg, or the use of antihypertensive medication verified by medical records. Smoking was defined as any tobacco use within 1 year prior to the CTA. Diabetes mellitus was diagnosed based on elevated plasma glucose levels (HbA1c ≥6.5%; fasting plasma glucose ≥126 mg/dl) or the use of antidiabetic medication or insulin therapy. Statin use was evaluated at both baseline and follow-up CT scans, defined as the use of statins at the time of these scans.

Anamnestic, anthropometric data, and CTA findings were documented using a structured reporting platform (Axis, Neumann Medical Ltd., Budapest, Hungary). The study received approval from the institutional review board and informed consent was waived (SE TUKEB 173/2016). All procedures adhered to local and federal regulations as well as the Declaration of Helsinki.

3.1.2 Coronary CTA acquisition and reconstruction protocol

All patients underwent prospectively ECG-triggered coronary CTA in accordance with SCCT guidelines (125). To control heart rate, premedication included oral metoprolol administered one hour before the CTA if the heart rate exceeded 65 beats per minute, and

intravenous metoprolol given five minutes before contrast agent injection if the heart rate exceeded 60 beats per minute. All patients received 0.8 mg of sublingual nitroglycerine prior to the CTA to enhance coronary visualization. Image acquisition was timed to diastole (75-81% of the R-R interval) or systole (37-43% of the R-R interval) based on the patient's heart rate (below or above 70 beats per minute) after premedication. The scanner settings were as follows: 270 ms rotation time, 128 x 0.625 mm collimation, tube voltage of 100-120 kVp and tube current of 200-300 mAs, adjusted for the patient's body mass index (BMI). A four-phase contrast injection protocol was utilized with 85-95 ml of contrast agent delivered at a flow rate of 4.5-5.5 ml/s (126).

3.1.3 Coronary CTA image analysis

Coronary CTA images were assessed for CAD by examining the location, morphology and stenosis severity of coronary lesions using an 18-segment coronary tree model (47). Coronary segments with a minimal diameter of 1.5 mm were evaluated. Coronary plaque was identified on CTA following the criteria established by Mahabadi et al and Achenbach et al (127, 128). Calcified plaques were defined as any discernible structure with a density of ≥130 Hounsfield units, while non-calcified plaques had a density of <130 Hounsfield units, both attributed to the vessel wall in at least two independent image planes. Baseline and follow-up images were evaluated simultaneously by the reader, who was blinded to patient characteristics, CTA dates, comorbidities and medical treatment, to detect changes in plaque composition or stenosis severity.

To quantify total CAD burden, SIS and SSS were calculated for all patients at baseline and follow-up scans. Inter-reader reproducibility of SSS and SIS had been previously assessed and published (25). CAD-RADS stenosis categories (0: 0%, 1: 1-24%, 2: 25-49%, 3: 50-69%, 4A: 70-99%, 4B: Left main >50% or three-vessel disease, 5: 100%) were also evaluated according to the CAD-RADS consensus document (129). The presence, extent, and severity of all lesions were entered into a structured reporting platform, which automatically generated CAD-RADS clinical recommendations (Axis, Neumann Medical Ltd., Budapest, Hungary) based on the reader's inputs. Different definitions of plaque progression were analyzed, including increases in SSS, SIS, or CAD-RADS category.

3.1.4 Statistical analysis

Continuous variables are presented as means with standard deviations, while categorical variables are presented as frequencies with percentages. A paired sample t-test was used to compare parameters describing coronary plaque burden between the two CTA examinations. Linear regression analysis identified predictors of annualized plaque progression. Additionally, linear mixed models were used to analyze repeated observations at non-standardized intervals. Taking into account intra-individual changes over time allowed for the simultaneous estimation of a predictor's effect on (I) the overall amount of the outcome (SSS, SIS, and CAD-RADS) and (II) the annual progression rate. This approach provides estimates on how a covariate affects both the overall outcome and its temporal changes, accounting for total plaque burden at baseline without requiring additional adjustments. Univariate linear mixed models were calculated to assess the effect of each predictor on the outcome (CAD definitions) and its annual progression. Predictors with a p-value <0.10 in either effect were included in a multivariate model. Clinical predictors of coronary plaque progression were included as predictors, with SIS, SSS, and CAD-RADS as outcomes.

Inter-observer reproducibility was also assessed in 25 patients by two observers using weighted kappa. Five plaques per stenosis category (minimal 1-24%, mild 25-49%, moderate 50-69%, severe 70-99%, and occluded 100%) were selected, including one plaque per patient. The kappa values were interpreted as follows: 0.00-0.20 poor; 0.21-0.40 fair; 0.41-0.60 moderate; 0.61-0.80 good; and 0.81-1.00 excellent agreement.

3.2 Study design for the association of quantitative plaque metrics and myocardial ischemia

3.2.1 Patient population

In our prospective, single-center study, patients with stable chest pain with CAD detected on rest coronary CTA were screened. The inclusion criteria required at least 30% stenosis in one of the main coronary arteries and excellent image quality for quantitative analysis of the entire coronary tree. Exclusion criteria included prior myocardial infarction, revascularization, heart transplantation, contraindications to regadenoson, or low image quality for quantitative coronary plaque assessment. Regadenoson stress DPCT was performed at a separate appointment. Subjects with low image quality for myocardial ischemia assessment were excluded. Patients meeting the inclusion and exclusion criteria were enrolled in the study (**Figure 11**).
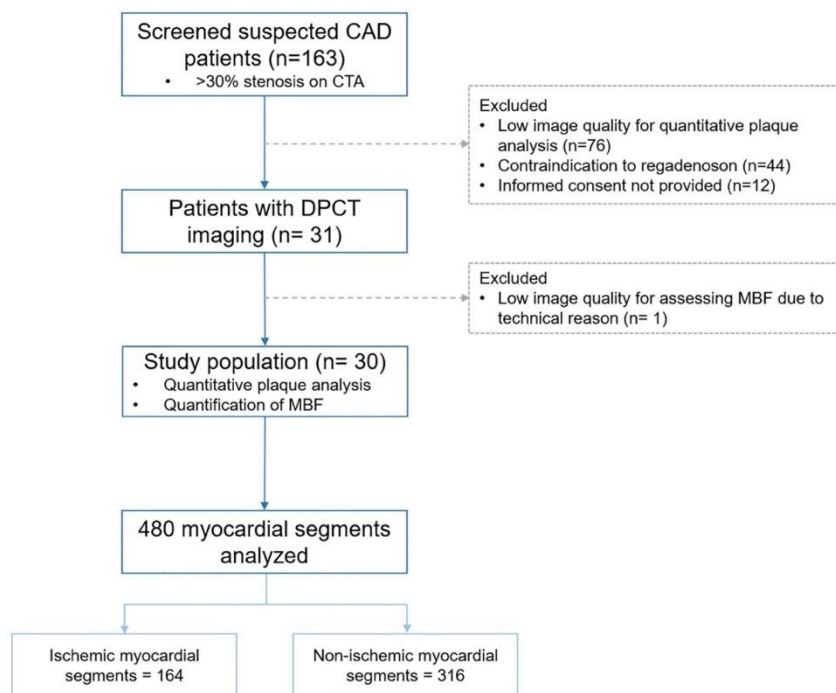
Figure 11. Flow-chart of the study.

(Source: Vattay B., et al. Front Cardiovasc Med. 2022;9:974805. CC BY 4.0)

CAD: coronary artery disease; CTA: computed tomography angiography; DPCT: dynamic perfusion computed tomography; MBF: myocardial blood flow

All patients provided written informed consent. The study received approval from the national ethical committee (National Institute of Pharmacy and Nutrition - OGYÉI/719/2017) and was conducted in accordance with the Declaration of Helsinki. Demographic data and comorbidities were collected by reviewing patients' medical records. Hypertension, hyperlipidemia, and diabetes mellitus were defined as previously described in section *3.1.1*.

3.2.2 Coronary CTA acquisition and reconstruction protocol

Coronary CTA acquisition protocol was identical to previous substudy of the thesis described at section *3.1.2*.

3.2.3 Dynamic myocardial perfusion CT protocol

The stress DPCT scan was conducted following the rest CTA at a separate appointment using the same CT scanner. A single intravenous dose of 400 µg of regadenoson (Rapiscan R, GE Healthcare) was administered to induce hyperemia. Stress imaging was performed during a single breath-hold at peak stress, one minute after the administration of regadenoson, covering 25 - 30 cardiac cycles. Patients' heart rate, oxygen saturation and blood pressure were monitored to ensure appropriate stress levels for perfusion imaging.

The contrast injection protocol included a bolus of 50 - 60 ml of contrast agent at a rate of 5 ml/s, followed by a 30 ml saline chaser. A prospective ECG-gated dynamic mode was used (with 64×1.25 mm collimation, 360-degree reconstruction, covering 8 cm), acquiring images in the systolic phase (35% of the R-R interval). Tube voltage ranged from 80 to 120 kVp, and tube current was adjusted between 100 and 250 mAs based on the patient's BMI. Images were reconstructed using hybrid iterative reconstruction (iDOSE4 level 5, Philips Healthcare, Cleveland, OH, United States) with a slice thickness of 2.0 mm and an increment of 2.0 mm.

3.2.4 Quantitative plaque analysis

Quantitative assessment of coronary plaques was conducted using dedicated software (QAngioCT Research Edition v3.1; Medis Medical Imaging Systems, Leiden, The Netherlands) on rest coronary CTA images. Coronary artery segments were delineated according to the 18-segment model recommended by SCCT guidelines (47). A single reader - blinded to patient data and myocardial perfusion parameters - analyzed all coronary vessels with a diameter greater than 1.5 mm.

The software automatically generated the coronary tree and performed initial contouring of the lumen and vessel wall. Manual corrections were applied, if necessary, in both longitudinal and cross-sectional views at 0.5 mm intervals. The reader defined the proximal and distal borders of coronary plaques for quantification. Plaque definition followed established criteria outlined in section *3.1.3*. No chronic total occlusions were observed in the study population.

Plaque composition was determined using predefined HU thresholds: LAP: -100 to 30 HU; NCP: 31 to 350 HU; CP: ≥351 HU. Volumes of total plaque, LAP, NCP, and CP were calculated. LAP burden, defined as the LAP volume divided by vessel volume and expressed as a percentage (LAP volume × 100%/vessel volume), was also calculated. Lumen area stenosis was quantified at the site of maximal luminal narrowing caused by coronary plaque. The RI was computed as the ratio of vessel wall area at the site of maximal luminal narrowing to the reference vessel wall area. HRP was defined by quantitative LAP burden >4% or a RI >1.1 (31, 71).

3.2.5 Myocardial perfusion analysis

DPCT images were analyzed using dedicated software (Intellispace Portal; Philips Healthcare, Cleveland, OH, United States). Elastic registration and temporal filtering techniques were applied to reduce motion artifacts. TAC generated in the left ventricular outflow tract served as arterial input functions for perfusion analysis. Short-axis views were generated to assess left ventricular myocardial tissue.

MBF was computed using a hybrid deconvolution method (130). Two readers independently assessed MBF in a random order, blinded to plaque data and patient characteristics. A ROI greater than 0.5 cm² was placed in each myocardial segment using a 16-segment model, excluding the apex and carefully avoiding any artifacts on short-axis images (131).

Segmental myocardial ischemia was defined as MBF < 101 ml/100 g/min based on criteria established by Pontone et al (131). Relative MBF (MBFi) for each segment was calculated as the ratio of absolute MBF to the reference MBF, defined as the 75th percentile of all MBF values for a given patient (132).

3.2.6 Integration of coronary anatomy and myocardial territories

Coronary lesions were allocated to their respective myocardial segments using a modified method based on the CORE320 trial as described by Cerci et al (133) (**Figure 12**).

Previous studies utilized vessel-based analyses to align myocardial territories with their supplying vessels. In our segment-based approach, we defined coronary artery segments supplying each of the 16 analyzed myocardial segments based on dominance and segment location relative to basal, mid-ventricular, or apical regions.

After adjudication, the total plaque volume (TPV), NCP volume, and CP volume from all relevant supplying coronary segments were aggregated for each myocardial segment. Additionally, LAP burden was calculated using the summed LAP volume and vessel volume. Summed plaque volumes, the highest degree of lumen area stenosis, and the presence of HRP (defined as LAP burden > 4% or RI > 1.1) in the supplying coronary segments were analyzed for each corresponding myocardial segment.
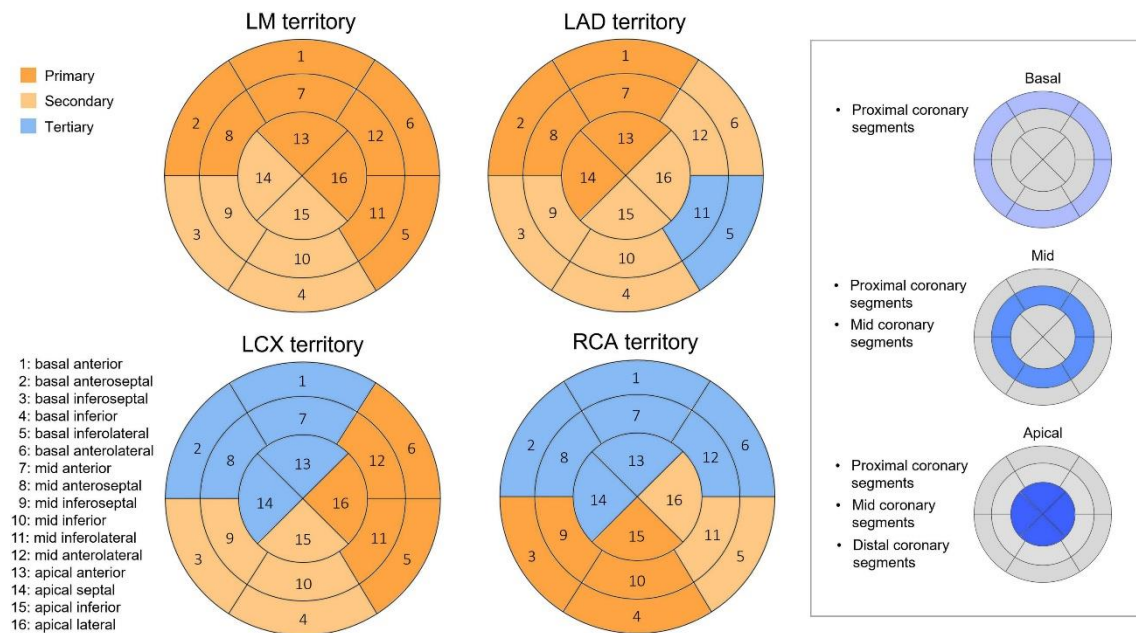
Figure 12. Integration of coronary anatomy and myocardial segments.

Vessel territories were defined based on the modified method after Cerci et al for the main coronary arteries. The following categories were determined for myocardial segments: primary: most commonly supplied segments in case of right dominance; secondary: might be supplied segments; tertiary: usually not supplied segments. In addition, lesion location was also taken into account based on coronary segments: basal myocardial segments were aligned with proximal, mid myocardial segments with proximal and mid, while apical myocardial segments with proximal, mid and distal coronary segments. *(Source: Vattay B., et al. Front Cardiovasc Med. 2022;9:974805. CC BY 4.0)*

LAD: left anterior descending; LCX: left circumflex; LM: left main; RCA: right coronary artery

3.2.7 Statistical analysis

An independent t-test was employed to compare parameters describing coronary plaque burden between ischemic and non-ischemic segments. Pearson correlation analysis was used to examine the associations between TPV, NCP volume, and CP volume.

Linear and logistic mixed models, adjusting for intra-patient clustering and clinical factors, were utilized to assess the relationships between TPV, maximal area stenosis, quantitative HRP features, and absolute MBF, relative MBF (MBFi), or myocardial ischemia (defined as MBF < 101 ml/100 g/min). The models were adjusted for established clinical risk factors of CAD and potential modifiers of ischemia, including hypertension, diabetes mellitus and statin therapy.

The intraclass correlation coefficient (ICC) for MBF was calculated using data from 160 segments of 10 randomly selected patients assessed by two readers. Additionally, the reproducibility of quantitative plaque assessment between two independent readers was evaluated based on 10 randomly selected plaques from patients. ICC values greater than 0.80 were considered indicative of good reproducibility, while values exceeding 0.90 were deemed excellent.

All statistical analyses were performed using SPSS (version 24.0) and R software (version 3.6.1). A significance level of $p < 0.05$ was used to determine statistical significance.

3.3 Study design for quantitative plaque characterization using photon-counting CT

3.3.1 Patient population

In our prospective, single-center study, consecutive patients referred for clinically indicated coronary CTA due to suspected or known CAD were screened. Inclusion criteria required (I) diagnostic image quality suitable for quantitative plaque analysis and (II) identification of discernible coronary lesions in at least one of the main coronary arteries. Exclusion criteria included (I) presence of stents or bypass grafts and (II) images affected by severe motion, breathing artifacts, beam-hardening artifacts or misalignment. The study received approval from the institutional ethics committee (IV/667–1/2022/EKU) and adhered to the principles outlined in the Helsinki Declaration. Written informed consent was obtained from all patients prior to their participation.

3.3.2 Coronary CTA acquisition and reconstruction protocol

ECG-triggered coronary CTA scans were performed using a first-generation dual-source PCCT scanner (NAEOTOM Alpha, Siemens Healthineers), following the guidelines of the SCCT (125). Scan parameters were standardized as follows: tube voltage of 120 kVp, automatic tube current modulation set to an image quality level (IQ-level) of 80, detector configuration of 144 mm × 0.4 mm, and rotation time of 0.25 s. Intravenous beta blocker was administered if the heart rate exceeded 65 beats/minute prior to the examination. Additionally, all patients received 0.8 mg of sublingual nitroglycerine if their systolic blood pressure was over 100 mmHg before the CTA scan. Depending on the heart rate and rhythm, different scan modes were utilized: high-pitch helical (TurboFlash) for heart rate below 70/min, sequential for heart rate above 70 beats/min and helical for irregular heart rhythm. Image acquisition was timed to diastole (65-85% of the R-R interval) or systole (200-400 ms) based on the heart rate (below or above 75 beats/minute). A four-phasic contrast injection protocol was implemented, administering 70-80 ml of contrast agent at a flow rate of 4.5-5.0 ml/s (126).

VMIs were reconstructed at various energy levels from 40 to 180 keV in 10-keV increments. Additionally, polychromatic images at 120 kVp (T3D) were generated as a reference standard for comparison. All reconstructed images adhered to the same parameters: 0.4 mm slice thickness with 0.4 mm increment, quantitative iterative reconstruction level set to 2, using a medium smooth kernel (Bv40) and a matrix size of 512×512.

3.3.3 Quantitative plaque analysis

Coronary atherosclerotic plaque was assessed on CTA images following the methodology established by Achenbach et al (128). Quantitative plaque analysis was conducted using dedicated semi-automated software (AutoPlaque 2.5; Cedars-Sinai Medical Center) by a single experienced reader. For each patient, the coronary lesion with the highest-grade stenosis based on visual assessment was selected and analyzed to mitigate potential intra-patient clustering effects.

The centerline of the chosen coronary artery was extracted, and the proximal and distal borders of the plaque were delineated on the T3D images. Automatic contouring of the vessel wall and lumen was performed, with manual adjustments made as necessary to avoid artifacts from metallic structures, beam-hardening, or misalignment (in sequential

scanning). Only high-quality images free from significant motion or breathing artifacts, as per exclusion criteria, were used for plaque quantification.

Segmentation masks from the T3D images were applied consistently across all VMIs to ensure uniform analysis of the same voxels (**Figure 13**). This approach minimized potential variations in contouring among different VMIs of the same patient, thereby focusing on the impact of VMI reconstructions on plaque composition while eliminating reader bias. Voxel data from the corresponding images were exported to the R environment (version 4.0.2) and analyzed using the Radiomics Image Analysis software package (RIA v.1.6.0) (134). Plaque volume calculations included CP, NCP and LAP. Plaque components were defined using two distinct methods (**Table 3**). These thresholds were employed to accurately categorize and quantify plaque components across the study cohort (135-137).

Table 3. Fixed HU thresholds commonly used for plaque quantification.

	Method 1	**Method 2**
LAP	-100 - 30 HU	<30 HU
NCP	30 - 350 HU	30 - 130 HU
CP	>350 HU	>130 HU

CP: calcified plaque; HU: Hounsfield unit; LAP: low attenuation plaque; NCP: non-calcified plaque

3.3.4 Image quality assessment

Quantitative image quality analysis was conducted for both VMI and T3D images using RadiAnt DICOM Viewer software (v2022.1.1) by a single reader. Image noise was defined as the standard deviation (SD) of attenuation values measured within a circular region of interest (ROI) of 200 mm² placed in the aortic root at the level of the left main coronary ostium (SDlumen). Circular ROIs were also positioned in the coronary lumen and adjacent pericoronary fat near the analyzed lesion to measure mean attenuation (HUlumen, HUfat). Careful attention was given to avoid artifacts and plaques while manually placing these ROIs.

ROIs were initially placed on the T3D images as the reference and then copied to the corresponding position on all reconstructed images to ensure uniform measurement of SD

and HU values across datasets. Signal-to-noise ratio (SNR) and CNR were calculated for each reconstructed dataset as follows: $SNR = HU_{lumen} / SD_{lumen}$ and $CNR = (HU_{lumen} - HU_{fat}) / SD_{lumen}$. This standardized approach enabled consistent assessment of image quality parameters across different image reconstructions.

3.3.5 Statistical analysis

We evaluated normality using Q-Q plots. Continuous variables are presented as mean and standard deviation for normally distributed data, and as medians and interquartile ranges for non-normally distributed data. Categorical parameters are described as frequencies with percentages.

To compare image quality metrics, average plaque attenuation, and plaque volumes across different monoenergetic levels, we employed one-way repeated measures analysis of variance (ANOVA) followed by post hoc comparisons. Our analysis involved two main comparisons: (1) each VMI group versus T3D images to identify significant differences among VMIs, and (2) each keV group versus the next incrementally to assess differences between consecutive VMIs. All multiple comparisons were done using pair t-tests and p values were corrected using the Bonferroni method.

Relative differences between T3D and all VMI reconstructions were calculated using the formula: $(VMI_{mean} - T3D_{mean}) / T3D_{mean} * 100\%$. All statistical analyses were conducted using R software (version 4.0.2) with the ggstatsplot (v.0.9.3) and rstatix (v0.7.0) packages. A two-sided p-value < 0.05 was considered statistically significant.
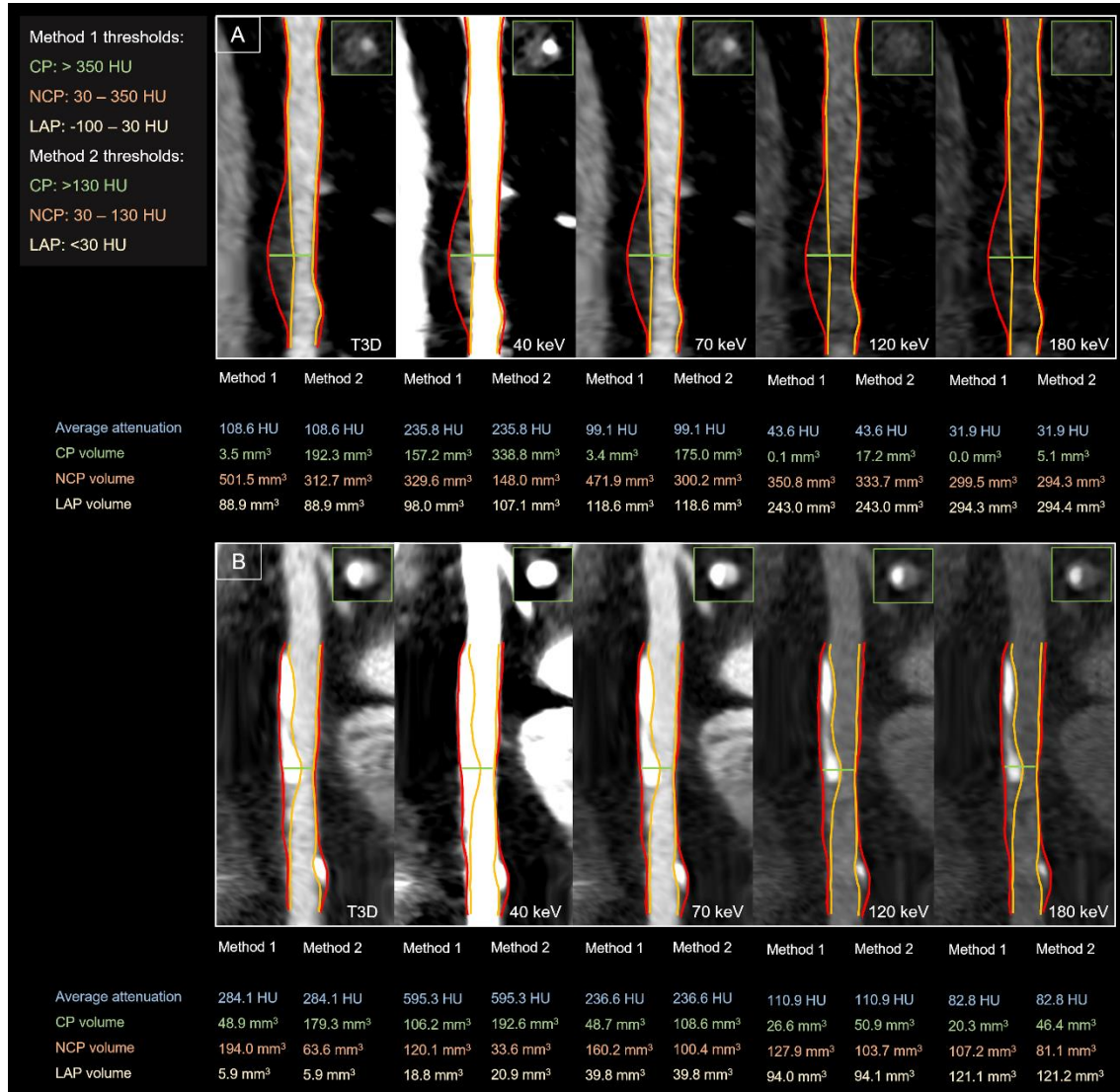
Figure 13. Representative case of quantitative plaque analysis on different reconstructions. Panel A shows a partially calcified-predominantly non-calcified plaque, panel B shows a partially calcified-predominantly calcified plaque reconstructed in T3D and different VMI reconstructions at 40, 70, 120, and 180 keV levels. Vessel wall border is depicted as red line, lumen border is shown as orange line. Cross-sectional images are also depicted at the point of the maximal narrowing of the lesion as green line. Identical window setting was applied for all represented images: window: 800; level: 250. *(Source: Vattay B., et al. Eur Radiol. 2023;33(12):8528-8539. CC BY 4.0)*

CP: calcified plaque; HU: Hounsfield unit; LAP: low-attenuation plaque; NCP: non-calcified plaque

4. RESULTS

4.1 Results of plaque progression assessment

The baseline characteristics of the 115 enrolled patients (mean age 60.1 ± 9.6 years, 27% female) are outlined in **Table 4**. The average interval between the two CTA examinations was 2.6 ± 1.1 years. A total of 1763 coronary artery segments were assessed at both time points. The mean effective radiation dose was 5.07 mSv at baseline and 5.09 mSv at follow-up (p = 0.822).

Table 4. Baseline characteristics of study population.

Patient data	Study population (n=115)
Age, years	60.1 ± 9.6
BMI, kg/m^2	28.4 ± 4.2
Female gender, n (%)	27 (23.5)
Cardiovascular risk factors at baseline, n (%)	
Hypertension	87 (75.7)
Diabetes mellitus	15 (13.0)
Dyslipidemia	63 (54.8)
Smoking	13 (11.3)
Family history of premature CAD	29 (25.2)
Statin use	47 (35.7)

BMI: body mass index, CAD: coronary artery disease

4.1.1 Characteristics of coronary plaque progression

A total of 105 out of 115 patients (91.3%) exhibited CAD at baseline. The remaining 10 patients (8.7%) initially had no plaque, but developed minimal stenosis on follow-up (CAD-RADS 1). No progression of CAD was detected in 54 patients (46.7%) and plaque regression was not observed in this study group. In terms of plaque numbers and types, we detected 397 plaques at baseline and 449 plaques at follow-up in the study population. Specifically, there were 142 calcified plaques at baseline compared to 154 at follow-up, 175 partially calcified plaques versus 203, and 80 non-calcified plaques versus 92, respectively.

Comparing the first and second coronary CTA images, significant increases were observed in SSS, SIS and CAD-RADS on the follow-up images: SSS: 4.63 ± 4.06 vs. 5.67 ± 5.10, p< 0.001; SIS: 3.43 ± 2.53 vs. 3.89 ± 2.65, p< 0.001; CAD-RADS 0: 8.7%

vs. 0.0%, 1: 44.3% vs. 40.9%, 2: 34.8% vs. 40.9%, 3: 7.0% vs. 9.6%, 4: 3.5% vs. 6.1%, 5: 1.7% vs. 2.6%, p< 0.001 at baseline and follow-up, respectively (**Table 5**).

The average annual progression rates were 0.41 ± 0.62 for SSS and 0.18 ± 0.34 for SIS. Progression in SSS, SIS, and CAD-RADS was observed in 53.0%, 29.6% and 28.7% of all cases, respectively (**Figure 14**). Notably, among patients without CAD-RADS progression during follow-up, 34.1% and 17.1% experienced progression in SSS and SIS, respectively (**Figure 15**). Among those who progressed based on SSS, only 54% showed changes in CAD-RADS scores. This could potentially lead to a false impression that CAD had not progressed over time despite novel plaque development only reflected by SSS changes.

Excellent agreement across stenosis categories was found between two observers who evaluated 25 plaques (5 from each stenosis category) (weighted kappa = 0.903).

Table 5. CAD features of the enrolled patient population.

	1. scan (n=115)	2. scan (n=115)	p value
SSS	**4.63 ± 4.06**	**5.67 ± 5.10**	**<0.001**
SIS	**3.43 ± 2.53**	**3.89 ± 2.65**	**<0.001**
CAD-RADS severity, n (%)			**<0.001**
0	10 (8.7)	0 (0.0)	
1	51 (44.3)	47 (40.9)	
2	40 (34.8)	47 (40.9)	
3	8 (7.0)	11 (9.6)	
4	4 (3.5)	7 (6.1)	
5	2 (1.7)	3 (2.6)	

CAD-RADS: coronary artery disease reporting and data system, SIS: segment involvement score, SSS: segment stenosis score

Figure 14. Sankey diagram depicting coronary plaque progression based on SSS and CAD-RADS.

Patient-based progression of coronary atherosclerosis using SSS and CAD-RADS severity is depicted on the Sankey diagram. This type of flow diagram depicts the number of patients with progression during follow-up, where the width of the arrow is proportional to the flow rate (number of patients). No progression was found in 54 patients' SSS and in 82 patients' CAD-RADS during the follow-up period (marked with light blue). The number of patients with increase in SSS and CAD-RADS are depicted at 1, 2 and ≥ 3 years based on serial CTA imaging (orange). CAD-RADS substantially underestimated changes in disease severity and extent of CAD. During the follow-up period we could identify three patients with SSS increase at 1 year (rapid progression of CAD), whereas most patients progressed later at 3 or more years. *(Source: Szilveszter B., Vattay B., et al. Eur Heart J Cardiovas Imaging. 2022;23(11):1530-1539. CC BY 4.0)*
CAD-RADS: coronary artery disease reporting and data system; SSS: segment stenosis score
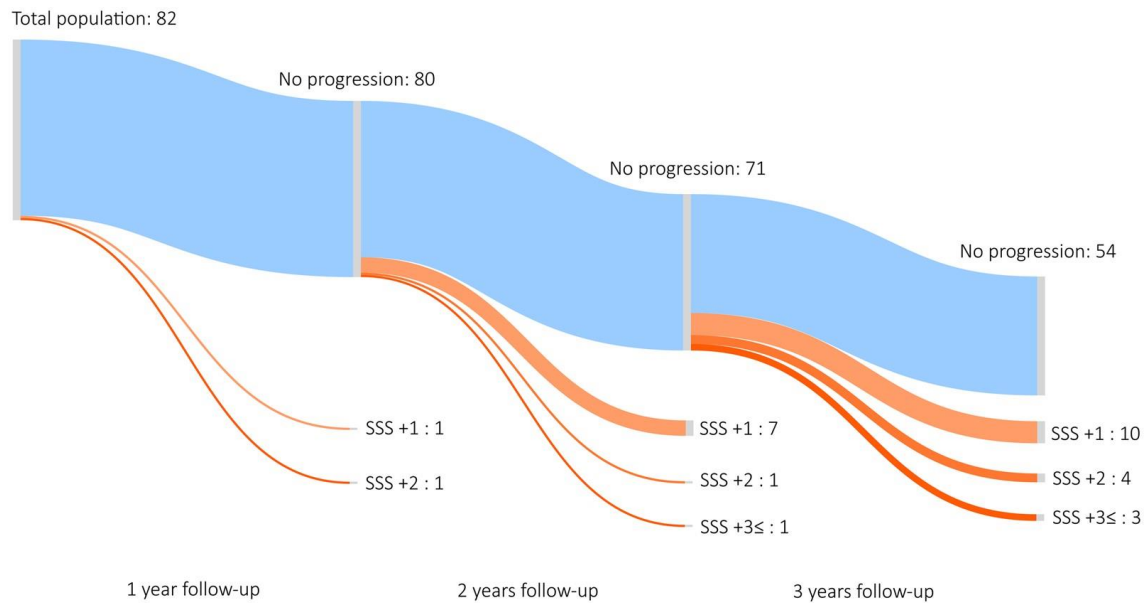
Figure 15. Sankey diagram depicting coronary plaque progression based on SSS among those with no progression in CAD-RADS classification for lesion severity.
A total of 82 patients in our study did not progress based on CAD-RADS severity, although a large proportion of patients demonstrated coronary plaque progression based on SSS. Increasing number of patients developed higher stenosis scores during follow-up period: 2 patients had higher SSS at 1 year, 9 patients had higher SSS at 2 years, and 17 patients had higher SSS at 3 years or more. Four patients had substantial increase in SSS (three or more) despite no changes in CAD-RADS classification. *(Source: Szilveszter B., Vattay B., et al. Eur Heart J Cardiovasc Imaging. 2022;23(11):1530-1539. CC BY 4.0) CAD-RADS: coronary artery disease reporting and data system; SSS: segment stenosis score*

4.1.2 Predictors of coronary plaque progression

Linear regression models were performed to identify predictors of plaque progression, defined as the annualized progression of SSS or SIS. Age was found to be associated with plaque progression based on SSS [$\beta = 0.013$, confidence interval (CI) 0.01-0.024, $p = 0.034$], but no association was observed with SIS progression ($p = 0.784$). Notably, none of the other predictors showed any significant association with the annualized progression rate of SSS, SIS or CAD-RADS (all $p > 0.05$). However, this approach does not account for temporal changes in covariates over time or consider the baseline values. Therefore, we also analyzed our data using linear mixed models.

4.1.3 Analysis of coronary plaque progression and progression rate using linear mixed models

Univariate linear mixed models revealed that age and gender influence the values of SSS and SIS in our population, while diabetes increased the annual progression rate of SSS by 0.34 per year [CI 0.01 - 0.66; p = 0.036] (**Table 6**). Multivariate analysis showed that smokers had a significantly increased annual progression rate of SSS by 0.37 per year [CI 0.07 - 0.67, p = 0.017] and a higher total extent of CAD as described by SIS compared with non-smokers [β = 0.77, CI 0.06 - 1.50, p = 0.034]. Diabetes mellitus increased the annual progression rate of SSS by 0.38 per year [CI 0.07 - 0.69, p = 0.016]. Age and gender affected the total amount of SSS and SIS (p < 0.001). Female gender was associated with an average of 2.86 lower SSS [CI -4.52 - (-1.20), p < 0.001] and 1.68 lower SIS [CI -2.65 - (-0.71), p = 0.001] compared to male gender. Notably, CAD-RADS was not influenced by any cardiovascular risk factor (all p ≥ 0.05). Detailed results of the multivariate analysis are summarized in **Table 7.**

Table 6. Linear mixed models to define the predictors of plaque progression (univariate).

| Predictors | SSS Univariate model | | | | | | SIS Univariate model | | | | | |
| | Effect on SSS | | | Effect on annual progression | | | Effect on SIS | | | Effect on annual progression | | |
	β	95% CI	p	β	95% CI	p	β	95% CI	p	β	95% CI	p
Age	**0.11**	**0.04; 0.19**	**0.004**	**0.01**	**0.00; 0.02**	**0.035**	**0.09**	**0.05; 0.14**	**<0.001**	0.00	0.00; 0.01	0.701
Female gender	**-2.31**	**-4.04; -0.58**	**0.010**	-0.08	-0.34; 0.17	0.516	**-1.38**	**-2.44; -0.31**	**0.013**	-0.01	-0.15; 0.13	0.898
BMI	-0.02	-0.13; 0.08	0.651	-0.01	-0.03; 0.02	0.609	0.04	-0.02; 0.10	0.182	-0.01	-0.02; 0.01	0.254
Hypertension	0.15	-1.22; 1.51	0.834	0.19	-0.06; 0.44	0.136	0.28	-0.51; 1.07	0.479	0.02	-0.11; 0.16	0.740
Diabetes mellitus	1.39	-0.84; 3.61	0.225	**0.34**	**0.02; 0.66**	**0.036**	0.81	-0.56; 2.18	0.251	0.06	-0.11; 0.24	0.473
Dyslipidemia	0.64	-0.47; 1.75	0.264	-0.12	-0.34; 0.09	0.269	0.28	-0.37; 0.93	0.390	-0.05	-0.17; 0.07	0.427
Smoking	0.67	-0.55; 1.88	0.281	0.33	0.00; 0.65	0.050	0.64	-0.08; 1.37	0.083	0.09	-0.08; 0.26	0.286
Statin use	-0.11	-0.92; 0.70	0.785	0.15	-0.08; 0.38	0.203	-0.16	-0.61; 0.30	0.498	0.05	-0.07; 0.18	0.413

BMI: body mass index; CI: confidence interval; SSS: segment stenosis score; SIS: segment involvement score

Table 6. Linear mixed models to define the predictors of plaque progression (univariate). *Continued.*

Predictors	CAD-RADS							
	Univariate model							
	Effect on CAD-RADS				Effect on annual progression			
	β	95% CI		p	β	95% CI		p
Age	0.01	0.00; 0.03		0.140	0.00	-0.01; 0.00		0.510
Female gender	-0.34	-0.76; 0.07		0.110	0.02	-0.07; 0.10		0.713
BMI	0.00	-0.03; 0.04		0.901	0.00	-0.01; 0.01		0.730
Hypertension	-0.12	-0.48; 0.25		0.523	0.05	-0.03; 0.13		0.229
Diabetes mellitus	0.17	-0.36; 0.70		0.527	0.05	-0.06; 0.15		0.377
Dyslipidemia	0.13	-0.18; 0.44		0.412	-0.06	-0.14; 0.01		0.083
Smoking	0.06	-0.38; 0.49		0.794	0.05	-0.05; 0.15		0.311
Statin use	0.12	-0.15; 0.38		0.378	-0.05	-0.12; 0.03		0.241

BMI: body mass index; CAD-RADS: coronary artery disease reporting and data system; CI: confidence interval

Table 7. Multivariate analysis of predictors of plaque progression using linear mixed models.

Predictors	SSS						SIS					
	Effect on SSS			Effect on annual progression			Effect on SIS			Effect on annual progression		
	β	95% CI	p	β	95% CI	p	β	95% CI	p	β	95% CI	p
Age	**0.12**	**0.05; 0.20**	**0.001**	**0.01**	**0.01; 0.03**	**0.013**	**0.10**	**0.06; 0.15**	**<0.001**	0.00	0.00; 0.01	0.369
Female gender	**-2.86**	**-4.52; -1.20**	**<0.001**	-0.23	-0.47; 0.01	0.06	**-1.68**	**-2.65; -0.71**	**0.001**	-0.03	-0.17; 0.11	0.646
Smoking	1.16	-0.03; 2.35	0.06	**0.37**	**0.07; 0.67**	**0.017**	**0.77**	**0.06; 1.50**	**0.034**	0.10	-0.07; 0.27	0.263
Diabetes mellitus	1.27	-0.86; 3.40	0.24	**0.38**	**0.07; 0.69**	**0.016**						

BMI: body mass index; CI: confidence interval; SSS: segment stenosis score; SIS: segment involvement score

Table 7. Multivariate analysis of predictors of plaque progression using linear mixed models. *Continued.*

Predictors	CAD-RADS					
	Effect on CAD-RADS			Effect on annual progression		
	β	95% CI	p	β	95% CI	p
Age			NS			NS
Female gender			NS			NS
Smoking			NS			NS

BMI: body mass index; CAD-RADS: coronary artery disease reporting and data system; CI: confidence interval

4.2 Results of the association of quantitative plaque metrics and myocardial ischemia

4.2.1 Patient characteristics

The baseline characteristics of the 30 analyzed patients (mean age 60.9 ± 8.3 years, 26.7% female, mean BMI 28.9 ± 3.8 kg/m²) are summarized in **Table 8**. Common comorbidities included hypertension (76.7%) and dyslipidemia (76.7%). The average interval between the two examinations was 13.0 ± 8.6 days. The mean effective radiation dose was 4.4 ± 1.1 mSv for rest CTA and 8.9 ± 4.0 mSv for DPCT. Quantitative analysis was performed on 496 coronary artery segments and 480 myocardial segments. The ICC between readers was 0.96 for MBF and 0.93 for TPV.

Table 8. Patient characteristics and concomitant medical therapy of study population.

	Patient population (n=30)
Age, years	60.9 ± 8.3
Male gender, n (%)	22 (73.3)
BMI, kg/m^2	28.9 ± 3.8
Hypertension, n (%)	23 (76.7)
Diabetes mellitus, n (%)	2 (6.7)
Dyslipidemia, n (%)	23 (76.7)
Smoking, n (%)	16 (53.3)
Cerebrovascular disease, n (%)	1 (3.3)
Peripheral artery disease, n (%)	3 (10.0)
Family history of premature CAD, n (%)	9 (30.0)
Oral anticoagulant therapy, n (%)	6 (20.0)
Statin therapy, n (%)	16 (53.3)
ACE-I / ARB therapy, n (%)	18 (60.0)
Beta-blocker therapy, n (%)	15 (50.0)

ACE-I: angiotensin-converting-enzyme inhibitor; ARB: angiotensin receptor blocker; BMI: body mass index; CAD: coronary artery disease

4.2.2 Quantitative plaque characteristics and myocardial ischemia

Total plaque volume, NCP volume, and CP volume differed significantly between ischemic and non-ischemic myocardial segments, measuring 120.5 ± 119.5 mm³ vs. 84.6 ± 82.2 mm³ (p = 0.001), 62.3 ± 59.5 mm³ vs. 51.4 ± 54.9 mm³ (p = 0.045), and 58.3 ± 91.8 mm³ vs. 33.3 ± 50.6 mm³ (p = 0.001), respectively (**Table 9**). The median and interquartile range (IQR) of plaque volumes for ischemic and non-ischemic myocardial segments were: TPV: 82.9 (31.1 - 179.6) vs. 68.7 (25.8 - 114.7) mm³; NCP volume: 46.1

(24.3 - 93.7) vs. 31.6 (12.4 - 73.8) mm³; CP volume: 15.9 (0.1 - 78.2) vs. 17.3 (2.2 - 46.1) mm³. **Figure 16** shows box plots of quantitative plaque volumes in coronary segments supplying ischemic and non-ischemic myocardial segments. On a patient level, the average maximal lumen area stenosis of the worst lesion was $54.7 \pm 15.9\%$. On a segmental level, the average maximal lumen area stenosis was $37.2 \pm 22.7\%$ for ischemic segments and $33.5 \pm 20.7\%$ for non-ischemic segments ($p = 0.072$). HRP was present in 21.3% of ischemic and 19.0% of non-ischemic territories ($p = 0.539$). The number of ischemic segments was 164 out of 480 (34.2%). The median MBF was 111 ml/100 g/min, while the median relative MBF (MBFi) was 0.94. TPV strongly correlated with NCP volume ($r = 0.73$, $p < 0.001$) and CP volume ($r = 0.83$, $p < 0.001$); therefore, TPV was included in the multivariate prediction models to avoid multicollinearity.

Table 9. Plaque features in ischemic and non-ischemic myocardial segments.

	Ischemic myocardial segments (n=164)	Non-ischemic myocardial segments (n=316)	p value
Total plaque volume, mm^3	**120.5 ± 119.5**	**84.6 ± 82.2**	**0.001**
NCP volume, mm^3	**62.3 ± 59.5**	**51.4 ± 54.9**	**0.045**
CP volume, mm^3	**58.3 ± 91.8**	**33.3 ± 50.6**	**0.001**
High-risk plaque, n (%)	35 (21.3)	60 (19.0)	0.539
Lumen area stenosis, %	37.2 ± 22.7	33.5 ± 20.7	0.072

CP: calcified plaque; NCP: non-calcified plaque
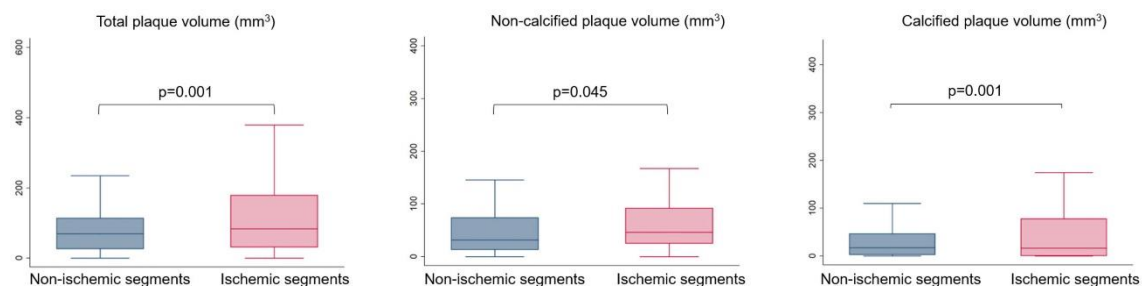
Figure 16. Box plots showing the distribution of total, NC and CP volumes related to ischemic and non-ischemic myocardial segments based on DPCT. *(Source: Vattay B., et al. Front Cardiovasc Med. 2022;9:974805. CC BY 4.0)*

CP: calcified plaque; DPCT: dynamic perfusion computed tomography; MBF, myocardial blood flow; NCP: non-calcified plaque volume

4.2.3 Predictors of myocardial blood flow

Using linear mixed models, univariate analysis showed that total plaque volume predicted both absolute and relative MBF values (**Table 10**). Clinical risk factors (such as hypertension, diabetes mellitus and statin use), HRP characteristics and stenosis severity were not associated with impaired myocardial perfusion based on MBF and MBFi. On multivariate analysis, an increase in TPV led to reduced absolute and relative MBF values, even after adjusting for clinical risk factors, lumen area stenosis and HRP features: per 10 mm³ increase, β = -0.035, $p < 0.01$ for MBF and β = -0.0002, $p < 0.01$ for MBFi. Notably, lumen area stenosis and quantitative HRP features were not linked to absolute or relative MBF values (all $p > 0.05$)

On univariate logistic regression, TPV and lumen area stenosis were significant predictors of myocardial ischemia based on MBF < 101 ml/100 g/min (**Table 11**). After adjusting for predefined clinical risk factors, stenosis severity and HRP, an increase in TPV was independently associated with myocardial ischemia: OR = 1.01, $p = 0.033$ (per 10 mm³). However, in multivariate analysis, HRP features and lumen area stenosis were not linked to ischemia (both $p > 0.05$).

Table 10. Quantitative segmental analysis of myocardial perfusion: predictors of absolute and relative myocardial blood flow.

Predictors	Absolute MBF		Relative MBF	
	Univariate model		Univariate model	
	β [95% CI]	p value	β [95% CI]	p value
TPV, (/10 mm^3)	**-0.025** **[-0.043; - 0.007]**	**0.006**	**-0.0002** **[-0.0003; - 0.0001]**	**0.004**
NCPV, (/10 mm^3)	-0.025 [-0.053; 0.003]	0.079	-0.0002 [-0.0004; 0.0000]	0.077
CPV, (/10 mm^3)	**-0.046** **[-0.078; - 0.014]**	**0.005**	**-0.0002** **[-0.0004; - 0.00006]**	**0.008**
Remodeling index	1.934 [-2.427; 6.295]	0.384	0.003 [-0.029; 0.036]	0.838
High-risk plaque	1.952 [-1.767; 5.672]	0.303	0.018 [-0.009; 0.045]	0.191
Area stenosis	-4.479 [-12.008; 3.050]	0.243	-0.042 [-0.093; 0.009]	0.108
Age, years	-0.172 [-1.208; 0.864]	0.736	0.0006 [-0.001; 0.002]	0.463
BMI, kg/m^2	-0.791 [-3.037; 1.455]	0.477	**0.004** **[0.0007; 0.007]**	**0.017**
Hypertension	-1.482 [-21.491; 18.527]	0.881	0.010 [-0.019; 0.039]	0.491
Diabetes mellitus	1.542 [-32.393; 35.478]	0.926	0.018 [-0.031; 0.068]	0.456
Smoking	1.536 [-15.424; 18.496]	0.854	0.013 [-0.011; 0.038]	0.274
Statin therapy	-3.201 [-20.127; 13.724]	0.701	-0.005 [-0.030; 0.020]	0.658

BMI: body mass index; CI: confidence interval; CPV: calcified plaque volume; DPCT: dynamic perfusion computed tomography; HRP: high-risk plaque; NCPV: non-calcified plaque volume; OR: odds ratio; TPV: total plaque volume

Table 11. Predictors of myocardial ischemia detected by DPCT using a clinical threshold (MBF < 101ml/100 g/min).

Predictors	Myocardial ischemia detected by DPCT		
	Univariate model		
	OR	95% CI	p value
TPV, (/10 mm^3)	**1.01**	**1.002; 1.012**	**0.003**
NCPV, (/10 mm^3)	**1.01**	**1.004; 1.018**	**0.002**
CPV, (/10 mm^3)	1.01	0.997; 1.015	0.172
Remodeling index	1.14	0.422; 3.059	0.801
HRP	0.79	0.333; 1.890	0.601
Area stenosis	**8.05**	**1.340; 48.333**	**0.023**
Age, years	1.03	0.839; 1.268	0.770
BMI, kg/m^2	1.26	0.787; 2.019	0.335
Hypertension	2.86	0.046; 177.116	0.617
Diabetes mellitus	1.74	0.003; 883.279	0.861
Smoking	0.96	0.031; 29.434	0.982
Statin therapy	4.06	0.108; 152.174	0.448

BMI: body mass index; CI: confidence interval; CPV: calcified plaque volume; DPCT: dynamic perfusion computed tomography; HRP: high-risk plaque; NCPV: non-calcified plaque volume; OR: odds ratio; TPV: total plaque volume

4.3 Results of quantitative plaque characterization using photon-counting CT

Patients with suspected or known CAD who underwent coronary CTA on our novel PCCT scanner were screened in our prospective single center study. Between April 2022 and June 2022, a total of 158 patients were screened. We excluded 22 patients due to inadequate image quality for plaque quantification and 85 patients without CAD. Consequently, 51 plaques from 51 patients were included in the analyses. The mean age was 65.1 ± 11.9 years, with 68.6% being male. Common comorbidities included hypertension (80.4%), diabetes mellitus (27.5%), and dyslipidemia (52.9%). The average TPV of the analyzed lesions was 270.2 ± 208.7 mm³ on T3D images. The mean effective radiation dose was 5.2 ± 4.3 mSv. Baseline demographic data and CT scan parameters are summarized in **Table 12**.

Table 12. Patient characteristics and imaging parameters.

Demographic data	Patient population (n=51)
Age, years	65.1 ± 11.9
Male gender	35 (68.6%)
BMI, kg/m^2	28.8 ± 4.7
Hypertension	41 (80%)
Diabetes mellitus	14 (28%)
Dyslipidemia	27 (53%)
Family history of premature CAD	8 (16%)
Smoking	11 (22%)
CT scan parameters	
Agatston score	444 ± 619
Total plaque volume, mm^3	270 ± 208
DLP, mGy cm	374 ± 309
Effective dose, mSv	5.2 ± 4.3

BMI: body mass index; CAD: coronary artery disease; CT: computed tomography; DLP: dose length product

4.3.1 Quantitative image quality of different VMI reconstructions

The mean attenuation of the analyzed plaques was 299 ± 209 HU on T3D images. The average plaque attenuation showed a significant graded decrease with increasing keV levels, ranging from 723 ± 501 HU at 40 keV to 120 ± 112 HU at 180 keV (p < 0.0001 for all comparisons). All VMIs demonstrated significant difference compared to T3D,

except for the 70 keV images (303 ± 225 HU, p = 0.15) (**Figure 17A; Table 13**). Image noise (SD of mean attenuation) also decreased with increasing keV levels, from 72 ± 12 HU at 40 keV to 33 ± 6 HU at 180 keV. However, significant difference in image noise between adjacent keV levels were not consistently observed. Images reconstructed at 80 keV showed similar image noise compared to T3D images (35 ± 5 HU vs. 35 ± 5 HU, respectively; p = 0.74) (**Figure 17B**). Trends for CNR and SNR were similar to those for mean attenuation. CNR was highest at 40 keV (22.1 ± 5.6) and lowest at 180 keV (5.3 ± 1.6), with each value significantly different from the adjacent keV level. Similarly, SNR was highest at 40 keV (20.0 ± 5.5) and lowest at 180 keV (3.3 ± 1.2) with each value significantly different from the adjacent keV level. T3D images yielded similar image quality based on CNR and SNR compared to 70 keV VMI reconstructions (CNR: 15.5 ± 3.7 vs. 15.8 ± 3.5, p = 0.32; SNR: 13.1 ± 3.6 vs. 13.2 ± 3.2, p = 0.69, respectively) (**Figure 17C and 17D**).
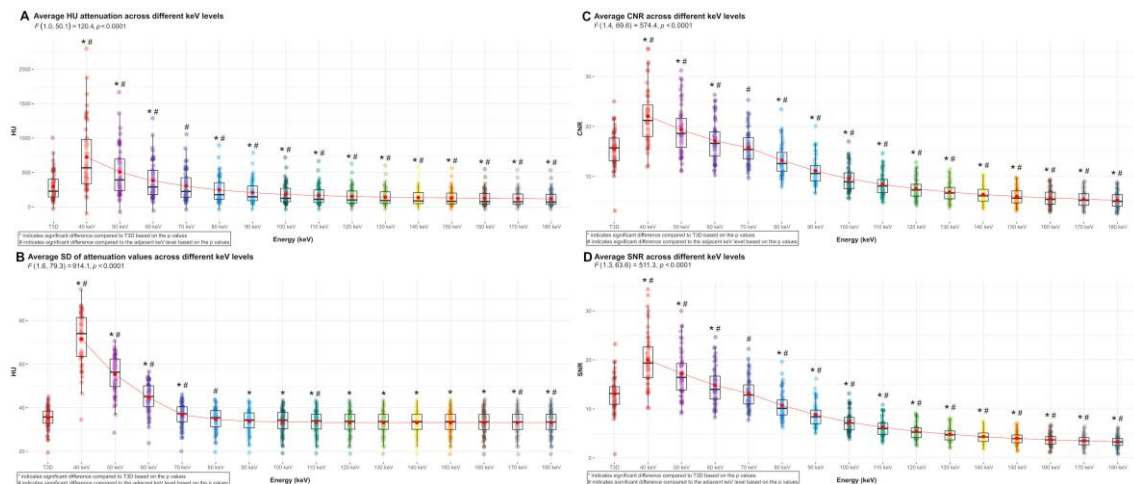
Figure 17. Box plots depicting the distribution of plaque attenuation and image quality parameters in T3D images and different VMI energy levels.

Panel **A:** distribution of HU attenuation values. Panel **B:** distribution of image noise (SD). Panel **C:** distribution of CNR. Panel **D:** distribution of SNR. *(Source: Vattay B., et al. Eur Radiol. 2023;33(12):8528-8539. CC BY 4.0)*

CNR: contrast-to-noise ratio; HU: Hounsfield unit; SD: standard deviation; SNR: signal-to-noise ratio; VMI: virtual monoenergetic image

Table 13. Mean attenuation and image quality values across different reconstructions.

VMI level (keV)	Attenuation (HU)		Image noise (SD)		CNR		SNR	
	Mean	SD	Mean	SD	Mean	SD	Mean	SD
T3D	299	209	35	5	15.5	3.7	13.1	3.6
40	723	501	72	12	22.1	5.6	20.0	5.5
50	509	361	55	9	19.4	4.9	17.2	4.7
60	382	277	45	7	17.2	4.0	14.8	3.8
70	303	225	37	6	15.8	3.5	13.2	3.2
80	247	190	35	5	13.2	3.2	10.7	2.8
90	210	167	34	5	11.1	2.9	8.8	2.4
100	184	151	34	6	9.5	2.5	7.3	2.1
110	167	140	33	6	8.4	2.3	6.3	1.8
120	154	132	33	6	7.6	2.1	5.4	1.6
130	144	127	33	6	6.9	1.9	4.8	1.5
140	137	122	33	6	6.4	1.8	4.4	1.4
150	131	119	33	6	6.0	1.8	4.0	1.3
160	127	116	33	6	5.7	1.7	3.7	1.3
170	123	114	33	6	5.5	1.7	3.5	1.2
180	120	112	33	6	5.3	1.6	3.3	1.2

CNR: contrast-to-noise ratio; HU: Hounsfield unit; SD: standard deviation; SNR: signal-to-noise ratio; VMI: virtual monoenergetic image

4.3.2 Plaque volume changes on different VMI reconstructions

We applied two threshold settings (method 1 and 2) for plaque quantification as described above in section *3.3.3.* (**Table 3**). Using method 1, the mean NCP volume was 161.0 ± 126.3 mm^3 on T3D images. The average NCP volume increased up to 70 keV and then decreased with each subsequent increment in VMI energy level. However, a significant difference in NCP volume between keV levels was not observed at every step. The lowest value was found using 40 keV (96.9 ± 86.8 mm^3), while the highest was seen using 70 keV (152.8 ± 122.0 mm^3). Mean NCP volume measured on 100 - 180 keV reconstructions did not differ significantly from T3D images ($p > 0.05$ for all) (**Figure 18A**). The average CP volume showed a significant graded decrease with increasing keV levels, from 138.7 ± 126.4 mm^3 at 40 keV to 38.5 ± 64.6 mm^3 at 180 keV ($p < 0.05$ for all). An increasing LAP volume was observed with each increment in keV level, showing a significant difference between each step (from 22.8 ± 24.9 mm^3 at 40 keV to 96.0 ± 76.3 mm^3 at 180 keV; $p < 0.0001$ for all) (**Figure 18B**). Mean LAP volumes differed

significantly between T3D and VMI reconstructions, except for the 50 keV images (28.0 ± 30.8 mm^3 and 28.6 ± 30.1 mm^3, respectively, p = 0.63) (**Figure 18C**) (**Table 14**). Method 2 yielded similar findings for plaque volume assessment. The mean NCP volume initially increased up to 100 keV and then decreased with higher keV levels, with no significant differences between each adjacent keV level. The average NCP volume on T3D was comparable to those at 70 and 140 - 180 keV energy levels (p > 0.05 for all) (**Figure 19A**). Similarly, the mean CP volume showed a decreasing trend with significant differences between each adjacent keV level (p < 0.01 for all). Mean CP volumes measured on each VMI reconstruction differed significantly from the reference T3D images (p < 0.001 for all) (**Figure 19B**). Additionally, the LAP volume increased with higher keV levels, with significant difference between each adjacent VMI (p < 0.05 for all). For LAP volume measurement, all VMIs showed significant differences compared to T3D, except for 40 keV images (p = 0.65) (**Figure 19C**) (**Table 15).**

4.3.3 Relative difference between standard and VMI reconstructions

The relative difference in attenuation and image quality parameters between the reference standard T3D and VMI reconstructions are summarized in **Table 16**. For plaque volumes using thresholds from method 1 for plaque characterization, the largest difference for CP and NCP volumes were observed on 40 keV images compared to T3D, with relative differences of 70.8% and -39.8%, respectively (p < 0.0001), The smallest relative differences were found using 70 keV images, with 0.9% and -5.1% difference, respectively (p < 0.0001). The mean LAP volume showed the largest discrepancy on 180 keV reconstruction, with 242.5% relative difference (p < 0.0001) and the smallest on 50 keV images, with a 1,9% difference (p = 0.63) (**Table 17**).

Using method 2 for plaque quantification, the greatest difference in CP volume was between 180 keV and T3D, with a relative difference of -48.9% (p < 0.0001). The lowest relative difference of CP volume was on 70 keV images (-4.0%, p < 0.001). For NCP volume compared to T3D, the greatest and smallest differences were found using 40 keV (-65.6%, p < 0.0001) and 70 keV (-1.5%, p = 0.54), respectively. The largest relative difference for LAP volume was seen on 180 keV images (243.3%, p < 0.0001), while the smallest on 40 keV images (-1.9%, p = 0.65) (**Table 18**).

Figure 18. Box plots depicting the distribution of plaque volumes (method 1) in T3D images and different VMI energy levels.

Panel **A**: distribution of NCP volume. Panel **B**: distribution of CP volume. Panel **C**: distribution of LAP volume. *(Source: Vattay B., et al. Eur Radiol. 2023;33(12):8528-8539. CC BY 4.0)*

CP: calcified plaque; HU: Hounsfield unit; LAP: low-attenuation non-calcified plaque; NCP: non-calcified plaque; VMI: virtual monoenergetic image

Table 14. Mean plaque volumes and their proportion to TPV (%) across different reconstructions method 1 thresholds for plaque characterization.

VMI keV	CP volume (>350 HU)			NCP volume (31 - 350 HU)			LAP volume (-100 - 30 HU)		
	Mean mm³	SD mm³	Mean/ TPV ratio (%)	Mean mm³	SD mm³	Mean/ TPV ratio (%)	Mean mm³	SD mm³	Mean/ TPV ratio (%)
T3D	81.2	110.1	30.0	161.0	126.3	59.6	28.0	30.8	10.4
40	138.7	126.4	51.3	96.9	86.8	35.9	22.8	24.9	8.4
50	111.1	121.5	41.1	128.3	106.9	47.5	28.6	30.1	10.6
60	88.2	113.3	32.6	149.9	120.1	55.5	31.8	32.9	11.8
70	81.9	111.4	30.3	152.8	122.0	56.6	35.5	35.0	13.1
80	75.9	105.1	28.1	149.3	120.7	55.3	45.0	41.4	16.7
90	67.0	95.6	24.8	149.1	123.0	55.2	54.1	47.6	20.0
100	58.9	87.1	21.8	148.8	122.6	55.1	62.5	53.3	23.1
110	53.0	81.0	19.6	147.2	120.9	54.5	69.9	58.4	25.9
120	48.8	76.5	18.1	145.2	118.9	53.7	76.0	62.7	28.1
130	45.9	73.1	17.0	143.0	117.1	52.9	81.1	66.3	30.0
140	43.6	70.4	16.1	141.0	115.5	52.2	85.4	69.3	31.6
150	41.9	68.5	15.5	139.2	114.3	51.5	88.9	71.5	32.9
160	40.5	66.9	15.0	137.7	113.3	51.0	91.8	73.5	34.0
170	39.4	65.6	14.6	136.4	112.6	50.5	94.1	75.0	34.8
180	38.5	64.6	14.3	135.4	111.9	50.1	96.0	76.3	35.5

CP: calcified plaque; HU: Hounsfield unit; LAP: low-attenuation plaque; NCP: non-calcified plaque; SD: standard deviation; TPV: total plaque volume on T3D images; VMI: virtual monoenergetic image
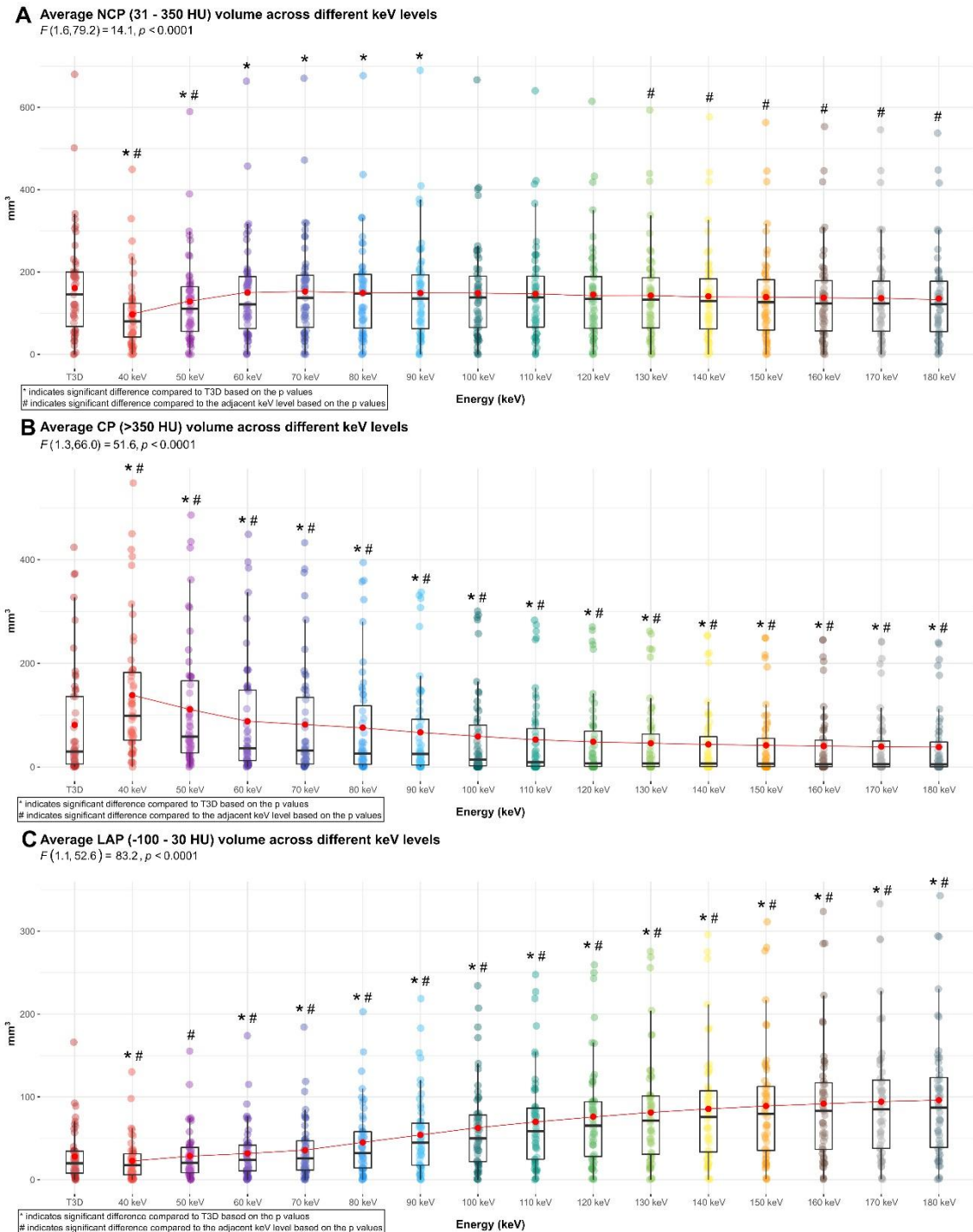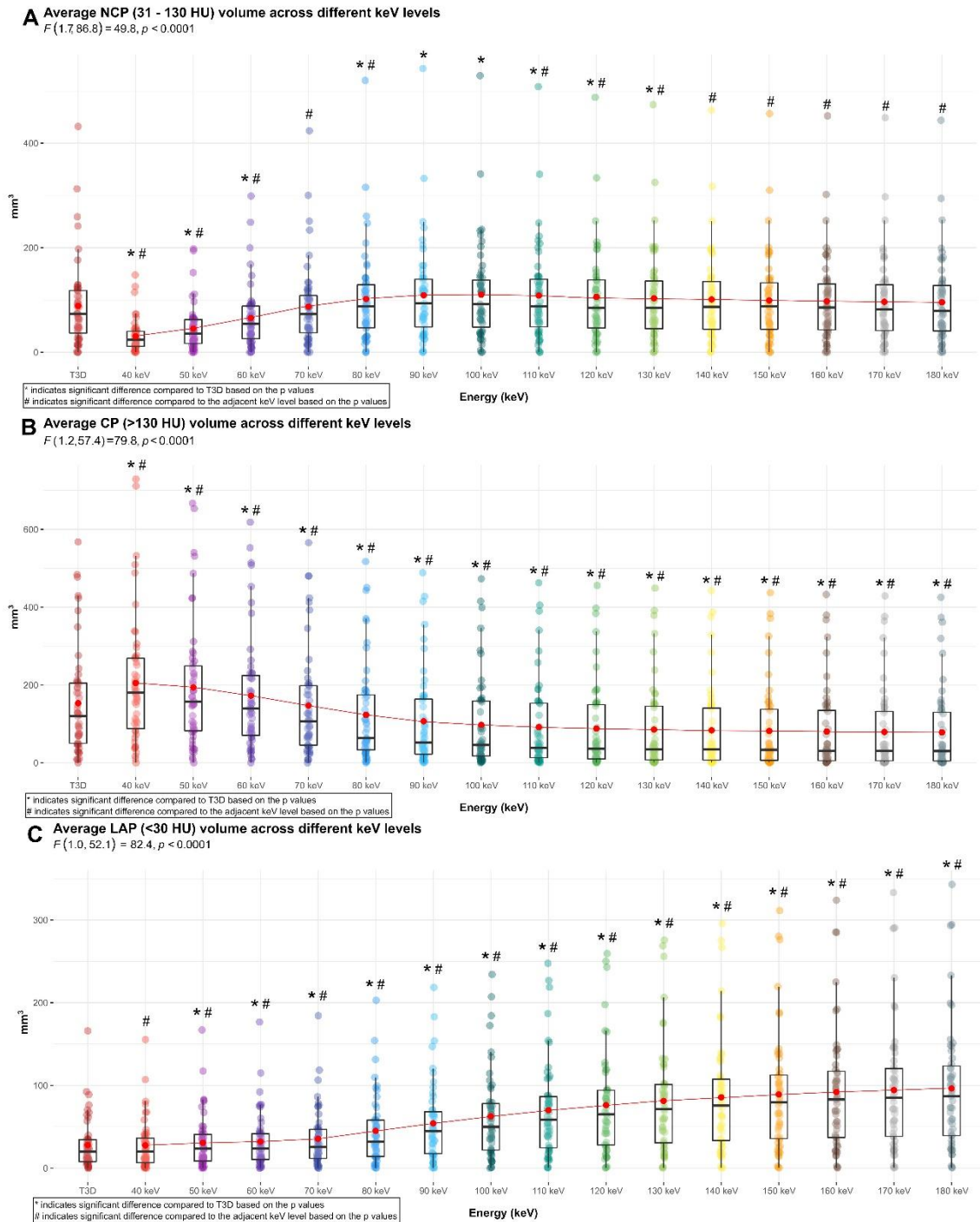
Figure 19. Box plots depicting the distribution of plaque volumes (method 2) in T3D images and different VMI energy levels.

Panel **A**: distribution of NCP volume. Panel **B**: distribution of CP volume. Panel **C**: distribution of LAP volume. *(Source: Vattay B., et al. Eur Radiol. 2023;33(12):8528-8539. CC BY 4.0)*

CP: calcified plaque; HU: Hounsfield unit; LAP: low-attenuation non-calcified plaque; NCP: non-calcified plaque; VMI: virtual monoenergetic image

Table 15. Mean plaque volumes and their proportion to TPV (%) across different reconstructions method 2 thresholds for plaque characterization.

VMI keV	CP volume (>130 HU)			NCP volume (31 - 130 HU)			LAP volume (<30 HU)		
	Mean mm^3	SD mm^3	Mean/ TPV ratio (%)	Mean mm^3	SD mm^3	Mean/ TPV ratio (%)	Mean mm^3	SD mm^3	Mean/ TPV ratio (%)
T3D	153.4	138.4	56.8	88.8	82.2	32.9	28.1	30.8	10.4
40	205.0	164.2	75.9	30.6	31.3	11.3	27.5	29.9	10.2
50	194.0	161.6	71.8	45.4	43.9	16.8	30.7	32.3	11.4
60	172.6	150.3	63.9	65.6	60.5	24.3	32.1	33.3	11.9
70	147.2	138.3	54.5	87.4	79.4	32.4	35.6	35.1	13.2
80	123.1	127.5	45.6	102.1	90.3	37.8	45.0	41.5	16.7
90	106.8	120.9	39.5	109.3	93.2	40.5	54.2	47.6	20.1
100	97.4	117.6	36.1	110.3	92.5	40.8	62.6	53.4	23.2
110	91.7	115.6	33.9	108.5	90.7	40.2	70.0	58.5	25.9
120	88.1	114.3	32.6	106.0	88.6	39.2	76.2	62.8	28.2
130	85.5	112.9	31.6	103.4	86.8	38.3	81.3	66.5	30.1
140	83.5	111.8	30.9	101.1	85.4	37.4	85.6	69.4	31.7
150	81.8	110.7	30.3	99.3	84.4	36.8	89.1	71.6	33.0
160	80.4	109.7	29.8	97.7	83.6	36.1	92.1	73.6	34.1
170	79.3	108.9	29.4	96.5	83.0	35.7	94.4	75.1	34.9
180	78.3	108.2	29.0	95.6	82.4	35.4	96.3	76.5	35.6

CP: calcified plaque; HU: Hounsfield unit; LAP: low-attenuation plaque; NCP: non-calcified plaque; SD: standard deviation; TPV: total plaque volume on T3D image; VMI: virtual monoenergetic image

Table 16. Relative difference in attenuation and image quality parameters between the reference standard T3D and VMI reconstructions.

VMI level (keV)	Attenuation (HU)		Image noise (SD)		CNR		SNR	
	Difference to T3D (%)	95 % CI	Difference to T3D (%)	95 % CI	Difference to T3D (%)	95 % CI	Difference to T3D (%)	95 % CI
40	142.0	114.3; 169.6	102.7	95.8 - 109.7	42.6	36.1; 49.0	52.7	45.1; 60.3
50	70.1	55.8; 84.5	56.8	52.4; 61.1	25.2	19.8; 30.5	31.7	25.5; 37.9
60	27.9	21.5; 34.4	27.0	24.2; 29.7	11.0	6.5; 15.4	13.4	8.4; 18.4
70	1.3*	- 0.5; 3.2	4.2	2.3; 6.1	1.8*	-1.8; 5.4	0.8*	-3.2; 4.8
80	-17.4	-19.7; -15.1	-1.7*	-4.1; 0.6	-14.4	-18.0; -10.8	-17.9	-21.8; -13.9
90	-29.9	-34.2; -25.6	-4.3	-6.9; -1.7	-28.0	-31.8; -24.1	-32.6	-36.8; -28.4
100	-38.3	-44.1; -32.5	-4.9	-7.6; -2.2	-38.3	-42.3; -34.3	-44.1	-48.7; -39.5
110	-44.3	- 51.1; -32.5	-5.7	-8.6; -2.9	-45.6	-49.8; -41.3	-52.2	-57.2; -47.2
120	-48.6	-56.2; -41.0	-5.9	-8.8; -3.0	-51.2	-55.7; -46.6	-58.4	-63.7; -53.0
130	-51.8	-60.0; -43.7	-5.9	-8.9; -3.0	-55.4	-60.1; -50.7	-63.0	-68.7; -57.4
140	-54.3	-62.9; -45.7	-6.0	-8.9; -3.0	-58.6	-63.5; -53.7	-66.6	-72.5; -60.7
150	-56.2	-65.1; -47.2	-5.9	-8.9; -3.0	-61.1	-66.1; -56.1	-69.4	-75.4; -63.3
160	-57.6	-66.9; -48.4	-5.9	-8.8; -2.9	-63.1	-68.2; -58.0	-71.6	-77.8; -65.4
170	-58.8	-68.3; -49.4	-5.9	-8.8; -2.9	-64.7	-69.9; -59.5	-73.3	-79.6; -67.0
180	-59.8	-69.4; -50.2	-5.8	-8.8; -2.9	-66.0	-71.2; -60.7	-74.7	-81.1; -68.3

*Differences and 95% CI are from pairwise t-tests. * indicates no statistical significance compared to T3D based on p value.*

CI: confidence interval; CNR: contrast to noise ratio; HU: Hounsfield unit; SD: standard deviation; SNR: signal to noise ratio; VMI: virtual monoenergetic image

Table 17. Difference in CP, NCP, and LAP volumes based on the thresholds of method 1 for different VMI levels compared to T3D.

VMI keV	CP (>350 HU)		NCP (31 - 350 HU)		LAP (-100 - 30 HU)	
	ΔT3D (%)	95% CI	ΔT3D (%)	95% CI	ΔT3D (%)	95% CI
40	70.8	54.2; 87.5	-39.8	-48.1; -31.5	-18.8	-29.0; -8.6
50	36.9	28.2; 45.6	-20.3	-25.2; -15.5	1.9*	-5.8; 9.6
60	8.7	5.4; 12.0	-6.9	-8.9; -4.9	13.6	7.5; 19.6
70	0.9	0.1; 1.6	-5.1	-6.4; -3.8	26.8	19.8; 33.7
80	-6.5	-9.4; -3.6	-7.3	-9.7; -4.9	60.5	46.9; 74.0
90	-17.5	-24.9; -10.0	-7.4	-11.4; -3.4	92.9	72.5; 113.3
100	-27.5	-38.2; -16.8	-7.6*	-13.2; -2.0	122.9	96.1; 149.7
110	-34.8	-47.6; -21.9	-8.6*	-15.3; -1.8	149.3	116.9; 181.8
120	-39.8	-54.2; -25.5	-9.8*	-17.5; -2.2	171.2	133.9; 208.4
130	-43.4	-58.9; -28.0	-11.2*	-19.6; -2.8	189.3	148.0; 230.5
140	-46.3	-62.5; -30.0	-12.4*	-21.4; -3.5	204.7	160.2; 249.2
150	-48.3	-65.3; -31.4	-13.6*	-23.0; -4.1	217.0	170.0; 263.9
160	-50.1	-67.6; -32.6	-14.5*	-24.3; -4.7	227.4	178.4; 276.4
170	-51.4	-69.4; -33.5	-15.3*	-25.4; -5.2	235.7	185.1; 286.3
180	-52.5	-70.9; -34.2	-15.9*	-26.3; -5.5	242.5	190.5; 294.6

*Differences and 95% CI are from pairwise t-tests. * indicates no statistical significance compared to T3D based on p value.*

CI: confidence interval; CP: calcified plaque; HU: Hounsfield unit; LAP: low-attenuation plaque; NCP: non-calcified plaque; VMI: virtual monoenergetic image

Table 18. Difference in CP, NCP, and LAP volumes based on the thresholds of method 2 for different VMI levels compared to T3D.

VMI keV	CP (>130 HU)		NCP (31 - 130 HU)		LAP (<30 HU)	
	ΔT3D (%)	95% CI	ΔT3D (%)	95% CI	ΔT3D (%)	95% CI
40	33.6	23.3; 44.0	-65.6	-82.4; -48.8	-1.9*	-10.1; 6.4
50	26.5	19.3; 33.6	-48.9	-61.6; -36.2	9.6	2.2; 17.0
60	12.5	8.4; 16.6	-26.2	-33.4; -18.9	14.4	8.4; 20.4
70	-4.0	-5.9; -2.1	-1.5*	-3.9; 0.9	26.8	19.8; 33.8
80	-19.7	-24.1; -15.4	15.0	9.8; 20.1	60.5	47.0; 74.1
90	-30.4	-36.7; -24.0	23.1	16.1; 30.1	93.0	72.6; 113.5
100	-36.5	-44.1; -29.0	24.2	16.0; 32.5	123.1	96.2; 149.9
110	-40.2	-48.6; -31.8	22.2	13.1; 31.3	149.6	117.1; 182.1
120	-42.6	-51.5; -33.7	19.4	9.7; 29.1	171.5	134.2; 208.9
130	-44.3	-53.5; -35.0	16.5	6.3; 26.7	189.7	148.4; 231.0
140	-45.6	-55.1; -36.0	13.9*	3.4; 24.4	205.2	160.7; 249.8
150	-46.7	-56.5; -36.8	11.8*	1.1; 22.6	217.6	170.6; 264.6
160	-47.6	-57.6; -37.5	10.1*	-0.9; 21.1	228.1	179.0; 277.2
170	-48.3	-58.5; -38.1	8.7*	-2.5; 19.9	236.5	185.7; 287.2
180	-48.9	-59.3; -38.5	7.7*	-3.7; 19.1	243.3	191.2; 295.5

*Differences and 95% CI are from pairwise t-tests. * indicates no statistical significance compared to T3D based on p value.*

CI: confidence interval; CP: calcified plaque; HU: Hounsfield unit; LAP: low-attenuation plaque; NCP: non-calcified plaque; VMI: virtual monoenergetic level

5. DISCUSSION

The aim of this thesis was to comprehensively evaluate the anatomical and functional aspects of chronic coronary syndrome by analyzing plaque progression, plaque burden, plaque composition, and myocardial ischemia using advanced CT imaging. The main findings summarized in the thesis are: (1) smoking, diabetes, age and male sex independently predicted coronary plaque progression, and the identification of plaque progression was underestimated based on CAD-RADS classification, (2) quantified total coronary plaque burden independently influenced corresponding quantified myocardial ischemia assessed by CT imaging, (3) using novel first-generation dual-source PCCT, different VMI reconstructions significantly influenced estimated coronary plaque volumes and quantitative image quality parameters.

5.1 Assessment of plaque progression

CTA is a uniquely suited imaging modality to monitor changes in the extent and severity of CAD and underlying plaque composition. Our longitudinal observational cohort study showed that age and gender influenced the severity and the extent of coronary atherosclerosis independent of established cardiovascular risk factors, while smoking and diabetes increased annual rate of plaque progression based on SSS, representing both disease severity and extent. Notably, CAD-RADS severity classification change was not observed in 46% and 41% of patients despite increased SSS and SIS during follow-up CTA scans. In addition, none of the risk factors influenced CAD-RADS, which is the currently endorsed clinical classification system for reporting CAD using CTA.

Coronary atherosclerosis progression has demonstrated significant prognostic value in predicting future cardiovascular events based on previous data. During a median follow-up of 4.1 years, plaque progression was an independent predictor of ACS based on serial coronary CTA imaging (31). Also, a growing body of evidence highlights the critical role of rapid plaque progression as a precursor to plaque rupture and subsequent myocardial infarction (138, 139). Coronary CTA offers accurate and reproducible assessment of atherosclerotic plaque changes and, as a non-invasive technique, provides a safe option for serial imaging in patients with high-risk atherosclerotic morphology. This makes it particularly valuable for monitoring progression and evaluating the effectiveness of preventive therapies over time. Motoyama et al. defined plaque progression as at least 1 grade increase in stenosis severity or a >1.1 increase in the RI ratio (31). **Table 19**

describes additional approaches to define plaque progression. Other studies defined progression based on newly diagnosed cases with at least 50% stenosis by the person-years during follow-up, or utilized CACS, SSS and SIS to describe plaque progression (140).

Table 19. Different approaches to detect plaque progression with coronary CTA.

Category	CT based parameters
Quantitative plaque measures	Positive remodeling index (>1.1)
	Increase in total plaque volume (TPV)
	Increase in non-calcified plaque burden
	Progression of fibrofatty plaque content
	Greater volume increase in LAP
	De novo obstructive lesion (>50%)
Calcium-based progression	Increase in CACS
	Higher rate of new calcium deposition
Segment-based stenosis progression	Increase in SSS (worsening stenosis severity)
	Increase in SIS (new segment involvement)

CACS: coronary artery calcium score; CTA: computed tomography angiography; LAP: low-attenuation plaque; SIS: segment involvement score; SSS: segment stenosis score; TPV: total plaque volume

Importantly, we used a novel approach to define the predictors of plaque progression using different definitions, including progression in SSS, SIS, or CAD-RADS classification category (**Figure 20**). In addition, while previous studies assessed plaque progression as the change between two timepoints, we applied linear mixed models. Our methodology allowed us to also account for one's baseline value, (i.e. individuals with more plaque may progress faster unless normalizing for the baseline plaque volume) or the possible changes in covariates over time (i.e. someone may develop diabetes over the follow-up period). Modeling intra-subject changes and analyzing both overall and individual patterns over time offer a more comprehensive assessment of how predictors influence plaque development.
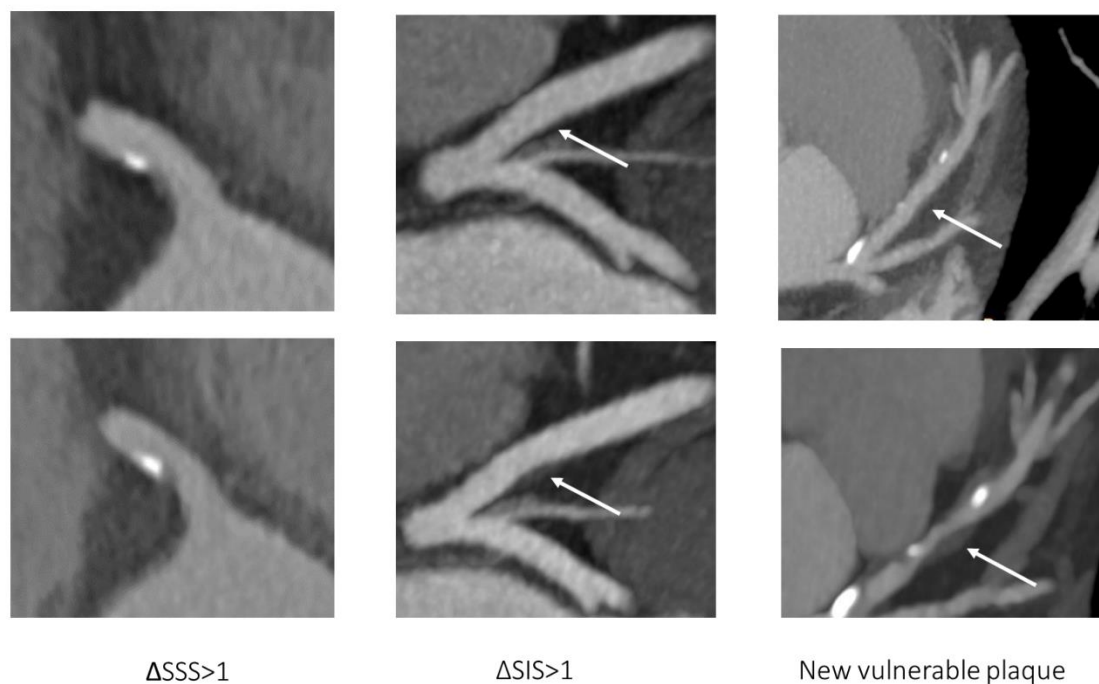
Figure 20. Coronary plaque progression defined as increase in SSS - severity increased on left panel, SIS - new plaque as shown in the middle panel, or the appearance of a vulnerable plaque - right panel. (Own material.)

SIS: segment involvement score; SSS: segment stenosis score

Although an increasing number of studies have utilized CT to detect coronary atherosclerosis, data on the predictors of plaque progression remain limited. Notably, these predictors vary depending on the chosen definition of plaque progression, and a wide range of definitions are used to assess CAD progression and characterize coronary atherosclerosis on CTA. Increased plaque progression was also linked to obesity, high low-density lipoprotein cholesterol level and smoking (141-144). Smoking contributes to atherogenesis through various mechanisms, including inflammation, endothelial dysfunction, altered platelet function, disruptions in cholesterol metabolism, and the promotion of thrombotic factors. Coronary CT imaging showed significantly higher CACS, SSS and SIS in diabetic patients compared to control groups during a 5-year follow-up study (145). In addition, SSS and SIS showed predictive value for clinical events in the same diabetic cohort. We also observed that male gender was linked to a larger SSS and SIS levels, and that smokers exhibited a greater extent of CAD.

Additionally, smoking and diabetes mellitus were found to be associated with the progression rate of SSS, as determined by linear mixed models.

Other recently published studies have focused on quantitative plaque analysis defining plaque progression based on volumetric changes. However, due to the small changes in plaque volume, these adjustments would not affect clinical scoring systems like SSS or CAD-RADS, nor alter clinical decision-making. Notably, limitations of quantitative plaque analysis also include lack of standardized protocols, inter-vendor, scan-rescan and inter-software variability. Total atherosclerotic plaque volume increase was used to evaluate the relationship between various diseases (HIV infection, non-alcoholic fatty liver disease, etc) and outcomes using mediation analysis (146, 147). However, the detected changes are comparable to interscan variability, requiring caution in their interpretation (148). Coronary CTA is being increasingly employed to monitor the effectiveness of anti-atherosclerotic drug therapy. Gu et al found that following long-term high-intensity statin therapy, females presented greater degree of coronary plaque regression compared to males based on CACS, SIS and SSS (140).

The introduction of the CAD-RADS multidisciplinary consensus document marks a significant step in standardizing and streamlining coronary CTA reporting, facilitating improved communication across medical disciplines by using a simplified and consistent terminology for CT findings. The CAD-RADS classification, which focuses on the most severe stenosis, proved however inadequate for detecting plaque progression based on our results. Patients with mild/moderate stenosis (CAD-RADS category 2-3), classified as non-obstructive, may still exhibit extensive CAD affecting >4 coronary segments. Bittencourt et al. demonstrated that such patients have comparable cardiovascular risk to those with obstructive CAD (57). Min et al evaluated 1,127 symptomatic patients undergoing CTA and demonstrated that increasing SIS - reflecting the number of coronary segments with plaque - strongly correlates with worsened all-cause mortality (149).

It is therefore encouraging that the new CAD-RADS 2.0 version now includes extent of CAD, addressing this limitation (150).

5.2 The association of quantitative plaque metrics and myocardial ischemia

In our prospective, single center study, we employed a novel method to assess the association of quantified coronary plaque metrics to myocardial ischemia across all coronary segments, focusing on lesions within the corresponding myocardial territory using CTA (**Figure 21**). This approach allowed us to evaluate the direct effect of a specific lesion or a combination of lesions on the corresponding myocardial segment.

Our findings revealed that TPV impacted myocardial ischemia, independent of stenosis severity, HRP, and risk factors. Furthermore, maximal luminal stenosis and the presence of HRP were not associated with myocardial ischemia as measured by MBF. We also detected excellent reproducibility of both TPV and MBF assessments.

Coronary CTA is a unique imaging modality that allows for the combined anatomical and functional assessment of CAD. CT has several advantages for evaluating myocardial ischemia, as compared with other modalities such as increased spatial resolution, comprehensive plaque assessment and reproducible quantitative measures of myocardial perfusion. However, radiation dose remains a limiting factor, particularly when utilizing dynamic CT protocols, restricting its applicability for a large subset of patients.

Previous studies have suggested that increased plaque burden correlates with visual perfusion defects, reinforcing the notion that morphological plaque characteristics play an important role in myocardial ischemia beyond just stenosis severity (151, 152). The CREDENCE trial showed a strong association between quantified plaque volume and invasive FFR (153). Liu et al. similarly found that low-density plaque volume and diameter stenosis were independently linked to myocardial ischemia (152). Driessen et al. analyzed 208 patients who underwent (^{15}O) H_2O PET-MPI and coronary CTA, concluding that plaque length and volume were inversely correlated with MBF (154). Additionally, this study identified a connection between decreased blood flow and non-calcified plaque volume or positive remodeling in a vessel-based analysis. The multicenter CORE 320 study demonstrated that the combination of coronary CTA and CTP exhibited excellent diagnostic accuracy for detecting flow-limiting lesions (greater than 50%) by invasive angiography and perfusion defects via SPECT. Van Rosendael et al used static stress CTP in 84 patients to examine the relationship between morphological plaque characteristics and visual perfusion deficits (155). While increasing stenosis

severity and lesion length were found to be predictors of ischemia, plaque volumes were not. However, prior studies also found higher TPV for ischemic patients as compared with non-ischemic individuals, and plaque burden improved the diagnosis of ischemia over stenosis (156). In our study, TPV for ischemic segments was 120.5 ± 119.5 mm³, while for non-ischemic segments it was 84.6 ± 82.2 mm³ indicating a substantial difference in plaque burden for ischemic segments. Studies have reported conflicting findings on whether ischemia is primarily driven by luminal narrowing, plaque composition and vulnerability, or overall plaque burden. However, these studies were limited to assessing the total plaque burden within a given vessel, without accounting for the individual variability in coronary arborization and myocardial perfusion territories (133). A distal coronary lesion does not restrict blood flow to the most basal myocardial segments, which could significantly impact the interpretation of results. Regarding stenosis severity, discrepancies between lesion severity and ischemia have been observed in both invasive and noninvasive studies (81, 157) . While previous clinical care primarily emphasized lesion severity, there is a growing shift toward assessing total coronary atherosclerotic burden. This broader approach can facilitate early intervention, guide the initiation of secondary prevention therapy, and contribute to disease stabilization ultimately reducing adverse events. Using patient-specific anatomical variations into our calculations, we ensured a more precise evaluation of the relationship between plaque burden and ischemia. In a recent study, Min et al. suggested stages of plaque burden for the detection of ischemia assessed by FFR (158). Whether there is certain cutoff for TPV that leads to definite requires future investigations.
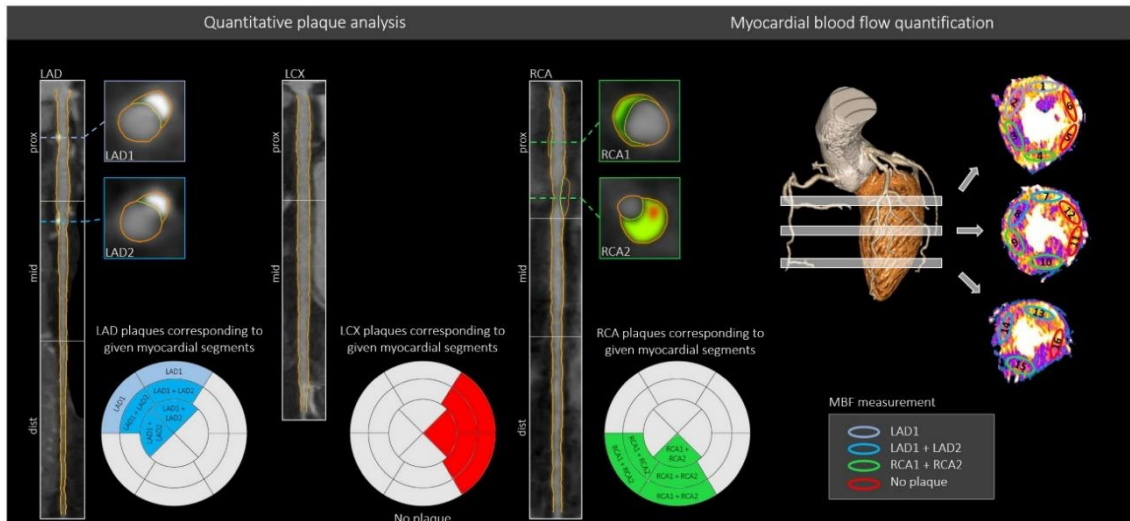
Figure 21. Comprehensive quantitative plaque and myocardial perfusion analysis using cardiac CTA. In this case, plaques were detected and quantified in the proximal LAD (LAD1), mid-LAD (LAD2) and proximal RCA (RCA1 + RCA2). All coronary plaques based on their location were matched for the corresponding myocardial territory. MBF was quantified for all 16 myocardial segments using DPCT images. By creating a myocardial vessel territory map for each coronary segment, we could derive the TPV that could influence MBF. In this case, basal anterior and basal anteroseptal myocardial segments were influenced by the proximal LAD (LAD1) lesion, while the mid anterior, mid anteroseptal, apical anterior , and apical septal myocardial segments were affected by two lesions: LAD1 and LAD2, as they are located more distally. LCX demonstrated no coronary lesions. Regarding the RCA, two plaques were detected in the proximal RCA segment (RCA1 and RCA2), therefore all myocardial segments corresponding to the RCA were influenced by two plaques (RCA1 and RCA2). Plaque volumes of the lesions aligned for a given myocardial segment were summed and accounted for in the analysis, while the highest degree of lumen area stenosis of the corresponding lesions was included in the analysis. Light blue color indicates LV segments related to proximal LAD lesion, dark blue color indicates LV territories related to both proximal and mid-LAD lesions, whereas green color shows myocardial territories corresponding to the RCA lesions. *(Source: Vattay B., et al. Front Cardiovasc Med. 2022;9:974805. CC BY 4.0)*

CAD: coronary artery disease; CTA: CT angiography; DPCT: dynamic perfusion CT; LAD: left anterior descending; LCX: left circumflex; LV: left ventricle; MBF: myocardial blood flow; RCA: right coronary artery

5.3 Quantitative plaque characterization using photon-counting CT

Novel photon-counting detector technology enables spectral imaging of coronary plaques using different virtual monoenergetic reconstructions. In our study, we demonstrated that the use of various VMI energy levels significantly impacts attenuation values and the corresponding volumes of coronary plaque components. Our main finding included: low-energy images (40-70 keV) enhanced CNR while increasing image noise, and resulted in higher CP but lower NCP and LAP volumes; CP volume measured at 70 keV showed the smallest relative difference compared to T3D images as reference; NCP volumes did not differ significantly across higher VMI levels (100-180 keV); LAP volume on low-energy images (40-50 keV) was not significantly different from T3D images.

Coronary CTA is a first line non-invasive imaging modality in the diagnosis of CAD in patients with stable chest pain (159). CT enables the assessment of CAD parameters with important prognostic value, including luminal stenosis, high-risk plaque morphology and plaque burden (31). Quantitative plaque analysis further enhances this capability by providing detailed assessment of plaque volume and composition. Emerging evidence supports the added prognostic value of quantitative over visual plaque assessment (160). Notably, LAP burden - defined by a fixed attenuation threshold of 30 HU - being an independent predictor of myocardial infarction at 5-year follow-up (71). As such, quantitative CTA-based plaque evaluation can improve risk stratification by identifying patients at elevated cardiovascular risk (161).

The recent introduction of dual-source PCCT systems into clinical practice offers potential advantages over conventional CT technology. Compared to traditional energy-integrating detectors, PCCT directly generate electronical signal proportional to the energy of each photon reaching the detector, resulting in superior spatial resolution, reduced image noise and beam-hardening artifacts (118). Additionally, PCCT allows for advanced tissue characterization through VMI reconstructions, which could improve coronary plaque assessment. However, VMI reconstructions also alter CT attenuation values, which can impact plaque characterization. Lower keV images increase contrast between the coronary lumen and vessel wall, improving visualization of plaques and intraluminal contrast. Although these images exhibit higher image noise, they also demonstrate improved image quality based on CNR and SNR, consistent with previous phantom studies (162). Conversely, higher keV levels reduce image noise and blooming

artifacts, thereby enhancing evaluation of calcified plaques, although resulting in reduced CNR and SNR. An optimal approach may involve viewing both low- and high-keV images side-by-side and enabling manual adjustment of segmentation contours on either reconstruction to mitigate artifacts. Ohta et al., using dual-energy CT, reported that different VMI levels yielded the highest CNR and SNR for specific plaque components, supporting our findings that multiple VMI levels may be needed for comprehensive plaque characterization (163).

Because VMI reconstructions alter voxel attenuation values, it is critical to consider how these changes affect quantitative plaque analysis. Our findings show that fixed threshold definitions applied to T3D images yield significantly different plaque volumes when used on VMIs. This is because VMI based attenuation varies depending on the tissue composition of each voxel (164-166). Thus, applying fixed thresholds across VMI levels results in inconsistent quantification, as demonstrated by the significant differences in plaque volumes across almost all VMI reconstructions relative to T3D. Moreover, demonstrated by our results, a single correction factor is insufficient, since the degree of volume discrepancy differs by plaque type even within the same VMI level. To ensure consistency across studies using different VMI or conventional datasets, standardized protocols and adaptive correction methods are needed to enable reliable conversion between volumetric estimates.

To date, no prior study has specifically evaluated the influence of VMI energy levels on coronary plaque composition using PCCT data. Symons et al. investigated similar effects using a third-generation dual-source CT scanner and found comparable trends in image quality, with higher CNR and SNR at lower keV levels and greater image noise. Although their analysis involved separate segmentations for each reconstruction, they reported similar tendencies regarding plaque types (167).

5.4 Limitations

Certain limitations of our investigations must be acknowledged. The study on plaque progression was a single center, retrospective analysis at a single center tertiary cardiology center, with variable time intervals between the two CT scans. To address this, we employed linear mixed models, which account for differences in follow-up duration and allow for a more detailed evaluation of the factors influencing plaque progression.

Another limitation was the incidental statin use without evaluating serum cholesterol levels. Prospective, multicenter studies are needed to assess whether the observed differences in CAD definitions could impact patient outcomes. Finally, smoking was defined as tobacco use within one year prior to CTA, capturing current smoking status but not accounting for the cumulative lifetime exposure and associated risk.

The study on the association of plaque volume and myocardial ischemia had a relatively reduced sample size due to the exclusion of patients with non-diagnostic image quality for quantitative plaque analysis or without intermediate stenosis. Since excellent image quality is essential for accurate quantitative plaque assessment, this may have introduced selection bias. Furthermore, quantitative plaque analysis is a time-intensive process and currently remains a research tool, not yet integrated into routine clinical practice. Nevertheless, its value in risk stratification is increasingly recognized by experts, and efforts are underway to develop automated quantification tools. Additionally, our study lacks sufficient power to evaluate robust outcome analyses.

The third study of current thesis has certain limitations, including that it was also a single center study involving a modest number of stable chest pain patients, although the sample size was sufficient to observe consistent trends in VMI based plaque quantification. Also, we used a single software platform for segmentation, and did not account for other technical factors - such as slice thickness, iterative reconstruction algorithms, or reconstruction kernels - that may also influence plaque volume measurements. Additionally, no reference standard such as histology or intravascular imaging was available. Nevertheless, T3D images are generally comparable to conventional 120-kV images from energy-integrating detector CT systems and the methods used have been validated against intravascular imaging in large cohorts (168, 169). Although variation in contrast media concentration and injection protocols can also influence attenuation, our standardized protocol allows minimal variation (170). More importantly, we compared VMI based measurements within the same patients, thereby minimizing the impact of such variation on our results.

5.5 Future perspectives

According to currently available literature and to our results, we propose the following to be incorporated in future clinical practice in the management of CCS. Accurate risk

assessment in CAD should move beyond the detection of stenosis alone. Emphasizing total plaque burden and plaque progression in clinical CTA reports - and ultimately within structured frameworks such as CAD-RADS - could better identify patients who may benefit from intensified preventive strategies or further functional testing. Integrating dynamic plaque metrics - whether semi-quantitative (e.g. SSS or SIS) or quantitative (e.g. volumetric plaque progression) - could refine risk stratification and support earlier, more personalized interventions. Future multicenter, prospective studies are warranted to validate these concepts and to establish their impact on patient outcomes. Advances in CT technology, such as PCCT, offer improved spatial resolution and more robust plaque quantification, but standardization of analysis across platforms remains essential. As quantitative plaque analysis tools mature and become automated, their integration into routine practice will likely become more feasible.

6. CONCLUSIONS

In conclusion, this thesis addressed three critical aims to enhance CAD assessment using advanced coronary CTA and PCCT imaging. It showed that stenosis-based classifications like CAD-RADS may underestimate disease progression, that total plaque volume better predicts myocardial ischemia than stenosis severity, and that spectral imaging parameters significantly affect plaque quantification requiring new clinical standards. These insights pave the way for more accurate, reproducible and clinically meaningful evaluation of coronary atherosclerosis, potentially improving patient care through better risk stratification and targeted therapies.

7. SUMMARY

This thesis aimed to improve the assessment of CAD burden, its progression and functional consequences by leveraging advanced coronary CTA postprocessing tools and PCCT imaging. The first objective was to define plaque progression using different CAD definitions applied to serial CTA scans, identifying predictors of progression and comparing detection rates across semi-quantitative CAD definitions, including the widely used CAD-RADS stenosis classification. Current CAD definitions vary, leading to inconsistent identification of patients with CAD progression and differing risk factor associations. Our study revealed important limitations in current CAD assessment methods. CAD-RADS failed to detect progression in nearly half of patients with serial CTA. This finding underscores the need for more comprehensive, standardized definitions incorporating semiquantitative plaque burden metrics.

The second objective focused on elucidating the relationship between quantitative coronary plaque metrics derived from coronary CTA and segmental myocardial ischemia as assessed by DPCT. This aimed to clarify whether plaque burden provides incremental value over stenosis severity in predicting ischemia, which is crucial for clinical decision-making. Importantly, TPV was independently associated with segmental myocardial ischemia based on MBF, whereas traditional measures were not. This suggests that total plaque burden is a more sensitive and clinically relevant marker for ischemia than stenosis alone, supporting a shift toward comprehensive plaque quantification in clinical practice to better identify ischemic myocardial territories.

The third objective investigated how quantitative measurements of individual plaque components change across different VMI reconstructions obtained from a novel PCCT system and assessed the quantitative image quality. Plaque volume estimates differed substantially between VMIs at different VMI levels, especially for LAP, which is currently defined by fixed HU thresholds. Since PCCT offers enhanced spectral imaging capabilities, understanding how HU values vary with energy levels is critical for establishing reliable plaque quantification protocols and therefore our results represent an important step towards normalization of coronary plaque volume using different VMIs. Collectively, these results show the potential of novel technologies to refine CAD diagnosis and management and might also improve personalized medicine in CAD management provided that standardized definitions and imaging protocols are adopted.

8. ÖSSZEFOGLALÓ

A disszertáció célja a koszorúér-betegség (CAD) kiterjedésének, progressziójának és funkcionális következményeinek vizsgálata volt a legmodernebb coronaria CT angiográfiás (CTA) eszközök, köztük a fotonszámláló CT (PCCT) alkalmazásával. Első célkitűzésünk a plakk progresszió prediktorainak elemzése volt különböző szemi-kvantitatív CAD definíciók mentén, és hogy ezek milyen mértékben alkalmasak a betegség előrehaladásának azonosítására. Az irodalomban többféle definíciót alkalmaznak a CAD progresszió leírására, ami eltérő eredményekhez vezethet. Eredményeink alapján a széles körben használt CAD-RADS klasszifikáció az esetek közel felében nem mutatta ki a plakkok progresszióját, ami alátámasztja a részletesebb, egységesebb definíciók és a CAD kiterjedését leíró szemi-kvantitatív paraméterek alkalmazásának fontosságát a klinikai gyakorlatban. Második célunk a CTA alapján meghatározott kvantitatív plakk jellemzők és a szegmentális myocardialis ischaemia közötti kapcsolat vizsgálata volt, dinamikus perfúziós CT (DPCT) alkalmazásával. Célunk volt elemezni, hogy a teljes plakk terheltség (TPV) - a szűkület mértékén túl - hozzáadott prognosztikus értékkel bír-e az ischaemia azonosításában. Eredményeink szerint a TPV függetlenül befolyásolta a DPCT-vel meghatározott ischaemiát, míg a hagyományos jellemzők nem mutattak hasonló összefüggést. Ez hangsúlyozza a TPV klinikai jelentőségét, amely érzékenyebb markernek bizonyult az ischaemia meghatározására, mint a szűkület mértéke. Harmadik célkitűzésként a VMI képrekonstrukciók hatását vizsgáltuk különböző plakk komponensek kvantifikációjára és a képminőségre PCCT-t alkalmazva. A különböző VMI energiaszinteken jelentős eltéréseket mértünk elsősorban az alacsony denzitású plakk (LAP) volumenben, melynek meghatározása jelenleg fix HU küszöbérték alapján történik. A PCCT által nyújtott spektrális képalkotás elterjedése révén elengedhetetlen annak pontos megértése, hogyan változnak a denzitás értékek különböző energiaszinteken, így eredményeink fontos lépést jelentenek a VMI-alapú plakk kvantifikáció egységesítése felé. Összefoglalásként elmondható, hogy a disszertáció három lényeges területen járult hozzá a CAD korszerűbb értékeléséhez az új generációs CTA technológiák alkalmazásával. Az eredmények ezen innovatív módszerek képesek pontosítani a CAD diagnosztikáját és kezelését, és új perspektívát nyithatnak a személyre szabott orvoslás területén - feltéve, hogy egységes képalkotási protokollokat és egységes definíciókat alkalmazunk.

9. REFERENCES

1.   Tsao CW, Aday AW, Almarzooq ZI, Anderson CAM, Arora P, Avery CL, et al. Heart Disease and Stroke Statistics-2023 Update: A Report From the American Heart Association. Circulation. 2023;147(8):e93-e621.

2.   Martin SS, Aday AW, Almarzooq ZI, Anderson CAM, Arora P, Avery CL, et al. 2024 Heart Disease and Stroke Statistics: A Report of US and Global Data From the American Heart Association. Circulation. 2024;149(8):e347-e913.

3.   Janosi A, Ferenci T, Komocsi A, Andreka P. [Short- and long-term prognostic significance of previous recanalization interventions in patients treated for myocardial infarction]. Orv Hetil. 2021;162(5):177-84.

4.   Ulambayar B, Ghanem AS, Kovacs N, Trefan L, More M, Nagy AC. Cardiovascular disease and risk factors in adults with diabetes mellitus in Hungary: a population-based study. Front Endocrinol (Lausanne). 2023;14:1263365.

5.   András J. Data on the care and prognosis of patients treated for myocardial infarction. Hungarian Myocardial Infarction. Registry 2023. Cardiologia Hungarica. 2024;54(3):243-51.

6.   Mensah GA, Fuster V, Murray CJL, Roth GA, Global Burden of Cardiovascular D, Risks C. Global Burden of Cardiovascular Diseases and Risks, 1990-2022. Journal of the American College of Cardiology. 2023;82(25):2350-473.

7.   Wong ND, Budoff MJ, Ferdinand K, Graham IM, Michos ED, Reddy T, et al. Atherosclerotic cardiovascular disease risk assessment: An American Society for Preventive Cardiology clinical practice statement. Am J Prev Cardiol. 2022;10:100335.

8.   Berger JS, Jordan CO, Lloyd-Jones D, Blumenthal RS. Screening for cardiovascular risk in asymptomatic patients. Journal of the American College of Cardiology. 2010;55(12):1169-77.

9.   Brown JC, Gerhardt TE, Kwon E. Risk Factors for Coronary Artery Disease. StatPearls. Treasure Island (FL)2024.

10.   Visseren FLJ, Mach F, Smulders YM, Carballo D, Koskinas KC, Back M, et al. 2021 ESC Guidelines on cardiovascular disease prevention in clinical practice. Eur Heart J. 2021;42(34):3227-337.

11. Marx N, Federici M, Schutt K, Muller-Wieland D, Ajjan RA, Antunes MJ, et al. 2023 ESC Guidelines for the management of cardiovascular disease in patients with diabetes. Eur Heart J. 2023;44(39):4043-140.

12. McDermott M, Meah MN, Khaing P, Wang KL, Ramsay J, Scott G, et al. Rationale and Design of SCOT-HEART 2 Trial: CT Angiography for the Prevention of Myocardial Infarction. JACC Cardiovasc Imaging. 2024;17(9):1101-12.

13. Zeitouni M, Nanna MG, Sun JL, Chiswell K, Peterson ED, Navar AM. Performance of Guideline Recommendations for Prevention of Myocardial Infarction in Young Adults. Journal of the American College of Cardiology. 2020;76(6):653-64.

14. Myerburg RJ, Junttila MJ. Sudden cardiac death caused by coronary heart disease. Circulation. 2012;125(8):1043-52.

15. Talha I, Elkhoudri N, Hilali A. Major Limitations of Cardiovascular Risk Scores. Cardiovasc Ther. 2024;2024:4133365.

16. Kheiri B, Simpson TF, Osman M, German DM, Fuss CS, Ferencik M. Computed Tomography vs Invasive Coronary Angiography in Patients With Suspected Coronary Artery Disease: A Meta-Analysis. JACC Cardiovasc Imaging. 2022;15(12):2147-9.

17. Group DT, Maurovich-Horvat P, Bosserdt M, Kofoed KF, Rieckmann N, Benedek T, et al. CT or Invasive Coronary Angiography in Stable Chest Pain. N Engl J Med. 2022;386(17):1591-602.

18. Kolossvary M, Szilveszter B, Merkely B, Maurovich-Horvat P. Plaque imaging with CT-a comprehensive review on coronary CT angiography based risk assessment. Cardiovasc Diagn Ther. 2017;7(5):489-506.

19. Bittner DO, Mayrhofer T, Budoff M, Szilveszter B, Foldyna B, Hallett TR, et al. Prognostic Value of Coronary CTA in Stable Chest Pain: CAD-RADS, CAC, and Cardiovascular Events in PROMISE. JACC Cardiovasc Imaging. 2020;13(7):1534-45.

20. Vattay B, Boussoussou M, Borzsák S, Vecsey-Nagy M, Simon J, Kolossváry M, et al. Myocardial perfusion imaging using computed tomography: Current status, clinical value and prognostic implications. Imaging. 2021;13(1):49-60.

21. Vattay B, Szilveszter B, Boussoussou M, Vecsey-Nagy M, Lin A, Konkoly G, et al. Impact of virtual monoenergetic levels on coronary plaque volume components using photon-counting computed tomography. Eur Radiol. 2023;33(12):8528-39.

22.	Vrints C, Andreotti F, Koskinas KC, Rossello X, Adamo M, Ainslie J, et al. 2024 ESC Guidelines for the management of chronic coronary syndromes. Eur Heart J. 2024;45(36):3415-537.

23.	Virani SS, Newby LK, Arnold SV, Bittner V, Brewer LC, Demeter SH, et al. 2023 AHA/ACC/ACCP/ASPC/NLA/PCNA Guideline for the Management of Patients With Chronic Coronary Disease: A Report of the American Heart Association/American College of Cardiology Joint Committee on Clinical Practice Guidelines. Circulation. 2023;148(9):e9-e119.

24.	Knuuti J, Ballo H, Juarez-Orozco LE, Saraste A, Kolh P, Rutjes AWS, et al. The performance of non-invasive tests to rule-in and rule-out significant coronary artery stenosis in patients with stable angina: a meta-analysis focused on post-test disease probability. Eur Heart J. 2018;39(35):3322-30.

25.	Kolossvary M, Szilveszter B, Edes IF, Nardai S, Voros V, Hartyanszky I, et al. Comparison of Quantity of Coronary Atherosclerotic Plaques Detected by Computed Tomography Versus Angiography. Am J Cardiol. 2016;117(12):1863-7.

26.	Szilveszter B, Vattay B, Bossoussou M, Vecsey-Nagy M, Simon J, Merkely B, et al. CAD-RADS may underestimate coronary plaque progression as detected by serial CT angiography. Eur Heart J Cardiovasc Imaging. 2022;23(11):1530-9.

27.	Szilveszter B, Kolossvary M, Pontone G, Williams MC, Dweck MR, Maurovich-Horvat P. How to quantify coronary atherosclerotic plaque using computed tomography. Eur Heart J Cardiovasc Imaging. 2022;23(12):1573-5.

28.	Min JK, Dunning A, Lin FY, Achenbach S, Al-Mallah M, Budoff MJ, et al. Age- and sex-related differences in all-cause mortality risk based on coronary computed tomography angiography findings results from the International Multicenter CONFIRM (Coronary CT Angiography Evaluation for Clinical Outcomes: An International Multicenter Registry) of 23,854 patients without known coronary artery disease. Journal of the American College of Cardiology. 2011;58(8):849-60.

29.	van Rosendael AR, Narula J, Lin FY, van den Hoogen IJ, Gianni U, Al Hussein Alawamlh O, et al. Association of High-Density Calcified 1K Plaque With Risk of Acute Coronary Syndrome. JAMA Cardiol. 2020;5(3):282-90.

30.	Chang HJ, Lin FY, Lee SE, Andreini D, Bax J, Cademartiri F, et al. Coronary Atherosclerotic Precursors of Acute Coronary Syndromes. Journal of the American College of Cardiology. 2018;71(22):2511-22.

31.	Motoyama S, Ito H, Sarai M, Kondo T, Kawai H, Nagahara Y, et al. Plaque Characterization by Coronary Computed Tomography Angiography and the Likelihood of Acute Coronary Events in Mid-Term Follow-Up. J Am Coll Cardiol. 2015;66(4):337-46.

32.	Douglas PS, Hoffmann U, Patel MR, Mark DB, Al-Khalidi HR, Cavanaugh B, et al. Outcomes of anatomical versus functional testing for coronary artery disease. N Engl J Med. 2015;372(14):1291-300.

33.	Andreini D, Pontone G, Mushtaq S, Bartorelli AL, Bertella E, Antonioli L, et al. A long-term prognostic value of coronary CT angiography in suspected coronary artery disease. JACC Cardiovasc Imaging. 2012;5(7):690-701.

34.	Dzaye O, Razavi AC, Blaha MJ, Mortensen MB. Evaluation of coronary stenosis versus plaque burden for atherosclerotic cardiovascular disease risk assessment and management. Current opinion in cardiology. 2021;36(6):769-75.

35.	Szilveszter B, Maurovich-Horvat P. Myocardial computed tomography perfusion: a synergy of form and function. Eur Heart J Cardiovasc Imaging. 2018;19(11):1232-3.

36.	Sliwicka O, Sechopoulos I, Baggiano A, Pontone G, Nijveldt R, Habets J. Dynamic myocardial CT perfusion imaging-state of the art. Eur Radiol. 2023;33(8):5509-25.

37.	Andreini D, Mushtaq S, Pontone G, Conte E, Collet C, Sonck J, et al. CT Perfusion Versus Coronary CT Angiography in Patients With Suspected In-Stent Restenosis or CAD Progression. JACC Cardiovasc Imaging. 2020;13(3):732-42.

38.	Zsarnoczay E, Varga-Szemes A, Emrich T, Szilveszter B, van der Werf NR, Mastrodicasa D, et al. Characterizing the Heart and the Myocardium With Photon-Counting CT. Invest Radiol. 2023;58(7):505-14.

39.	Szilveszter B, Elzomor H, Karolyi M, Kolossvary M, Raaijmakers R, Benke K, et al. The effect of iterative model reconstruction on coronary artery calcium quantification. Int J Cardiovasc Imaging. 2016;32(1):153-60.

40.	Vattay B, Boussoussou M, Vecsey-Nagy M, Kolossvary M, Juhasz D, Kerkovits N, et al. Qualitative and quantitative image quality of coronary CT angiography using

photon-counting computed tomography: Standard and Ultra-high resolution protocols. Eur J Radiol. 2024;175:111426.

41.   den Harder AM, Willemink MJ, de Ruiter QM, Schilham AM, Krestin GP, Leiner T, et al. Achievable dose reduction using iterative reconstruction for chest computed tomography: A systematic review. Eur J Radiol. 2015;84(11):2307-13.

42.   Mergen V, Sartoretti T, Baer-Beck M, Schmidt B, Petersilka M, Wildberger JE, et al. Ultra-High-Resolution Coronary CT Angiography With Photon-Counting Detector CT: Feasibility and Image Characterization. Invest Radiol. 2022;57(12):780-8.

43.   Shaw LJ, Blankstein R, Bax JJ, Ferencik M, Bittencourt MS, Min JK, et al. Society of Cardiovascular Computed Tomography / North American Society of Cardiovascular Imaging - Expert Consensus Document on Coronary CT Imaging of Atherosclerotic Plaque. J Cardiovasc Comput Tomogr. 2021;15(2):93-109.

44.   Narula J, Chandrashekhar Y, Ahmadi A, Abbara S, Berman DS, Blankstein R, et al. SCCT 2021 Expert Consensus Document on Coronary Computed Tomographic Angiography: A Report of the Society of Cardiovascular Computed Tomography. J Cardiovasc Comput Tomogr. 2021;15(3):192-217.

45.   de Knegt MC, Haugen M, Linde JJ, Kuhl JT, Nordestgaard BG, Kober LV, et al. Reproducibility of quantitative coronary computed tomography angiography in asymptomatic individuals and patients with acute chest pain. PLoS One. 2018;13(12):e0207980.

46.   Cheng VY, Nakazato R, Dey D, Gurudevan S, Tabak J, Budoff MJ, et al. Reproducibility of coronary artery plaque volume and composition quantification by 64-detector row coronary computed tomographic angiography: an intraobserver, interobserver, and interscan variability study. J Cardiovasc Comput Tomogr. 2009;3(5):312-20.

47.   Leipsic J, Abbara S, Achenbach S, Cury R, Earls JP, Mancini GJ, et al. SCCT guidelines for the interpretation and reporting of coronary CT angiography: a report of the Society of Cardiovascular Computed Tomography Guidelines Committee. J Cardiovasc Comput Tomogr. 2014;8(5):342-58.

48.   Sakai K, Shin D, Singh M, Malik S, Dakroub A, Sami Z, et al. Diagnostic Performance and Clinical Impact of Photon-Counting Detector Computed Tomography

in Coronary Artery Disease. Journal of the American College of Cardiology. 2025;85(4):339-48.

49.   Nakanishi R, Li D, Blaha MJ, Whelton SP, Darabian S, Flores FR, et al. All-cause mortality by age and gender based on coronary artery calcium scores. Eur Heart J Cardiovasc Imaging. 2016;17(11):1305-14.

50.   Budoff MJ, Shaw LJ, Liu ST, Weinstein SR, Mosler TP, Tseng PH, et al. Long-term prognosis associated with coronary calcification: observations from a registry of 25,253 patients. Journal of the American College of Cardiology. 2007;49(18):1860-70.

51.   Miedema MD, Dardari ZA, Kianoush S, Virani SS, Yeboah J, Knickelbine T, et al. Statin Eligibility, Coronary Artery Calcium, and Subsequent Cardiovascular Events According to the 2016 United States Preventive Services Task Force (USPSTF) Statin Guidelines: MESA (Multi-Ethnic Study of Atherosclerosis). J Am Heart Assoc. 2018;7(12).

52.   Mitchell JD, Fergestrom N, Gage BF, Paisley R, Moon P, Novak E, et al. Impact of Statins on Cardiovascular Outcomes Following Coronary Artery Calcium Scoring. J Am Coll Cardiol. 2018;72(25):3233-42.

53.   Nasir K. Message for 2018 Cholesterol Management Guidelines Update: Time to Accept the Power of Zero. J Am Coll Cardiol. 2018;72(25):3243-5.

54.   Taylor AJ, Raggi J, Raggi P. The power of nothing: the zero calcium score. J Cardiovasc Comput Tomogr. 2007;1(3):160-1.

55.   van Rosendael AR, van den Hoogen IJ, Gianni U, Ma X, Tantawy SW, Bax AM, et al. Association of Statin Treatment With Progression of Coronary Atherosclerotic Plaque Composition. JAMA Cardiol. 2021;6(11):1257-66.

56.   Lima TP, Assuncao AN, Bittencourt MS, Liberato G, Arbab-Zadeh A, Lima JAC, et al. Coronary computed tomography plaque-based scores predict long-term cardiovascular events. Eur Radiol. 2023;33(8):5436-45.

57.   Bittencourt MS, Hulten E, Ghoshhajra B, O'Leary D, Christman MP, Montana P, et al. Prognostic value of nonobstructive and obstructive coronary artery disease detected by coronary computed tomography angiography to identify cardiovascular events. Circ Cardiovasc Imaging. 2014;7(2):282-91.

58. Maurovich-Horvat P, Schlett CL, Alkadhi H, Nakano M, Otsuka F, Stolzmann P, et al. The napkin-ring sign indicates advanced atherosclerotic lesions in coronary CT angiography. JACC Cardiovasc Imaging. 2012;5(12):1243-52.

59. Thomsen C, Abdulla J. Characteristics of high-risk coronary plaques identified by computed tomographic angiography and associated prognosis: a systematic review and meta-analysis. Eur Heart J Cardiovasc Imaging. 2016;17(2):120-9.

60. Szilveszter B, Celeng C, Maurovich-Horvat P. Plaque assessment by coronary CT. Int J Cardiovasc Imaging. 2016;32(1):161-72.

61. Motoyama S, Kondo T, Sarai M, Sugiura A, Harigaya H, Sato T, et al. Multislice computed tomographic characteristics of coronary lesions in acute coronary syndromes. Journal of the American College of Cardiology. 2007;50(4):319-26.

62. Ozaki Y, Okumura M, Ismail TF, Motoyama S, Naruse H, Hattori K, et al. Coronary CT angiographic characteristics of culprit lesions in acute coronary syndromes not related to plaque rupture as defined by optical coherence tomography and angioscopy. Eur Heart J. 2011;32(22):2814-23.

63. Taylor AJ, Bindeman J, Feuerstein I, Cao F, Brazaitis M, O'Malley PG. Coronary calcium independently predicts incident premature coronary heart disease over measured cardiovascular risk factors: mean three-year outcomes in the Prospective Army Coronary Calcium (PACC) project. Journal of the American College of Cardiology. 2005;46(5):807-14.

64. Kataoka Y, Wolski K, Uno K, Puri R, Tuzcu EM, Nissen SE, et al. Spotty calcification as a marker of accelerated progression of coronary atherosclerosis: insights from serial intravascular ultrasound. Journal of the American College of Cardiology. 2012;59(18):1592-7.

65. Ehara S, Kobayashi Y, Yoshiyama M, Shimada K, Shimada Y, Fukuda D, et al. Spotty calcification typifies the culprit plaque in patients with acute myocardial infarction: an intravascular ultrasound study. Circulation. 2004;110(22):3424-9.

66. Motoyama S, Sarai M, Harigaya H, Anno H, Inoue K, Hara T, et al. Computed tomographic angiography characteristics of atherosclerotic plaques subsequently resulting in acute coronary syndrome. Journal of the American College of Cardiology. 2009;54(1):49-57.

67.   Seifarth H, Schlett CL, Nakano M, Otsuka F, Karolyi M, Liew G, et al. Histopathological correlates of the napkin-ring sign plaque in coronary CT angiography. Atherosclerosis. 2012;224(1):90-6.

68.   Maurovich-Horvat P, Ferencik M, Voros S, Merkely B, Hoffmann U. Comprehensive plaque assessment by coronary CT angiography. Nature reviews Cardiology. 2014;11(7):390-402.

69.   Otsuka K, Fukuda S, Tanaka A, Nakanishi K, Taguchi H, Yoshikawa J, et al. Napkin-ring sign on coronary CT angiography for the prediction of acute coronary syndrome. JACC Cardiovasc Imaging. 2013;6(4):448-57.

70.   Nadjiri J, Hausleiter J, Jahnichen C, Will A, Hendrich E, Martinoff S, et al. Incremental prognostic value of quantitative plaque assessment in coronary CT angiography during 5 years of follow up. J Cardiovasc Comput Tomogr. 2016;10(2):97-104.

71.   Williams MC, Kwiecinski J, Doris M, McElhinney P, D'Souza MS, Cadet S, et al. Low-Attenuation Noncalcified Plaque on Coronary Computed Tomography Angiography Predicts Myocardial Infarction: Results From the Multicenter SCOT-HEART Trial (Scottish Computed Tomography of the HEART). Circulation. 2020;141(18):1452-62.

72.   Vecsey-Nagy M, Kolossvary M, Varga-Szemes A, Boussoussou M, Vattay B, Nagy M, et al. Low-attenuation coronary plaque burden and troponin release in chronic coronary syndrome: A mediation analysis. J Cardiovasc Comput Tomogr. 2024;18(1):18-25.

73.   Nieman K, Garcia-Garcia HM, Hideo-Kajita A, Collet C, Dey D, Pugliese F, et al. Standards for quantitative assessments by coronary computed tomography angiography (CCTA): An expert consensus document of the society of cardiovascular computed tomography (SCCT). J Cardiovasc Comput Tomogr. 2024;18(5):429-43.

74.   Lee SE, Chang HJ, Sung JM, Park HB, Heo R, Rizvi A, et al. Effects of Statins on Coronary Atherosclerotic Plaques: The PARADIGM Study. JACC Cardiovasc Imaging. 2018;11(10):1475-84.

75.   Mergen V, Eberhard M, Manka R, Euler A, Alkadhi H. First in-human quantitative plaque characterization with ultra-high resolution coronary photon-counting CT angiography. Front Cardiovasc Med. 2022;9:981012.

76. Vecsey-Nagy M, Szilveszter B, Tremamunno G, Schoepf U, Zsarnóczay E, Maurovich-Horvat P, et al. Ultrahigh-resolution Photon-counting Detector Ct Detects A Significantly Lower Coronary Plaque Volume Than Energy-integrating Detector Ct. Journal of Cardiovascular Computed Tomography. 2025;19(1):S30.

77. Cury RC, Leipsic J, Abbara S, Achenbach S, Berman D, Bittencourt M, et al. CAD-RADS 2.0 - 2022 Coronary Artery Disease-Reporting and Data System: An Expert Consensus Document of the Society of Cardiovascular Computed Tomography (SCCT), the American College of Cardiology (ACC), the American College of Radiology (ACR), and the North America Society of Cardiovascular Imaging (NASCI). J Cardiovasc Comput Tomogr. 2022;16(6):536-57.

78. Pontone G, Baggiano A, Andreini D, Guaricci A, Guglielmo M, Muscogiuri G. Stress computed tomography perfusion versus fractional flow reserve CT derived in suspected coronary artery disease: the perfection study. JACC Cardiovasc Imaging. 2019;12(8 Pt 1):1487.

79. Baggiano A, Fusini L, Del Torto A, Vivona P, Guglielmo M, Muscogiuri G. Sequential strategy including FFRCT plus stress-CTP impacts on management of patients with stable chest pain: the stress-CTP RIPCORD study. J Clin Med. 2020;9(7).

80. Vattay B, Boussoussou M, Borzsák S, Vecsey-Nagy M, Simon J, Kolossváry M, et al. Myocardial perfusion imaging using computed tomography: Current status, clinical value and prognostic implications %J Imaging. 2021;13(1):49-60.

81. Tonino PA, Fearon WF, De Bruyne B, Oldroyd KG, Leesar MA, Ver Lee PN, et al. Angiographic versus functional severity of coronary artery stenoses in the FAME study fractional flow reserve versus angiography in multivessel evaluation. Journal of the American College of Cardiology. 2010;55(25):2816-21.

82. De Bruyne B, Pijls NH, Kalesan B, Barbato E, Tonino PA, Piroth Z, et al. Fractional flow reserve-guided PCI versus medical therapy in stable coronary disease. N Engl J Med. 2012;367(11):991-1001.

83. Boden W, O'Rourke R, Teo K, Hartigan P, Maron D, Kostuk W. Optimal medical therapy with or without PCI for stable coronary disease. 2007;356(15):1503.

84. Hachamovitch R, Hayes S, Friedman J, Cohen I, Berman D. Comparison of the short-term survival benefit associated with revascularization compared with medical

therapy in patients with no prior coronary artery disease undergoing stress myocardial perfusion single photon emission computed tomography. 2003;107(23):2900.

85.   Curzen N, Rana O, Nicholas Z, Golledge P, Zaman A, Oldroyd K. Does routine pressure wire assessment influence management strategy at coronary angiography for diagnosis of chest pain?: the RIPCORD study. 2014;7(2):248.

86.   Schuijf J, Wijns W, Jukema J, Atsma D, de Roos A, Lamb H. Relationship between noninvasive coronary angiography with multi-slice computed tomography and myocardial perfusion imaging. 2006;48(12):2508.

87.   Patel A, Bamberg F, Branch K, Carrascosa P, Chen M, Cury R. Society of cardiovascular computed tomography expert consensus document on myocardial computed tomography perfusion imaging. 2020;14(1):87.

88.   Techasith T, Cury R. Stress myocardial CT perfusion: an update and future perspective. 2011;4(8):905.

89.   Baxa J, Hromadka M, Sedivy J, Stepankova L, Molacek J, Schmidt B. Regadenoson-stress dynamic myocardial perfusion improves diagnostic performance of CT angiography in assessment of intermediate coronary artery stenosis in asymptomatic patients. 2015;2015:105629.

90.   Seitun S, Castiglione Morelli M, Budaj I, Boccalini S, Galletto Pregliasco A, Valbusa A. Stress computed tomography myocardial perfusion imaging: a new topic in cardiology. 2016;69(2):188.

91.   Bischoff B, Bamberg F, Marcus R, Schwarz F, Becker H, Becker A. Optimal timing for first-pass stress CT myocardial perfusion imaging. 2013;29(2):435.

92.   George R, Jerosch-Herold M, Silva C, Kitagawa K, Bluemke D, Lima J. Quantification of myocardial perfusion using dynamic 64-detector computed tomography. 2007;42(12):815.

93.   Danad I, Szymonifka J, Schulman-Marcus J, Min J. Static and dynamic assessment of myocardial perfusion by computed tomography. 2016;17(8):836.

94.   Pontone G, Baggiano A, Andreini D, Guaricci A, Guglielmo M, Muscogiuri G. Dynamic stress computed tomography perfusion with a whole-heart coverage scanner in addition to coronary computed tomography angiography and fractional flow reserve computed tomography derived. 2019;12(12):2460.

95.   Rossi A, Dharampal A, Wragg A, Davies L, van Geuns R, Anagnostopoulos C. Diagnostic performance of hyperaemic myocardial blood flow index obtained by dynamic computed tomography: does it predict functionally significant coronary lesions? 2014;15(1):85.

96.   Bamberg F, Marcus R, Becker A, Hildebrandt K, Bauner K, Schwarz F. Dynamic myocardial CT perfusion imaging for evaluation of myocardial ischemia as determined by MR imaging. 2014;7(3):267.

97.   Bamberg F, Becker A, Schwarz F, Marcus R, Greif M, von Ziegler F. Detection of hemodynamically significant coronary artery stenosis: incremental diagnostic value of dynamic CT-based myocardial perfusion imaging. 2011;260(3):689.

98.   Coenen A, Rossi A, Lubbers M, Kurata A, Kono A, Chelu R. Integrating CT myocardial perfusion and CT-FFR in the work-up of coronary artery disease. 2017;10(7):760.

99.   Kono A, Coenen A, Lubbers M, Kurata A, Rossi A, Dharampal A. Relative myocardial blood flow by dynamic computed tomographic perfusion imaging predicts hemodynamic significance of coronary stenosis better than absolute blood flow. 2014;49(12):801.

100.   Rossi A, Wragg A, Klotz E, Pirro F, Moon J, Nieman K. Dynamic computed tomography myocardial perfusion imaging: comparison of clinical analysis methods for the detection of vessel-specific ischemia. 2017;10(4).

101.   Greif M, von Ziegler F, Bamberg F, Tittus J, Schwarz F, D'Anastasi M. CT stress perfusion imaging for detection of haemodynamically relevant coronary stenosis as defined by FFR. 2013;99(14):1004.

102.   Kikuchi Y, Oyama-Manabe N, Naya M, Manabe O, Tomiyama Y, Sasaki T. Quantification of myocardial blood flow using dynamic 320-row multi-detector CT as compared with (1)(5)O-H(2)O PET. Eur Radiol. 2014;24(7):1547.

103.   Bettencourt N, Chiribiri A, Schuster A, Ferreira N, Sampaio F, Pires-Morais G. Direct comparison of cardiac magnetic resonance and multidetector computed tomography stress-rest perfusion imaging for detection of coronary artery disease. J Am College Cardiol. 2013;61(10):1099.

104. Ko B, Cameron J, Meredith I, Leung M, Antonis P, Nasis A. Computed tomography stress myocardial perfusion imaging in patients considered for revascularization: a comparison with fractional flow reserve. Eur Heart J. 2012;33(1):67.

105. Tamarappoo B, Gutstein A, Cheng V, Nakazato R, Gransar H, Dey D. Assessment of the relationship between stenosis severity and distribution of coronary artery stenoses on multislice computed tomographic angiography and myocardial ischemia detected by single photon emission computed tomography. J Nucl Cardiol. 2010;17(5):791.

106. George R, Mehra V, Chen M, Kitagawa K, Arbab-Zadeh A, Miller J. Myocardial CT perfusion imaging and SPECT for the diagnosis of coronary artery disease: a head-to-head comparison from the CORE320 multicenter diagnostic performance study. Radiology. 2014;272(2):407.

107. Takx R, Blomberg B, El Aidi H, Habets J, de Jong P, Nagel E. Diagnostic accuracy of stress myocardial perfusion imaging compared to invasive coronary angiography with fractional flow reserve meta-analysis. Circ Cardiovasc Imaging. 2015;8(1).

108. Sorgaard M, Kofoed K, Linde J, George R, Rochitte C, Feuchtner G. Diagnostic accuracy of static CT perfusion for the detection of myocardial ischemia. A systematic review and meta-analysis. J Cardiovasc Comput Tomogr. 2016;10(6):450.

109. Vrints C, Andreotti F, Koskinas KC, Rossello X, Adamo M, Ainslie J, et al. 2024 ESC Guidelines for the management of chronic coronary syndromes: Developed by the task force for the management of chronic coronary syndromes of the European Society of Cardiology (ESC) Endorsed by the European Association for Cardio-Thoracic Surgery (EACTS). European Heart Journal. 2024;45(36):3415-537.

110. Hoffmann U, Ferencik M, Udelson JE, Picard MH, Truong QA, Patel MR, et al. Prognostic Value of Noninvasive Cardiovascular Testing in Patients With Stable Chest Pain: Insights From the PROMISE Trial (Prospective Multicenter Imaging Study for Evaluation of Chest Pain). Circulation. 2017;135(24):2320-32.

111. Investigators S-H, Newby DE, Adamson PD, Berry C, Boon NA, Dweck MR, et al. Coronary CT Angiography and 5-Year Risk of Myocardial Infarction. N Engl J Med. 2018;379(10):924-33.

112. Hadamitzky M, Achenbach S, Al-Mallah M, Berman D, Budoff M, Cademartiri F, et al. Optimized Prognostic Score for Coronary Computed Tomographic Angiography. JACC. 2013;62(5):468-76.

113. Ferencik M, Hoffmann U. High-Risk Coronary Plaque on Computed Tomography Angiography: Time to Recognize a New Imaging Risk Factor. Circ Cardiovasc Imaging. 2018;11(1):e007288.

114. Williams MC, Moss AJ, Dweck M, Adamson PD, Alam S, Hunter A, et al. Coronary Artery Plaque Characteristics Associated With Adverse Outcomes in the SCOT-HEART Study. J Am Coll Cardiol. 2019;73(3):291-301.

115. Ferencik M, Mayrhofer T, Bittner DO, Emami H, Puchner SB, Lu MT, et al. Use of High-Risk Coronary Atherosclerotic Plaque Detection for Risk Stratification of Patients With Stable Chest Pain: A Secondary Analysis of the PROMISE Randomized Clinical Trial. JAMA Cardiol. 2018;3(2):144-52.

116. Gannon MP, Cerci RJ, Valdiviezo C, Ostovaneh MR, Vavere AL, de Vasconcellos HD, et al. Combined Computed Tomography Angiography-Computed Tomography Perfusion in the Identification and Prognostic Assessment of Myocardial Bridging from the CORE320 Study: 5-Year Follow-Up. The American Journal of Cardiology. 2023;207:314-21.

117. Sandfort V, Persson M, Pourmorteza A, Noel PB, Fleischmann D, Willemink MJ. Spectral photon-counting CT in cardiovascular imaging. J Cardiovasc Comput Tomogr. 2021;15(3):218-25.

118. Willemink MJ, Persson M, Pourmorteza A, Pelc NJ, Fleischmann D. Photon-counting CT: Technical Principles and Clinical Prospects. Radiology. 2018;289(2):293-312.

119. Grant KL, Flohr TG, Krauss B, Sedlmair M, Thomas C, Schmidt B. Assessment of an advanced image-based technique to calculate virtual monoenergetic computed tomographic images from a dual-energy examination to improve contrast-to-noise ratio in examinations using iodinated contrast media. Invest Radiol. 2014;49(9):586-92.

120. Boussel L, Coulon P, Thran A, Roessl E, Martens G, Sigovan M, et al. Photon counting spectral CT component analysis of coronary artery atherosclerotic plaque samples. Br J Radiol. 2014;87(1040):20130798.

121. Vecsey-Nagy M, Tremamunno G, Schoepf UJ, Gnasso C, Zsarnoczay E, Fink N, et al. Intraindividual Comparison of Ultrahigh-Spatial-Resolution Photon-Counting Detector CT and Energy-Integrating Detector CT for Coronary Stenosis Measurement. Circ Cardiovasc Imaging. 2024;17(10):e017112.

122. Vecsey-Nagy M, Tremamunno G, Schoepf UJ, Gnasso C, Zsarnoczay E, Fink N, et al. Coronary Plaque Quantification with Ultrahigh-Spatial-Resolution Photon-counting Detector CT: Intraindividual Comparison with Energy-integrating Detector CT. Radiology. 2025;314(3):e241479.

123. Simon J, Hrenko A, Kerkovits NM, Nagy K, Vertes M, Balogh H, et al. Photon-counting detector CT reduces the rate of referrals to invasive coronary angiography as compared to CT with whole heart coverage energy-integrating detector. J Cardiovasc Comput Tomogr. 2024;18(1):69-74.

124. Vecsey-Nagy M, Emrich T, Tremamunno G, Kravchenko D, Taha Hagar M, Laux GS, et al. Cost-effectiveness of ultrahigh-resolution photon-counting detector coronary CT angiography for the evaluation of stable chest pain. J Cardiovasc Comput Tomogr. 2025;19(1):106-12.

125. Abbara S, Blanke P, Maroules CD, Cheezum M, Choi AD, Han BK, et al. SCCT guidelines for the performance and acquisition of coronary computed tomographic angiography: A report of the society of Cardiovascular Computed Tomography Guidelines Committee: Endorsed by the North American Society for Cardiovascular Imaging (NASCI). J Cardiovasc Comput Tomogr. 2016;10(6):435-49.

126. Karady J, Panajotu A, Kolossvary M, Szilveszter B, Jermendy AL, Bartykowszki A, et al. The effect of four-phasic versus three-phasic contrast media injection protocols on extravasation rate in coronary CT angiography: a randomized controlled trial. Eur Radiol. 2017;27(11):4538-43.

127. Mahabadi AA, Bamberg F, Toepker M, Schlett CL, Rogers IS, Nagurney JT, et al. Association of aortic valve calcification to the presence, extent, and composition of coronary artery plaque burden: from the Rule Out Myocardial Infarction using Computer Assisted Tomography (ROMICAT) trial. Am Heart J. 2009;158(4):562-8.

128. Achenbach S, Moselewski F, Ropers D, Ferencik M, Hoffmann U, MacNeill B, et al. Detection of calcified and noncalcified coronary atherosclerotic plaque by contrast-

enhanced, submillimeter multidetector spiral computed tomography: a segment-based comparison with intravascular ultrasound. Circulation. 2004;109(1):14-7.

129.   Cury RC, Abbara S, Achenbach S, Agatston A, Berman DS, Budoff MJ, et al. CAD-RADS: Coronary Artery Disease - Reporting and Data System: An Expert Consensus Document of the Society of Cardiovascular Computed Tomography (SCCT), the American College of Radiology (ACR) and the North American Society for Cardiovascular Imaging (NASCI). Endorsed by the American College of Cardiology. J Am Coll Radiol. 2016;13(12 Pt A):1458-66 e9.

130.   Tanabe Y, Kido T, Uetani T, Kurata A, Kono T, Ogimoto A, et al. Differentiation of myocardial ischemia and infarction assessed by dynamic computed tomography perfusion imaging and comparison with cardiac magnetic resonance and single-photon emission computed tomography. Eur Radiol. 2016;26(11):3790-801.

131.   Pontone G, Baggiano A, Andreini D, Guaricci AI, Guglielmo M, Muscogiuri G, et al. Dynamic Stress Computed Tomography Perfusion With a Whole-Heart Coverage Scanner in Addition to Coronary Computed Tomography Angiography and Fractional Flow Reserve Computed Tomography Derived. JACC Cardiovasc Imaging. 2019;12(12):2460-71.

132.   Nous FMA, Geisler T, Kruk MBP, Alkadhi H, Kitagawa K, Vliegenthart R, et al. Dynamic Myocardial Perfusion CT for the Detection of Hemodynamically Significant Coronary Artery Disease. JACC Cardiovasc Imaging. 2022;15(1):75-87.

133.   Cerci RJ, Arbab-Zadeh A, George RT, Miller JM, Vavere AL, Mehra V, et al. Aligning coronary anatomy and myocardial perfusion territories: an algorithm for the CORE320 multicenter study. Circ Cardiovasc Imaging. 2012;5(5):587-95.

134.   Kolossvary M, Karady J, Szilveszter B, Kitslaar P, Hoffmann U, Merkely B, et al. Radiomic Features Are Superior to Conventional Quantitative Computed Tomographic Metrics to Identify Coronary Plaques With Napkin-Ring Sign. Circ Cardiovasc Imaging. 2017;10(12):e006843.

135.   Kolossvary M, Bluemke DA, Fishman EK, Gerstenblith G, Celentano D, Mandler RN, et al. Temporal assessment of lesion morphology on radiological images beyond lesion volumes-a proof-of-principle study. Eur Radiol. 2022;32(12):8748-60.

136.   Kolossvary M, Gerstenblith G, Bluemke DA, Fishman EK, Mandler RN, Kickler TS, et al. Contribution of Risk Factors to the Development of Coronary Atherosclerosis

as Confirmed via Coronary CT Angiography: A Longitudinal Radiomics-based Study. Radiology. 2021;299(1):97-106.

137.   Ferencik M, Mayrhofer T, Puchner SB, Lu MT, Maurovich-Horvat P, Liu T, et al. Computed tomography-based high-risk coronary plaque score to predict acute coronary syndrome among patients with acute chest pain--Results from the ROMICAT II trial. J Cardiovasc Comput Tomogr. 2015;9(6):538-45.

138.   Ahmadi A, Leipsic J, Blankstein R, Taylor C, Hecht H, Stone GW, et al. Do plaques rapidly progress prior to myocardial infarction? The interplay between plaque vulnerability and progression. Circ Res. 2015;117(1):99-104.

139.   Ahmadi A, Argulian E, Leipsic J, Newby DE, Narula J. From Subclinical Atherosclerosis to Plaque Progression and Acute Coronary Events: JACC State-of-the-Art Review. J Am Coll Cardiol. 2019;74(12):1608-17.

140.   Gu H, Lu B, Gao Y, Hou Z, Yang S, Yuan X, et al. Prognostic Value of Atherosclerosis Progression for Prediction of Cardiovascular Events in Patients with Nonobstructive Coronary Artery Disease. Acad Radiol. 2021;28(7):980-7.

141.   Won KB, Lee SE, Lee BK, Park HB, Heo R, Rizvi A, et al. Longitudinal quantitative assessment of coronary plaque progression related to body mass index using serial coronary computed tomography angiography. Eur Heart J Cardiovasc Imaging. 2019;20(5):591-9.

142.   Lehman SJ, Schlett CL, Bamberg F, Lee H, Donnelly P, Shturman L, et al. Assessment of coronary plaque progression in coronary computed tomography angiography using a semiquantitative score. JACC Cardiovasc Imaging. 2009;2(11):1262-70.

143.   Nakanishi R, Ceponiene I, Osawa K, Luo Y, Kanisawa M, Megowan N, et al. Plaque progression assessed by a novel semi-automated quantitative plaque software on coronary computed tomography angiography between diabetes and non-diabetes patients: A propensity-score matching study. Atherosclerosis. 2016;255:73-9.

144.   Won KB, Lee SE, Lee BK, Park HB, Heo R, Rizvi A, et al. Longitudinal assessment of coronary plaque volume change related to glycemic status using serial coronary computed tomography angiography: A PARADIGM (Progression of AtheRosclerotic PlAque DetermIned by Computed TomoGraphic Angiography Imaging) substudy. J Cardiovasc Comput Tomogr. 2019;13(2):142-7.

145.   Nadjiri J, Hausleiter J, Deseive S, Will A, Hendrich E, Martinoff S, et al. Prognostic value of coronary CT angiography in diabetic patients: a 5-year follow up study. Int J Cardiovasc Imaging. 2016;32(3):483-91.

146.   Yu MM, Tang XL, Zhao X, Chen YY, Xu ZH, Wang QB, et al. Plaque progression at coronary CT angiography links non-alcoholic fatty liver disease and cardiovascular events: a prospective single-center study. Eur Radiol. 2022;32(12):8111-21.

147.   Kolossvary M, Fishman EK, Gerstenblith G, Bluemke DA, Mandler RN, Celentano D, et al. Cardiovascular risk factors and illicit drug use may have a more profound effect on coronary atherosclerosis progression in people living with HIV. Eur Radiol. 2021;31(5):2756-67.

148.   Symons R, Morris JZ, Wu CO, Pourmorteza A, Ahlman MA, Lima JA, et al. Coronary CT Angiography: Variability of CT Scanners and Readers in Measurement of Plaque Volume. Radiology. 2016;281(3):737-48.

149.   Min JK, Shaw LJ, Devereux RB, Okin PM, Weinsaft JW, Russo DJ, et al. Prognostic value of multidetector coronary computed tomographic angiography for prediction of all-cause mortality. Journal of the American College of Cardiology. 2007;50(12):1161-70.

150.   Cury RC, Leipsic J, Abbara S, Achenbach S, Berman D, Bittencourt M, et al. CAD-RADS™ 2.0 - 2022 Coronary Artery Disease-Reporting and Data System: An Expert Consensus Document of the Society of Cardiovascular Computed Tomography (SCCT), the American College of Cardiology (ACC), the American College of Radiology (ACR), and the North America Society of Cardiovascular Imaging (NASCI). Journal of Cardiovascular Computed Tomography. 2022;16(6):536-57.

151.   Diaz-Zamudio M, Fuchs TA, Slomka P, Otaki Y, Arsanjani R, Gransar H, et al. Quantitative plaque features from coronary computed tomography angiography to identify regional ischemia by myocardial perfusion imaging. Eur Heart J Cardiovasc Imaging. 2017;18(5):499-507.

152.   Liu T, Yuan X, Wang C, Sun M, Jin S, Dai X. Quantification of plaque characteristics detected by dual source computed tomography angiography to predict myocardial ischemia as assessed by single photon emission computed tomography myocardial perfusion imaging. Quant Imaging Med Surg. 2019;9(4):711-21.

153. Stuijfzand WJ, van Rosendael AR, Lin FY, Chang HJ, van den Hoogen IJ, Gianni U, et al. Stress Myocardial Perfusion Imaging vs Coronary Computed Tomographic Angiography for Diagnosis of Invasive Vessel-Specific Coronary Physiology: Predictive Modeling Results From the Computed Tomographic Evaluation of Atherosclerotic Determinants of Myocardial Ischemia (CREDENCE) Trial. JAMA Cardiol. 2020;5(12):1338-48.

154. Driessen RS, Stuijfzand WJ, Raijmakers PG, Danad I, Min JK, Leipsic JA, et al. Effect of Plaque Burden and Morphology on Myocardial Blood Flow and Fractional Flow Reserve. J Am Coll Cardiol. 2018;71(5):499-509.

155. van Rosendael AR, Kroft LJ, Broersen A, Dijkstra J, van den Hoogen IJ, van Zwet EW, et al. Relation between quantitative coronary CTA and myocardial ischemia by adenosine stress myocardial CT perfusion. J Nucl Cardiol. 2017;24(4):1253-62.

156. Kero T, Bar S, Saraste A, Klen R, Bax JJ, Knuuti J, et al. Plaque burden improves the detection of ischemic CAD over stenosis from coronary computed tomography angiography. Int J Cardiovasc Imaging. 2025.

157. Schuijf JD, Wijns W, Jukema JW, Atsma DE, de Roos A, Lamb HJ, et al. Relationship between noninvasive coronary angiography with multi-slice computed tomography and myocardial perfusion imaging. Journal of the American College of Cardiology. 2006;48(12):2508-14.

158. Min JK, Chang HJ, Andreini D, Pontone G, Guglielmo M, Bax JJ, et al. Coronary CTA plaque volume severity stages according to invasive coronary angiography and FFR. J Cardiovasc Comput Tomogr. 2022;16(5):415-22.

159. Gulati M, Levy PD, Mukherjee D, Amsterdam E, Bhatt DL, Birtcher KK, et al. 2021 AHA/ACC/ASE/CHEST/SAEM/SCCT/SCMR Guideline for the Evaluation and Diagnosis of Chest Pain: Executive Summary: A Report of the American College of Cardiology/American Heart Association Joint Committee on Clinical Practice Guidelines. Circulation. 2021;144(22):e368-e454.

160. Nadjiri J, Hausleiter J, Jähnichen C, Will A, Hendrich E, Martinoff S, et al. Incremental prognostic value of quantitative plaque assessment in coronary CT angiography during 5 years of follow up. Journal of Cardiovascular Computed Tomography. 2016;10(2):97-104.

161. Chang H-J, Lin FY, Lee S-E, Andreini D, Bax J, Cademartiri F, et al. Coronary Atherosclerotic Precursors of Acute Coronary Syndromes. Journal of the American College of Cardiology. 2018;71(22):2511-22.

162. Sartoretti T, McDermott M, Mergen V, Euler A, Schmidt B, Jost G, et al. Photon-counting detector coronary CT angiography: impact of virtual monoenergetic imaging and iterative reconstruction on image quality. Br J Radiol. 2023;96(1143):20220466.

163. Ohta Y, Kitao S, Watanabe T, Kishimoto J, Yamamoto K, Ogawa T. Evaluation of image quality of coronary artery plaque with rapid kVp-switching dual-energy CT. Clinical Imaging. 2017;43:42-9.

164. Rajendran K, Petersilka M, Henning A, Shanblatt ER, Schmidt B, Flohr TG, et al. First Clinical Photon-counting Detector CT System: Technical Evaluation. Radiology. 2022;303(1):130-8.

165. Mergen V, Ried E, Allmendinger T, Sartoretti T, Higashigaito K, Manka R, et al. Epicardial Adipose Tissue Attenuation and Fat Attenuation Index: Phantom Study and In Vivo Measurements With Photon-Counting Detector CT. AJR Am J Roentgenol. 2022;218(5):822-9.

166. Eberhard M, Mergen V, Higashigaito K, Allmendinger T, Manka R, Flohr T, et al. Coronary Calcium Scoring with First Generation Dual-Source Photon-Counting CT-First Evidence from Phantom and In-Vivo Scans. Diagnostics (Basel). 2021;11(9).

167. Symons R, Choi Y, Cork TE, Ahlman MA, Mallek M, Bluemke DA, et al. Optimized energy of spectral coronary CT angiography for coronary plaque detection and quantification. J Cardiovasc Comput Tomogr. 2018;12(2):108-14.

168. Matsumoto H, Watanabe S, Kyo E, Tsuji T, Ando Y, Otaki Y, et al. Standardized volumetric plaque quantification and characterization from coronary CT angiography: a head-to-head comparison with invasive intravascular ultrasound. Eur Radiol. 2019;29(11):6129-39.

169. Meah MN, Singh T, Williams MC, Dweck MR, Newby DE, Slomka P, et al. Reproducibility of quantitative plaque measurement in advanced coronary artery disease. J Cardiovasc Comput Tomogr. 2021;15(4):333-8.

170. Cademartiri F, Mollet NR, Runza G, Bruining N, Hamers R, Somers P, et al. Influence of intracoronary attenuation on coronary plaque measurements using multislice

computed tomography: observations in an ex vivo model of coronary computed tomography angiography. Eur Radiol. 2005;15(7):1426-31.

10. BIBLIOGRAPHY OF THE CANDIDATE'S PUBLICATIONS (Σ IF: 145.228)

10.1 Publications discussed in the present thesis (Σ IF: 14.6)

1. Szilveszter B*, **Vattay B***, Bossoussou M, Vecsey-Nagy M, Simon J, Merkely B, Maurovich-Horvat P, Kolossvary M. (2022) CAD-RADS may underestimate coronary plaque progression as detected by serial CT angiography. Eur Heart J Cardiovasc Imaging, 23: 1530-1539. **(SJR: D1; IF: 6.3)**

2. **Vattay B**, Borzsak S, Boussoussou M, Vecsey-Nagy M, Jermendy Á L, Suhai F I, Maurovich-Horvat P, Merkely B, Kolossvary M, Szilveszter B. (2022) Association between coronary plaque volume and myocardial ischemia detected by dynamic perfusion CT imaging. Front Cardiovasc Med, 9: 974805. **(SJR: Q1; IF: 3.6)**

3. **Vattay B**, Szilveszter B, Boussoussou M, Vecsey-Nagy M, Lin A, Konkoly G, Kubovje A, Schwarz F, Merkely B, Maurovich-Horvat P, Williams M C, Dey D, Kolossvary M. (2023) Impact of Virtual Monoenergetic Levels on Coronary Plaque Volume Components using Photon-Counting Computed Tomography. Eur Radiol 33: 8528-8539 **(SJR: D1; IF: 4.7)**

4. **Vattay B**, Boussoussou M, Borzsák S, Vecsey-Nagy M, Simon J, Kolossváry M, Merkely B, Szilveszter B. (2021) Myocardial perfusion imaging using computed tomography: Current status, clinical value and prognostic implications. Imaging, 13: 49-60. **(SJR: Q4; IF: 0)**

10.2 Publications not related to the present thesis

1. Juhász D, Vecsey-Nagy M, Jermendy ÁL, Szilveszter B, Simon J, **Vattay B**, Boussoussou M, Dávid D, Maurovich-Horvát P, Merkely B, Apor A, Molnár L, Dósa E, Rakovics M, Johnson J, Manouras A, Nagy AI. (2025) Prognostic and therapeutic implications of a low aortic valve calcium score in patients with low-gradient aortic stenosis. Eur Heart J Cardiovasc Imaging. 26(2): 287-298.

2. Kravchenko D, Hagar MT, Vecsey-Nagy M, Tremamunno G, Szilveszter B, **Vattay B**, Zsarnóczay E, Beke S, Maurovich-Horvat P, Emrich T, Varga-Szemes A. (2025) Value of Ultrahigh-Resolution Photon-Counting Detector Computed Tomography in Cardiac Imaging. Echocardiography. 42(2): e70100.

3. Vecsey-Nagy M, Kolossváry M, Varga-Szemes A, Boussoussou M, **Vattay B**, Nagy M, Juhász D, Merkely B, Radovits T, Szilveszter B. (2024) Low-attenuation coronary plaque burden and troponin release in chronic coronary syndrome: A mediation analysis. J Cardiovasc Comput Tomogr. 18(1): 18-25.

4. Simon J, Hrenkó Á, Kerkovits NM, Nagy K, Vértes M, Balogh H, Nagy N, Munkácsi T, Emrich T, Varga-Szemes A, Boussoussou M, **Vattay B**, Vecsey-Nagy M, Kolossváry M, Szilveszter B, Merkely B, Maurovich-Horvat P. (2024) Photon-counting detector CT reduces the rate of referrals to invasive coronary angiography as compared to CT with whole heart coverage energy-integrating detector. J Cardiovasc Comput Tomogr. 18(1): 69-74.

5. Weichsel L, Giesen A, André F, Renker M, Baumann S, Breitbart P, Beer M, Maurovitch-Horvat P, Szilveszter B, **Vattay B**, Buss SJ, Marwan M, Giannopoulos AA, Kelle S, Frey N, Korosoglou G. (2024) Comparison of Two Contemporary Quantitative Atherosclerotic Plaque Assessment Tools for Coronary Computed Tomography Angiography: Single-Center Analysis and Multi-Center Patient Cohort Validation. Diagnostics (Basel). 9;14(2):154.

6. **Vattay B**, Boussoussou M, Vecsey-Nagy M, Kolossváry M, Juhász D, Kerkovits N, Balogh H, Nagy N, Vértes M, Kiss M, Kubovje A, Merkely B, Maurovich Horvat P, Szilveszter B. (2024) Qualitative and quantitative image quality of coronary CT angiography using photon-counting computed tomography: Standard and Ultra-high resolution protocols. Eur J Radiol. 175: 111426.

7. Vecsey-Nagy M, Varga-Szemes A, Schoepf UJ, Tremamunno G, Fink N, Zsarnoczay E, Szilveszter B, Graafen D, Halfmann MC, **Vattay B**, Boussoussou M, O'Doherty J, Suranyi PS, Maurovich-Horvat P, Emrich T. (2024) Ultra-high resolution coronary CT angiography on photon-counting detector CT: bi-centre study on the impact of quantum iterative reconstruction on image quality and accuracy of stenosis measurements. Eur J Radiol. 176: 111517.

8. Sipos B, Vecsey-Nagy M, **Vattay B**, Boussoussou M, Jokkel Z, Borzsák S, Jermendy Á, Panajotu A, Gonda X, Rihmer Z, Merkely B, Szilveszter B, Nemcsik J. (2024) Association between affective temperaments and the severity and the extent of coronary artery disease as obtained by coronary CT angiography. J Affect Disord. 363: 47-54.

9. Weichsel L, André F, Renker M, Breitbart P, Overhoff D, Beer M, Giesen A, **Vattay B**, Buss S, Marwan M, Schlett CL, Giannopoulos AA, Kelle S, Frey N, Korosoglou G, Giusca S, Schütz M, Weberling LD, Schmitt R, Schoenberg SO, Kuru M, Klömpken S, Bálint Sz, Maurovich-Horvat P, Görich J, Emami M, Kaufmann PA, Doeblin P, Solowjawa N, Weiss KJ, Baumann S, Stach K, The LOCATE Investigators. (2024) Effects of high- versus low-intensity lipid-lowering treatment in patients undergoing serial coronary computed tomography angiography: results of the multi-center LOCATE study. Clin Res Cardiol.

10. Boussoussou M, **Vattay B**, Szilveszter B, Simon J, Lin A, Vecsey-Nagy M, Konkoly G, Merkely B, Maurovich-Horvat P, Dey D, Kolossváry M. (2023) The effect of patient and imaging characteristics on coronary CT angiography assessed pericoronary adipose tissue attenuation and gradient. J Cardiovasc Comput Tomogr. 17(1): 34-42.

11. Panajotu A, Vecsey-Nagy M, Jermendy ÁL, Boussoussou M, **Vattay B**, Kolossváry M, Dombrády ÖZs, Csobay-Novák Cs, Merkely B, Szilveszter B. (2023) Coronary CTA Amidst the COVID-19 Pandemic: A Quicker Examination Protocol with Preserved Image Quality Using a Dedicated Cardiac Scanner. Diagnostics (Basel) 13(3).

12. Vecsey-Nagy M, Jokkel Zs, Jermendy ÁL, Nagy M, Boussoussou M, **Vattay B**, Kolossváry M, Csobay-Novák Cs, Amin-Spector S, Merkely B, Szilveszter B. (2023) The Impact of Novel Reconstruction Algorithms on Calcium Scoring: Results on a Dedicated Cardiac CT Scanner. Diagnostics (Basel) 13(4).

13. Boussoussou M, Édes IF, Nowotta F, **Vattay B**, Vecsey-Nagy M, Drobni Z, Simon J, Kolossváry M, Németh B, Jermendy ÁL, Becker D, Leipsic J, Rogers C, Collinsworth A, Maurovich-Horvat P, Merkely B, Szilveszter B. (2023) Coronary CT-based FFR in patients with acute myocardial infarction might predict follow-up invasive FFR: The XPECT-MI study. J Cardiovasc Comput Tomogr. 17(4): 269-276.

14. Vecsey-Nagy M, Varga-Szemes A, Emrich T, Zsarnóczai E, Nagy N, Fink N, Schmidt B, Nowak T, Kiss M, **Vattay B**, Boussouss M, Kolossváry M, Kubovje A, Merkely B, Maurovich-Horvat P, Szilveszter B. (2023) Calcium scoring on coronary computed angiography tomography with photon-counting detector technology: Predictors of performance. J Cardiovasc Comput Tomogr 17(5): 328-335.

15. Nagy FT, Olajos D, **Vattay B**, Borzsák S, Boussoussou M, Deák M, Vecsey-Nagy M, Sipos B, Jermendy ÁL, Tóth GG, Nemes B, Merkely B, Szili-Török T, Ruzsa Z, Szilveszter B. (2023) Dynamic Perfusion Computed Tomography for the Assessment of Concomitant Coronary Artery Disease in Patients with a History of Percutaneous Transluminal Angioplasty for Chronic Limb-Threatening Ischemia-A Pilot Study. J Cardiovasc Dev Dis. 10(11): 443.

16. Juhász D, **Vattay B**, Boussoussou M, Vecsey-Nagy M, Jokkel Zs, Jermendy ÁL, Merkely B, Édes IF, Szilveszter B. (2023) Korszerű koronáriaintervenció CT-vezérléssel: terápiás tervezés és előnyök. CARDIOLOGIA HUNGARICA 53: 571-576.

17. Simon J, Herczeg Sz, Borzsák S, Csőre J, Kardos AS, Mérges G, Zsarnóczay E, Szegedi N, Boussoussou M, **Vattay B**, Kolossváry M, Szilveszter B, Gellér L, Merkely B, Maurovich-Horvat P. (2022) Extracardiac findings on cardiac computed tomography in patients undergoing atrial fibrillation catheter ablation. Imaging 14: 52-59.

18. Boussoussou M, Szilveszter B, **Vattay B**, Kolossváry M, Vecsey-Nagy M, Salló Z, Orbán G, Perge P, Piros K, Nagy KV, Osztheimer I, Maurovich-Horvat P, Merkely B, Gellér L, Szegedi N. (2022) The effect of left atrial wall thickness and pulmonary vein sizes on the acute procedural success of atrial fibrillation ablation. Int J Cardiovasc Imaging 38(7): 1601-1611.

19. Vecsey-Nagy M, Szilveszter B, Kolossváry M, Boussoussou M, **Vattay B**, Merkely B, Maurovich-Horvat P, Radovits T, Nemcsik J. (2022) Correlation between Coronary Artery Calcium- and Different Cardiovascular Risk Score-Based Methods for the Estimation of Vascular Age in Caucasian Patients. J Clin Med 11(4).

20. **Vattay B**, Nagy A I, Apor A, Kolossváry M, Manouras A, Vecsey-Nagy M, Molnár L, Boussoussou M, Bartykowszki A, Jermendy ÁL, Kováts T, Zsarnóczay E, Maurovich-Horvat P, Merkely B, Szilveszter B. (2022) The Predictive Value of Left Atrial Strain Following Transcatheter Aortic Valve Implantation on Anatomical and Functional Reverse Remodeling in a Multi-Modality Study. Front Cardiovasc Med 9: 841658.

21. Vecsey-Nagy M, Szilveszter B, Kolossváry M, Boussoussou M, **Vattay B**, Gonda X, Rihmer Z, Merkely B, Maurovich-Horvat P, Nemcsik J. (2022) Cyclothymic

affective temperament is independently associated with left ventricular hypertrophy in chronic hypertensive patients. J Psychosom Res 160: 110988.

22. Vecsey-Nagy M, Jermendy ÁL, Kolossváry M, **Vattay B**, Boussoussou M, Suhai FI, Panajotu A, Csőre J, Borzsák S, Fontanini DM, Csobay-Novák Cs, Merkely B, Maurovich-Horvat P, Szilveszter B. (2022) Heart Rate-Dependent Degree of Motion Artifacts in Coronary CT Angiography Acquired by a Novel Purpose-Built Cardiac CT Scanner. J Clin Med 11(15).

23. Papp S, Bárczi Gy, Karády J, Kolossváry M, Drobni ZsD, Simon J, Boussoussou M, **Vattay B**, Szilveszter B, Jermendy Gy, Merkely B, Maurovich-Horvat P. (2021) Coronary plaque burden of the left anterior descending artery in patients with or without myocardial bridge: A case-control study based on coronary CT-angiography. Int J Cardiol 327: 231-235.

24. Piros E A, Szilveszter B, **Vattay B**, Maurovich-Horvat P, Szalai K, Dósa E, Merkely B, Holló P. (2021) Novel anti-inflammatory therapies to reduce cardiovascular burden of psoriasis. Dermatol Ther 34(1): e14721.

25. Boussoussou M, **Vattay B**, Szilveszter B, Kolossváry M, Simon J, Vecsey-Nagy M, Merkely B, Maurovich-Horvat P. (2021) Functional assessment of coronary plaques using CT based hemodynamic simulations: current status, technical principles and clinical value. Imaging 13: 37-48.

26. Vecsey-Nagy M, Szilveszter B, Kolossváry M, Boussoussou M, **Vattay B**, Gonda X, Rihmer Zs, Merkely B, Maurovich-Horvat P, Nemcsik J. (2021) The association between accelerated vascular aging and cyclothymic affective temperament in women. J Psychosom Res 145: 110423.

27. Stengl R, Ágg B, Szilveszter B, Benke K, Daradics N, Ruskó B, **Vattay B**, Merkely B, Pólos M, Szabolcs Z. (2021) Case Report: Morphological Characterization and Long-Term Observation of Bilateral Sequential Internal Mammary Artery Aneurysms in a Patient With Confirmed FBN1 Mutation. Front Cardiovasc Med 8: 697591.

28. Vecsey-Nagy M, Szilveszter B, Kolossváry M, Boussoussou M, **Vattay B**, Gonda X, Rihmer Z, Merkely B, Maurovich-Horvat P, Nemcsik J. (2021) Association between affective temperaments and severe coronary artery disease. J Affect Disord 295: 914-919.

29. Vecsey-Nagy M, Jermendy ÁL, Suhai FI, Panajotu A, Csőre J, Borzsák S, Fontanini D M, Kolossváry M, **Vattay B**, Boussoussou M, Csobay-Novák Cs, Merkely B, Maurovich-Horvat P, Szilveszter B. (2021) Model-based adaptive filter for a dedicated cardiovascular CT scanner: Assessment of image noise, sharpness and quality. Eur J Radiol 145: 110032.

30. Szilveszter B, Oren D, Molnár L, Apor A, Nagy A, Molnár A, **Vattay B**, Kolossváry M, Karády J, Bartykowszki A, Jermendy Á L, Suhai F I, Panajotu A, Maurovich-Horvat P, Merkely B. (2020) 1. Subclinical leaflet thrombosis is associated with impaired reverse remodelling after transcatheter aortic valve implantation. Eur Heart J Cardiovasc Imaging, 21(10): 1144-1151.

31. Szilveszter B, Nagy A I, **Vattay B**, Apor A, Kolossváry M, Bartykowszki A, Simon J, Drobni Z D, Tóth A, Suhai F I, Merkely B, Maurovich-Horvat P. (2020). Left ventricular and atrial strain imaging with cardiac computed tomography: Validation against echocardiography. J Cardiovasc Comput Tomogr 14(4): 363-369.

32. Simon J, Szaraz L, Szilveszter B, Panajotu A, Jermendy Á L, Bartykowszki A, Boussoussou M, **Vattay B**, Drobni ZD, Merkely B, Maurovich-Horvat P, Kolossvary M. (2020). Calcium scoring: a personalized probability assessment predicts the need for additional or alternative testing to coronary CT angiography. Eur Radiol 30(10): 5499-5506.

11. ACKNOWLEDGEMENTS

The work presented in this thesis would not have been possible without the advice, encouragement, and support of several individuals. I would like to express my deepest gratitude to all those who contributed to the completion of this PhD journey.

First and foremost, I would like to sincerely thank my mentor and supervisor, Dr. Bálint Szilveszter, for his invaluable guidance, support, and dedication throughout my PhD years. His mentorship has played a key role in shaping both my scientific thinking and professional development.

I am especially grateful to Professor Béla Merkely for providing me with the opportunity to carry out my research at the Heart and Vascular Center. His intellectual insight, professional, and financial support laid the foundation for my scientific work and research career.

I would also like to thank to my friends and colleagues Melinda Boussoussou, Milan Vecsey-Nagy, Márton Kolossváry, Zsófia Jokkel, and Ádám Jermendy for their helpful suggestions, thoughtful advice and continuous encouragement throughout the years. Your support and friendship have been a constant source of motivation and inspiration.

My sincere thanks go to Professor Pál Maurovich Horvat, who was my first mentor during my university studies. His collaborative spirit, critical insights, and technical contributions were instrumental in shaping this thesis and supporting my academic growth.

I am grateful to all my former and current colleagues at the Heart and Vascular Center for their ongoing support and collaboration in various aspects of my research.

It has also been a great privilege to work with Professor Gianluca Pontone and his outstanding team in Milan. I am truly thankful for the opportunity to collaborate with such an inspiring and internationally respected group, and I look forward to continuing our joint efforts in the future.

I would also like to express my gratitude to Anna Polgár Kelemenné for her valuable help in creating the figures, which greatly enhanced the clarity and visual appeal of this thesis.

Lastly, I wish to express my deepest appreciation to my family - especially my parents and sister - for their unconditional love, patience and support throughout my academic and personal journey. This achievement would not have been possible without you.

ESC
European Society
of Cardiology

ORIGINAL PAPER

CAD-RADS may underestimate coronary plaque progression as detected by serial CT angiography

Bálint Szilveszter [1]*[†], **Borbála Vattay**[1][†], **Melinda Bossoussou**[1],
Milán Vecsey-Nagy[1], **Judit Simon** [1], **Béla Merkely**[1],
Pál Maurovich-Horvat [1,2], and **Márton Kolossváry** [1]

[1]MTA-SE Cardiovascular Imaging Research Group, Heart and Vascular Center, Semmelweis University, 68 Városmajor st, 1122 Budapest, Hungary; and [2]Medical Imaging Centre, Semmelweis University, 2 Korányi Sándor st, 1083 Budapest, Hungary

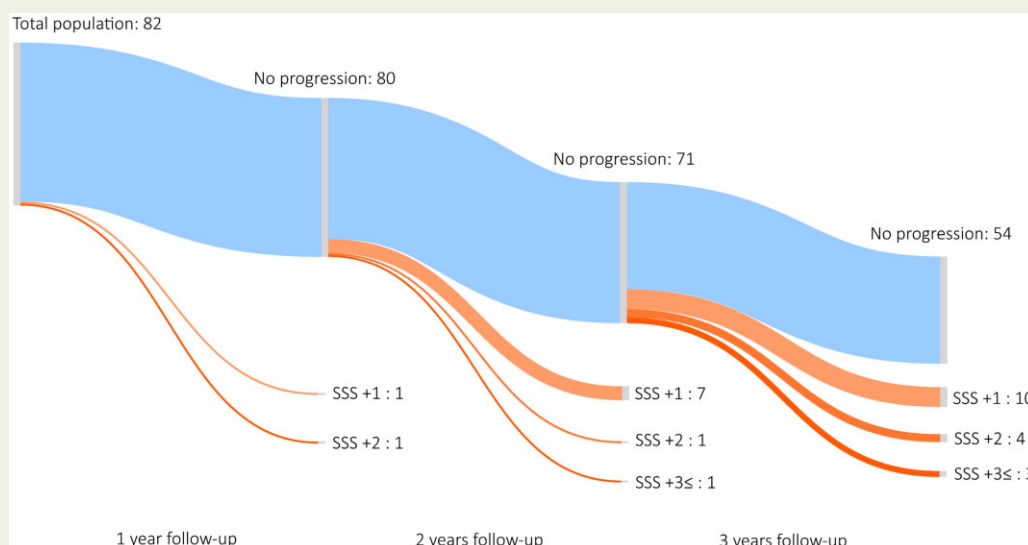|	
Aims	We wished to assess whether different clinical definitions of coronary artery disease (CAD) [segment stenosis and involvement score (SSS, SIS), Coronary Artery Disease—Reporting and Data System (CAD-RADS)] affect which patients are considered to progress and which risk factors affect progression.
Methods and results	We enrolled 115 subsequent patients (60.1 ± 9.6 years, 27% female) who underwent serial coronary computed tomography angiography (CTA) imaging with >1year between the two examinations. CAD was described using SSS, SIS, and CAD-RADS. Linear mixed models were used to investigate the effects of risk factors on the overall amount of CAD and the effect on annual progression rate of different definitions. Coronary plaque burdens were SSS 4.63 ± 4.06 vs. 5.67 ± 5.10, $P < 0.001$; SIS 3.43 ± 2.53 vs. 3.89 ± 2.65, $P < 0.001$; CAD-RADS 0:8.7% vs. 0.0% 1:44.3% vs. 40.9%, 2:34.8% vs. 40.9%, 3:7.0% vs. 9.6% 4:3.5% vs. 6.1% 5:1.7% vs. 2.6%, $P < 0.001$, at baseline and follow-up, respectively. Overall, 53.0%, 29.6%, and 28.7% of patients progressed over time based on SSS, SIS, and CAD-RADS, respectively. Of the patients who progressed based on SSS, only 54% showed changes in CAD-RADS. Smoking and diabetes increased the annual progression rate of SSS by 0.37/year and 0.38/year, respectively (both $P < 0.05$). Furthermore, each year increase in age raised SSS by 0.12 [confidence interval (CI) 0.05–0.20, $P = 0.001$] and SIS 0.10 (CI 0.06–0.15, $P < 0.001$), while female sex was associated with 2.86 lower SSS (CI -4.52 to -1.20, $P < 0.001$) and 1.68 SIS values (CI -2.65 to -0.77, $P = 0.001$).
Conclusion	CAD-RADS could not capture the progression of CAD in almost half of patients with serial CTA. Differences in CAD definitions may lead to significant differences in patients who are considered to progress, and which risk factors are considered to influence progression.

---

* Corresponding author. Tel: +36 20 666 3857; Fax: +36 1 458 6842. E-mail: szilveszter.balint@gmail.com
† These authors contributed equally to this work.

Graphical Abstract

Total population: 82
No progression: 80
No progression: 71
No progression: 54

SSS +1 : 1
SSS +2 : 1

SSS +1 : 7
SSS +2 : 1
SSS +3≤ : 1

SSS +1 : 10
SSS +2 : 4
SSS +3≤ : 3

1 year follow-up   2 years follow-up   3 years follow-up

Introduction

Coronary artery disease (CAD) is a chronic disease with dynamic temporal changes in plaque size and composition.[1,2] Coronary computed tomography angiography (CTA) is a robust, non-invasive diagnostic test to characterize CAD.[3,4] Coronary CTA allows the accurate assessment of the presence, extent and severity of coronary atherosclerosis, and has received class I recommendation (level of evidence B) for the evaluation of CAD among patients with stable chest pain in the latest guidelines.[5] Recent studies have proposed CAD progression as a prognosticator of adverse events, irrespectively from stenosis severity using CTA.[1] However, many clinical definitions and metrics of coronary plaque progression (PP) have been proposed.[6,7] Nevertheless, there are still limited data on the predictors of coronary PP with respect to different metrics of CAD quantity.

Therefore, we aimed to evaluate the predictors of CAD progression using different clinical definitions of plaque burden on serial computed tomography (CT) imaging. In addition, we sought to compare the identification of PP by three different semiquantitative definitions of CAD including the stenosis classification of the Coronary Artery Disease—Reporting and Data System (CAD-RADS).

Methods

Patient population

From 7233 patients in our structured reporting registry of coronary CTA, 316 had at least two coronary CTAs with at least 1 year between the two examinations using the same 256-slice scanner (Philips Brilliance

iCT, Best, The Netherlands) between 1 January 2015 and 6 January 2020. Indications for serial testing were the planning of radiofrequency ablation in patients with paroxysmal atrial fibrillation (23.4%) or recurrent angina after initial CTA (76.6%). Exclusion criteria for our analysis were myocardial infarction, percutaneous coronary intervention, heart transplantation, or coronary bypass graft surgery prior to any CTA imaging and nondiagnostic CT image quality. Overall, we found 115 symptomatic and stable patients who met the inclusion and exclusion criteria (*Figure 1*). Anamnestic, anthropometric data and CTA findings were recorded in a structured reporting platform (Axis, Neumann Medical Ltd. Budapest, Hungary).

The study was approved by the institutional review board and informed consent was waived due to the retrospective nature of the study. All procedures used in this study were in accordance with local and federal regulations, and the Declaration of Helsinki.

Demographics and comorbidities

Medical chart review was performed to gather data on patient demographics and comorbidities. Both at baseline and follow-up, patients underwent detailed interview on risk factors, medical history, and medication. Hyperlipidaemia was defined as having elevated plasma cholesterol levels (total cholesterol >200 mg/dL) or the use of lipid-lowering therapy. Hypertension was defined as systolic blood pressure >140 mmHg and/or diastolic blood pressure >90 mmHg or antihypertensive medication use verified by medical records. Smoking was defined as prior tobacco use within 1 year prior CTA (both baseline and follow-up time point evaluated). Diagnosis of diabetes mellitus (DM) was established based on elevated plasma glucose levels (fasting plasma glucose ≥ 126 mg/dL; HbA1c ≥ 6.5%) or the use of antidiabetic medication or insulin therapy. Statin use was recorded at baseline and follow-up at the time of the CT scanning and was defined as the use of statin at the time of the scans.
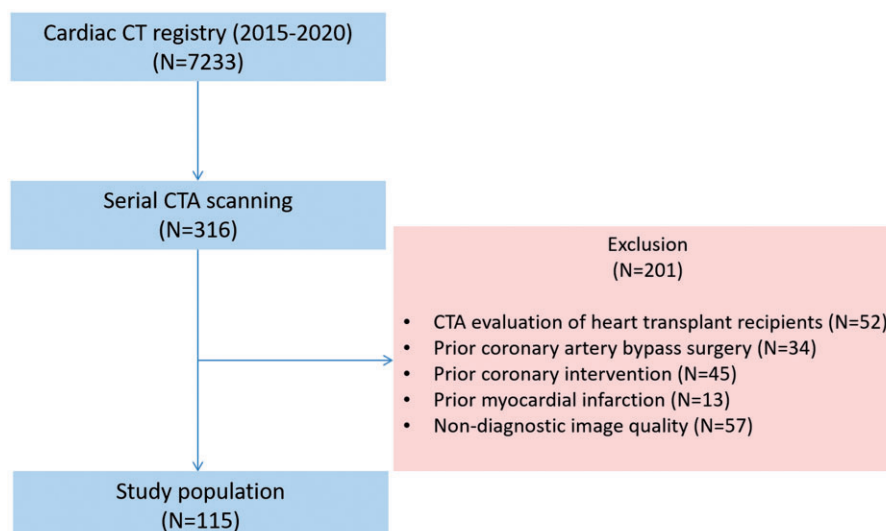
Figure 1 Flow chart of the study. CT, computed tomography; CTA, computed tomography angiography.

CT Image acquisition

We performed prospectively triggered CTA of the heart according to the guidelines of the SCCT.[8] Per os metoprolol was administered in case of heart rate exceeded 65 beats per minute 1 h before the coronary CTA examination and if not contraindicated. All patients received 0.8 mg of sublingual nitroglycerine prior to the CTA and intravenous beta-blocker was also administered if heart rate was still above 60 beats/min. Image acquisition was performed at diastole (75–81% of the R–R interval) or at systole (37–43% of the R–R interval) if heart rate was above 70 bpm despite premedication. The following scanner settings were used: 270 ms rotation time, 128 × 0.625 mm collimation, tube voltage of 100–120 kVp, and tube current of 200–300 mAs based on patient's body mass index (BMI). Axial images were reconstructed with 0.4 mm slice thickness using iterative reconstruction.

Coronary CTA analysis

A single reader with 7 years of experience in cardiovascular CT imaging (B.S.) assessed the location, morphology, and severity of coronary lesions using an 18-segment coronary tree model.

Coronary plaque was defined on the CTA based on former publications by Mahabadi *et al.* and Achenbach *et al.*[9,10] Calcified and non-calcified plaques were defined as any discernible structure with a density of ≥130 and <130 Hounsfield units, respectively, which were assigned to the vessel wall in at least two independent image planes. Coronary segments with a diameter of >1.5 mm were analysed. The reader evaluated baseline and follow-up images simultaneously to detect changes in plaque composition (on visual evaluation) or stenosis severity and was blinded to patient characteristics, CTA date, comorbidities, and medical treatment.

To quantify total CAD burden segment involvement score (SIS) (sum of all coronary segments affected with plaque) and segment stenosis score (SSS) (sum of coronary segments involved with plaque weighted with stenosis severity: 0%: 0, 1–24%: 1, 25–49%: 2, 50–69%: 3, 70–99%:4, 100%: 5) were calculated in all 18 segments of all patients at baseline and follow-up scans.[6] Inter-reader reproducibility of SSS and SIS was assessed previously.[11] CAD-RADS stenosis categories (0: 0%, 1: 1–24%, 2:

25–49%, 3: 50–69%, 4A 70–99%, 4B: Left main >50% or three-vessel disease, 5: 100%) were assessed according to the CAD-RADS consensus document.[12] The presence, extent, and severity for all lesions were entered into a structured reporting platform that automatically generated CAD-RADS clinical recommendation (Axis, Neumann Medical Ltd. Budapest, Hungary)[12] based on these conditional inputs of the reader.

Statistical analysis

Continuous variables are presented as mean and standard deviation, whereas categorical parameters are presented as frequency with percentages. Paired sample *t*-test was used to compare parameters describing coronary plaque burden of the two CTA examinations. First, we used linear regression analysis to identify predictors of annualized PP. Furthermore, we applied a more complex approach using linear mixed models to analyse repeated observations at non-standardized intervals.[13–15]

By analysing intra-individual changes over time we can simultaneously estimate the effect of a predictor on (i) overall amount of the outcome (SSS, SIS, and CAD-RADS) and (ii) effect on annual progression rate.[15,16] Using this information, the model is able to provide an estimate on the effect of a covariate on overall amount of the outcome, irrespective of time (e.g. statin users tend to have more plaque, as statin is initiated in patients with increased plaque burdens), but it also provides estimates on how the covariate affects temporal changes (e.g. statin users will have slower progression as compared to the average). This method also already accounts for the total plaque burden at baseline, therefore no additional adjustment is needed in the models. We calculated univariate linear mixed models to assess the effect of each predictor on the outcome (CAD definitions) and annual progression of the outcome. If either effect had a *P*-value <0.10, we included that predictor in a multivariate model. Clinical predictors of coronary PP were included in the models as predictors with SIS, SSS, and CAD-RADS as outcomes. Inter-observer reproducibility was assessed in 25 patients by two observers using weighted kappa. We selected five plaques per stenosis category (minimal 1–24%, mild 25–49%, moderate 50–69%, severe 70–99%, and occluded 100%), including one plaque per patient. The *k* values were interpreted as

Table 1 Patient characteristics

Patient data	Study population (N = 115)
Age (years)	60.1 ± 9.6
BMI (kg/m^2)	28.4 ± 4.2
Female gender, n (%)	27 (23.5)
Cardiovascular risk factors at baseline, n (%)	
Hypertension	87 (75.7)
Diabetes mellitus	15 (13.0)
Dyslipidaemia	63 (54.8)
Smoking	13 (11.3)
Family history of premature CAD	29 (25.2)
Statin use	47 (35.7)

BMI, body mass index; CAD, coronary artery disease.

Table 2 Coronary plaque burden at baseline and follow-up

	1. Scan (n = 115)	2. Scan (n = 115)	P-value
SSS	4.63 ± 4.06	5.67 ± 5.10	<0.001
SIS	3.43 ± 2.53	3.89 ± 2.65	<0.001
CAD-RADS severity, n (%)			<0.001
0	10 (8.7)	0 (0.0)	
1	51 (44.3)	47 (40.9)	
2	40 (34.8)	47 (40.9)	
3	8 (7.0)	11 (9.6)	
4	4 (3.5)	7 (6.1)	
5	2 (1.7)	3 (2.6)	

CAD-RADS, Coronary Artery Disease—Reporting and Data System; SIS, segment involvement score; SSS, segment stenosis score.

follows: 0.00–0.20 poor; 0.21–0.40 fair; 0.41–0.60 moderate; 0.61–0.80 good; and 0.81–1.00 excellent agreement.

All analyses were conducted in the R environment v3.6.1 and STATA v13.0. A two-sided P-value smaller than 0.05 was considered statistically significant.

Results

The baseline characteristics of the 115 enrolled patients (mean age 60.1 ± 9.6 years, 27% female) are summarized in Table 1. On average, 2.6 ± 1.1 years has passed between the CTA examinations. A total of 1763 coronary artery segments were evaluated at both time points. Mean effective radiation dose was 5.07 and 5.09 mSv (P = 0.822) for baseline and follow-up.

Characteristics of coronary PP

A total of 105 (91.3%) patients had any CAD at baseline. The remaining 10 patients (8.7%) had no plaque on baseline and all developed minimal stenosis on follow-up (CAD-RADS 1). We detected no progression of disease in 54 patients with CAD (46.7%), furthermore, plaque regression was not observed in this patient population.

We detected a total of 397 plaques at baseline vs. 449 plaques at follow-up in the total population. Regarding plaque types, we found 142 vs. 154 calcified, 175 vs. 203 partially calcified, and 80 vs. 92 non-calcified plaques on baseline vs. follow-up scans, respectively. Comparing the first and second coronary CTA images we found that SSS, SIS, and CAD-RADS significantly increased on the follow-up images: SSS 4.63 ± 4.06 vs. 5.67 ± 5.10, P < 0.001; SIS 3.43 ± 2.53 vs. 3.89 ± 2.65, P < 0.001; CAD-RADS 0: 8.7% vs. 0.0% 1: 44.3% vs. 40.9%, 2: 34.8% vs. 40.9%, 3: 7.0% vs. 9.6% 4: 3.5% vs. 6.1% 5: 1.7% vs. 2.6%, P < 0.001, at baseline and follow-up, respectively (see Table 2). The average annual progression rate was 0.41 ± 0.62 for SSS and 0.18 ± 0.34 for SIS. Any progression in SSS, SIS, and CAD-RADS was found in 53.0%, 29.6%, and 28.7% of all cases. Importantly, among patients without progression in CAD-RADS during the follow-up period, 34.1% and 17.1% had progression in SSS and SIS, respectively. Of the patients who progressed based on SSS, only 54% showed changes in CAD-RADS scores.

Representative case of CAD progression is seen on Figure 2, changes in SSS and CAD-RADS during follow-up are summarized on a Sankey diagram (Figure 3). SSS-based progression is depicted among those with no changes in CAD-RADS severity on a Sankey diagram (Figure 4).

We found excellent agreement across stenosis categories evaluating 25 plaques (5 from each stenosis category) by two observers (weighted kappa = 0.903).

Predictors of coronary PP

Linear regression models were carried out to identify predictors of PP described as annualized progression of SSS or SIS. Age was associated with PP based on SSS [β = 0.013, confidence interval (CI) 0.01–0.024, P = 0.034] but showed no association with SIS progression (P = 0.784). Importantly, none of the other predictors showed any association with the annualized progression rate of SSS, SIS, or CAD-RADS (all P > 0.05). However, this approach does not account for the temporal changes of covariates over time and does not account for the one's baseline value, therefore we also analysed our data using linear mixed models.

Linear mixed models for the analysis of coronary PP and progression rate

Univariate linear mixed models showed that age and gender affect the value of SSS and SIS in our population, whereas diabetes increased the annual progression rate of SSS by 0.34/year (CI 0.01–0.66; P = 0.036) (see Table 3).

On multivariate analysis, patients who smoked had significantly increased annual progression rate of SSS by 0.37/year (CI 0.07–0.67, P = 0.017) and higher total extent of CAD as described by SIS as compared with non-smokers (β = 0.77, CI 0.06–1.50, P = 0.034). DM increased the annual progression rate of SSS by 0.38/year (CI 0.07–0.69, P = 0.016). Age and gender affected the total amount of SSS and SIS (P ≤ 0.001, all): 1-year increase in age lead to an estimated increase of 0.12 (CI 0.05–0.20, P = 0.001) in SSS and 0.10 (CI 0.06–0.15, P < 0.001) in SIS. Female gender is associated with an average of 2.86 lower SSS (CI -4.52 to -1.20, P < 0.001) and 1.68 lower SIS (CI -2.65 to -0.71, P = 0.001) than male gender. Importantly, CAD-RADS was
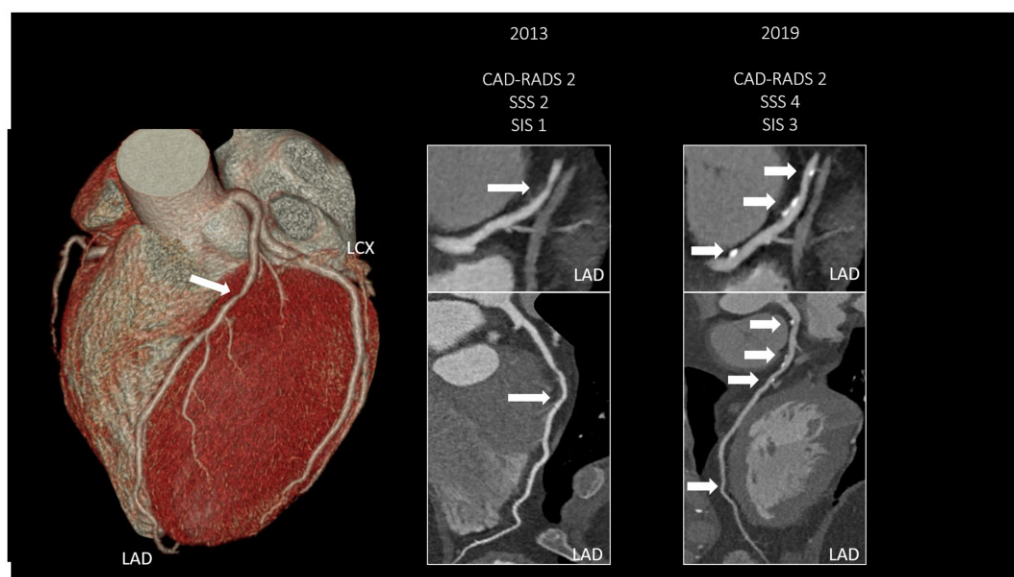
Figure 2 Representative case of plaque progression. A 51-year-old male patient underwent serial CTA scanning due to stable chest pain. In 2013, the patient had one affected coronary segment (mid-LAD) with plaque. The figure shows the LAD with a non-calcified plaque leading to mild stenosis (CAD-RADS 2, SSS 2, SIS 1). We detected coronary plaque progression on the proximal and distal LAD segment of LAD 6 years later, including *de novo* calcified plaque development. The total segment involvement and segment stenosis scores were both higher on follow-up (SSS 4 and SIS 3), however, based on the worst stenosis CAD-RADS score of 2 was assigned. CAD-RADS, Coronary Artery Disease—Reporting and Data System; LAD, left anterior descending artery; LCX, Left circumflex artery; SIS, segment involvement score; SSS, segment stenosis score.

not influenced by any cardiovascular risk factor (all $P \geq 0.05$). Detailed results of multivariate analysis are summarized in *Table 4*.

Discussion

In our longitudinal observation cohort study, we found that age and gender influenced the severity and the extent of CAD after correcting for the effects of other conventional cardiovascular risk factors. Smoking and DM were significant factors increasing annual progression rates of SSS, reflecting both the severity and the extent of the disease. Importantly, among those with increased SSS and SIS on follow-up CTA, in 46% and 41% of patients the CAD-RADS severity classification did not change. On the other hand, none of the risk factors seem to influence CAD-RADS, the currently recommended clinical classification framework for reporting CAD.

Coronary atherosclerosis is a dynamic and progressive disease that may lead to the obstruction of the coronary lumen and induce ischaemia.[17] CTA is a uniquely suited imaging modality to monitor changes in the extent and severity of CAD and underlying plaque composition.[18] Quantifying coronary plaque burden improves risk assessment using both semi-quantitative (SSS, SIS) or quantitative (volumetric) plaque metrics.[19,20] Recent studies incorporated the degree of stenosis, plaque morphology, and SSS for the detection of PP. Although quantitative plaque analysis (volumetric change in atheroma burden) is not used routinely in clinical setting, this biomarker has been increasingly utilized for monitoring anti-atherosclerotic drug therapy.[21]

Despite increasing number of studies utilizing CT imaging for the detection of the plaque development, there are limited data on the predictors of atherosclerosis progression. Moreover, there is a huge variety of definitions in use to quantify CAD progression and to characterize coronary atherosclerosis on CTA per se. Motoyama *et al.*[1] defined disease progression as either an increase in stenosis by at least 1 grade or an increase in the remodelling index ratio of >1.1, and found that increase in plaque burden might be the strongest predictor of adverse events. In other studies, progression was defined based on newly diagnosed cases with 50% or more coronary stenosis by the person-years of follow-up,[22] whereas Gu *et al.*[23] used coronary calcium score, SSS, and SIS for describing progression. More recent investigations focused on quantitative plaque analysis and defined PP based on volumetric changes ($\geq$10%) compared to baseline volume[24] or simply evaluated the change in plaque volume.[25] Notably, most of these changes in plaque volume are relatively small and would not change clinical scoring systems such as SSS or CAD-RADS classification and clinical decision-making. Other limitations of using volumetric plaque analysis include insufficient image quality, lack of standardized protocols regarding acquisition protocols and iterative reconstruction.[26,27] Furthermore, many concerns have been raised regarding the inter-vendor, scan–rescan, inter-software, and inter-reader variability of quantitative plaque analysis which limits its widespread clinical use.[28–30]

Importantly, the methodology of the aforementioned studies differed as compared to our analysis, since we are the first to use linear mixed models to define the effect of risk factors on CAD metrics and the progression rate. Most of the prior studies analysed two
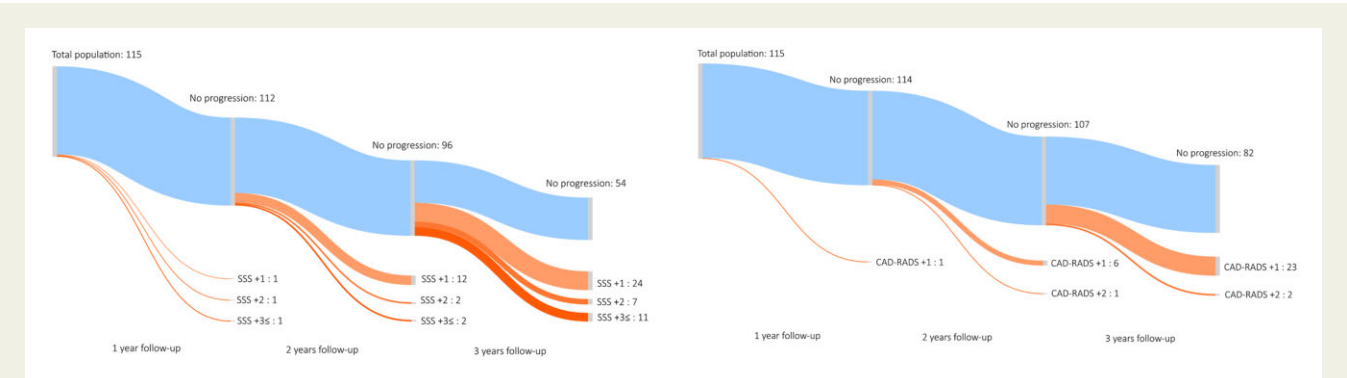
Figure 3 Sankey diagram depicting coronary plaque progression based on SSS and CAD-RADS. Patient-based progression of coronary atherosclerosis using SSS and CAD-RADS severity is depicted on the Sankey diagram. This type of flow diagram depicts the number of patients with progression during follow-up, where the width of the arrow is proportional to the flow rate (number of patients). No progression was found in 54 patients' SSS and in 82 patients' CAD-RADS during the follow-up period (marked with light blue). The number of patients with increase in SSS and CAD-RADS are depicted at 1, 2, and ≥3 years based on serial CTA imaging (orange). CAD-RADS substantially underestimates changes in disease severity and extent of CAD. During the follow-up period we could identify three patients with SSS increase at 1 year (rapid progression of CAD), whereas most patients progressed later at 3 or more years. CAD-RADS, Coronary Artery Disease—Reporting and Data System; SSS, segment stenosis score.
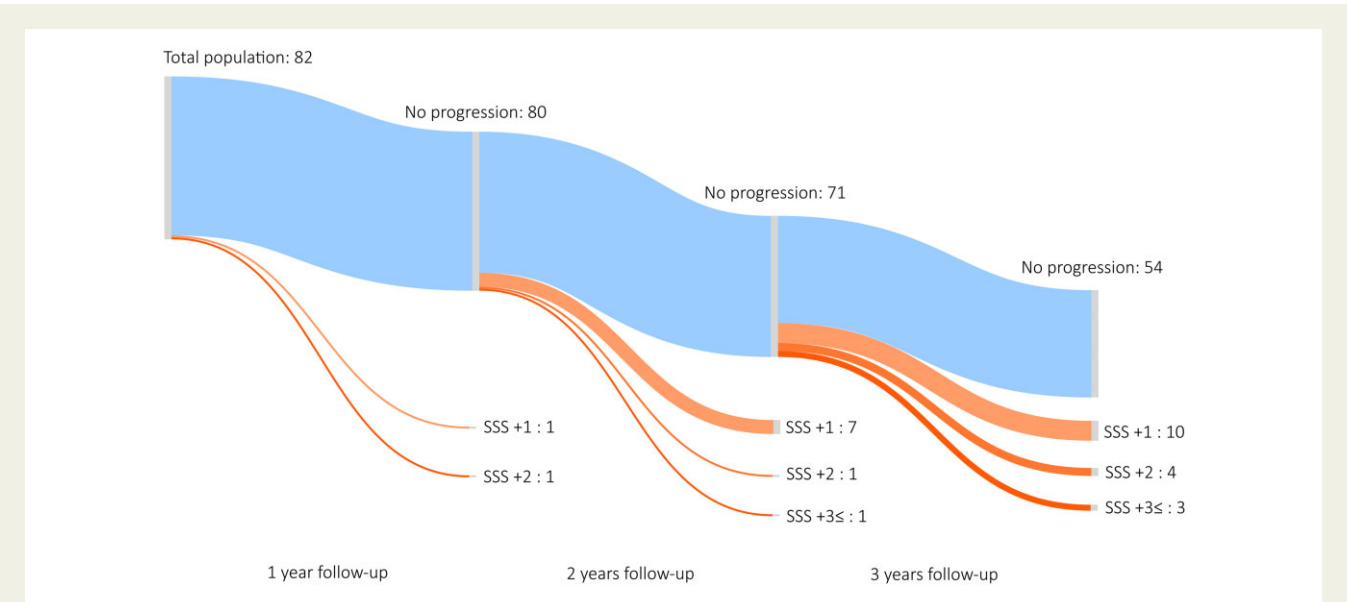

Figure 4 Sankey diagram depicting coronary plaque progression based on SSS among those with no progression in CAD-RADS classification for lesion severity. A total of 82 patients in our study did not progress based on CAD-RADS severity, although a large proportion of patients demonstrated coronary plaque progression based on SSS. Increasing number of patients developed higher stenosis scores during follow-up period: 2 patients had higher SSS at 1 year, 9 patients had higher SSS at 2 years, and 17 patients had higher SSS at 3 years or more. Four patients had substantial increase in SSS (three or more) despite no changes in CAD-RADS classification. SSS, segment stenosis score.

timepoints defining progression as the change in mean values of plaque parameters of a given population, but this approach might not account for the one's baseline value (i.e. individuals with more plaque may progress faster unless normalizing for the baseline plaque volume) or the possible changes in covariates over time (i.e. someone may develop DM over the follow-up period). Moreover, some studies enrolled patients with non-standardized follow-up times for serial scanning, which—also based on our observation of PP rate—can significantly influence results. Linear mixed models provide flexible

modelling of intra-subject changes and enable to assess overall and individual patterns in time. This method enables to assess the impact of predictors in both timepoints on the outcomes.[15]

To incorporate the main findings of coronary CTA in a unified and standardized framework, experts of the field have proposed the use of the CAD-RADS classification in clinical practice. Maroules *et al.*[31] found high inter-observer agreement for both experienced and early career readers when assessing CAD-RADS categories, except for vulnerability. Importantly, the currently used CAD-RADS

Table 3 Univariate analysis of predictors of plaque progression using linear mixed models

Predictors	SSS						SIS						CAD-RADS severity					
	Univariate model						Univariate model						Univariate model					
	Effect on SSS			Effect on annual progression			Effect on SIS			Effect on annual progression			Effect on CAD-RADS			Effect on annual progression		
	β	95% CI	P-value	β	95% CI	P-value	β	95% CI	P-value	β	95% CI	P-value	β	95% CI	P-value	β	95% CI	P-value
Age	**0.11**	**0.04–0.19**	**0.004**	**0.01**	**0.00–0.02**	**0.035**	**0.09**	**0.05–0.14**	**<0.001**	0.00	0.00–0.01	0.701	0.01	0.00–0.03	0.140	0.00	-0.01 to 0.00	0.510
Gender	**−2.31**	**−4.04 to −0.58**	**0.010**	-0.08	-0.34 to 0.17	0.516	**−1.38**	**−2.44 to −0.31**	**0.013**	-0.01	-0.15 to 0.13	0.898	-0.34	-0.76 to 0.07	0.110	0.02	-0.07 to 0.10	0.713
BMI	-0.02	-0.13 to 0.08	0.651	-0.01	-0.03 to 0.02	0.609	0.04	-0.02 to 0.10	0.182	-0.01	-0.02 to 0.01	0.254	0.00	-0.03 to 0.04	0.901	0.00	-0.01 to 0.01	0.730
Hypertension	0.15	-1.22 to 1.51	0.834	0.19	-0.06 to 0.44	0.136	0.28	-0.51 to 1.07	0.479	0.02	-0.11 to 0.16	0.740	-0.12	-0.48 to 0.25	0.523	0.05	-0.03 to 0.13	0.229
Diabetes mellitus	1.39	-0.84 to 3.61	0.225	**0.34**	**0.02–0.66**	**0.036**	0.81	-0.56 to 2.18	0.251	0.06	-0.11 to 0.24	0.473	0.17	-0.36 to 0.70	0.527	0.05	-0.06 to 0.15	0.377
Dyslipidaemia	0.64	-0.47 to 1.75	0.264	-0.12	-0.34 to 0.09	0.269	0.28	-0.37 to 0.93	0.390	-0.05	-0.17 to 0.07	0.427	0.13	-0.18 to 0.44	0.412	-0.06	-0.14 to 0.01	0.083
Smoking	0.67	-0.55 to 1.88	0.281	0.33	0.00–0.65	0.050	0.64	-0.08 to 1.37	0.083	0.09	-0.08 to 0.26	0.286	0.06	-0.38 to 0.49	0.794	0.05	-0.05 to 0.15	0.311
Statin use	-0.11	-0.92 to 0.70	0.785	0.15	-0.08 to 0.38	0.203	-0.16	-0.61 to 0.30	0.498	0.05	-0.07 to 0.18	0.413	0.12	-0.15 to 0.38	0.378	-0.05	-0.12 to 0.03	0.241

Univariate linear mixed models demonstrating the effects of risk factors on SSS, SIS, and CAD-RADS. Significant predictors are marked in bold letters. The effect of each risk factor on the total amount of SSS, SIS, and CAD-RADS is described by the model. Yearly progression rate of each predictor is also described by the effect of progression rate. All models incorporate the baseline value of CAD metrics.
BMI, body mass index; CAD-RADS, Coronary Artery Disease—Reporting and Data System; CI, confidence interval; SIS, segment involvement score; SSS, segment stenosis score.

Table 4 Multivariate analysis of predictors of plaque progression using linear mixed models

Predictors	SSS				SIS				CAD-RADS Severity			
	Effect on SSS β (95% CI)	P-value	Effect on annual progression β (95% CI)	P-value	Effect on SIS β (95% CI)	P-value	Effect on annual progression β (95% CI)	P-value	Effect on CAD-RADS β (95% CI)	P-value	Effect on annual progression β (95% CI)	P-value
Age	0.12 (0.05–0.20)	0.001	0.01 (0.01–0.03)	0.013	0.10 (0.06–0.15)	<0.001	0.00 (0.00–0.01)	0.369		NS		NS
Female gender	−2.86 (−4.52 to −1.20)	<0.001	−0.23 (−0.47 to 0.01)	0.06	−1.68 (−2.65 to −0.71)	0.001	−0.03 (−0.17 to 0.11)	0.646		NS		NS
Smoking	1.16 (−0.03 to 2.35)	0.06	0.37 (0.07–0.67)	0.017	0.77 (0.06–1.50)	0.034	0.10 (−0.07 to 0.27)	0.263		NS		NS
Diabetes mellitus	1.27 (−0.86 to 3.40)	0.24	0.38 (0.07–0.69)	0.016								

Multivariate linear mixed models including independent predictors of coronary plaque progression. Significant predictors are marked in bold letters.
CAD-RADS, Coronary Artery Disease—Reporting and Data System; CI, confidence interval; NS, Non-significant; SIS, segment involvement score; SSS, segment stenosis score.

classification scheme only describes the plaque with the largest degree of stenosis and does not account for the extent of disease. For example, patients with mild or moderate stenosis (CAD-RADS category 2 or 3)—who are classified as non-obstructive patients—could also demonstrate extensive CAD affecting more than four coronary segments. Bittencourt et al.[32] demonstrated that extensive, but non-obstructive CAD patients have comparable risk profile as those with obstructive CAD. CAD burden scores (SSS and SIS) used in current study also incorporate the number of segments affected with plaques. Figure 2 shows a representative case of our study highlighting the importance of using different scores when describing PP. In this case, the patient had de novo plaques on two additional segments whereas the CAD-RADS category remained the same and thus might create the false impression that CAD did not progress throughout the years. Coronary PP is a strong prognosticator of events and therefore should also be implemented in CAD-RADS recommendation. Proper risk assessment is crucial to better define a subset of patients who require a more aggressive secondary prevention therapy or downstream testing.

We detected substantial changes in SSS and SIS during follow-up imaging; however, the CAD-RADS classification was not able to identify changes in the extent and severity of CAD and thus might not recognize increased risk for future events. CAD-RADS classification has been proposed to guide further testing and secondary prevention therapy; however, based on our data, it would miss almost every second patient with increased plaque severity or extent which have been previously shown to increase adverse events. The use of CAD-RADS underestimates coronary PP as it heavily focuses on the worst plaque of a given patient and only includes three-vessel obstructive ≥70% disease in grade 4B when assessing plaque burden. Coronary CTA provides, however, rich information on the distribution, extent, and vulnerability of coronary atherosclerosis. The novel version of the classification scheme could improve risk assessment by combining the stenosis severity and plaque burden, moreover, experts of the field also suggested adding flow-limiting lesions and coronary artery calcium score information as well. Further outcome studies are warranted to evaluate the prognostic value of the current CAD-RADS classification and possible future versions in terms of plaque severity vs. the extent of CAD. Also, PP should be included in the classification and its predictive value should be tested in large contemporary cohort of outpatients with stable angina.

Prior investigations report conflicting results regarding the predictors of PP, which might originate from the differences in the definition of progression and the use of CAD scoring systems. Increased PP might be promoted by male gender, obesity, high low-density lipoprotein cholesterol level, DM, and smoking.[33,34] Among conventional cardiovascular risk factors, DM, BMI, and smoking induced PP in other studies.[35,36] Smoking can promote atherogenesis involving pathways of inflammation, endothelial dysfunction, platelet function, cholesterol metabolism, and thrombotic factors.[37–39] We also found that male gender was associated with larger SSS and SIS, moreover, patients who smoked had larger extent of CAD. Among cardiovascular risk factors smoking and DM were related to the progression rate of SSS using linear mixed models.

We acknowledge the limitations of our study. First, we retrospectively analysed patients who underwent serial CTA at a single tertiary centre for Cardiology with different time interval between the two

coronary CTA examinations. We therefore used linear mixed models that account for differences in follow-up times and provide detailed information on the factors of PP. Another limitation is the incidental statin use without routine cholesterol measurements and strict control of adherence to the drug. Also, prospective, multicentre trials are warranted to analyse whether the observed discrepancies between different CAD definitions could influence patient outcomes. Furthermore, smoking was defined as prior tobacco use within 1 year prior CTA reflecting current smoking and not life-long accumulated hazards of smoking.

Conclusion

CAD-RADS did not capture the progression of CAD in almost half of stable angina patients with serial CT imaging. Age and gender influenced segment stenosis and plaque extent as described by segment stenosis and involvement scores. Smoking and diabetes affected the progression rate of PP based on SSS. Differences in CAD definitions may lead to significant differences in patients who are considered to progress. Therefore, unified plaque metrics are needed that are capable to properly describe the extent and severity of CAD for CT-based risk prediction and clinical management.

Funding

Data availability

The data underlying this article will be shared on reasonable request to the corresponding author.

References

1. Motoyama S, Ito H, Sarai M, Kondo T, Kawai H, Nagahara Y *et al.* Plaque characterization by coronary computed tomography angiography and the likelihood of acute coronary events in mid-term follow-up. *J Am Coll Cardiol* 2015;**66**:337–46.
2. Ito H, Motoyama S, Sarai M, Kawai H, Harigaya H, Kan S *et al.* Characteristics of plaque progression detected by serial coronary computed tomography angiography. *Heart Vessels* 2014;**29**:743–9.
3. Celeng C, Leiner T, Maurovich-Horvat P, Merkely B, de Jong P, Dankbaar JW *et al.* Anatomical and functional computed tomography for diagnosing hemodynamically significant coronary artery disease: a meta-analysis. *JACC Cardiovasc Imaging* 2019;**12**:1316–25.
4. Budoff MJ, Dowe D, Jollis JG, Gitter M, Sutherland J, Halamert E *et al.* Diagnostic performance of 64-multidetector row coronary computed tomographic angiography for evaluation of coronary artery stenosis in individuals without known coronary artery disease: results from the prospective multicenter ACCURACY (Assessment by Coronary Computed Tomographic Angiography of Individuals Undergoing Invasive Coronary Angiography) trial. *J Am Coll Cardiol* 2008;**52**:1724–32.
5. Knuuti J, Wijns W, Saraste A, Capodanno D, Barbato E, Funck-Brentano C *et al.*; ESC Scientific Document Group. 2019 ESC Guidelines for the diagnosis and management of chronic coronary syndromes. *Eur Heart J* 2019;**41**:407–77.
6. Voros S, Elashoff MR, Wingrove JA, Budoff MJ, Thomas GS, Rosenberg S. A peripheral blood gene expression score is associated with atherosclerotic plaque burden and stenosis by cardiovascular CT-angiography: results from the PREDICT and COMPASS studies. *Atherosclerosis* 2014;**233**:284–90.
7. Min JK, Shaw LJ, Devereux RB, Okin PM, Weinsaft JW, Russo DJ *et al.* Prognostic value of multidetector coronary computed tomographic angiography for prediction of all-cause mortality. *J Am Coll Cardiol* 2007;**50**:1161–70.
8. Wu FZ, Wu MT. 2014 SCCT Guidelines for the interpretation and reporting of coronary CT angiography: a report of the Society of Cardiovascular Computed Tomography Guidelines Committee. *J Cardiovasc Comput Tomogr* 2015;**9**:e3.
9. Mahabadi AA, Bamberg F, Toepker M, Schlett CL, Rogers IS, Nagurney JT *et al.* Association of aortic valve calcification to the presence, extent, and composition of coronary artery plaque burden: from the Rule Out Myocardial Infarction using Computer Assisted Tomography (ROMICAT) trial. *Am Heart J* 2009;**158**:562–8.
10. Achenbach S, Moselewski F, Ropers D, Ferencik M, Hoffmann U, MacNeill B *et al.* Detection of calcified and noncalcified coronary atherosclerotic plaque by contrast-enhanced, submillimeter multidetector spiral computed tomography: a segment-based comparison with intravascular ultrasound. *Circulation* 2004;**109**:14–7.
11. Kolossvary M, Szilveszter B, Edes IF, Nardai S, Voros V, Hartyanszky I *et al.* Comparison of quantity of coronary atherosclerotic plaques detected by computed tomography versus angiography. *Am J Cardiol* 2016;**117**:1863–7.
12. Cury RC, Abbara S, Achenbach S, Agatston A, Berman DS, Budoff MJ *et al.* CAD-RADS: coronary artery disease—reporting and data system: an expert consensus document of the Society of Cardiovascular Computed Tomography (SCCT), the American College of Radiology (ACR) and the North American Society for Cardiovascular Imaging (NASCI). Endorsed by the American College of Cardiology. *J Am Coll Radiol* 2016;**13**:1458–66.e9.
13. Kolossvary M, Fishman EK, Gerstenblith G, Bluemke DA, Mandler RN, Celentano D *et al.* Cardiovascular risk factors and illicit drug use may have a more profound effect on coronary atherosclerosis progression in people living with HIV. *Eur Radiol* 2021;**31**:2756–67.
14. Kolossvary M, Gerstenblith G, Bluemke DA, Fishman EK, Mandler RN, Kickler TS *et al.* Contribution of risk factors to the development of coronary atherosclerosis as confirmed via coronary CT angiography: a longitudinal radiomics-based study. *Radiology* 2021;**299**:97–106.
15. Fleg JL, Morrell CH, Bos AG, Brant LJ, Talbot LA, Wright JG *et al.* Accelerated longitudinal decline of aerobic capacity in healthy older adults. *Circulation* 2005;**112**:674–82.
16. Verbeke G, Molenberghs G. *Linear Mixed Models for Longitudinal Data.* New York: Springer; 2000. pxxii, 568.
17. Nabel EG, Braunwald E. A tale of coronary artery disease and myocardial infarction. *N Engl J Med* 2012;**366**:54–63.
18. Sandfort V, Lima JA, Bluemke DA. Noninvasive imaging of atherosclerotic plaque progression: status of coronary computed tomography angiography. *Circ Cardiovasc Imaging* 2015;**8**:e003316.
19. Tesche C, Plank F, De Cecco CN, Duguay TM, Albrecht MH, Varga-Szemes A *et al.* Prognostic implications of coronary CT angiography-derived quantitative markers for the prediction of major adverse cardiac events. *J Cardiovasc Comput Tomogr* 2016;**10**:458–65.
20. Gnanenthiran SR, Naoum C, Leipsic JA, Achenbach S, Al-Mallah MH, Andreini D *et al.* Long-term prognostic utility of computed tomography coronary angiography in older populations. *Eur Heart J Cardiovasc Imaging* 2019;**20**:1279–86.
21. Taron J, Lee S, Aluru J, Hoffmann U, Lu MT. A review of serial coronary computed tomography angiography (CTA) to assess plaque progression and therapeutic effect of anti-atherosclerotic drugs. *Int J Cardiovasc Imaging* 2020;**36**:2305–17.
22. Lai H, Stitzer M, Treisman G, Moore R, Brinker J, Gerstenblith G *et al.* Cocaine abstinence and reduced use associated with lowered marker of endothelial dysfunction in African Americans: a preliminary study. *J Addict Med* 2015;**9**:331–9.
23. Gu H, Gao Y, Wang H, Hou Z, Han L, Wang X *et al.* Sex differences in coronary atherosclerosis progression and major adverse cardiac events in patients with suspected coronary artery disease. *J Cardiovasc Comput Tomogr* 2017;**11**:367–72.

24. Yu M, Li W, Lu Z, Wei M, Yan J, Zhang J. Quantitative baseline CT plaque characterization of unrevascularized non-culprit intermediate coronary stenosis predicts lesion volume progression and long-term prognosis: A serial CT follow-up study. *Int J Cardiol* 2018;**264**:181–6.

25. Won KB, Lee BK, Park HB, Heo R, Lee SE, Rizvi A *et al.* Quantitative assessment of coronary plaque volume change related to triglyceride glucose index: the Progression of AtheRosclerotic PlAque DetermIned by Computed TomoGraphic Angiography IMaging (PARADIGM) registry. *Cardiovasc Diabetol* 2020;**19**:113.

26. Sande EP, Martinsen AC, Hole EO, Olerud HM. Interphantom and interscanner variations for Hounsfield units—establishment of reference values for HU in a commercial QA phantom. *Phys Med Biol* 2010;**55**:5123–35.

27. Cademartiri F, Mollet NR, Runza G, Bruining N, Hamers R, Somers P *et al.* Influence of intracoronary attenuation on coronary plaque measurements using multislice computed tomography: observations in an ex vivo model of coronary computed tomography angiography. *Eur Radiol* 2005;**15**:1426–31.

28. Symons R, Morris JZ, Wu CO, Pourmorteza A, Ahlman MA, Lima JA *et al.* Coronary CT angiography: variability of CT scanners and readers in measurement of plaque volume. *Radiology* 2016;**281**:737–48.

29. Kolossváry M, Szilveszter B, Karády J, Drobni ZD, Merkely B, Maurovich-Horvat P. Maurovich-Horvat P. Effect of image reconstruction algorithms on volumetric and radiomic parameters of coronary plaques. *J Cardiovasc Comput Tomogr* 2019;**13**:325–30.

30. Kolossvary M, Javorszky N, Karady J, Vecsey-Nagy M, David TZ, Simon J. Effect of vessel wall segmentation on volumetric and radiomic parameters of coronary plaques with adverse characteristics. *J Cardiovasc Comput Tomogr* 2021;**15**:137–45.

31. Maroules CD, Hamilton-Craig C, Branch K, Lee J, Cury RC, Maurovich-Horvat P *et al.* Coronary artery disease reporting and data system (CAD-RADS(TM)): inter-observer agreement for assessment categories and modifiers. *J Cardiovasc Comput Tomogr* 2018;**12**:125–30.

32. Bittencourt MS, Hulten E, Ghoshhajra B, O'Leary D, Christman MP, Montana P *et al.* Prognostic value of nonobstructive and obstructive coronary artery disease detected by coronary computed tomography angiography to identify cardiovascular events. *Circ Cardiovascular Imaging* 2014;**7**:282–91.

33. Won KB, Lee SE, Lee BK, Park HB, Heo R, Rizvi A *et al.* Longitudinal quantitative assessment of coronary plaque progression related to body mass index using serial coronary computed tomography angiography. *Eur Heart J Cardiovasc Imaging* 2019;**20**:591–9.

34. Lehman SJ, Schlett CL, Bamberg F, Lee H, Donnelly P, Shturman L *et al.* Assessment of coronary plaque progression in coronary computed tomography angiography using a semiquantitative score. *JACC Cardiovasc Imaging* 2009;**2**:1262–70.

35. Nakanishi R, Ceponiene I, Osawa K, Luo Y, Kanisawa M, Megowan N *et al.* Plaque progression assessed by a novel semi-automated quantitative plaque software on coronary computed tomography angiography between diabetes and non-diabetes patients: a propensity-score matching study. *Atherosclerosis* 2016;**255**:73–9.

36. Won KB, Lee SE, Lee BK, Park HB, Heo R, Rizvi A *et al.* Longitudinal assessment of coronary plaque volume change related to glycemic status using serial coronary computed tomography angiography: A PARADIGM (Progression of AtheRosclerotic PlAque DetermIned by Computed TomoGraphic Angiography Imaging) substudy. *J Cardiovasc Comput Tomogr* 2019;**13**:142–7.

37. Huxley RR, Woodward M. Cigarette smoking as a risk factor for coronary heart disease in women compared with men: a systematic review and meta-analysis of prospective cohort studies. *Lancet* 2011;**378**:1297–305.

38. Li WJ, Zhang HY, Miao CL, Tang RB, Du X, Shi JH *et al.* Cigarette smoking inhibits the anti-platelet activity of aspirin in patients with coronary heart disease. *Chin Med J (Engl)* 2011;**124**:1569–72.

39. Leone A, Giannini D, Bellotto C, Balbarini A. Passive smoking and coronary heart disease. *Curr Vasc Pharmacol* 2004;**2**:175–82.

frontiers | Frontiers in **Cardiovascular Medicine**

Association between coronary plaque volume and myocardial ischemia detected by dynamic perfusion CT imaging

Borbála Vattay[1], Sarolta Borzsák[1], Melinda Boussoussou[1], Milán Vecsey-Nagy[1], Ádám L. Jermendy[1], Ferenc I. Suhai[1], Pál Maurovich-Horvat[1,2], Béla Merkely[1], Márton Kolossváry[1] and Bálint Szilveszter[1]*

[1]Cardiovascular Imaging Research Group, Heart and Vascular Center, Semmelweis University, Budapest, Hungary, [2]Medical Imaging Center, Semmelweis University, Budapest, Hungary

Introduction: We aimed to evaluate the relationship between quantitative plaque metrics derived from coronary CT angiography (CTA) and segmental myocardial ischemia using dynamic perfusion CT (DPCT).

Methods: In a prospective single-center study, patients with > 30% stenosis on rest CTA underwent regadenoson stress DPCT. 480 myocardium segments of 30 patients were analyzed. Quantitative plaque assessment included total plaque volume (PV), area stenosis, and remodeling index (RI). High-risk plaque (HRP) was defined as low-attenuation plaque burden > 4% or RI > 1.1. Absolute myocardial blood flow (MBF) and relative MBF (MBFi: MBF/75th percentile of all MBF values) were quantified. Linear and logistic mixed models correcting for intra-patient clustering and clinical factors were used to evaluate the association between total PV, area stenosis, HRP and MBF or myocardial ischemia (MBF < 101 ml/100 g/min).

Results: Median MBF and MBFi were 111 ml/100 g/min and 0.94, respectively. The number of ischemic segments were 164/480 (34.2%). Total PV of all feeding vessels of a given myocardial territory differed significantly between ischemic and non-ischemic myocardial segments ($p = 0.001$). Area stenosis and HRP features were not linked to MBF or MBFi (all $p > 0.05$). Increase in PV led to reduced MBF and MBFi after adjusting for risk factors including hypertension, diabetes, and statin use (per 10 mm^3; $\beta = -0.035$, $p < 0.01$ for MBF; $\beta = -0.0002$, $p < 0.01$ for MBFi). Similarly, using multivariate logistic regression total PV was associated with ischemia (OR = 1.01, $p = 0.033$; per 10 mm^3) after adjustments for clinical risk factors, area stenosis and HRP.

Conclusion: Total PV was independently associated with myocardial ischemia based on MBF, while area stenosis and HRP were not.

Introduction

Currently luminal stenosis is the most dominant factor in the management of coronary artery disease (CAD) (1). Quantitative plaque assessment and adverse plaque characteristics may further improve cardiovascular risk prediction and patient management (2). Furthermore, anatomical and functional assessment of CAD could also improve clinical outcomes (3), however, the link between stenosis severity and myocardial ischemia is controversial (4).

CT angiography (CTA) is a uniquely suited imaging modality that can simultaneously evaluate plaque morphology and ischemia (5). Also, CTA allows accurate characterization and quantification of coronary plaques over stenosis assessment. Moreover, myocardial dynamic perfusion CT (DPCT) provides functional data and can quantitatively assess myocardial perfusion during pharmacological stress (6).

Former observational studies evaluated the link between coronary plaque burden and global myocardial ischemia using qualitative/visual assessment by either static CT perfusion (CTP) (7), stress echocardiography (8) or SPECT (9). Based on these studies, whether stenosis severity, adverse plaque features or coronary plaque burden is predictive for ischemia remains uncertain. Also, it is unknown whether quantitative plaque characterization can predict segmental ischemia as assessed by quantitative DPCT imaging. Previous studies exclusively reported vessel-based data, however, we applied a novel segment-based analysis considering only coronary lesions corresponding to myocardial territories.

Our aim was to elucidate the association between quantitative atherosclerotic plaque metrics derived from coronary CTA and segmental myocardial ischemia based on myocardial blood flow (MBF) as detected by DPCT imaging.

Materials and methods

Study population and protocol

Patients with stable chest pain and > 30% coronary stenosis detected on rest CTA were screened for our prospective, single-center study. Inclusion criteria were at least 30% stenosis in one of the main coronary arteries and excellent image quality for the quantitative analysis of the whole coronary tree. Exclusion criteria were prior myocardial infarction or revascularization, heart transplantation, contraindication to regadenoson or low image quality for quantitative assessment of coronary lesions. Regadenoson stress DPCT was performed at a separate appointment after written informed consent was obtained from all patients. Subjects with low image quality for the assessment of myocardial ischemia were excluded ($n = 1$). Patients were enrolled in the analysis if found eligible based on

inclusion and exclusion criteria. Flow chart of the study is shown in **Figure 1**.

The study was approved by the national ethical committee (National Institute of Pharmacy and Nutrition—OGYÉI/719/2017) and was performed in accordance with the Helsinki declaration.

Demographic data and comorbidities were collected by reviewing patients' medical records. Hypertension was determined as systolic blood pressure > 140 mmHg and/or diastolic blood pressure > 90 mmHg based on office measurements or the use of antihypertensive therapy. Diagnosis of hyperlipidemia was based on total cholesterol level > 200 mg/dL or the administration of lipid-lowering medication. Diabetes mellitus was defined as elevated plasma glucose levels (fasting plasma glucose $\geq$ 126 mg/dL; HbA1C $\geq$ 6.5%) or the use of antidiabetic medication or insulin therapy.

Coronary CT angiography protocol

Prospectively triggered CTA scan of the heart was performed according to the guidelines of the Society of Cardiovascular Computed Tomography (SCCT) with a 256-slice multidetector row CT (Brilliance iCT, Philips Healthcare, Cleveland, OH, United States) (10). *Per os* beta blocker was administered 1 h prior examination if the heart rate (HR) was above 65 beats/min. All patients received 0.8 mg of sublingual nitroglycerine before CTA scanning if systolic blood pressure was > 100 mmHg, and in case of HR > 60 beats per minute intravenous beta blocker was additionally administered. Image acquisition was performed at diastole (75–81% of the R–R interval) or at systole (37–43% of the R–R interval) in case of HR > 70 beats per minute despite premedication. The following scan parameters were applied: 270 ms gantry rotation time, 128 × 0.625 mm collimation, tube voltage 100–120 kVp, and tube current 200–300 mAs based on patient's body mass index (BMI). A four-phasic contrast injection protocol was used with 85–95 ml contrast agent at a flow rate of 4.5–5.5 ml/s. Axial images were reconstructed with 0.6 mm slice thickness using iterative reconstruction (iDose4 Level 5, Philips Healthcare, Cleveland, OH, United States).

Dynamic perfusion CT protocol

Stress DPCT scan was performed after rest CTA at a separate appointment with the same scanner. Hyperemia was induced using single dose of 400 μg intravenous regadenoson (Rapiscan®, GE Healthcare) (11). Stress acquisition was performed during a single breath-hold in inspiration, 1 min after bolus regadenoson was administered during peak stress covering 25–30 cardiac cycles (12). Patients' HR, oxygen saturation and blood pressure were monitored to confirm
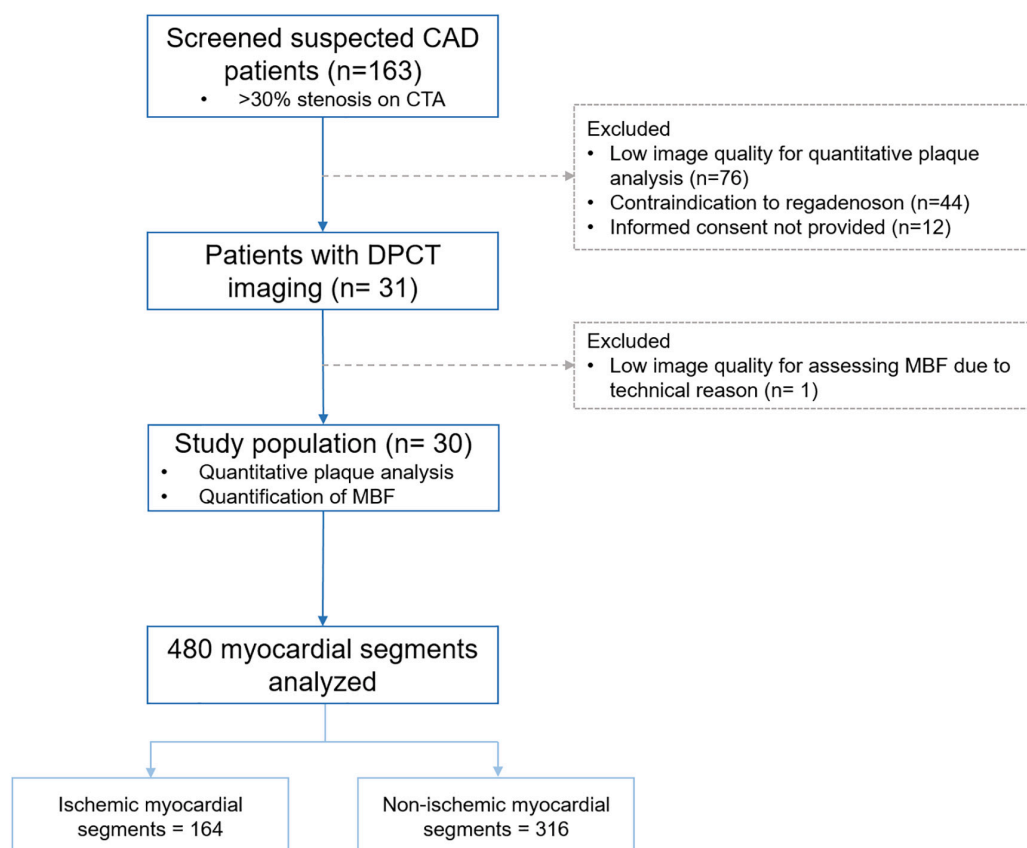
FIGURE 1

Flow-chart of the study. CAD, Coronary artery disease; CTA, CT angiography; DPCT, Dynamic perfusion CT; MBF, Myocardial blood flow.

appropriate levels of stress for CTP imaging. Contrast injection protocol included 50–60 ml contrast bolus at an infusion rate of 5 ml/s, followed by 30 ml saline chaser. Prospective electrocardiogram (ECG)-gated dynamic mode (with 64 × 1.25 mm collimation, 360° reconstruction, 8 cm coverage) was acquired in systolic phase (35% of the RR interval), with tube voltage of 80–120 kVp and tube current of 100–250 mAs based on patient's BMI. Images were reconstructed using hybrid iterative reconstruction (iDOSE4 level 5, Philips Healthcare, Cleveland, OH, United States) with 2.0 mm slice thickness and 2.0 mm increment.

Quantitative plaque analysis

Coronary artery segments were defined using an 18-segment model as recommended by the SCCT guidelines (10). CTA images were transferred into a dedicated software tool (QAngioCT Research Edition v3.1; Medis Medical Imaging Systems, Leiden, The Netherlands) for quantitative plaque analysis. Images were analyzed by a single reader (BV, 3 years of experience with cardiac CT) blinded to patient's data and

perfusion parameters. The software automatically extracted the coronary tree. All coronary vessels with a diameter > 1.5 mm were evaluated. After automatic contouring of the lumen and vessel wall, manual correction was performed—if needed—in both longitudinal and cross-sectional views at 0.5 mm increments. The proximal and distal borders of coronary plaques were defined for quantification. Coronary plaque was defined on the CTA based on former publications (13). Chronic total occlusions were not present in current patient population. Plaque composition was determined using fixed thresholds: low-attenuation plaque (LAP): −100–30 HU; non-calcified plaque (NCP): 31–350 HU; calcified plaque (CP): $\geq$ 351 HU. Volumes of total plaque, LAP, NCP and CP were calculated. LAP burden defined as the ratio of LAP volume and vessel volume (LAP volume × 100%/vessel volume) was also determined. Lumen area stenosis was defined at the site of the maximal luminal stenosis of the coronary plaque. Remodeling index (RI) was calculated as the ratio of the vessel wall area at the site of the maximal luminal narrowing and the reference vessel wall area. High-risk plaque (HRP) was defined based on quantitative LAP burden > 4% or a RI > 1.1 (2, 14).
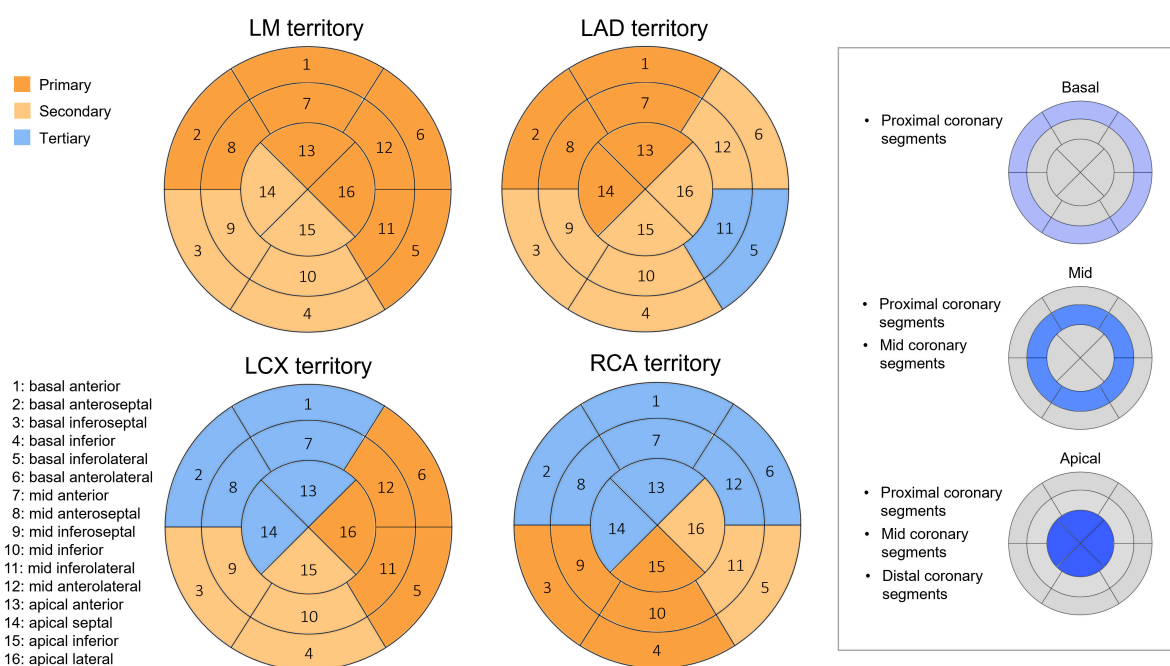
FIGURE 2
Integration of coronary anatomy and myocardial territories. Vessel territories were defined based on the modified method after Cerci et al. for LM, LAD, LCX, and RCA. The following categories were determined for myocardial segments: primary—most commonly supplied territories in case of right dominance; secondary—might be supplied territories in case of normal variations; tertiary—usually not supplied territories. In addition, coronary segment-based analysis was also used, taking lesion location into account. For that, basal segments were aligned with proximal, mid segments with proximal and mid, and apical segments with proximal, mid and distal coronary segments. LAD, Left anterior descending; LCX, Left circumflex; LM, Left main; RCA, Right coronary artery.

Myocardial perfusion analysis

DPCT images were analyzed using a dedicated software (Intellispace Portal; Philips Healthcare, Cleveland, OH, United States). Elastic registration and temporal filtering were applied for motion artifact reduction. Time-attenuation curves (TAC) created in the left ventricular outflow tract were used as arterial input function for perfusion analysis. Short-axis views were created for the assessment of the left ventricular myocardial tissue. MBF was computed applying a hybrid deconvolution method (12). The assessment of MBF was obtained by two readers (B.V and S.B, 3 and 4 years of experience with cardiac CT) in random order blinded to plaque data and patient characteristics. A ROI > 0.5 cm2 was set in each myocardial segment (intramural) using a 16-segment model excluding the apex carefully avoiding any artifacts on short-axial images (15). Segmental myocardial ischemia was defined as MBF < 101 ml/100 g/min based on Pontone et al. (16). In addition, relative MBF (MBFi) for each segment was also calculated as the ratio of absolute MBF to reference MBF, latter defined as the 75th percentile of all MBF values of a given patient (17).

Integration of coronary anatomy and myocardial territories

Coronary lesions were assigned to the corresponding myocardial segment based on the modified method after Cerci et al. for the CORE320 (Coronary Artery Evaluation Using 320-Row Multidetector CTA) trial (18). Former studies performed vessel-based analysis for the alignment of myocardial territories and supplying vessels. For our segment-based approach, we defined all coronary artery segments that supply a given myocardial segment of the 16 analyzed segments based on dominance, segment location in relation to basal, mid-ventricular or apical regions (Figure 2).

After the adjudication was performed by B.S.,—with 8 years of experience in cardiac imaging—volumes for total, NCP and CP of all relevant supplying coronary segments were summed for each myocardial segment. LAP burden was also calculated from the summed LAP and vessel volume. If LAP burden exceeded 4% of all plaque supplying a given segment, or the highest RI of the corresponding lesions was > 1.1, we marked as HRP. Summed plaque volumes (PVs), the highest degree of lumen area stenosis and HRP

(LAP burden > 4% or a RI > 1.1) of the supplying coronary segments were analyzed for the corresponding myocardial segment.

Statistical analysis

Continuous variables are presented as mean and standard deviation, whereas categorical parameters are presented as frequency with percentages. Independent t-test was used to compare parameters describing coronary plaque burden between ischemic and non-ischemic segments. Pearson correlation was used to define the association between total, NCP and CP volumes. Linear and logistic mixed models correcting for intra-patient clustering and clinical factors were used to assess the association between total PV, maximal area stenosis, quantitative HRP features and absolute MBF, MBFi or myocardial ischemia using 101 ml/100 g/min as cut-off value for MBF. Models were adjusted for predefined clinical risk factors of CAD and possible modifiers of ischemia including hypertension, diabetes mellitus and statin therapy.

Intraclass correlation coefficient (ICC) of MBF was calculated for 160 segments of 10 randomly selected patients between two readers with 3 or more years of experience in cardiac CT imaging (BV and SB). ICC values greater than 0.80 were considered good, values above 0.90 were considered to have excellent reproducibility. Also, reproducibility of quantitative plaque assessment was evaluated between two independent readers based on 10 plaques of randomly selected patients. All statistical analyses were performed using SPSS (version 24.0) and R software (version 3.6.1). $P < 0.05$ was defined as statistically significant.

Results

Patient characteristics

The baseline characteristics of the 30 analyzed patients (mean age 60.9 ± 8.3 years, 26.7% female, mean BMI 28.9 ± 3.8 kg/m^2) are summarized in **Table 1**. Common comorbidities were hypertension (76.7%) and dyslipidemia (76.7%).

On average, 13.0 ± 8.6 days have passed between the two examinations. Mean effective radiation dose was 4.4 ± 1.1 mSv for rest CTA and 8.9 ± 4.0 mSv for DPCT. A total of 496 coronary artery segments and 480 myocardial segments were evaluated quantitatively. ICC between readers was 0.96 and 0.93 for MBF and total PV, respectively.

TABLE 1 Patient characteristics.

	Patient population $N = 30$
Age, years	60.9 ± 8.3
Male gender, n (%)	22 (73.3)
BMI, kg/m^2	28.9 ± 3.8
Hypertension, n (%)	23 (76.7)
Diabetes mellitus, n (%)	2 (6.7)
Dyslipidemia, n (%)	23 (76.7)
Smoking, n (%)	16 (53.3)
Cerebrovascular disease, n (%)	1 (3.3)
Peripheral artery disease, n (%)	3 (10.0)
Family history of premature CAD, n (%)	9 (30.0)
Oral anticoagulant therapy, n (%)	6 (20.0)
Statin therapy, n (%)	16 (53.3)
ACE-I/ARB therapy, n (%)	18 (60.0)
Beta-blocker therapy, n (%)	15 (50.0)

Continuous variables are described as mean ± SD, whereas categorical variables are represented as frequencies and percentage.
ACE-I, Angiotensin-converting-enzyme inhibitor; ARB, Angiotensin receptor blocker; BMI, Body mass index; CAD, Coronary artery disease.

Plaque characteristics and segmental myocardial ischemia

Total PV, NCP volume, and CP volume differed significantly between ischemic and non-ischemic myocardial segments, 120.5 ± 119.5 mm^3 vs. 84.6 ± 82.2 mm^3, $p = 0.001$; 62.3 ± 59.5 mm^3 vs. 51.4 ± 54.9 mm^3, $p = 0.045$; 58.3 ± 91.8 mm^3 vs. 33.3 ± 50.6 mm^3, $p = 0.001$; respectively (**Table 2**). Median and interquartile range (IQR) of PVs for ischemic and non-ischemic myocardial segments were: total PV: 82.9 (31.1–179.6) vs. 68.7 (25.8–114.7) mm^3; NCP volume: 46.1 (24.3–93.7) vs. 31.6 (12.4–73.8) mm^3; CP volume: 15.9 (0.1–78.2) vs. 17.3 (2.2–46.1) mm^3. **Figure 3** demonstrates box plots of quantitative PVs in coronary segments supplying ischemic and non-ischemic myocardial segments. On a patient level, the average of maximal lumen area stenosis of the worst lesion was 54.7 ± 15.9%. On a segmental level, the average of the maximal lumen area stenosis was 37.2 ± 22.7% for ischemic and 33.5 ± 20.7% for non-ischemic myocardial segments ($p = 0.072$). HRP was present in 21.3% in ischemic and 19.0% in non-ischemic territories ($p = 0.539$).

Number of ischemic segments were 164/480 (34.2%). Median MBF was 111 ml/100 g/min, while median MBFi was 0.94.

Total PV strongly correlated with NCP volume ($r = 0.73$, $p < 0.001$) and CP volume ($r = 0.83$, $p < 0.001$), we therefore included total PV in the multivariate prediction models to avoid multicollinearity.
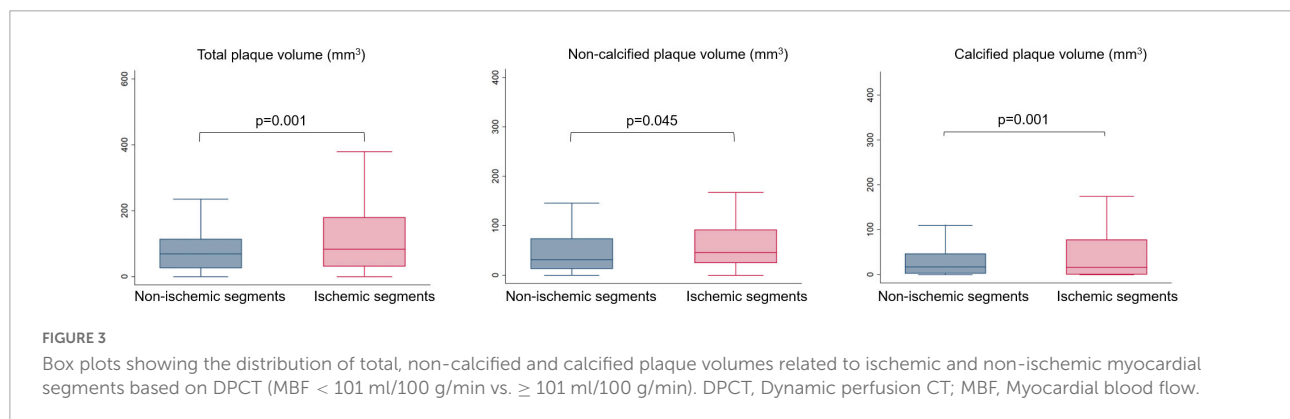
TABLE 2   Coronary plaque characteristics in ischemic and non-ischemic myocardial segments.

	Ischemic myocardial segments $N = 164$	Non-ischemic myocardial segments $N = 316$	P
Total plaque volume, mm³	120.5 ± 119.5	84.6 ± 82.2	**0.001**
NCP volume, mm³	62.3 ± 59.5	51.4 ± 54.9	**0.045**
CP volume, mm³	58.3 ± 91.8	33.3 ± 50.6	**0.001**
High-risk plaque, n (%)	35 (21.3)	60 (19.0)	0.539
Lumen area stenosis,%	37.2 ± 22.7	33.5 ± 20.7	0.072

Myocardial ischemia was defined as MBF < 101 ml/100 g/min. Continuous variables are described as mean ± SD, whereas categorical variables are represented as frequencies and percentage.
Bold values indicate significant differences based on the p-values.
CP, Calcified plaque; MBF, Myocardial blood flow; NCP, Non-calcified plaque.

FIGURE 3

Box plots showing the distribution of total, non-calcified and calcified plaque volumes related to ischemic and non-ischemic myocardial segments based on DPCT (MBF < 101 ml/100 g/min vs. ≥ 101 ml/100 g/min). DPCT, Dynamic perfusion CT; MBF, Myocardial blood flow.

Predictors of absolute and relative myocardial blood flow

Using linear mixed models, univariate analysis revealed that total PV predicted both absolute and relative MBF values (Table 3). Clinical risk factors (including hypertension, diabetes mellitus, and statin use), HRP and stenosis severity were not associated with impaired myocardial perfusion based on MBF and MBFi.

On multivariate analysis, total PV increase led to reduced absolute and relative MBF values even after adjusting for clinical risk factors, lumen area stenosis and HRP features: per 10 mm³; $\beta = -0.035$, $p < 0.01$ for MBF and $\beta = -0.0002$, $p < 0.01$ for MBFi. Notably, lumen area stenosis and quantitative HRP features were not linked to absolute or relative MBF values (all $p > 0.05$).

Predictors of myocardial ischemia based on myocardial blood flow threshold

On univariate logistic regression total PV and lumen area stenosis were significant predictors of myocardial ischemia based on MBF < 101 ml/100 g/min (Table 4). After adjusting for predefined clinical risk factors, stenosis severity and

HRP, increase in total PV was independently associated with myocardial ischemia: OR: 1.01, $p = 0.033$ (per 10 mm³). However, on multivariate analysis HRP feature and lumen area stenosis were not linked to ischemia (both $p > 0.05$).

Discussion

We used a novel approach to define the contribution of coronary PV to limited flow (ischemia) of all feeding coronary segments considering only coronary lesions prior to a given myocardial territory. We established that total PV influenced myocardial perfusion on a segmental level, independent from stenosis severity, HRP and risk factors. Moreover, maximal luminal area stenosis and the presence of HRP were not linked to myocardial ischemia based on MBF. Reproducibility was excellent for the evaluation of MBF or total PV.

While there are several alternative imaging modalities to analyze the hemodynamic consequence of coronary plaques, CT is the only non-invasive modality for the combined assessment of morphology and function of CAD. CT can provide several additional anatomical parameters that could be incremental as compared with traditional evaluation focusing on luminal stenosis or lesion length. In agreement with our findings, total PV was linked to visual perfusion defects as assessed by SPECT (9, 19). Liu et al. also reported that low-density PV

TABLE 3 Univariate analysis of the predictors of absolute and relative myocardial blood flow (MBFi) detected by DPCT using linear mixed models.

Predictors	Absolute MBF detected by DPCT			Relative MBF detected by DPCT		
	Univariate model			Univariate model		
	β	95% CI	P	β	95% CI	P
Total plaque volume, per 10 mm^3	**-0.025**	**-0.043—-0.007**	**0.006**	**-0.0002**	**-0.0003—-0.0001**	**0.004**
NCP volume, per 10 mm^3	−0.025	−0.053–0.003	0.079	−0.0002	−0.0004–0.0000	0.077
CP volume, per 10 mm^3	**-0.046**	**-0.078—-0.014**	**0.005**	**-0.0002**	**-0.0004—-0.00006**	**0.008**
Remodeling index	1.934	−2.427–6.295	0.384	0.003	−0.029–0.036	0.838
High-risk plaque	1.952	−1.767–5.672	0.303	0.018	−0.009–0.045	0.191
Lumen area stenosis	−4.479	−12.008–3.050	0.243	−0.042	−0.093–0.009	0.108
Age, years	−0.172	−1.208–0.864	0.736	0.0006	−0.001–0.002	0.463
BMI, kg/m^2	−0.791	−3.037–1.455	0.477	**0.004**	**0.0007–0.007**	**0.017**
Hypertension	−1.482	−21.491–18.527	0.881	0.010	−0.019–0.039	0.491
Diabetes mellitus	1.542	−32.393–35.478	0.926	0.018	−0.031–0.068	0.456
Smoking	1.536	−15.424–18.496	0.854	0.013	−0.011–0.038	0.274
Statin therapy	−3.201	−20.127–13.724	0.701	−0.005	−0.030–0.020	0.658

Bold values indicate significant differences based on the p-values.
CP, Calcified plaque; BMI, Body mass index; DPCT, Dynamic perfusion CT; MBF, Myocardial blood flow; MBFi, Myocardial blood flow index; NCP, Non-calcified plaque.

TABLE 4 Univariate logistic regression analysis of the predictors of myocardial ischemia detected by DPCT.

Predictors	Myocardial ischemia detected by DPCT		
	Univariate model		
	OR	95% CI	P
Total plaque volume, per 10 mm^3	**1.01**	**1.002–1.012**	**0.003**
NCP volume, per 10 mm^3	**1.01**	**1.004–1.018**	**0.002**
CP volume, per 10 mm^3	1.01	0.997–1.015	0.172
Remodeling index	1.14	0.422–3.059	0.801
High-risk plaque	0.79	0.333–1.890	0.601
Lumen area stenosis	**8.05**	**1.340–48.333**	**0.023**
Age, years	1.03	0.839–1.268	0.770
BMI, kg/m^2	1.26	0.787–2.019	0.335
Hypertension	2.86	0.046–177.116	0.617
Diabetes mellitus	1.74	0.003–883.279	0.861
Smoking	0.96	0.031–29.434	0.982
Statin therapy	4.06	0.108–152.174	0.448

Myocardial ischemia was defined as MBF < 101 ml/100 g/min.
Bold values indicate significant differences based on the p-values.
CP, Calcified plaque; BMI, Body mass index; DPCT, Dynamic perfusion CT; MBF, Myocardial blood flow; NCP, Non-calcified plaque.

and diameter stenosis were also independently associated with myocardial ischemia. Driessen et al. evaluated 208 patients who underwent (^{15}O) H$_2$O PET-MPI and coronary CTA and found that plaque length and volume were inversely associated with MBF in a sub-study of the PACIFIC trial (20). Moreover,

this study suggested a link between decreased flow and NCP volume or positive remodeling in a vessel-based analysis. The multicenter CORE 320 study demonstrated that combined CTA and CTP has excellent diagnostic performance to detect flow-limiting lesions (more than 50%) by invasive angiography and perfusion defects by SPECT. van Rosendael et al. utilized static stress CTP in a total of 84 patients to evaluate the relationship between morphological plaque features and visual perfusion deficits (7). Interestingly, increasing stenosis severity and lesion length were predictors of ischemia, however PVs were not. Previous studies examining the association between PV and ischemia in stable angina patients reported highly variable mean values for total PV: 69.0 ± 16.8 mm^3 vs. 49.6 ± 17.2 mm^3 by van Rosendael et al. (7), 114 ± 118 mm^3 vs. 62 ± 89 mm^3 by Diaz-Zamudio et al. (9), and 694.6 ± 485.1 mm^3 vs. 422.3 ± 387.9 mm^3 by Min et al. (21), for ischemic and non-ischemic myocardial territories, respectively. In our current study, total PV for ischemic segments were 120.5 ± 119.5 mm^3 while for non-ischemic segments it was 84.6 ± 82.2 mm^3.

As highlighted above, there are conflicting results on whether luminal narrowing, plaque composition and vulnerability or plaque burden precipitate ischemia. This could originate from the high inter-vendor, inter-scanner, inter-protocol variability of coronary plaque assessment and from the methodology used for the characterization of ischemia. To our knowledge, there are currently no studies evaluating both myocardial ischemia and CAD quantitatively, on a segment level using CT imaging. Also, most of the former studies used visual assessment for detecting perfusion defects. However, quantitative methods are more reproducible and might provide
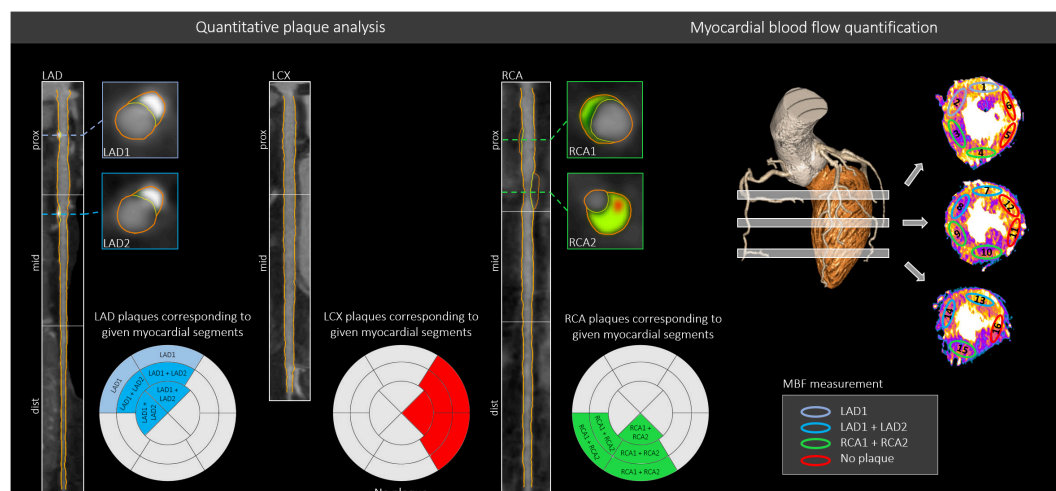
FIGURE 4
Comprehensive plaque assessment and the evaluation of myocardial ischemia based on CT images. A representative case of our study depicts the images of a 62-year-old male patient who underwent coronary CTA and DPCT imaging for the evaluation of CAD and corresponding myocardial ischemia. In this case, plaques were detected and quantified in the proximal LAD (LAD1), mid-LAD (LAD2) and proximal RCA (RCA1 + RCA2) coronary segments. All coronary plaques based on their location were matched for a given myocardial territory. MBF was quantified for all 16 myocardial segments using DPCT images. By creating a myocardial vessel territory map for each coronary segment, we could derive the total plaque volume that possibly influences the blood flow quantified as MBF on DPCT to any of the 16 analyzed LV territories (see **Figure 2** for segmental classification). In this case, basal anterior (1) and basal anteroseptal (2) myocardial segments were influenced by the proximal LAD (LAD1) lesion, while the mid anterior (7), mid anteroseptal (8), apical anterior (13), and apical septal (14) myocardial segments were affected by two lesions: LAD1 and LAD2 (mid LAD segment) as they are located more distally. No plaques were present in the LCX. Regarding the RCA, two plaques were detected in the proximal RCA segment (RCA1 and RCA2), therefore all myocardial segments corresponding to the RCA were influenced by two plaques (RCA1 and RCA2). Plaque volumes of the lesions aligned for a given myocardial segment were summed and accounted for in the analysis, while the highest degree of lumen area stenosis of the corresponding lesions was included in the analysis. Light blue color indicates LV segments related to proximal LAD lesion, dark blue color indicates LV territories related to both proximal and mid-LAD lesions, whereas green color shows myocardial territories corresponding to the RCA lesions. LCX demonstrated no coronary lesions. ROI-s were placed in each myocardial segment on short-axial images. CAD, Coronary artery disease; CTA, CT angiography; DPCT, Dynamic perfusion CT; LAD, Left anterior descending; LCX, Left circumflex; LV, Left ventricle; MBF, Myocardial blood flow; RCA, Right coronary artery.

a more detailed analysis of LV blood flow based on different perfusion markers. One of the largest challenges is the precise alignment of a myocardial territory to its feeding vessels. The most common approach is to calculate an accumulated PV for a given vessel, however this could not tailor unique variations in coronary anatomy and lesions on the distal coronary segments should not be taken into consideration when assessing perfusion in the basal myocardium. Authors of the CORE320 trial sought to assign coronary lesions to the corresponding myocardial segment taking anatomical variations and coronary dominance into account (18). For our segment-based approach, we defined all coronary artery segments that supply a given myocardial segment (16-segment model) based on dominance, segment location in relation to basal, mid-ventricular or apical regions (**Figure 2**). A representative case and the detailed description of our methodology are demonstrated on **Figure 4**. Using this approach, we aimed to overcome a main limitation of former studies which performed vessel-based analysis when evaluating ischemia. However, a distally localized lesion in the coronary vessel does not limit the flow of the most basal segments and this could substantially influence the results. Also, apical region of the heart can be supplied by several contributing

vessel segments and therefore all of the lesions should be taken into consideration.

The discordance between stenosis severity and ischemia has been reported using both non-invasive and invasive methods. As previously described by Schuijf et al. in patients with obstructive CAD detected on coronary CTA, only 50% had ischemia using SPECT, while ischemia was detected in 15% of patients without obstructive CAD (4). Similarly, in the FAME study discrepancy was identified between anatomic and functional stenosis severity assessed by invasive angiography and FFR (22). Despite these findings, our current clinical management heavily relies on treating coronary lesions based on ischemic burden. However, total coronary plaque burden might step forward as the target of early interventions to stabilize HRPs, reduce the progression of coronary PV and luminal stenosis and thus ultimately to prevent adverse events.

Conflicting results regarding the relationship of plaques and ischemia may originate from the different capabilities of the modality utilized in the trials. CT has several advantages as compared with other techniques such as better spatial resolution, robust plaque assessment and reproducible quantitative measures of perfusion. CT imaging can define the

hemodynamic significance of CAD by defining either lesion-specific ischemia using CT derived fractional flow reserve (FFR) or global ischemia on DPCT imaging. Radiation dose however still limits its use—especially using dynamic CT protocols—for a large subset of patients. Growing body of evidence suggests that anatomical information derived from CTA outperforms traditional ischemia testing for defining lesion-specific ischemia as obtained from invasive FFR. The CREDENCE trial demonstrated a strong association between atherosclerotic PVs, lumen size and invasive FFR (23). Our study provides unique insight in the interplay of coronary plaque burden, stenosis severity, HRP anatomy and corresponding myocardial ischemia on CTA. While HRP was linked to lesion-specific ischemia based on several trials (24), we did not see an association with reduced MBF on a segmental level. We found that considering all possible plaque on the feeding vessels of a given myocardial territory, total PV aggravates MBF or MBFi (per 10 mm^3; β = −0.035, $p < 0.01$ for MBF and β = −0.0002, $p < 0.01$ for MBFi). This observation seems valid across different stages of stenosis severity and thus detailed plaque quantification could effectively guide secondary prevention therapy in a large spectrum of contemporary chest pain patients. Integrating plaque burden in the clinical CTA reports and thus in personalized patient management should be in the focus rather than luminal narrowing *per se*.

We acknowledge the limitations of our study. First, the sample size is limited after excluding patients with non-diagnostic image quality for quantitative plaque analysis or patients without intermediate stenosis. Excellent image quality is a prerequisite for quantitative plaque analysis. This could result in selection bias for our analysis. Quantitative plaque analysis is time-consuming and currently only a research tool, not used in routine clinical practice. However, experts of the field underline its role in risk prediction and tools are being developed for automated quantification in the near future. Also, our study is underpowered for the assessment of gender differences in CAD and corresponding ischemia or for outcome analysis.

Conclusion

Total coronary PV was independently associated with myocardial ischemia based on MBF derived from DPCT imaging, while area stenosis and HRP were not. Incorporating these quantitative plaque characteristics in a comprehensive coronary CTA evaluation could improve the prediction of ischemic CAD, independently of lesion severity.

Data availability statement

The data that support the findings of this study are available from the corresponding author, upon reasonable request.

Ethics statement

The studies involving human participants were reviewed and approved by National Institute of Pharmacy and Nutrition—OGYÉI/719/2017. The patients/participants provided their written informed consent to participate in this study.

Author contributions

Funding

Conflict of interest

The authors declare that the research was conducted in the absence of any commercial or financial relationships that could be construed as a potential conflict of interest.

Publisher's note

All claims expressed in this article are solely those of the authors and do not necessarily represent those of their affiliated organizations, or those of the publisher, the editors and the reviewers. Any product that may be evaluated in this article, or claim that may be made by its manufacturer, is not guaranteed or endorsed by the publisher.

References

1. Knuuti J, Wijns W, Saraste A, Capodanno D, Barbato E, Funck-Brentano C, et al. 2019 ESC Guidelines for the diagnosis and management of chronic coronary syndromes. *Eur Heart J.* (2020) 41:407–77.

2. Williams MC, Kwiecinski J, Doris M, McElhinney P, D'Souza MS, Cadet S, et al. Low-Attenuation noncalcified plaque on coronary computed tomography angiography predicts myocardial infarction: results from the multicenter SCOT-HEART trial (Scottish Computed Tomography of the HEART). *Circulation.* (2020) 141:1452–62. doi: 10.1161/CIRCULATIONAHA.120.049840

3. Xaplanteris P, Fournier S, Pijls NHJ, Fearon WF, Barbato E, Tonino PAL, et al. Five-year outcomes with PCI guided by fractional flow reserve. *N Engl J Med.* (2018) 379:250–9. doi: 10.1056/NEJMoa1803538

4. Schuijf JD, Wijns W, Jukema JW, Atsma DE, de Roos A, Lamb HJ, et al. Relationship between noninvasive coronary angiography with multi-slice computed tomography and myocardial perfusion imaging. *J Am Coll Cardiol.* (2006) 48:2508–14. doi: 10.1016/j.jacc.2006.05.080

5. Pontone G, Rossi A, Guglielmo M, Dweck MR, Gaemperli O, Nieman K, et al. Clinical applications of cardiac computed tomography: a consensus paper of the european association of cardiovascular imaging-part I. *Eur Heart J Cardiovasc Imaging.* (2022) 23:299–314. doi: 10.1093/ehjci/jeab293

6. Nieman K, Balla S. Dynamic CT myocardial perfusion imaging. *J Cardiovasc Comput Tomogr.* (2020) 14:303–6. doi: 10.1016/j.jcct.2019.09.003

7. van Rosendael AR, Kroft LJ, Broersen A, Dijkstra J, van den Hoogen IJ, van Zwet EW, et al. Relation between quantitative coronary CTA and myocardial ischemia by adenosine stress myocardial CT perfusion. *J Nucl Cardiol.* (2017) 24:1253–62. doi: 10.1007/s12350-016-0393-7

8. Eskerud I, Gerdts E, Larsen TH, Simon J, Maurovich-Horvat P, Lonnebakken MT. Total coronary atherosclerotic plaque burden is associated with myocardial ischemia in non-obstructive coronary artery disease. *Int J Cardiol Heart Vasc.* (2021) 35:100831. doi: 10.1016/j.ijcha.2021.100831

9. Diaz-Zamudio M, Fuchs TA, Slomka P, Otaki Y, Arsanjani R, Gransar H, et al. Quantitative plaque features from coronary computed tomography angiography to identify regional ischemia by myocardial perfusion imaging. *Eur Heart J Cardiovasc Imaging.* (2017) 18:499–507. doi: 10.1093/ehjci/jew274

10. Abbara S, Blanke P, Maroules CD, Cheezum M, Choi AD, Han BK, et al. SCCT guidelines for the performance and acquisition of coronary computed tomographic angiography: a report of the society of cardiovascular computed tomography guidelines committee: endorsed by the north american society for cardiovascular imaging (NASCI). *J Cardiovasc Comput Tomogr.* (2016) 10:435–49. doi: 10.1016/j.jcct.2016.10.002

11. Iskandrian AE, Bateman TM, Belardinelli L, Blackburn B, Cerqueira MD, Hendel RC, et al. Adenosine versus regadenoson comparative evaluation in myocardial perfusion imaging: results of the ADVANCE phase 3 multicenter international trial. *J Nucl Cardiol.* (2007) 14:645–58. doi: 10.1016/j.nuclcard.2007.06.114

12. Tanabe Y, Kido T, Uetani T, Kurata A, Kono T, Ogimoto A, et al. Differentiation of myocardial ischemia and infarction assessed by dynamic computed tomography perfusion imaging and comparison with cardiac magnetic resonance and single-photon emission computed tomography. *Eur Radiol.* (2016) 26:3790–801. doi: 10.1007/s00330-016-4238-1

13. Achenbach S, Moselewski F, Ropers D, Ferencik M, Hoffmann U, MacNeill B, et al. Detection of calcified and noncalcified coronary atherosclerotic plaque by contrast-enhanced, submillimeter multidetector spiral computed tomography: a segment-based comparison with intravascular ultrasound. *Circulation.* (2004) 109:14–7. doi: 10.1161/01.CIR.0000111517.69230.0F

14. Motoyama S, Sarai M, Harigaya H, Anno H, Inoue K, Hara T, et al. Computed tomographic angiography characteristics of atherosclerotic plaques subsequently resulting in acute coronary syndrome. *J Am Coll Cardiol.* (2009) 54:49–57. doi: 10.1016/j.jacc.2009.02.068

15. Cerqueira MD, Weissman NJ, Dilsizian V, Jacobs AK, Kaul S, Laskey WK, et al. Standardized myocardial segmentation and nomenclature for tomographic imaging of the heart. a statement for healthcare professionals from the cardiac imaging committee of the council on clinical cardiology of the american heart association. *Circulation.* (2002) 105:539–42. doi: 10.1161/hc0402.102975

16. Pontone G, Baggiano A, Andreini D, Guaricci AI, Guglielmo M, Muscogiuri G, et al. Dynamic stress computed tomography perfusion with a whole-heart coverage scanner in addition to coronary computed tomography angiography and fractional flow reserve computed tomography derived. *JACC Cardiovasc Imaging.* (2019) 12:2460–71. doi: 10.1016/j.jcmg.2019.02.015

17. Nous FMA, Geisler T, Kruk MBP, Alkadhi H, Kitagawa K, Vliegenthart R, et al. Dynamic myocardial perfusion CT for the detection of hemodynamically significant coronary artery disease. *JACC Cardiovasc Imaging.* (2022) 15:75–87. doi: 10.1016/j.jcmg.2021.07.021

18. Cerci RJ, Arbab-Zadeh A, George RT, Miller JM, Vavere AL, Mehra V, et al. Aligning coronary anatomy and myocardial perfusion territories: an algorithm for the CORE320 multicenter study. *Circ Cardiovasc Imaging.* (2012) 5:587–95. doi: 10.1161/CIRCIMAGING.111.970608

19. Liu T, Yuan X, Wang C, Sun M, Jin S, Dai X. Quantification of plaque characteristics detected by dual source computed tomography angiography to predict myocardial ischemia as assessed by single photon emission computed tomography myocardial perfusion imaging. *Quant Imaging Med Surg.* (2019) 9:711–21. doi: 10.21037/qims.2019.04.07

20. Driessen RS, Stuijfzand WJ, Raijmakers PG, Danad I, Min JK, Leipsic JA, et al. Effect of plaque burden and morphology on myocardial blood flow and fractional flow reserve. *J Am Coll Cardiol.* (2018) 71:499–509. doi: 10.1016/j.jacc.2017.11.054

21. Min JK, Chang HJ, Andreini D, Pontone G, Guglielmo M, Bax JJ. Coronary CTA plaque volume severity stages according to invasive coronary angiography and FFR. *J Cardiovasc Comput Tomogr.* (2022). doi: 10.1016/j.jcct.2022.03.001 [Epub ahead of print].

22. Tonino PA, Fearon WF, De Bruyne B, Oldroyd KG, Leesar MA, Ver Lee PN, et al. Angiographic versus functional severity of coronary artery stenoses in the FAME study fractional flow reserve versus angiography in multivessel evaluation. *J Am Coll Cardiol.* (2010) 55:2816–21. doi: 10.1016/j.jacc.2009.11.096

23. Stuijfzand WJ, van Rosendael AR, Lin FY, Chang HJ, van den Hoogen IJ, Gianni U, et al. Stress myocardial perfusion imaging vs coronary computed tomographic angiography for diagnosis of invasive vessel-specific coronary physiology: predictive modeling results from the computed tomographic evaluation of atherosclerotic determinants of myocardial ischemia (CREDENCE) Trial. *JAMA Cardiol.* (2020) 5:1338–48. doi: 10.1001/jamacardio.2020.3409

24. Danad I, Raijmakers PG, Driessen RS, Leipsic J, Raju R, Naoum C, et al. Comparison of Coronary CT Angiography, SPECT, PET, and Hybrid Imaging for Diagnosis of Ischemic Heart Disease Determined by Fractional Flow Reserve. *JAMA Cardiol.* (2017) 2:1100–7. doi: 10.1001/jamacardio.2017.2471

CARDIAC

Impact of virtual monoenergetic levels on coronary plaque volume components using photon-counting computed tomography

Borbála Vattay[1] · Bálint Szilveszter[1] · Melinda Boussoussou[1] · Milán Vecsey-Nagy[1] · Andrew Lin[2] · Gábor Konkoly[1] · Anikó Kubovje[3] · Florian Schwarz[4] · Béla Merkely[1] · Pál Maurovich-Horvat[3] · Michelle C. Williams[5] · Damini Dey[2] · Márton Kolossváry[6,7]

Abstract

Objectives Virtual monoenergetic images (VMIs) from photon-counting CT (PCCT) may change quantitative coronary plaque volumes. We aimed to assess how plaque component volumes change with respect to VMIs.

Methods Coronary CT angiography (CTA) images were acquired using a dual-source PCCT and VMIs were reconstructed between 40 and 180 keV in 10-keV increments. Polychromatic images at 120 kVp (T3D) were used as reference. Quantitative plaque analysis was performed on T3D images and segmentation masks were copied to VMI reconstructions. Calcified plaque (CP; > 350 Hounsfield units, HU), non-calcified plaque (NCP; 30 to 350 HU), and low-attenuation NCP (LAP; − 100 to 30 HU) volumes were calculated using fixed thresholds.

Results We analyzed 51 plaques from 51 patients (67% male, mean age 65 ± 12 years). Average attenuation and contrast-to-noise ratio (CNR) decreased significantly with increasing keV levels, with similar values observed between T3D and 70 keV images (299 ± 209 vs. 303 ± 225 HU, $p = 0.15$ for mean HU; 15.5 ± 3.7 vs. 15.8 ± 3.5, $p = 0.32$ for CNR). Mean NCP volume was comparable between T3D and 100–180-keV reconstructions. There was a monotonic decrease in mean CP volume, with a significant difference between all VMIs and T3D ($p < 0.05$). LAP volume increased with increasing keV levels and all VMIs showed a significant difference compared to T3D, except for 50 keV (28.0 ± 30.8 mm^3 and 28.6 ± 30.1 mm^3, respectively, $p = 0.63$).

Conclusions Estimated coronary plaque volumes significantly differ between VMIs. Normalization protocols are needed to have comparable results between future studies, especially for LAP volume which is currently defined using a fixed HU threshold.

Clinical relevance statement Different virtual monoenergetic images from photon-counting CT alter attenuation values and therefore corresponding plaque component volumes. New clinical standards and protocols are required to determine the optimal thresholds to derive plaque volumes from photon-counting CT.

Key Points
- *Utilizing different VMI energy levels from photon-counting CT for the analysis of coronary artery plaques leads to sub stantial changes in attenuation values and corresponding plaque component volumes.*

✉ Bálint Szilveszter
szilveszter.balint@med.semmelweis-univ.hu

✉ Márton Kolossváry
marton.kolossvary@gokvi.hu

1 MTA-SE "Lendület" Cardiovascular Imaging Research Group, Semmelweis University Heart and Vascular Center, Városmajor Street 68., 1122 Budapest, Hungary

2 Biomedical Imaging Research Institute, Cedars-Sinai Medical Center, 116 N Robertson Blvd, Suite 400, CA 90048 Los Angeles, USA

3 Semmelweis University Medical Imaging Center, Korányi Sándor Street 2., 1082 Budapest, Hungary

4 Clinic for Diagnostic and Interventional Radiology and Neuroradiology, University Hospital Augsburg, Stenglinstr. 2, 86156 Augsburg, Germany

5 University of Edinburgh/British Heart Foundation Centre for Cardiovascular Science, 47 Little France Crescent, Edinburgh EH16 4TJ, UK

6 Gottsegen National Cardiovascular Center, 29 Haller Utca, 1096 Budapest, Hungary

7 Physiological Controls Research Center, University Research and Innovation Center, Óbuda University, Bécsi Út 96/B, 1034 Budapest, Hungary

- *Low-energy images (40–70 keV) improved contrast-to-noise ratio, however also increased image noise.*
- *Normalization protocols are needed to have comparable results between future studies, especially for low-attenuation plaque volume which is currently defined using a fixed HU threshold.*

Abbreviations

CAD	Coronary artery disease
CNR	Contrast-to-noise ratio
CP	Calcified plaque
CTA	Computed tomography angiography
HU	Hounsfield unit
LAP	Low-attenuation non-calcified plaque
NCP	Non-calcified plaque
PCCT	Photon-counting computed tomography
ROI	Region of interest
SD	Standard deviation
SNR	Signal-to-noise ratio
VMI	Virtual monoenergetic image

Introduction

Coronary computed tomography angiography (CTA) allows characterization of atherosclerotic plaque in addition to luminal stenosis [1]. Quantifying coronary plaque burden and adverse plaque characteristics may improve cardiovascular risk prediction. Notably, low-attenuation non-calcified plaque (LAP) burden is an independent predictor of myocardial infarction [2].

Novel photon-counting CT (PCCT) is a promising technique for the assessment of coronary arteries with superior spatial and temporal resolution as compared with current-generation scanners [3]. Compared to conventional energy-integrating detectors, photon-counting detectors register the energy of each individual photon and directly convert x-ray photons to electrical signals without the need of reflecting septa, resulting in improved spatial resolution, noise reduction, and better soft tissue contrast [4]. It has previously been demonstrated on histological atherosclerotic plaque samples that different plaque components and vessel lumen can be accurately differentiated using spectral data from a PCCT system [5]. Furthermore, this allows for virtual monoenergetic images (VMIs) which may help evaluation of coronary CTA due to improvements in blooming artefact reduction and contrast-to-noise ratio (CNR) [6]. Also, PCCT allows for sharper delineation of structures such as calcifications, as it provides superior spatial resolution. Therefore, using different VMI reconstructions may improve coronary plaque detection due to changes in intraluminal contrast attenuation and CNR. However, VMIs also change the Hounsfield unit (HU) values of the voxels and therefore may impact plaque volume estimates which are often done using fixed HU thresholds.

Therefore, our aim was to assess how quantification of individual plaque components changes with respect to different monoenergetic levels obtained using PCCT.

Materials and methods

Study design and patient population

Consecutive patients referred for clinically indicated coronary CTA due to suspected or known coronary artery disease (CAD) were screened in our prospective, single-center study between April 2022 and June 2022. Inclusion criteria were (1) diagnostic image quality for quantitative plaque analysis and (2) discernible coronary lesion in at least one of the main coronary arteries. Exclusion criteria were (1) presence of stents or bypass grafts and (2) images with severe motion, breathing, beam-hardening, or misalignment artifacts.

The study was approved by the institutional ethical committee (IV/667–1/2022/EKU) and was performed in accordance with the Helsinki declaration. Written informed consent was obtained from all patients.

Coronary CTA acquisition and reconstruction

ECG-triggered CTA scans of the heart were performed using a first-generation dual-source PCCT scanner (NAEOTOM Alpha, Siemens Healthineers). Coronary CTA imaging was obtained according to the guidelines of the Society of Cardiovascular Computed Tomography [7]. Scan parameters for all patients were as follows: tube voltage = 120 kVp, automatic tube current modulation with image quality level (IQ-level) = 80, detector configuration = 144 mm × 0.4 mm, rotation time = 0.25 s. Intravenous beta blocker was administered if heart rate (HR) was > 65 beats/minute before examination. All patients received 0.8 mg of sublingual nitroglycerine before CTA scanning if systolic blood pressure was > 100 mmHg. High-pitch helical (TurboFlash) scan mode was used if HR was regular and below 70/min, sequential scan mode was applied in case of regular HR > 70 beats/min, and helical scan mode was used if HR was irregular. Images were acquired in diastole (65–85% of the R-R interval) or systole (200–400 ms) depending on the HR (< or > 75 beats/minute). A four-phasic contrast injection protocol was used with 70–80 mL contrast agent at a flow rate of 4.5–5.0 mL/s [8].

For all patients, VMIs were reconstructed at different energy levels from 40 to 180 keV in 10-keV increments
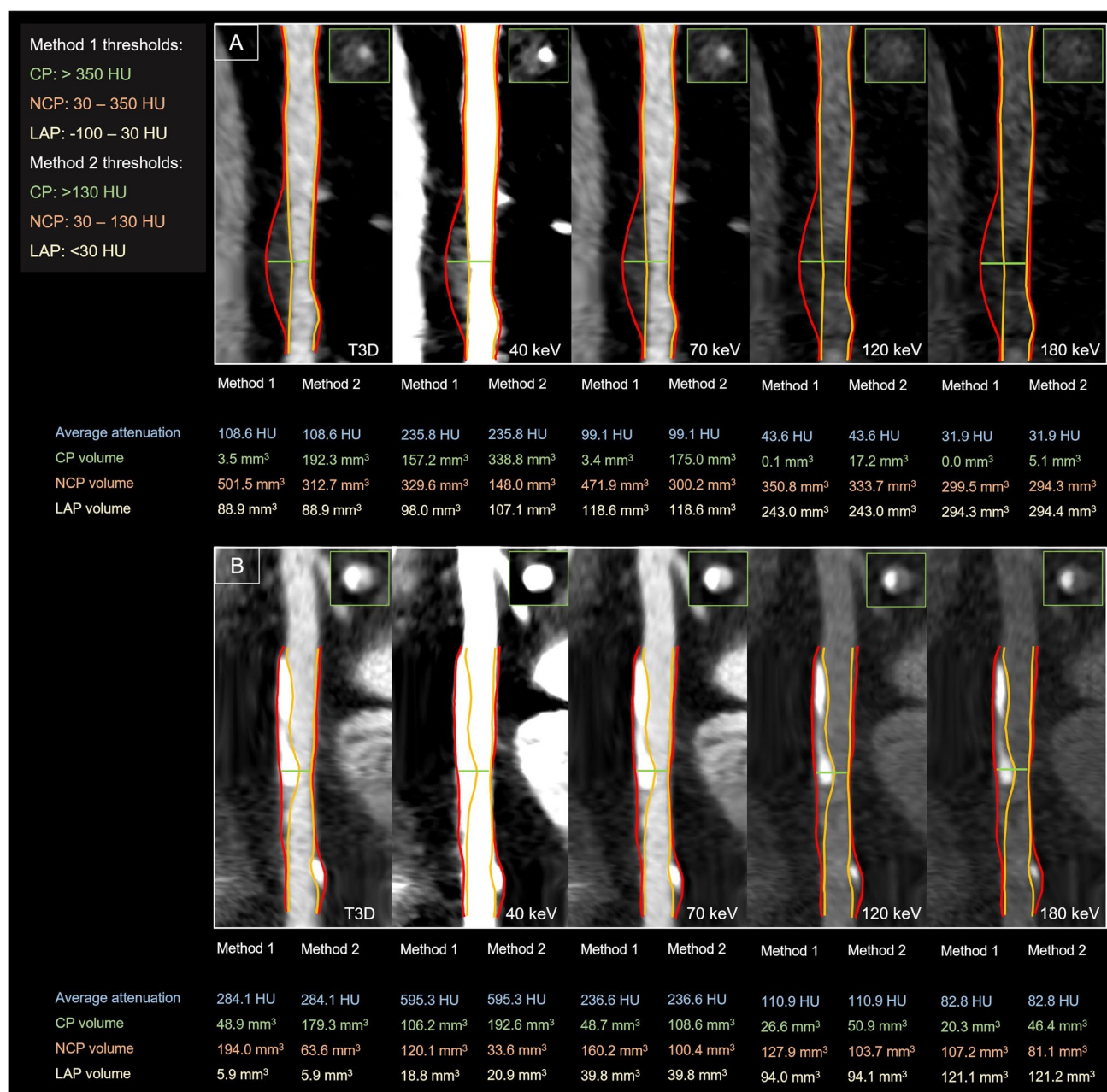
A T3D | 40 keV | 70 keV | 120 keV | 180 keV

Method 1 thresholds:
CP: > 350 HU
NCP: 30 – 350 HU
LAP: -100 – 30 HU
Method 2 thresholds:
CP: >130 HU
NCP: 30 – 130 HU
LAP: <30 HU

	Method 1	Method 2	Method 1	Method 2	Method 1	Method 2	Method 1	Method 2	Method 1	Method 2
Average attenuation	108.6 HU	108.6 HU	235.8 HU	235.8 HU	99.1 HU	99.1 HU	43.6 HU	43.6 HU	31.9 HU	31.9 HU
CP volume	3.5 mm³	192.3 mm³	157.2 mm³	338.8 mm³	3.4 mm³	175.0 mm³	0.1 mm³	17.2 mm³	0.0 mm³	5.1 mm³
NCP volume	501.5 mm³	312.7 mm³	329.6 mm³	148.0 mm³	471.9 mm³	300.2 mm³	350.8 mm³	333.7 mm³	299.5 mm³	294.3 mm³
LAP volume	88.9 mm³	88.9 mm³	98.0 mm³	107.1 mm³	118.6 mm³	118.6 mm³	243.0 mm³	243.0 mm³	294.3 mm³	294.4 mm³

B T3D | 40 keV | 70 keV | 120 keV | 180 keV

	Method 1	Method 2	Method 1	Method 2	Method 1	Method 2	Method 1	Method 2	Method 1	Method 2
Average attenuation	284.1 HU	284.1 HU	595.3 HU	595.3 HU	236.6 HU	236.6 HU	110.9 HU	110.9 HU	82.8 HU	82.8 HU
CP volume	48.9 mm³	179.3 mm³	106.2 mm³	192.6 mm³	48.7 mm³	108.6 mm³	26.6 mm³	50.9 mm³	20.3 mm³	46.4 mm³
NCP volume	194.0 mm³	63.6 mm³	120.1 mm³	33.6 mm³	160.2 mm³	100.4 mm³	127.9 mm³	103.7 mm³	107.2 mm³	81.1 mm³
LAP volume	5.9 mm³	5.9 mm³	18.8 mm³	20.9 mm³	39.8 mm³	39.8 mm³	94.0 mm³	94.1 mm³	121.1 mm³	121.2 mm³

Fig. 1 Representative CTA images of coronary plaques reconstructed in T3D and different VMI energy levels (40, 70, 120, and 180 keV). Quantitative plaque analyses of a partially calcified-predominantly non-calcified (panel **A**) and partially calcified-predominantly calcified (panel **B**) plaque are shown in T3D and different VMI reconstructions at 40, 70, 120, and 180 keV levels. The red line illustrates the border of the vessel wall and the orange line illustrates the lumen border segmented on T3D images. Corresponding cross-sectional images are also depicted at the point of the maximal narrowing of the lesion. The same window setting was applied for all represented images: window: 800; level: 250. Abbreviations: CP, calcified plaque; HU, Hounsfield unit; LAP, low-attenuation non-calcified plaque; NCP, non-calcified plaque

(Fig. 1). In addition, polychromatic images at 120 kVp (T3D) were also created as reference standard for comparison. All images were reconstructed with the same settings: 0.4-mm slice thickness with 0.4-mm increment, quantitative iterative reconstruction level of 2, using a medium smooth kernel (Bv40) and a matrix of 512×512.

Image quality assessment

Quantitative image quality analysis was performed for all VMI and T3D images. RadiAnt (Medixant) DICOM Viewer software (v2022.1.1) was used to measure quantitative image quality parameters by a single reader. Image noise was defined

as the standard deviation (SD) of attenuation values measured by placing a circular region of interest (ROI; 200 mm^2) in the aortic root at the level of the left main coronary ostium (SD$_{lumen}$). Circular regions of interest (ROIs) were also placed in the coronary lumen and pericoronary fat adjacent to the analyzed lesion to measure mean attenuation in HU (HU$_{lumen}$, HU$_{fat}$). Artifacts and plaques were carefully avoided while manually placing ROIs. ROIs were copied from T3D images as reference and pasted to the same position on all reconstructed images for identical measurement of SD and HU values. Signal-to-noise ratio (SNR) and CNR were calculated for all reconstructed datasets, as SNR = HU$_{lumen}$/SD$_{lumen}$, and CNR = (HU$_{lumen}$ − HU$_{fat}$) / SD$_{lumen}$.

Quantitative plaque analysis

Coronary atherosclerotic plaque was determined on the CTA images based on prior work by Achenbach et al [9]. Quantitative plaque analysis was performed using dedicated semi-automated software (AutoPlaque 2.5; Cedars-Sinai Medical Center) by a single experienced reader (B.V.). Each coronary lesion with the highest-grade stenosis based on visual assessment was defined and analyzed per patient. We selected one lesion per patient to avoid potential intra-patient clustering effects. The centerline of the selected coronary artery was extracted; then, proximal and distal borders of the plaque were marked on the T3D images. Contouring of the vessel wall and lumen was automatic, with manual adjustment as required. Artifacts from metallic structures, beam-hardening or — in case of sequential scanning — misalignment were carefully avoided. Also, only high-quality images were used for plaque quantification that were not severely affected by motion or breathing artifacts as per exclusion criteria. Segmentation masks were copied from the T3D image to all other VMIs guaranteeing that the same voxels were analyzed on all images; therefore, potential differences in contouring on the different VMIs of the same patient did not affect our results. Our method removes the reader's bias and focuses on the impact of different VMI reconstructions on plaque composition.

Voxels from the corresponding images were exported into the R environment (version 4.0.2) and analyzed using the Radiomics Image Analysis software package (RIA v.1.6.0) [10]. We calculated the volume of calcified plaque (CP), non-calcified plaque (NCP), and LAP. Plaque components were defined using two different methods with the following threshold ranges: method 1: LAP: − 100 to 30 HU; NCP: 30 to 350 HU; CP: > 350 HU [11, 12] and method 2: LAP: < 30 HU; NCP: 30 to 130 HU; CP: > 130 HU [13].

Statistical analysis

Normality was assessed using Q-Q plots. Continuous variables are presented as mean and standard deviation for normally distributed data and as medians and interquartile ranges for non-normally distributed data, whereas categorical parameters are presented as frequency with percentages in the text.

We used one-way, repeated measure analysis of variances (ANOVA) and post hoc comparison analysis to compare image quality metrics, average plaque attenuation, and plaque volumes between the different monoenergetic levels. We performed two comparisons: (1) each VMI group versus T3D images as reference to answer which VMIs have significantly different values; (2) each keV group versus the next group incrementally to evaluate whether each subsequent VMI is different from the previous one. All multiple comparisons were done using pair t-tests and p values were corrected using the Bonferroni method. We calculated the relative difference between the reference T3D and all VMI reconstructions as follows: as (VMImean − T3Dmean / T3Dmean) * 100. All statistical analyses were performed using R software (version 4.0.2) using packages: ggstatsplot (v.0.9.3) [14] and rstatix (v0.7.0). A two-sided $p < 0.05$ was considered as statistically significant.

Results

In total, 158 patients with suspected or known CAD underwent coronary CTA using our PCCT scanner between April 2022 and June 2022. We excluded 22 patients due to inadequate image quality for plaque quantification and 85 patients without CAD. A total of 51 plaques from 51 patients were included in the analyses. Mean age was 65.1 ± 11.9 years and 68.6% were male. Common comorbidities included hypertension (80.4%), diabetes mellitus (27.5%), and dyslipidemia

Table 1 Patient characteristics and CT scan parameters

Demographic data	Patient population $n = 51$
Age, years	65.1 ± 11.9
Male gender	35 (68.6%)
BMI, kg/m^2	28.8 ± 4.7
Hypertension	41 (80%)
Diabetes mellitus	14 (28%)
Dyslipidemia	27 (53%)
Family history of premature CAD	8 (16%)
Smoking	11 (22%)
CT scan parameters	
Agatston score	444 ± 619
Total plaque volume, mm^3	270 ± 208
DLP, mGy cm	374 ± 309
Effective dose, mSv	5.2 ± 4.3

Continuous variables are described as mean ± SD, whereas categorical variables are represented as frequencies and percentage

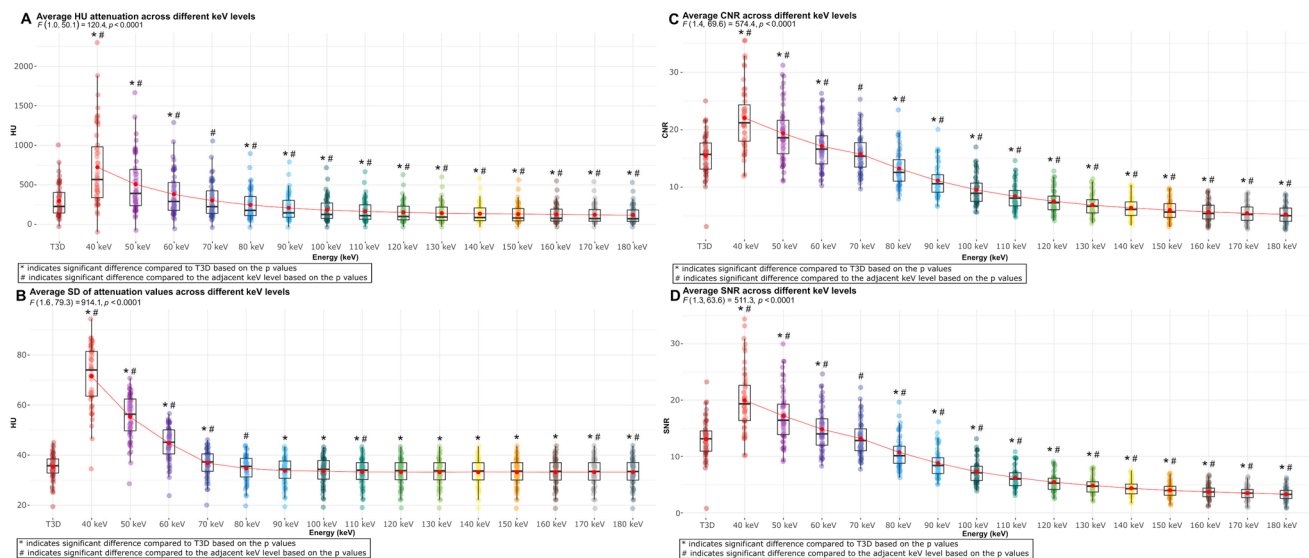*BMI*, body mass index; *CAD*, coronary artery disease; *DLP*, dose-length product

Fig. 2 Box plots showing the distribution of plaque attenuation and quantitative image quality parameters (SD, CNR, SNR) in different VMI energy levels and T3D images. Panel **A** depicts the distribution of attenuation values across different energy levels. Panel **B** depicts the distribution of image noise based on SD across different energy levels. Panel **C** depicts the distribution CNR across different energy levels. Panel **D** depicts the distribution SNR across different energy levels. Abbreviations: CNR, contrast-to-noise ratio; HU, Hounsfield unit; SD, standard deviation; SNR, signal-to-noise ratio

(52.9%). The average total plaque volume of the analyzed lesions was 270.2 ± 208.7 mm^3 on T3D images. Mean effective radiation dose was 5.2 ± 4.3 mSv. Baseline demographic data and CT scan parameters are summarized in Table 1.

Mean plaque attenuation and quantitative image quality parameters on VMIs

Mean attenuation of the analyzed plaques was 299 ± 209 HU on T3D images. The average plaque attenuation showed a significant graded decrease with increasing keV levels (from 723 ± 501 HU on 40 keV to 120 ± 112 HU on 180 keV, $p < 0.0001$ for all). All VMIs showed a significant difference compared to T3D, except for the 70-keV images (303 ± 225 HU, $p = 0.15$) (Fig. 2A; Supplementary table 1).

There was also a decrease in image noise (SD of mean attenuation) with increasing keV levels (from 72 ± 12 HU on 40 keV to 33 ± 6 HU on 180 keV). However, a significant difference in image noise between adjacent keV levels was not uniformly observed. Images reconstructed at 80 keV showed similar image noise compared to T3D images (35 ± 5 HU vs. 35 ± 5 HU, respectively; $p = 0.74$) (Fig. 2B).

Tendencies for CNR (highest at 40 keV: 22.1 ± 5.6 and lowest at 180 keV: 5.3 ± 1.6; each value significantly different from the adjacent keV level) and SNR (highest at 40 keV: 20.0 ± 5.5 and lowest at 180 keV: 3.3 ± 1.2; each value significantly different from the adjacent keV level) were similar to those for mean attenuation. T3D images yielded similar

image quality based on CNR and SNR as compared with 70-keV VMI reconstructions (15.5 ± 3.7 vs. 15.8 ± 3.5, $p = 0.32$ for CNR and 13.1 ± 3.6 vs. 13.2 ± 3.2, $p = 0.69$ for SNR, respectively) (Fig. 2C and D, respectively).

Changes in plaque volumes using different VMI reconstructions

We applied two threshold settings for plaque quantification: method 1: LAP: -100 to 30 HU; NCP: 30 to 350 HU; CP: > 350 HU [11, 12] and method 2: LAP: < 30 HU; NCP: 30 to 130 HU; CP: > 130 HU [13] (Figs. 3 and 4, respectively).

Using method 1, mean NCP volume was 161.0 ± 126.3 mm^3 on T3D images. The average NCP volume showed an increase up to 70 keV, followed by a decrease with each subsequent increment in VMI energy level. A significant difference in NCP volume between keV levels was not observed at every step. The lowest value was found using 40 keV (96.9 ± 86.8 mm^3), whereas the highest was seen using 70 keV (152.8 ± 122.0 mm^3). Mean NCP volume measured on 100–180-keV reconstructions did not differ significantly from T3D images ($p > 0.05$ for all) (Fig. 3A). The average CP volume showed a significant graded decrease with increasing keV levels, from 138.7 ± 126.4 mm^3 on 40 keV to 38.5 ± 64.6 mm^3 on 180 keV ($p < 0.001$ for all). Mean CP volume measured on each VMI reconstruction differed significantly from the reference T3D images ($p < 0.05$ for all) (Fig. 3B). An increasing LAP volume for each
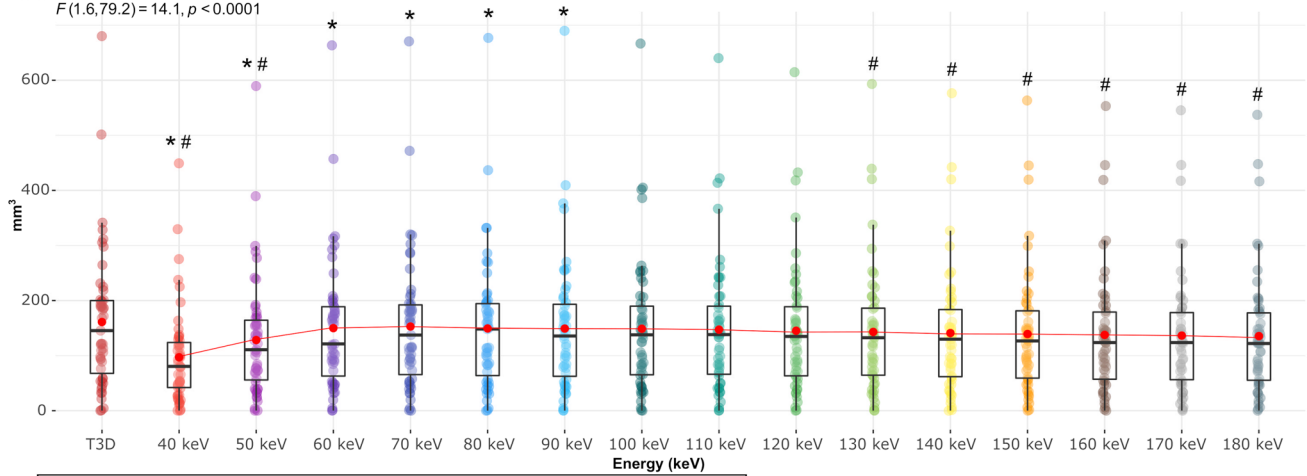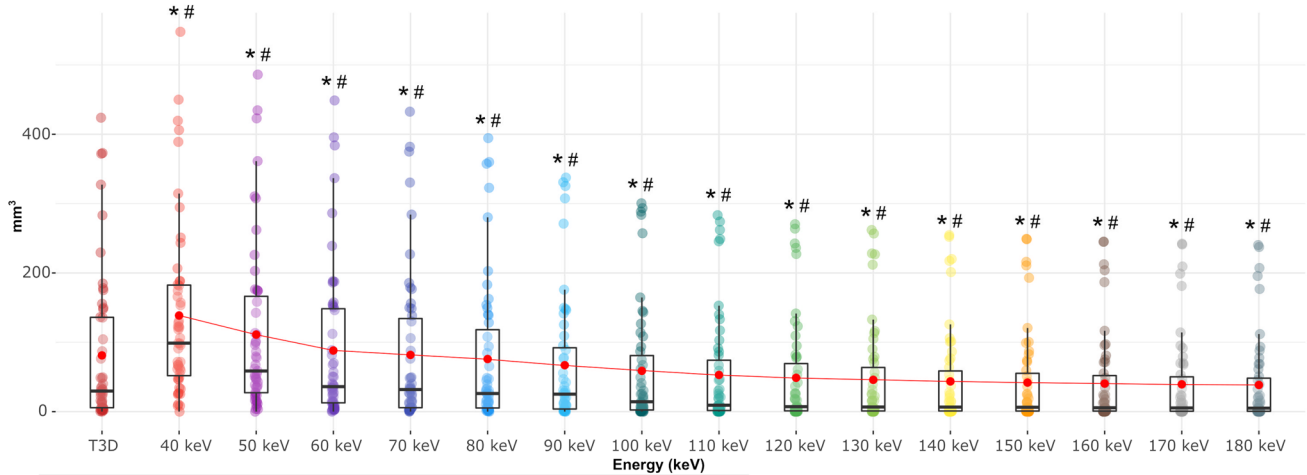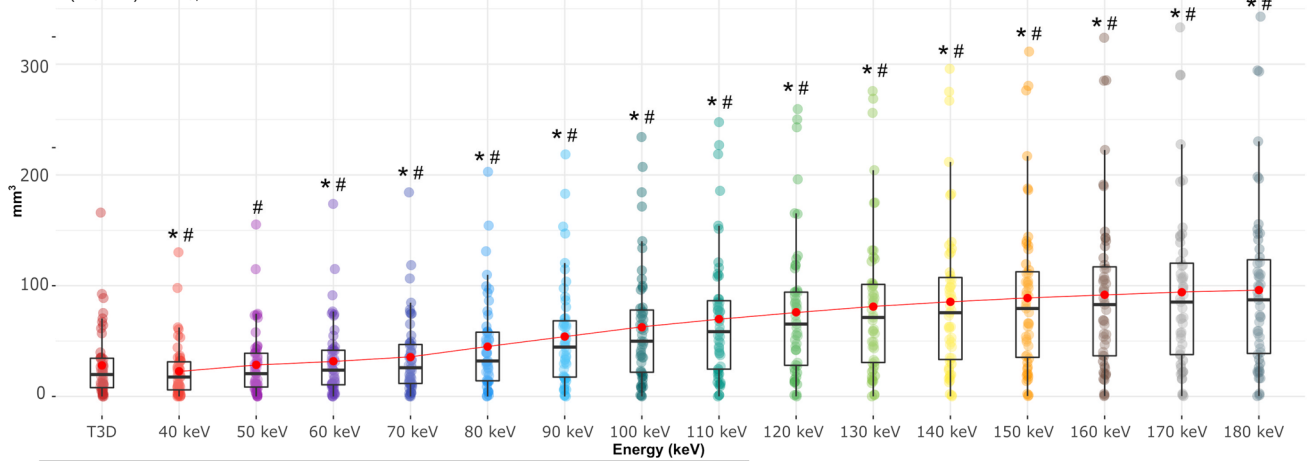
A Average NCP (31 - 350 HU) volume across different keV levels
$F(1.6, 79.2) = 14.1, p < 0.0001$

* indicates significant difference compared to T3D based on the p values
# indicates significant difference compared to the adjacent keV level based on the p values

B Average CP (>350 HU) volume across different keV levels
$F(1.3, 66.0) = 51.6, p < 0.0001$

* indicates significant difference compared to T3D based on the p values
# indicates significant difference compared to the adjacent keV level based on the p values

C Average LAP (-100 - 30 HU) volume across different keV levels
$F(1.1, 52.6) = 83.2, p < 0.0001$

* indicates significant difference compared to T3D based on the p values
# indicates significant difference compared to the adjacent keV level based on the p values

◄**Fig. 3** Box plots showing the distribution of plaque volumes in different VMI energy levels and T3D images using the thresholds of method 1 for plaque characterization. Panel **A** shows the distribution of NCP volume across different energy levels using threshold of −100 to 350 HU. Panel **B** shows the distribution of CP volume across different energy levels using the threshold of > 350 HU. Panel **C** shows the distribution of LAP volume across different energy levels using the threshold of −100 to 30 HU. Abbreviations: CP, calcified plaque; HU, Hounsfield unit; LAP, low-attenuation non-calcified plaque; NCP, non-calcified plaque; SD, standard deviation

increment in keV level was observed, with a significant difference between each step (from 22.8 ± 24.9 mm^3 on 40 keV to 96.0 ± 76.3 mm^3 on 180 keV; $p < 0.0001$ for all). Mean LAP volume differed significantly between T3D and VMI reconstructions, except for 50-keV images (28.0 ± 30.8 mm^3 and 28.6 ± 30.1 mm^3, respectively, $p = 0.63$) (Fig. 3C; Supplementary table 2).

Method 2 yielded similar findings for the assessment of plaque volumes. Mean NCP volume showed an initial increase up to 100 keV, followed by a decrease with increasing keV levels, with no significant difference between each adjacent keV level. Average NCP volume on T3D was comparable with 70- and 140–180-keV energy levels ($p > 0.05$ for all) (Fig. 4A). Similarly, mean CP volume showed a decreasing tendency with significant difference between each adjacent keV level ($p < 0.01$ for all). Mean CP volume measured on each VMI reconstructions differed significantly from the reference T3D images ($p < 0.001$ for all) (Fig. 4B). Also, an increasing tendency of LAP volume was observed by increasing keV levels, with significant difference between each adjacent VMI ($p < 0.05$ for all). When measuring LAP volume, all VMIs showed a significant difference compared to T3D, except for 40 keV ($p = 0.65$) (Fig. 4C; Supplementary table 3).

Relative difference between T3D and VMI reconstructions

The relative difference regarding attenuation and image quality parameters between the reference standard T3D and VMI reconstructions are summarized in Table 2. Regarding plaque volumes using thresholds of method 1 for plaque characterization, the highest difference for CP and NCP volume was measured on 40-keV images compared to T3D (70.8% and −39.8%, respectively, $p < 0.0001$), whereas the lowest relative difference was measured using 70-keV images (0.9% and −5.1%, respectively, $p < 0.0001$). Mean LAP volume showed the largest discrepancy on 180-keV reconstruction with 242.5% relative difference ($p < 0.0001$) and the smallest on 50-keV images (1.9%, $p = 0.63$) (Table 3).

Applying method 2 for plaque quantification, the greatest difference in CP volume was observed between 180 keV and T3D, with a relative differe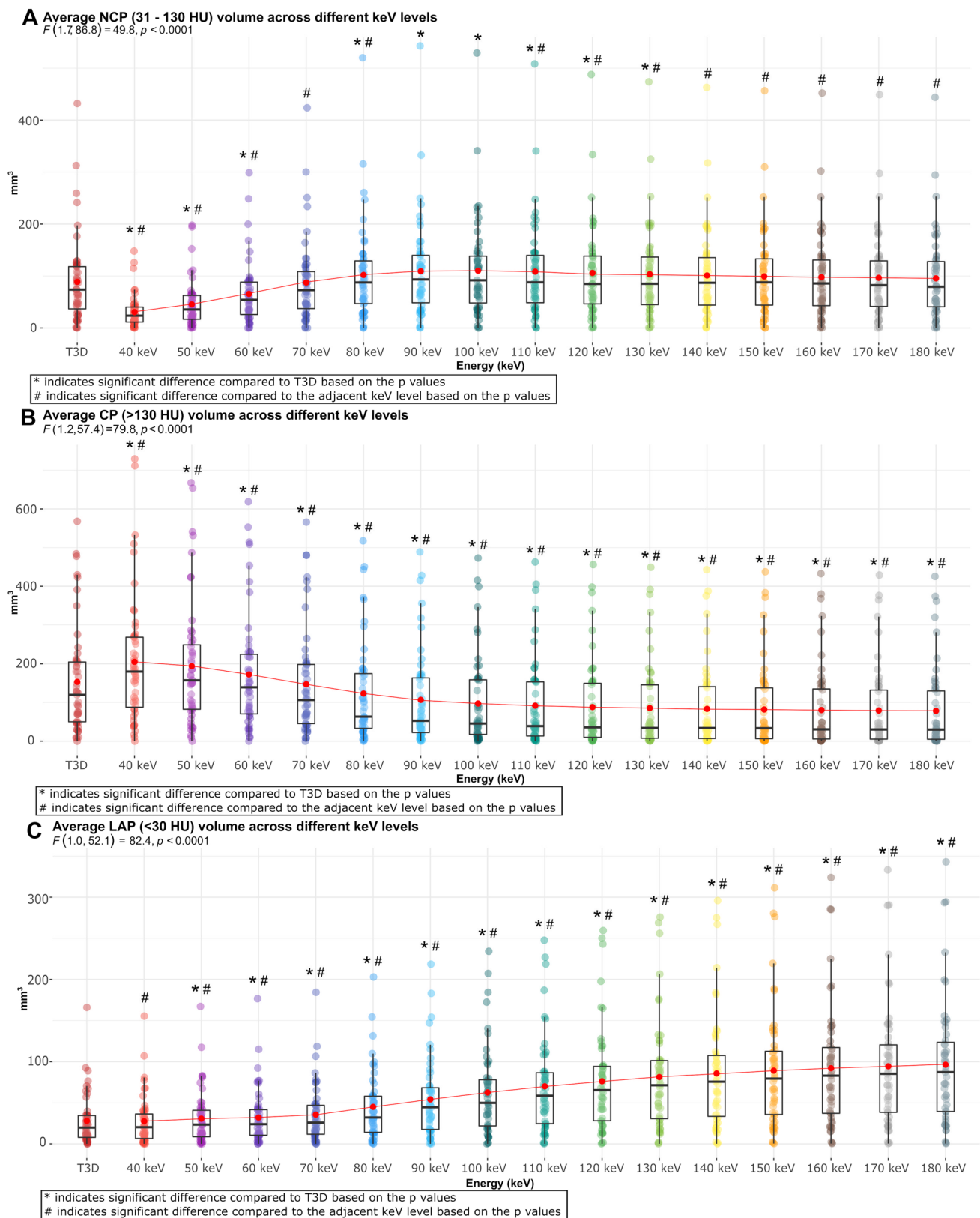nce of −48.9% ($p < 0.0001$), while the lowest relative difference of CP volume was observed at 70-keV images (−4.0%, $p < 0.001$). For NCP volume as compared with T3D, the greatest and smallest differences were observed using 40 (−65.6%, $p < 0.0001$) and 70 keV (−1.5%, $p = 0.54$), respectively. The largest relative difference for LAP volume was seen on 180-keV images (243.3%, $p < 0.0001$), and the lowest on 40-keV images (−1.9%, $p = 0.65$) (Table 4).

Discussion

In our study, we demonstrate that utilizing different VMI energy levels from PCCT for the analysis of coronary artery plaques leads to substantial changes in attenuation values and corresponding plaque component volumes. Our primary findings are as follows: (1) Low-energy images (40–70 keV) improved CNR and resulted in higher CP but lower NCP and LAP volumes, however also increased image noise; (2) CP volume quantified on 70 keV exhibited the lowest relative difference compared to T3D images; (3) No significant differences were observed in NCP volume using higher VMI levels (100–180 keV); (4) LAP volume was not significantly different on low-energy images (40–50 keV) when compared to T3D as reference.

Coronary CTA is a well-established non-invasive modality for the assessment of CAD in patients presenting with stable chest pain [15]. In addition to luminal stenosis, CTA uniquely allows for the evaluation of overall plaque burden and high-risk plaque characteristics, which are strong predictors of subsequent cardiovascular events [1]. Moreover, quantitative plaque analysis provides comprehensive assessment of coronary plaque volume and composition. A growing body of evidence suggests the additional prognostic value of quantitative plaque metrics over visual assessment alone [16]. In particular, LAP (defined using a fixed HU threshold of 30) burden independently predicted myocardial infarction at 5 years' follow-up in patients with stable chest pain [2]. Accordingly, using CTA for the quantitative evaluation of CAD can improve risk stratification by identifying patients at high risk [17].

A novel dual-source PCCT system has recently been introduced in clinical practice with the potential to overcome several limitations of conventional CT scanners. Photon-counting detectors directly generate electronical signal proportional to photon energy by measuring the energy of each individual photon reaching the detector. Compared to traditional energy-integrating detectors, PCCT is characterized by superior spatial resolution, reduction of image noise, and beam-hardening artifacts [4]. In addition, this technology enables advanced tissue characterization with the use of virtual monoenergetic reconstructions and therefore may provide improved plaque assessment. However, VMIs also change the CT attenuation values which may affect plaque characterization.

A Average NCP (31 - 130 HU) volume across different keV levels
$F(1.7, 86.8) = 49.8, p < 0.0001$

* indicates significant difference compared to T3D based on the p values
# indicates significant difference compared to the adjacent keV level based on the p values

B Average CP (>130 HU) volume across different keV levels
$F(1.2, 57.4) = 79.8, p < 0.0001$

* indicates significant difference compared to T3D based on the p values
# indicates significant difference compared to the adjacent keV level based on the p values

C Average LAP (<30 HU) volume across different keV levels
$F(1.0, 52.1) = 82.4, p < 0.0001$

* indicates significant difference compared to T3D based on the p values
# indicates significant difference compared to the adjacent keV level based on the p values

In general, the benefit of lower keV images is the increased contrast between the coronary lumen and vessel wall, aiding better discrimination of coronary plaques and intraluminal contrast. Despite showing higher image noise, lower keV level images yield better image quality based on CNR and SNR as demonstrated also in previous phantom

◀**Fig. 4** Box plots showing the distribution of plaque volumes in different VMI energy levels and T3D images using the thresholds of method 2 for plaque characterization. Panel **A** shows the distribution of NCP volume across different energy levels using threshold of < 130 HU. Panel **B** shows the distribution of CP volume across different energy levels using the threshold of > 130 HU. Panel **C** shows the distribution of LAP volume across different energy levels using the threshold of < 30 HU. Abbreviations: CP, calcified plaque; HU, Hounsfield unit; LAP, low-attenuation non-calcified plaque; NCP, non-calcified plaque; SD, standard deviation

studies [18]. On the other hand, higher keV level images decrease blooming and image noise, which can enhance calcified plaque analysis. However, higher keV levels result in decreased CNR and SNR. To utilize the advantages from both high- and low-energy level images, it would be advantageous to view the different keV images side-by-side and have the ability to manually edit segmentation contours on either image to minimize the effects of different artefacts. Ohta et al demonstrated using dual-energy CT datasets that different VMI energy levels showed the highest CNR and SNR for each coronary plaque component. In line with our results, these findings also suggested that different VMIs should be used simultaneously for coronary plaque assessment to apply the advantage of each energy levels [19].

As different keV images change the attenuation values of the voxels, it is also important to consider how these changes affect the quantification of plaque composition. Based on our results, plaque compositional volumes defined using fixed

threshold settings on T3D images yielded similar results in different VMI reconstructions for the different plaque components. This is due to the fact that attenuation values change on different VMIs as a function of the tissue composition of the given voxel [20–22]. Therefore, fixed threshold setting will not work on VMIs which is emphasized by our results as we observed significantly different plaque volumes on almost all VMIs as compared to T3D as a reference. Furthermore, one universal correction factor is not enough as we show that the relative difference in plaque volumes is different for each component on the same VMI. Therefore, to utilize the information from VMIs and have comparable results between future studies and previous investigations, we need to develop standardized protocols and adaptive correction factors which may allow conversions between volumetric estimates done using different VMIs and/or conventional images.

To the best of our knowledge, no previous study has investigated the influence of different VMI energy levels on coronary plaque composition using PCCT datasets. Symons et al examined the impact of different VMI energy levels on coronary plaque segmentation and quantification using 3rd-generation dual-source CT scanner. They reported similar tendencies in image quality parameters to our results, with better CNR and SNR, and higher image noise on lower keV images. Although a different method was applied during plaque analysis — as segmentation was performed individually on every reconstruction — similar tendencies were also observed regarding plaque types [23].

Table 2 Difference in CT attenuation and quantitative image quality parameters (SD, CNR, SNR) for different energy levels compared to T3D

Energy level (keV)	Attenuation (HU)		Image noise (SD)		CNR		SNR	
	Difference to T3D (%)	95% CI	Difference to T3D (%)	95% CI	Difference to T3D (%)	95% CI	Difference to T3D (%)	95% CI
40	142.0	114.3 to 169.6	102.7	95.8 to 109.7	42.6	36.1 to 49.0	52.7	45.1 to 60.3
50	70.1	55.8 to 84.5	56.8	52.4 to 61.1	25.2	19.8 to 30.5	31.7	25.5 to 37.9
60	27.9	21.5 to 34.4	27.0	24.2 to 29.7	11.0	6.5 to 15.4	13.4	8.4 to 18.4
70	1.3*	− 0.5 to 3.2	4.2	2.3 to 6.1	1.8*	− 1.8 to 5.4	0.8*	− 3.2 to 4.8
80	− 17.4	− 19.7 to − 15.1	− 1.7*	− 4.1 to 0.6	− 14.4	− 18.0 to − 10.8	− 17.9	− 21.8 to − 13.9
90	− 29.9	− 34.2 to − 25.6	− 4.3	− 6.9 to − 1.7	− 28.0	− 31.8 to − 24.1	− 32.6	− 36.8 to − 28.4
100	− 38.3	− 44.1 to − 32.5	− 4.9	− 7.6 to − 2.2	− 38.3	− 42.3 to − 34.3	− 44.1	− 48.7 to − 39.5
110	− 44.3	− 51.1 to − 37.5	− 5.7	− 8.6 to − 2.9	− 45.6	− 49.8 to − 41.3	− 52.2	− 57.2 to − 47.2
120	− 48.6	− 56.2 to − 41.0	− 5.9	− 8.8 to − 3.0	− 51.2	− 55.7 to − 46.6	− 58.4	− 63.7 to − 53.0
130	− 51.8	− 60.0 to − 43.7	− 5.9	− 8.9 to − 3.0	− 55.4	− 60.1 to − 50.7	− 63.0	− 68.7 to − 57.4
140	− 54.3	− 62.9 to − 45.7	− 6.0	− 8.9 to − 3.0	− 58.6	− 63.5 to − 53.7	− 66.6	− 72.5 to − 60.7
150	− 56.2	− 65.1 to − 47.2	− 5.9	− 8.9 to − 3.0	− 61.1	− 66.1 to − 56.1	− 69.4	− 75.4 to − 63.3
160	− 57.6	− 66.9 to − 48.4	− 5.9	− 8.8 to − 2.9	− 63.1	− 68.2 to − 58.0	− 71.6	− 77.8 to − 65.4
170	− 58.8	− 68.3 to − 49.4	− 5.9	− 8.8 to − 2.9	− 64.7	− 69.9 to − 59.5	− 73.3	− 79.6 to − 67.0
180	− 59.8	− 69.4 to − 50.2	− 5.8	− 8.8 to − 2.9	− 66.0	− 71.2 to − 60.7	− 74.7	− 81.1 to − 68.3

Differences and 95% confidence intervals (CI) are from pairwise *t*-tests

* indicates no statistical significance compared to T3D based on *p* value

CNR, contrast-to-noise ratio; *HU*, Hounsfield unit; *SD*, standard deviation; *SNR*, signal-to-noise ratio

Table 3 Difference in CP, NCP, and LAP volumes based on the thresholds of method 1 (CP > 350 HU; NCP: 31 to 350 HU; LAP: − 100 to 30 HU) for different energy levels compared to T3D

Energy level (keV)	CP (> 350 HU)		NCP (31 to 350 HU)		LAP (− 100 to 30 HU)	
	Difference to T3D (%)	95% CI	Difference to T3D (%)	95% CI	Difference to T3D (%)	95% CI
40	70.8	54.2 to 87.5	− 39.8	− 48.1 to − 31.5	− 18.8	− 29.0 to − 8.6
50	36.9	28.2 to 45.6	− 20.3	− 25.2 to − 15.5	1.9*	− 5.8 to 9.6
60	8.7	5.4 to 12.0	− 6.9	− 8.9 to − 4.9	13.6	7.5 to 19.6
70	0.9	0.1 to 1.6	− 5.1	− 6.4 to − 3.8	26.8	19.8 to 33.7
80	− 6.5	− 9.4 to − 3.6	− 7.3	− 9.7 to − 4.9	60.5	46.9 to 74.0
90	− 17.5	− 24.9 to − 10.0	− 7.4	− 11.4 to − 3.4	92.9	72.5 to 113.3
100	− 27.5	− 38.2 to − 16.8	− 7.6*	− 13.2 to − 2.0	122.9	96.1 to 149.7
110	− 34.8	− 47.6 to − 21.9	− 8.6*	− 15.3 to − 1.8	149.3	116.9 to 181.8
120	− 39.8	− 54.2 to − 25.5	− 9.8*	− 17.5 to − 2.2	171.2	133.9 to 208.4
130	− 43.4	− 58.9 to − 28.0	− 11.2*	− 19.6 to − 2.8	189.3	148.0 to 230.5
140	− 46.3	− 62.5 to − 30.0	− 12.4*	− 21.4 to − 3.5	204.7	160.2 to 249.2
150	− 48.3	− 65.3 to − 31.4	− 13.6*	− 23.0 to − 4.1	217.0	170.0 to 263.9
160	− 50.1	− 67.6 to − 32.6	− 14.5*	− 24.3 to − 4.7	227.4	178.4 to 276.4
170	− 51.4	− 69.4 to − 33.5	− 15.3*	− 25.4 to − 5.2	235.7	185.1 to 286.3
180	− 52.5	− 70.9 to − 34.2	− 15.9*	− 26.3 to − 5.5	242.5	190.5 to 294.6

Differences and 95% confidence intervals (CI) are from pairwise *t*-tests

* indicates no statistical significance compared to T3D based on *p* value

CP, calcified plaque; *HU*, Hounsfield unit; *LAP*, low-attenuation non-calcified plaque; *NCP*, non-calcified plaque

We acknowledge the limitations of our study. First, this was a single-center study focusing on plaque quantification in a relatively small population of stable chest pain patients. However, we believe that the sample was large enough to evaluate the trends in using different VMI reconstructions for plaque assessment. Second, we only used a single

Table 4 Difference in CP, NCP, and LAP volumes based on the thresholds of method 2 (CP > 130 HU; NCP: 31 to 130 HU; LAP: < 30 HU) for different energy levels compared to T3D

Energy level (keV)	CP (> 130 HU)		NCP (31 to 130 HU)		LAP (< 30 HU)	
	Difference to T3D (%)	95% CI	Difference to T3D (%)	95% CI	Difference to T3D (%)	95% CI
40	33.6	23.3 to 44.0	− 65.6	− 82.4 to − 48.8	− 1.9*	− 10.1 to 6.4
50	26.5	19.3 to 33.6	− 48.9	− 61.6 to − 36.2	9.6	2.2 to 17.0
60	12.5	8.4 to 16.6	− 26.2	− 33.4 to − 18.9	14.4	8.4 to 20.4
70	− 4.0	− 5.9 to − 2.1	− 1.5*	− 3.9 to 0.9	26.8	19.8 to 33.8
80	− 19.7	− 24.1 to − 15.4	15.0	9.8 to 20.1	60.5	47.0 to 74.1
90	− 30.4	− 36.7 to − 24.0	23.1	16.1 to 30.1	93.0	72.6 to 113.5
100	− 36.5	− 44.1 to − 29.0	24.2	16.0 to 32.5	123.1	96.2 to 149.9
110	− 40.2	− 48.6 to − 31.8	22.2	13.1 to 31.3	149.6	117.1 to 182.1
120	− 42.6	− 51.5 to − 33.7	19.4	9.7 to 29.1	171.5	134.2 to 208.9
130	− 44.3	− 53.5 to − 35.0	16.5	6.3 to 26.7	189.7	148.4 to 231.0
140	− 45.6	− 55.1 to − 36.0	13.9*	3.4 to 24.4	205.2	160.7 to 249.8
150	− 46.7	− 56.5 to − 36.8	11.8*	1.1 to 22.6	217.6	170.6 to 264.6
160	− 47.6	− 57.6 to − 37.5	10.1*	− 0.9 to 21.1	228.1	179.0 to 277.2
170	− 48.3	− 58.5 to − 38.1	8.7*	− 2.5 to 19.9	236.5	185.7 to 287.2
180	− 48.9	− 59.3 to − 38.5	7.7*	− 3.7 to 19.1	243.3	191.2 to 295.5

Differences and 95% confidence intervals (CI) are from pairwise *t*-tests

* indicates no statistical significance compared to T3D based on *p* value

CP, calcified plaque; *HU*, Hounsfield unit; *LAP*, low-attenuation non-calcified plaque; *NCP*, non-calcified plaque

software for plaque segmentation. Furthermore, there are additional parameters that could alter plaque volumes (such as slice thickness, iterative reconstruction, kernels) — that has previously been investigated — which were not part of our analysis [24, 25]. Also, we had no reference standard. Histology or intravascular imaging was not available in these individuals. Nevertheless, T3D polychromatic images are considered to be comparable to conventional 120-kV polychromatic images on energy-integrating detector CT scanner and the methods used have been validated to intravascular imaging and tested in large cohorts on conventional images [2, 26, 27]. Using different flow rates, contrast media concentrations and dosing could lead to different attenuation values in the coronaries. However, our protocol only allows for small changes in the given contrast media dose using the same concentration. Furthermore, we evaluated changes within the same patient on different VMIs, and thus, the potential effect of contrast administration on plaque volumes should be consistent within each patient [28].

In conclusion, low-energy monoenergetic reconstructions significantly alter plaque attenuation and plaque volumes with fixed plaque attenuation thresholds. Therefore, caution is required when using different VMI reconstructions and fixed plaque attenuation thresholds for plaque characterization. New standards and protocols are required to determine which monoenergetic or polyenergetic images are optimal to derive plaque volumes. This will aid the adoption of PCCT plaque analysis in both the clinical and research setting.

Declarations

Guarantor The scientific guarantor of this publication is Márton Kolossváry MD PhD.

Conflict of interest The authors of this manuscript declare relationships with the following companies:

Michelle C Williams has given talks for Canon Medical Systems and Siemens Healthineers.

Damini Dey has received software royalties from Cedars Sinai Medical Center.

Florian Schwarz and University Hospital Augsburg have received speaker honoraria from Siemens Healthineers.

Statistics and biometry One of the authors has significant statistical expertise.

Informed consent Written informed consent was obtained from all subjects (patients) in this study.

Ethical approval Institutional Review Board approval was obtained.

Study subjects or cohorts overlap Not applicable.

Methodology
- prospective
- cross-sectional study
- performed at one institution

References

1. Motoyama S, Ito H, Sarai M et al (2015) Plaque Characterization by Coronary Computed Tomography Angiography and the Likelihood of Acute Coronary Events in Mid-Term Follow-Up. J Am Coll Cardiol 66:337–346
2. Williams MC, Kwiecinski J, Doris M et al (2020) Low-Attenuation Noncalcified Plaque on Coronary Computed Tomography Angiography Predicts Myocardial Infarction: Results From the Multicenter SCOT-HEART Trial (Scottish Computed Tomography of the HEART). Circulation 141:1452–1462
3. Sandfort V, Persson M, Pourmorteza A, Noel PB, Fleischmann D, Willemink MJ (2021) Spectral photon-counting CT in cardiovascular imaging. J Cardiovasc Comput Tomogr 15:218–225
4. Willemink MJ, Persson M, Pourmorteza A, Pelc NJ, Fleischmann D (2018) Photon-counting CT: Technical Principles and Clinical Prospects. Radiology 289:293–312
5. Boussel L, Coulon P, Thran A et al (2014) Photon counting spectral CT component analysis of coronary artery atherosclerotic plaque samples. Br J Radiol 87:20130798
6. Grant KL, Flohr TG, Krauss B, Sedlmair M, Thomas C, Schmidt B (2014) Assessment of an advanced image-based technique to calculate virtual monoenergetic computed tomographic images from a dual-energy examination to improve contrast-to-noise ratio in examinations using iodinated contrast media. Invest Radiol 49:586–592
7. Abbara S, Blanke P, Maroules CD et al (2016) SCCT guidelines for the performance and acquisition of coronary computed

tomographic angiography: A report of the society of Cardiovascular Computed Tomography Guidelines Committee: Endorsed by the North American Society for Cardiovascular Imaging (NASCI). J Cardiovasc Comput Tomogr 10:435–449

8. Karady J, Panajotu A, Kolossvary M et al (2017) The effect of four-phasic versus three-phasic contrast media injection protocols on extravasation rate in coronary CT angiography: a randomized controlled trial. Eur Radiol 27:4538–4543

9. Achenbach S, Moselewski F, Ropers D et al (2004) Detection of calcified and noncalcified coronary atherosclerotic plaque by contrast-enhanced, submillimeter multidetector spiral computed tomography: a segment-based comparison with intravascular ultrasound. Circulation 109:14–17

10. Kolossvary M, Karady J, Szilveszter B et al (2017) Radiomic Features Are Superior to Conventional Quantitative Computed Tomographic Metrics to Identify Coronary Plaques With Napkin-Ring Sign. Circ Cardiovasc Imaging 10:e006843

11. Kolossvary M, Bluemke DA, Fishman EK et al (2022) Temporal assessment of lesion morphology on radiological images beyond lesion volumes-a proof-of-principle study. Eur Radiol 32:8748–8760

12. Kolossvary M, Gerstenblith G, Bluemke DA et al (2021) Contribution of Risk Factors to the Development of Coronary Atherosclerosis as Confirmed via Coronary CT Angiography: A Longitudinal Radiomics-based Study. Radiology 299:97–106

13. Ferencik M, Mayrhofer T, Puchner SB et al (2015) Computed tomography-based high-risk coronary plaque score to predict acute coronary syndrome among patients with acute chest pain–Results from the ROMICAT II trial. J Cardiovasc Comput Tomogr 9:538–545

14. Patil I (2021) Visualizations with statistical details: The 'ggstatsplot' approach. J Open Source Softw 6(61):3167

15. Writing Committee M, Gulati M, Levy PD et al (2021) 2021 AHA/ACC/ASE/CHEST/SAEM/SCCT/SCMR Guideline for the Evaluation and Diagnosis of Chest Pain: A Report of the American College of Cardiology/American Heart Association Joint Committee on Clinical Practice Guidelines. J Am Coll Cardiol 78:e187–e285

16. Nadjiri J, Hausleiter J, Jahnichen C et al (2016) Incremental prognostic value of quantitative plaque assessment in coronary CT angiography during 5 years of follow up. J Cardiovasc Comput Tomogr 10:97–104

17. Chang HJ, Lin FY, Lee SE et al (2018) Coronary Atherosclerotic Precursors of Acute Coronary Syndromes. J Am Coll Cardiol 71:2511–2522

18. Sartoretti T, McDermott M, Mergen V et al (2023) Photon-counting detector coronary CT angiography: impact of virtual monoenergetic imaging and iterative reconstruction on image quality. Br J Radiol 96:20220466

19. Ohta Y, Kitao S, Watanabe T, Kishimoto J, Yamamoto K, Ogawa T (2017) Evaluation of image quality of coronary artery plaque with rapid kVp-switching dual-energy CT. Clin Imaging 43:42–49

20. Rajendran K, Petersilka M, Henning A et al (2022) First Clinical Photon-counting Detector CT System: Technical Evaluation. Radiology 303:130–138

21. Mergen V, Ried E, Allmendinger T et al (2022) Epicardial Adipose Tissue Attenuation and Fat Attenuation Index: Phantom Study and In Vivo Measurements With Photon-Counting Detector CT. AJR Am J Roentgenol 218:822–829

22. Eberhard M, Mergen V, Higashigaito K et al (2021) Coronary Calcium Scoring with First Generation Dual-Source Photon-Counting CT-First Evidence from Phantom and In-Vivo Scans. Diagnostics (Basel) 11:1708

23. Symons R, Choi Y, Cork TE et al (2018) Optimized energy of spectral coronary CT angiography for coronary plaque detection and quantification. J Cardiovasc Comput Tomogr 12:108–114

24. Mergen V, Eberhard M, Manka R, Euler A, Alkadhi H (2022) First in-human quantitative plaque characterization with ultra-high resolution coronary photon-counting CT angiography. Front Cardiovasc Med 9:981012

25. Mergen V, Sartoretti T, Baer-Beck M et al (2022) Ultra-High-Resolution Coronary CT Angiography With Photon-Counting Detector CT: Feasibility and Image Characterization. Invest Radiol 57:780–788

26. Matsumoto H, Watanabe S, Kyo E et al (2019) Standardized volumetric plaque quantification and characterization from coronary CT angiography: a head-to-head comparison with invasive intravascular ultrasound. Eur Radiol 29:6129–6139

27. Meah MN, Singh T, Williams MC et al (2021) Reproducibility of quantitative plaque measurement in advanced coronary artery disease. J Cardiovasc Comput Tomogr 15:333–338

28. Cademartiri F, Mollet NR, Runza G et al (2005) Influence of intracoronary attenuation on coronary plaque measurements using multislice computed tomography: observations in an ex vivo model of coronary computed tomography angiography. Eur Radiol 15:1426–1431

Myocardial perfusion imaging using computed tomography: Current status, clinical value and prognostic implications

BORBÁLA VATTAY[*] ◉, MELINDA BOUSSOUSSOU, SAROLTA BORZSÁK, MILÁN VECSEY-NAGY, JUDIT SIMON, MÁRTON KOLOSSVÁRY, BÉLA MERKELY and BÁLINT SZILVESZTER

MTA-SE Cardiovascular Imaging Research Group, Heart and Vascular Center, Semmelweis University, Budapest, Hungary

IMAGING

REVIEW ARTICLE

ABSTRACT

Combined anatomical and functional evaluation of coronary artery disease (CAD) using computed tomography (CT) has recently emerged as an accurate, robust, and non-invasive tool for the evaluation of ischemic heart disease. Cardiac CT has become a one-stop-shop imaging modality that allows the simultaneous depiction, characterization, and quantification of coronary atherosclerosis and the assessment of myocardial ischemia. Advancements in scanner technology (improvements in spatial and temporal resolution, dual-energy imaging, wide detector panels) and the implementation of iterative reconstruction algorithms enables the detection of myocardial ischemia in both qualitative and quantitative fashion using low-dose scanning protocols. The addition of CT perfusion (CTP) to standard coronary CT angiography is a reliable tool to improve diagnostic accuracy. CTP using static first-pass imaging enables qualitative assessment of the myocardial tissue, whereas dynamic perfusion imaging can also provide quantitative information on myocardial blood flow. Myocardial tissue assessment by CTP holds the potential to refine risk in stable chest pain or microvascular dysfunction. CTP can aid the detection of residual ischemia after coronary intervention. Comprehensive evaluation of CAD using CTP might therefore improve the selection of patients for aggressive secondary prevention therapy or coronary revascularization with high diagnostic certainty. In addition, prognostic information provided by perfusion CT imaging could improve patient outcomes by quantifying the ischemic burden of the left ventricle. The current review focuses on the clinical value of myocardial perfusion imaging by CT, current status of CTP imaging and the use of myocardial CTP in various patient populations for the diagnosis of ischemic heart disease.

*Corresponding author. Tel.: +36 20 666 3857.
E-mail: bori.vattay@gmail.com

Introduction

The evaluation of symptomatic patients suggestive of myocardial ischemia is fundamental challenge in clinical care. The use of functional imaging in cardiology has led to a high number of unnecessary catheterizations with no obstructive disease [1]. On the other hand, anatomical evaluation by using coronary computed tomography angiography (CTA) has emerged as a reliable and accurate diagnostic tool for the evaluation of coronary artery disease (CAD) [2, 3]. Due to its high sensitivity and negative predictive value it is an accurate tool to rule out CAD in patients with low-to intermediate risk of obstructive disease [4, 5], however finding the proper test for the assessment of patients with suspected CAD without generating unnecessary downstream testing and to guide patient management is challenging.

Limitations of coronary CTA include that it tends to overestimate the severity of stenosis especially in the case of intermediate to severe lumen stenosis, multivessel disease, and extensive calcification, consequently lowering its specificity and positive predictive value. CT perfusion (CTP) imaging has emerged as a robust tool to complement traditional anatomical assessment of CAD by CTA. CTP imaging has the potential to also improve diagnosis in patients with higher likelihood of CAD or with microvascular disease and to detect residual ischemia after percutaneous coronary intervention. Current review focuses on the clinical value of myocardial perfusion imaging by CT, current status of CTP imaging and the use of myocardial CTP in various patient populations for the diagnosis of ischemic heart disease.

Coronary CTA for the evaluation of stable chest pain: current status

In the 2019 European Society of Cardiology guidelines CTA received class I recommendation for the evaluation of chronic coronary syndrome in patients with stable symptoms [6]. Two main studies were performed to underline the pivotal role of anatomical testing using CTA for stable angina. The results of the randomized SCOT-HEART (Scottish Computed Tomography of the Heart, NCT01149590) trial have shown that CTA based patient management could substantially improve long term outcomes as compared to standard care alone [7]. The PROMISE (Prospective Multicenter Imaging Study for Evaluation of Chest Pain, NCT01174550) trial has evaluated 10,003 symptomatic patients who were randomized either to functional or anatomical strategy to prove that CTA is non-inferior to functional testing [8]. Although the trial found no difference in the primary outcome, it did emphasize the prognostic value of CTA findings. Importantly, CTA also permits the detection of prognostically relevant non-obstructive CAD (between 1 and 69% luminal narrowing) that has been identified as an important predictor of adverse cardiac events [9]. Anatomical assessment using CTA provided better prognostic information as compared with functional testing that resulted also from the indiscriminatory nature of ischemia testing.

Despite its excellent capability to detect atherosclerotic plaque burden, the physiologic significance of the identified lesions remains unknown. In the FAME (Fractional Flow Reserve versus Angiography for Multivessel Evaluation, NCT00267774) study combining anatomical and functional evaluation (invasive measurement of lesion specific ischemia) of patients with suspected CAD improved clinical outcome [10]. Similarly, the combination of coronary CTA and CT perfusion imaging can improve diagnostic accuracy and proper identification of patients who require revascularization. The ISCHEMIA (International Study of Comparative Health Effectiveness with Medical and Invasive Approaches, NCT01471522) trial further improved our understanding on the management of patients with stable angina and proven ischemia [11]. Optimal medical therapy proved to be non-inferior to percutaneous intervention for adverse events, although latter could improve symptoms of angina. Notably, in the ISCHEMIA trial anatomical severity of CAD increased risk for adverse events, whereas proven ischemia did not.

CT perfusion imaging for the detection of myocardial ischemia

As an anatomical imaging test, traditional coronary CTA does not allow the detection of myocardial ischemia. Physiological evaluation of CAD is of utmost importance for patient management since ischemia driven revascularization could provide better outcomes [12–15]. Also, there is a remarkable discrepancy between luminal stenosis and detectable ischemia by either single-photon emission computed tomography (SPECT) or invasive fractional flow reserve (FFR). In the RICPORD (Does Routine Pressure Wire Assessment Influence Management Strategy at Coronary Angiography for Diagnosis of Chest Pain? NCT01070771) study after visual assessment of coronary stenosis by invasive coronary angiography (ICA), additional FFR measurement changed patient management in one-quarter of patients with stable angina [16]. Similarly, only 50% of patients with obstructive CAD on CTA had abnormal perfusion parameters assessed with SPECT [17].

Patients with less than 30% stenosis would possibly not benefit from ischemia testing, whereas lesions above 80% stenosis proved to be predominantly hemodynamically relevant [18]. Notably, revascularization does not improve symptoms or outcome in patients with no detectable ischemia, whereas some evidence suggests that more than 10% ischemia is associated with better prognosis after revascularization [19].

Functional testing includes stress echocardiography, stress magnetic resonance imaging (MRI), SPECT or positron-emission tomography (PET) imaging based on local expertise and accessibility. CTP imaging was introduced as a new-comer modality for ischemia detection. CTP is able to detect hypo-attenuated areas corresponding to myocardial injury in the left ventricle (LV) during first-pass of the contrast agent (see Central illustration). Advancements in CT scanner technology led to an improved spatial and temporal resolution with lower radiation exposure and contrast agent use by implementing iterative reconstruction algorithms. Also, wide detector CT scanners provide complete coverage (up to 16 cm z-axis coverage) of the heart volume. Rest CTA images are performed either as first to rule out CAD with subsequent ischemia provocation using vasodilator stressor agents (predominantly adenosine and regadenoson) or after stress imaging to avoid pre-enhancement of the myocardial tissue [20]. There are no guidelines on the exact order of stress and rest imaging, however in general it is recommended to start with a rest scan for lower
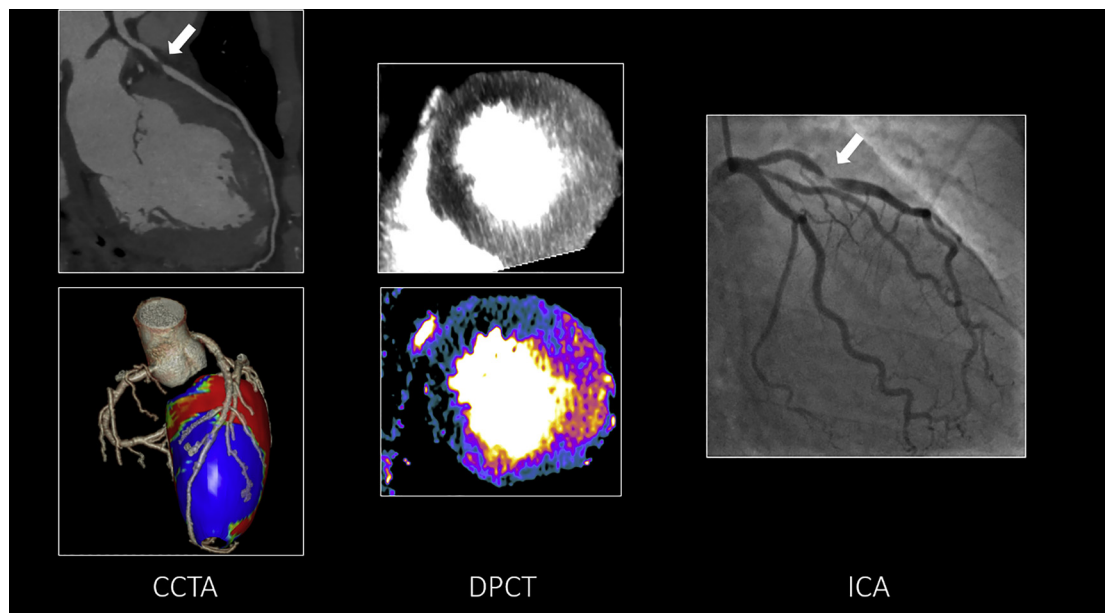
Central illustration. The addition of CTP to CCTA for the detection of hemodynamically relevant coronary lesions. Representative case of a patient presenting with stable chest pain. Panel left: CTA image of the left anterior descending (LAD) with high-grade stenosis in the proximal segment (white arrow). Panel middle: Dynamic CTP image showing hypoattenuated regions in the mid-anterior and mid-anteroseptal segments of the left ventricle. Panel right: ICA shows significant stenosis in LAD (white arrow). CCTA: coronary CT angiography; CTA: CT angiography; CTP: CT perfusion; DPCT: dynamic perfusion CT; ICA: invasive coronary angiography; LAD: left anterior descending

risk patients, and conversely, an initial stress scan should be performed for higher risk patients based on traditional risk scores and/or coronary calcium scoring. Notably, different stressor agents are in use to provoke ischemia during the CT scan. Recent investigations used regadenoson – a selective A2A agonist – in a single 10 second bolus that can be used in the same intravenous line as for the contrast injection [21]. Regadenoson provides adequate long and effective vasodilator stress for CTP and can be safely used without dose modulations for patients' size or co-morbidities [22].

Currently two different acquisitions are available to perform CTP with the aim to diagnose perfusion abnormalities through the myocardial tissue: static and dynamic myocardial perfusion CT. Furthermore, static stress CTP imaging can be performed using monoenergetic or dual-energy CT acquisition, where rest images are derived from the coronary CTA. Static CTP shows the peak blood flow of the myocardium (myocardial blood flow in one specific timepoint) allowing qualitative and semi-quantitative analysis of myocardial perfusion (Fig. 1). Therefore, the optimal timing for static CTP is crucial [20, 23]. Investigations demonstrated that dual-energy perfusion imaging using iodine mapping improves the detection of ischemia as compared to monoenergetic static CTP [24, 25]. On the other hand, dynamic CTP (usually stress imaging only) depicts contrast distribution in the LV wall during several cardiac cycles in order to obtain time attenuation curves (TACs) and the arterial input function curve (upslope method) to calculate myocardial blood flow. TAC curves for normal and ischemic myocardial segments differ markedly

[26] (Fig. 2). It therefore also enables assessment of semi-quantitative and quantitative parameters of myocardial perfusion such as the upslope, peak enhancement, time to peak (TTP), area under the curve, absolute, and relative myocardial blood flow (MBF) values, and myocardial blood volume (MBV). Dynamic stress CTP also allows for more precise and reproducible detection of balanced ischemia in multivessel disease as compared with static CTP. Although growing body of evidence suggest the improved diagnostic accuracy of CTP using dynamic stress perfusion protocols with quantitative assessment, this method is associated with increased radiation exposure (approx. 4–15 mSv) [20, 27]. Importantly, wide variability exists in both the imaging protocols and the cut-off values of perfusion parameters for discriminating ischemic myocardial segments. Previous studies reported a wide range of MBF thresholds for the detection of myocardial ischemia from 75 to even 103 mL/100 mL/min measured using a region of interest in a given segment [27–35]. Also, data are limited on the prognostic value of quantitative CTP parameters. Vendor specific technical aspects of CTP protocols are summarized in prior publications [18, 20, 24, 36]. Detailed description of technical aspects and outcomes are summarized in Table 1.

Earlier this year, the Society of Cardiovascular Computed Tomography (SCCT) released a consensus document on myocardial perfusion imaging [37]. This long-anticipated document summarizes the technical principles, diagnostic value, patient selection, image acquisition and interpretation of CTP imaging and also defines the key elements of reporting the results for the referring physician. Notably, the
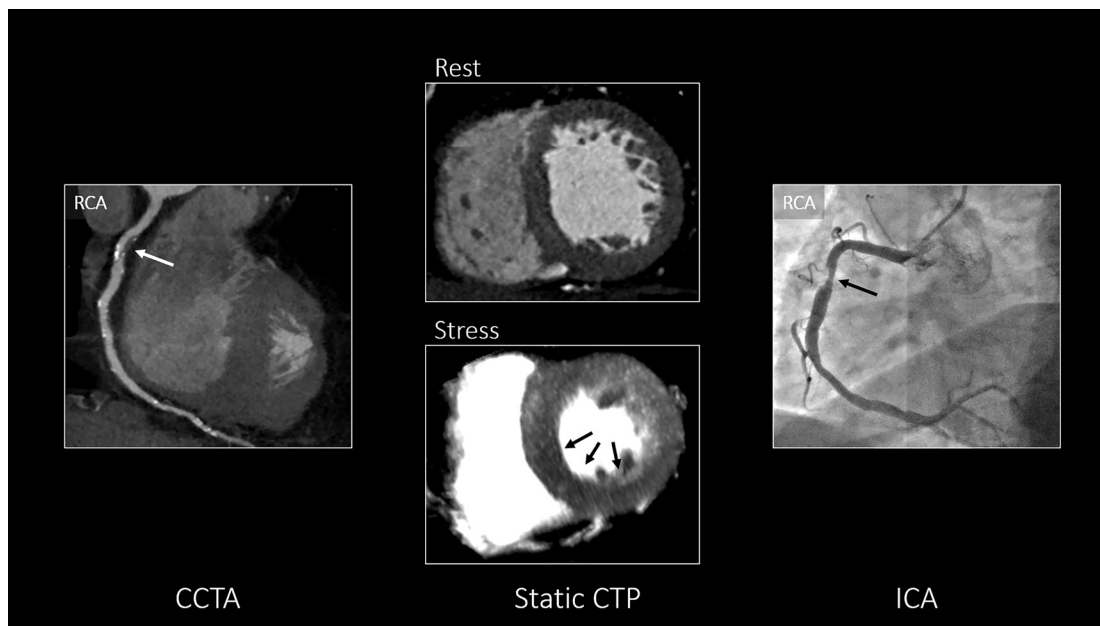
Fig. 1. Static CT perfusion imaging for detecting hemodynamically significant CAD in patients with stable chest pain and intermediate lesion. Representative images of a patient presenting with stable chest pain. Static CT perfusion allows for the visual assessment (qualitative or semi-quantitative) of perfusion defects. Panel left: CTA image of the right coronary artery (RCA) with moderate stenosis in the proximal segment (white arrow). Panel middle: Rest and stress static CTP images. No perfusion defect was observed on the rest CT scan, while hypoattenuated regions in the mid-inferior and mid-inferoseptal segments of the left ventricular wall was present under stress (black arrows). Panel right: ICA shows significant stenosis in the proximal RCA with an invasive FFR value of 0.72 (black arrow). CAD: coronary artery disease; CCTA: coronary CT angiography; CTA: CT angiography; CTP: CT perfusion; FFR: fractional flow reserve; ICA: invasive coronary angiography; RCA: right coronary artery
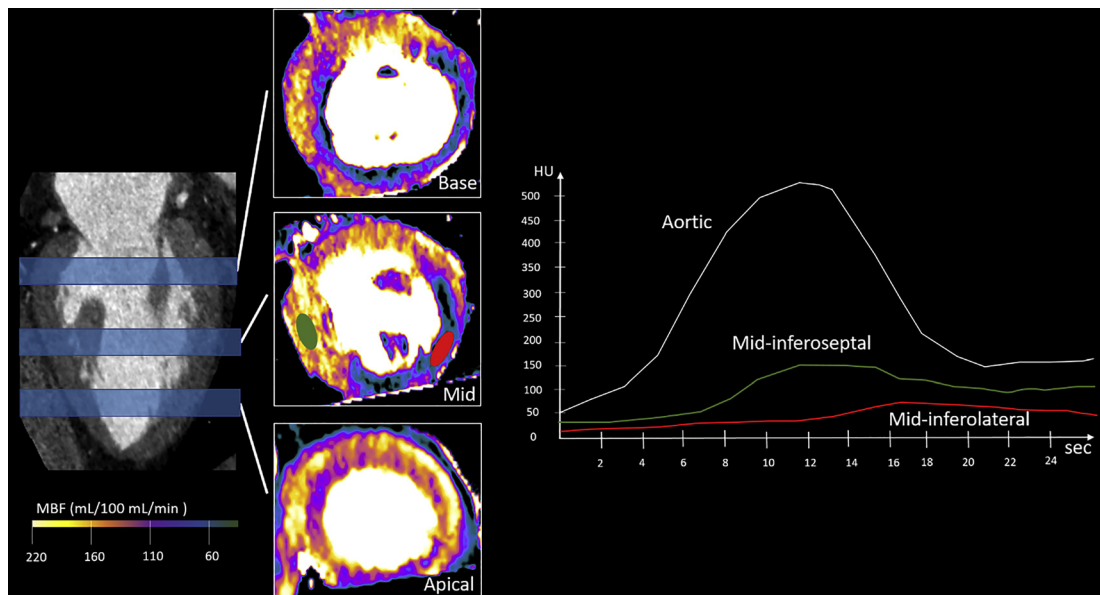

Fig. 2. Dynamic CT perfusion for the detection of myocardial ischemia. Dynamic CT perfusion enables the quantification of myocardial hemodynamics during stress. TAC curves are generated for the aorta and the selected myocardial segments. The red region of interest (ROI) represents the mid-inferolateral segment, whereas the green ROI stands for the mid-inferoseptal segment. Substantial differences are observed in the TAC curves and CTP revealed perfusion deficit of the inferolateral wall (reduced MBF values of 61 mL/100 mL/min in the inferolateral and normal perfusion of 143 mL/100 mL/min in the inferoseptal segment). CTP: CT perfusion; HU: Hounsfield unit; MBF: myocardial blood flow; TAC: time attenuation curve; ROI: region of interest

Table 1. Technical aspects and main outcomes of static and dynamic CTP studies

Author, year	Patient number	CT scanner	Stress agent	Analysis	Reference standard	Radiation dose of CTP (mSv)	Outcome
Static CTP							
Bettencourt et al. [70]	101	64-slice	Adenosine	Visual	FFR, MRI	5.0*	CTA + CTP for detecting significant CAD: SE: 90%; SP: 81%; PPV: 80%; NPV: 90%
Rochitte et al. [71]	381	320-slice	Adenosine	Semi-quantitative	SPECT	5.31	CTA + CTP: SE: 80%; SP: 74%; PPV: 65%; NPV: 86%
Cury et al. [43]	110	Multivendor	Regadenoson	Semi-quantitative	SPECT	17.70*	CTP was non-inferior; agreement rate: 0.87; SE: 90%; SP: 84%
Pontone et al. [46]	147	256-slice	Adenosine	Visual	FFR	2.5	CCTA + CTP patient based SE: 98%; SP: 87%; NPV: 99%; PPV: 86%
Andreini et al. [72]	150	256-slice	Adenosine	Visual	QCA	2.26	Highest diagnostic accuracy using CTP + CTA 95.8% in the territory-based analysis
Static dual-energy CTP							
Delgado et al. [73]	56	DS 2G	Adenosine	Iodine map	MRI	5.2	SE: 76%; SP: 99%; PPV: 89%; NPV: 98% per segment analysis
Meinel et al. [74]	55	DS 2G	Adenosine	Iodine map	SPECT	7.1	SE: 99%; SP: 97%; PPV: 92%; NPV: 100% per segment analysis
Kim et al. [75]	50	DS 2G	Adenosine	Iodine map	MRI	6.5	SE: 77%; SP: 94%; PPV: 53%; NPV: 98% per segment analysis
Ko et al. [76]	100	DS 1G	Adenosine	Iodine map	QCA + MRI	4.2	SE: 87%; SP: 79%; PPV: 71%; NPV: 91% vessel based analysis
Sánchez-Gracián et al. [77]	36	DS 2G	Adenosine	Iodine map	MRI	5.42	Threshold: 2.1 mg/mL; SE: 75%; SP: 73.6%
Dynamic CTP							
Bamberg et al. [30]	31	DS 2G	Adenosine	Quantitative	MRI	11.08	Estimated MBF threshold for perfusion defect 88 mL/mg/min; SE: 77.8%; SP: 75.4%; PPV: 50.6%; NPV: 91.3%
Rossi et al. [29]	80	DS 2G	Adenosine	Quantitative	FFR	9.4	78 mL/100 mL/min cut-off value for MBF index; SP was 89% for intermediate lesions
Coenen et al. [32]	74	DS 3G	Adenosine	Quantitative	ICA/FFR	9.3	CT MPI (indexed MBF) and CT-FFR had comparable accuracy
Nishiyama et al. [78]	38	256-slice	Adenosine	Quantitative	ICA/FFR	10.2	MBF cutoff 1.26 mL/g/min for detecting obstructive CAD
Yi et al. [79]	60	DS 3G	Adenosine	Quantitative	ICA/FFR	NA	Relative MBF ratio with highest segmental MBF provided optimal diagnostic accuracy (versus average and 3rd quartile segmental MBF)
Yang et al. [80]	82	DS 2G	Adenosine	Quantitative	ICA/FFR	3.5	AUC was 0.91 for the combination of stenosis ≥50% by CTA and SFR (ratio of hyperemic MBF in a stenosed artery versus in a non-diseased artery)
Pontone et al. [28]	85	256-slice	Adenosine	Quantitative	ICA/FFR	5.3	The sequential strategy of CCTA + FFRCT + CTP showed the highest AUC (0.919; $P < 0.05$) as compared with all other strategies. Threshold for absolute MBF 101 mL/100 g/min
Alessio et al. [81]	34	256-slice	Regadenoson	Quantitative	PET	8.4	Global MBF highly correlated with PET ($r = 0.92$; $P < 0.001$); mean difference: 0.7 ± 26.4%
Yi et al. [82]	60	DS 3G	Adenosine	Quantitative	ICA/FFR	NA	Absolute MBF value was superior than relative MBF ratio (AUC:0.955 versus 0.906 $P = 0.02$); cut-off for absolute MBF:115.7 mL/100 mL/min
Li et al. [83]	62	DS 3G	Adenosine	Quantitative	FFR	3.0	AUC: 0.942 for absolute MBF and AUC: 0.956 for relative MBF lesion based analysis

*Radiation dose for both rest and stress CTA.

1G: first-generation scanner; 2G: second-generation scanner; 3G: third-generation scanner; AUC: area under the curve; CAD: coronary artery disease; CTA: CT angiography; CCTA: coronary CT angiography; CTP: CT perfusion; DS: dual-source scanner; FFR: fractional flow reserve; MBF: myocardial blood flow; MPI: myocardial perfusion imaging; MRI: magnetic resonance imaging; mSv: millisievert; NA: non-assessable; NPV: negative predictive value; PET: positron emission tomography; PPV: positive predictive value; QCA: quantitative coronary angiography; SE: sensitivity; SFR: stress myocardial blood flow ratio; SP: specificity; SPECT: single-photon emission computed tomography.

consensus document encourages the use of CTP in patients with high likelihood of ischemic heart disease, known CAD, prior coronary intervention or extensive calcification.

Diagnostic performance of different CTP imaging protocols

CTP is an emerging technology that was developed to improve the diagnostic performance of coronary CTA. In single center studies CTP had excellent diagnostic performance compared to SPECT, CMR, PET, ICA, and invasive FFR [38–41]. In the CORE320 (Combined Non-invasive Coronary Angiography and Myocardial Perfusion Imaging Using 320 Detector Computed Tomography, NCT00934037) multicenter study static stress myocardial CTP and SPECT perfusion were compared in patients with known significant CAD detected by ICA and found higher overall diagnostic performance for static CTP [42]. In another multicenter study Cury et al. found that CTP was non-inferior to SPECT in the detection of reverse myocardial ischemia [43]. According to the meta-analysis of Takx et al., CTP had a pooled sensitivity and specificity of 88 and 80% using ICA with FFR as reference standard [44]. Furthermore, the diagnostic performance of CTP was similar to PET and stress MRI and higher than SPECT and echocardiography. A meta-analysis of CTP studies found similar diagnostic accuracy for static and dynamic techniques with a sensitivity and specificity of 82 and 78% for static and 77 and 89% for dynamic CTP. Sørgaard et al. in their meta-analysis found that compared to coronary CTA alone, combining CTP, and coronary CTA improved specificity from 62 to 84% when using ICA as reference standard [45]. CTP is therefore a promising and accessible tool that has superior spatial resolution as compared with SPECT to detect even smaller territories of myocardial ischemia. While there are several alternative, extensively validated modalities to provide functional information on CAD, CT is the only non-invasive modality for the combined assessments of morphology and function to guide patient management.

The PERFECTION (Comparison Between Stress Cardiac Computed Tomography Perfusion Versus Fractional Flow Reserve Measured by Computed Tomography Angiography In the Evaluation of Suspected Coronary Artery Disease) prospective study aimed to compare the diagnostic accuracy of CTA with combined CTA + CT-FFR and CTA + static stress-CTP in detecting functionally significant CAD using invasive FFR as the reference standard. The study enrolled 147 consecutive symptomatic patients, and found that complementary functional information obtained by either CT-FFR or CTP significantly improves diagnostic performance, but no significant difference was detected between CTA + CT-FFR versus CTA + CTP [46]. Even though both CT-FFR and CT + CTP yielded statistically similar diagnostic performance, combined CT and static or dynamic CTP might provide additive diagnostic value in patients with inconclusive CT-FFR due to the higher specificity and positive predictive value [47]. CT-FFR provides information on the lesion-specific ischemia and is derived from rest CTA images therefore highly dependent on image quality. Dynamic CTP on the other hand could quantify total myocardial burden and thus might be useful in patients with extensive CAD or microvascular disease.

Growing body of evidence suggests that using CT for the detection of myocardial perfusion defects is feasible and reliable compared to other non-invasive and invasive methods. However, the lack of standardized methods regarding image acquisition, stress protocols and particularly image analysis limits its widespread use. Moreover, there is no unified MBF cutoff value for the detection of ischemic myocardium. Although the number of CTP tests is increasing as part of routine clinical assessment of intermediate lesions, there are limited data on the clinical value of CTP in specific patient populations prone to have ischemic heart disease.

Potential role of myocardial perfusion imaging by CT in clinical practice

Studies examining the potential role of CTP in clinical practice are scarce. In the evaluation of ischemic heart disease using additional stress CTP has a higher sensitivity compared to anatomical assessment alone mainly due to the reduction of false positive findings. Therefore, CTA could become a more robust gatekeeper by reducing unnecessary invasive procedures. Table 2 summarizes the potential role of CTP for a wide spectrum of ischemic heart disease patients.

Stable angina

Myocardial perfusion imaging by CT can improve patient management in stable angina. In the multicenter prospective CRESCENT-II (Comprehensive Cardiac CT Versus Exercise Testing in Suspected Coronary Artery Disease 2, NCT02291484) trial a diagnostic pathway including CTP was compared with traditional functional testing in patients with stable chest pain and found to be an effective and safe alternative for the diagnosis of CAD by lowering rates of ICA without coronary revascularization [48]. Similarly, in another study including 240 consecutive patients, adding dynamic CTP to CTA significantly reduced the number of unnecessary invasive testing in patients with intermediate risk for CAD (CTA only: 50.0% [29/58] versus CTA + CTP: 10.8% [4/37], $P < 0.0001$) [49]. Myocardial ischemia was determined as MBF $\leq$ 100 mL/100 mL/min. In addition, van Rosendael et al. found a five-fold reduction of performing ICA in patients with obstructive CAD in case of normal myocardial perfusion on static stress CTP images [50].

Patients with extensive coronary calcification detected on native CT scans could be an optimal target for stress CTP. In challenging cases such as severe calcification (coronary calcium score $\geq$ 400), combined CTA and CTP is superior to CTA alone by providing additional functional information

Table 2. Potential clinical use of CTP in the spectrum of ischemic heart disease

	Potential role of CTP
Stable angina	Improve patient management in stable angina by detecting ischemic segments. Better gatekeeper function of FFR by reducing unnecessary invasive procedures. Superior spatial resolution as compared with SPECT. Useful in patients with extensive calcification (blooming artifacts). Multivessel CAD evaluation to select vessel(s) for revascularization (dynamic CTP). Prognostic information provided by combining plaque burden and ischemic load. Ischemia detection in the presence of previously implanted stents. Evaluation of microvascular dysfunction using parameters of myocardial tissue hemodynamics.
Acute chest pain	Exclude obstructive CAD in patients with low risk for ACS.
Post-myocardial infarction	Improve risk prediction in patients after MI by evaluating infarcted territories.
Extensive non-obstructive CAD	Global ischemia detection by quantitative CTP parameters.
Diabetes mellitus and arterial hypertension	Early identification of epicardial coronary atherosclerosis, microvascular dysfunction and impaired myocardial perfusion in patients at higher risk.

ACS: acute coronary syndrome; CAD: coronary artery disease; CCTA: coronary CT angiography; CTP: CT perfusion; FFR: fractional flow reserve; MI: myocardial infarction; SPECT: single-photon emission computed tomography.

of coronary lesions (AUC = 0.97 versus AUC = 0.088, P = 0.030). However, in patients with high pretest probability or known CAD combining CTA and CTP did not improve diagnostic performance in case of low Agatston calcium score (coronary calcium score < 400) [51].

More recent studies also examined the impact of MBF as assessed by dynamic CTP on clinical outcomes and found that it has an additive prognostic value over coronary CTA and is an independent predictor of major adverse cardiovascular events (MACEs). Using dynamic CTP, a summed stress score based on MBF values proved to be prognostically relevant after adjusted for obstructive CAD on CTA with hazard ratio (HR) of 5.7 (CI: 1.9–16.9, P = 0.002) [52]. Also, myocardial perfusion defect defined by low index-MBF (<0.88) calculated as a ratio between each segment and global MBF values was associated with MACE after adjusting for coronary CTA, CT-FFR findings, age, sex, and risk factors (HR: 10.1, CI: 2.1–48.8, P = 0.004) [53]. Notably, dynamic CTP derived perfusion parameters had additive prognostic value beyond clinical risk factors and stenosis severity assessed by coronary CTA [54]. Moreover, the extent of myocardial perfusion defect was also a prognosticator of MACE.

Currently, two large, randomized trials aimed to evaluate the clinical utility and prognostic value of CTP. The CTP-PRO (Impact of Stress Cardiac Computed Tomography Myocardial Perfusion on Downstream Resources and Prognosis in Patients with Suspected or Known Coronary Artery Disease, NCT03976921) study is an international, multicenter, prospective, open-label, randomized trial focusing on the cost-effectiveness of combined CTA + CTP strategy versus usual care in 2,000 intermediate-high risk patients with suspected or known CAD [55]. The PERFUSE RCT (Prospective Evaluation of Myocardial Perfusion Computed Tomography Trial, NCT02208388) sought to investigate the safety and effectiveness of CTP guided revascularization versus FFR guided revascularization in 1,000 patients with suspected stable CAD.

Besides the assessment of epicardial coronary arteries, CTP allows for the detection of microvascular dysfunction, although regarding data are scarce. Coronary flow reserve can also be accurately evaluated using specific dynamic CTP protocols in rest and stress phase [56]. In a recent study, quantified MBF using dynamic CTP also appeared to be significantly lower in myocardial segments affected by microvascular obstruction and had excellent diagnostic

accuracy compared to the reference CMR data (AUC = 0.996, $P < 0.001$) [57].

A sub-study of the CORE320 prospective trial divided patients into 3 groups based on the presence of obstructive CAD or perfusion defect defined by either coronary CTA and CTP or ICA and SPECT. Patients with ischemia but no obstructive stenosis (INOCA) were identified using CTA and static CTP. Interestingly, higher prevalence of positive remodeling, greater total and low attenuation atheroma volume was present in the INOCA group as compared to patients without either obstructive CAD or ischemia [58].

CTP after coronary intervention

Although only few studies are available, the use of CTP could also be beneficial in patients with prior coronary intervention for detecting residual ischemia. Due to the metallic artifacts the evaluation of coronary stents by CTA is limited. Adding stress CTP to rest CTA aids the diagnosis of in-stent-restenosis and helps the identification of patients who need further intervention (AUC = 0.82 for CTP and CTA versus AUC = 0.69 for CTA alone, $P < 0.001$) [59].

Acute chest pain

For patients presenting with acute on-set chest pain with low risk for acute coronary syndrome (ACS) coronary CTA is a reliable tool to exclude obstructive CAD [60]. The use of CTA can result in decreased time to diagnosis and to discharge, however it could also drive revascularization rates higher. In the CATCH-2 (Cardiac CT in the Treatment of Acute Chest Pain 2, NCT02014311) randomized controlled trial combined CTA + CTP was compared to CTA alone for the diagnosis and treatment of ischemic heart disease. The trial included patients with acute chest pain after ACS was ruled out by standard care. The combined protocol decreased the number of further invasive examinations and helped in guiding patient management [61]. In addition, in a similar patient population visual and semi-quantitative perfusion defect assessed by static CTP was associated with MACE with a median follow-up of 19 months independently of the patient's pretest probability. For visual perfusion defect the adjusted hazard ratio was 39 (CI: 11–134, $P < 0.0001$), while for impaired perfusion based on TPR (cut-off 0.89) hazard ratio was 0.99 (CI: 0.98–0.99, $P < 0.0001$). Moreover, poor prognosis was related to cases where >10% of left ventricular myocardium was affected [62].

Post-myocardial infarction patients

It has been suggested that the evaluation of infarcted area after acute myocardial infarction (AMI) could improve risk prediction, as irreversible myocardial damage is a strong long-term prognosticator. Analyzing irreversibly damaged myocardial areas is feasible using CTP parameters [63]. Nakauchi et al. quantified MBF parameters using dynamic CTP with deconvolution analysis in patients after AMI and measured significant differences in tissue blood flow and blood volume between infarcted and non-infarcted myocardial territories (mean MBF: 51.96 versus 108.84 mL/ 100 g/min, $P < 0.01$) [64]. In patients with ST-segment elevation myocardial infarction and successful revascularization Pan et al. found that MBF derived from dynamic CTP significantly and inversely correlated with peak Troponin T levels ($r = -0.682$, $P < 0.001$) and left ventricular function at 6 months ($r = 0.585$, $P = 0.001$) [65].

Extensive non-obstructive CAD

In cases of large atherosclerotic plaque burden without obstructive stenosis the assessment of ischemia by CT could help in identifying patients at highest cardiovascular risk. Meinel et al. demonstrated that dynamic CTP is suitable for the evaluation of global myocardial perfusion parameters [66]. Global MBF, MBV, and volume transfer constant (K_{trans}) were analyzed and correlated well with the severity and extent of CAD on coronary CTA and visual perfusion defects. In addition, after a follow up of 6, 12, and 18 months MBF predicted cardiovascular outcomes with a two-fold increased risk for major events in case of global MBF < 121 mL/100 mL/min [67]. Global MBF also showed incremental prognostic value over age, gender, clinical risk factors and stenosis severity on coronary CTA.

Diabetes mellitus and arterial hypertension

Dynamic CTP provides global quantification of LV myocardium that could improve early recognition of developing ischemic heart disease in different conditions such as diabetes mellitus or hypertension. Using dynamic CTP lower global perfusion values were found in patients with hypertension and diabetes mellitus with suspected CAD (hypertension versus normotension: MBV 18.5 ± 3.0 versus 19.7 ± 2.3 mL/100 mL, $P < 0.05$; diabetes versus no diabetes: MBV 17.9 ± 2.4 versus 19.4 ± 2.8 mL/100 mL, $P < 0.05$) [68]. Furthermore, longer duration of diabetes was associated with lower MBF assessed by dynamic CTP, yearly 6% additional risk was detected for decreased MBF [69]. Further larger studies are needed to establish the role of CTP in the diagnosis of common comorbidities such as diabetes and hypertension.

Conclusion and future perspectives

CTP is a promising tool for the identification of the presence and severity of perfusion abnormalities using either qualitative or quantitative analysis in patients with stable or even acute chest pain. Patients with extensive CAD and diffuse calcifications are optimal candidates to further improve the gatekeeper functionality of CTA. CTP can substantially increase the diagnostic accuracy of coronary CTA to identify possible candidates for revascularization and aggressive secondary prevention. However, differences in image acquisition protocols, image analysis, and artifacts limit the widespread clinical use of CTP. Advancements in scanner technology, post-processing software, and image reconstruction may help

overcome the limitations of CTP. Also, further studies are warranted to establish proper indications for patients, who could benefit the most from CTP imaging (i.e., patients with diabetes, post-PCI, multivessel-disease, microvascular dysfunction). Furthermore, spectral CT imaging might help detect true perfusion defects using iodine density reconstructions in the future. Also, radiomic and machine learning analysis of the left ventricle may help overcome the limitations of CTP interpretation, especially the subjectivity of visual assessment. Furthermore, radiomics and machine learning may help in identifying new imaging biomarkers of the myocardium from CTP scans which may better identify myocardial injury and assist clinical decision making.

Authors' contribution: All authors reviewed the final version of the manuscript and agreed to submit it to IMAGING for publication.

Conflict of interest: The authors have no conflict of interest to disclose.

REFERENCES

[1] Patel MR, Peterson ED, Dai D, Brennan JM, Redberg RF, Anderson HV, et al.: Low diagnostic yield of elective coronary angiography. N Engl J Med 2010; 362(10): 886.

[2] Maurovich-Horvat P, Ferencik M, Voros S, Merkely B, Hoffmann U: Comprehensive plaque assessment by coronary CT angiography. Nat Rev Cardiol 2014; 11(7): 390.

[3] Yang L, Zhou T, Zhang R, Xu L, Peng Z, Ding J, et al.: Meta-analysis: diagnostic accuracy of coronary CT angiography with prospective ECG gating based on step-and-shoot, Flash and volume modes for detection of coronary artery disease. Eur Radiol 2014; 24(10): 2345.

[4] Shaw LJ, Hausleiter J, Achenbach S, Al-Mallah M, Berman DS, Budoff MJ, et al.: Coronary computed tomographic angiography

[5] Moss AJ, Williams MC, Newby DE, Nicol ED: The updated NICE guidelines: cardiac CT as the first-line test for coronary artery disease. Curr Cardiovasc Imaging Rep 2017; 10(5): 15.

[6] Knuuti J, Wijns W, Saraste A, Capodanno D, Barbato E, Funck-Brentano C, et al.: ESC guidelines for the diagnosis and management of chronic coronary syndromes: the task force for the diagnosis and management of chronic coronary syndromes of the European Society of Cardiology (ESC). Eur Heart J 2019; 41(3): 407.

[7] Investigators S-H, Newby DE, Adamson PD, Berry C, Boon NA, Dweck MR, et al.: Coronary CT Angiography and 5-Year Risk of Myocardial Infarction. N Engl J Med 2018; 379(10): 924.

[8] Douglas PS, Hoffmann U, Patel MR, Mark DB, Al-Khalidi HR, Cavanaugh B, et al.: Outcomes of anatomical versus functional testing for coronary artery disease. N Engl J Med 2015; 372(14): 1291.

[9] Hoffmann U, Ferencik M, Udelson JE, Picard MH, Truong QA, Patel MR, et al.: Prognostic value of noninvasive cardiovascular testing in patients with stable chest pain: insights from the PROMISE trial (prospective multicenter imaging study for evaluation of chest pain). Circulation 2017; 135(24): 2320.

[10] Tonino PA, De Bruyne B, Pijls NH, Siebert U, Ikeno F, van' t Veer M, et al.: Fractional flow reserve versus angiography for guiding percutaneous coronary intervention. N Engl J Med 2009; 360(3): 213.

[11] Maron DJ, Hochman JS, Reynolds HR, Bangalore S, O'Brien SM, Boden WE, et al.: Initial invasive or conservative strategy for stable coronary disease. N Engl J Med 2020; 382(15): 1395.

[12] Iwasaki K: Myocardial ischemia is a key factor in the management of stable coronary artery disease. World J Cardiol 2014; 6(4): 130.

[13] Tonino PA, Fearon WF, De Bruyne B, Oldroyd KG, Leesar MA, Ver Lee PN, et al.: Angiographic versus functional severity of coronary artery stenoses in the FAME study fractional flow reserve versus angiography in multivessel evaluation. J Am College Cardiol 2010; 55(25): 2816.

[14] De Bruyne B, Pijls NH, Kalesan B, Barbato E, Tonino PA, Piroth Z, et al.: Fractional flow reserve-guided PCI versus medical therapy in stable coronary disease. N Engl J Med 2012; 367(11): 991.

[15] Boden WE, O'Rourke RA, Teo KK, Hartigan PM, Maron DJ, Kostuk WJ, et al.: Optimal medical therapy with or without PCI for stable coronary disease. N Engl J Med 2007; 356(15): 1503.

[16] Curzen N, Rana O, Nicholas Z, Golledge P, Zaman A, Oldroyd K, et al.: Does routine pressure wire assessment influence management strategy at coronary angiography for diagnosis of chest pain?: the RIPCORD study. Circ Cardiovasc Interv 2014; 7(2): 248.

[17] Schuijf JD, Wijns W, Jukema JW, Atsma DE, de Roos A, Lamb HJ, et al.: Relationship between noninvasive coronary angiography with multi-slice computed tomography and myocardial perfusion imaging. J Am Coll Cardiol 2006; 48(12): 2508.

[18] Seitun S, De Lorenzi C, Cademartiri F, Buscaglia A, Travaglio N, Balbi M, et al.: CT myocardial perfusion imaging: a new frontier in cardiac imaging. Biomed Res Int 2018; 2018: 7295460.

[19] Hachamovitch R, Hayes SW, Friedman JD, Cohen I, Berman DS: Comparison of the short-term survival benefit associated with

as a gatekeeper to invasive diagnostic and surgical procedures: results from the multicenter CONFIRM (Coronary CT Angiography Evaluation for Clinical Outcomes: an International Multicenter) registry. J Am College Cardiol 2012; 60(20): 2103.

revascularization compared with medical therapy in patients with no prior coronary artery disease undergoing stress myocardial perfusion single photon emission computed tomography. Circulation 2003; 107(23): 2900.

[20] Seitun S, Castiglione Morelli M, Budaj I, Boccalini S, Galletto Pregliasco A, Valbusa A, et al.: Stress computed tomography myocardial perfusion imaging: a new topic in cardiology. Rev Esp Cardiol (Engl Ed) 2016; 69(2): 188.

[21] Techasith T, Cury RC: Stress myocardial CT perfusion: an update and future perspective. JACC Cardiovasc Imaging 2011; 4(8): 905.

[22] Baxa J, Hromadka M, Sedivy J, Stepankova L, Molacek J, Schmidt B, et al.: Regadenoson-stress dynamic myocardial perfusion improves diagnostic performance of CT angiography in assessment of intermediate coronary artery stenosis in asymptomatic patients. Biomed Res Int 2015; 2015: 105629.

[23] Bischoff B, Bamberg F, Marcus R, Schwarz F, Becker HC, Becker A, et al.: Optimal timing for first-pass stress CT myocardial perfusion imaging. Int J Cardiovasc Imaging 2013; 29(2): 435.

[24] Cademartiri F, Seitun S, Clemente A, La Grutta L, Toia P, Runza G, et al.: Myocardial blood flow quantification for evaluation of coronary artery disease by computed tomography. Cardiovasc Diagn Ther 2017; 7(2): 129.

[25] Arnoldi E, Lee YS, Ruzsics B, Weininger M, Spears JR, Rowley CP, et al.: CT detection of myocardial blood volume deficits: dual-energy CT compared with single-energy CT spectra. J Cardiovasc Comput Tomogr 2011; 5(6): 421.

[26] George RT, Jerosch-Herold M, Silva C, Kitagawa K, Bluemke DA, Lima JA, et al.: Quantification of myocardial perfusion using dynamic 64-detector computed tomography. Invest Radiol 2007; 42(12): 815.

[27] Danad I, Szymonifka J, Schulman-Marcus J, Min JK: Static and dynamic assessment of myocardial perfusion by computed tomography. Eur Heart J Cardiovasc Imaging 2016; 17(8): 836.

[28] Pontone G, Baggiano A, Andreini D, Guaricci AI, Guglielmo M, Muscogiuri G, et al.: Dynamic stress computed tomography perfusion with a whole-heart coverage scanner in addition to coronary computed tomography angiography and fractional flow reserve computed tomography derived. JACC Cardiovasc Imaging 2019; 12(12): 2460.

[29] Rossi A, Dharampal A, Wragg A, Davies LC, van Geuns RJ, Anagnostopoulos C, et al.: Diagnostic performance of hyperaemic myocardial blood flow index obtained by dynamic computed tomography: does it predict functionally significant coronary lesions? Eur Heart J Cardiovasc Imaging 2014; 15(1): 85.

[30] Bamberg F, Marcus RP, Becker A, Hildebrandt K, Bauner K, Schwarz F, et al.: Dynamic myocardial CT perfusion imaging for evaluation of myocardial ischemia as determined by MR imaging. JACC Cardiovasc Imaging 2014; 7(3): 267.

[31] Bamberg F, Becker A, Schwarz F, Marcus RP, Greif M, von Ziegler F, et al.: Detection of hemodynamically significant coronary artery stenosis: incremental diagnostic value of dynamic CT-based myocardial perfusion imaging. Radiology 2011; 260(3): 689.

[32] Coenen A, Rossi A, Lubbers MM, Kurata A, Kono AK, Chelu RG, et al.: Integrating CT myocardial perfusion and CT-FFR in the work-up of coronary artery disease. JACC Cardiovasc Imaging 2017; 10(7): 760.

[33] Kono AK, Coenen A, Lubbers M, Kurata A, Rossi A, Dharampal A, et al.: Relative myocardial blood flow by dynamic computed

tomographic perfusion imaging predicts hemodynamic significance of coronary stenosis better than absolute blood flow. Invest Radiol 2014; 49(12): 801.

[34] Rossi A, Wragg A, Klotz E, Pirro F, Moon JC, Nieman K, et al.: Dynamic computed tomography myocardial perfusion imaging: comparison of clinical analysis methods for the detection of vessel-specific ischemia. Circ Cardiovasc Imaging 2017; 10(4).

[35] Greif M, von Ziegler F, Bamberg F, Tittus J, Schwarz F, D'Anastasi M, et al.: CT stress perfusion imaging for detection of haemodynamically relevant coronary stenosis as defined by FFR. Heart 2013; 99(14): 1004.

[36] Brusen R, Branch K: Myocardial CT perfusion: a review of current modalities, technology, and clinical performance. Current Cardiovasc Imaging Report 2017; 10(8): 25.

[37] Patel AR, Bamberg F, Branch K, Carrascosa P, Chen M, Cury RC, et al.: Society of cardiovascular computed tomography expert consensus document on myocardial computed tomography perfusion imaging. J Cardiovasc Comput Tomogr 2020; 14(1): 87.

[38] Kikuchi Y, Oyama-Manabe N, Naya M, Manabe O, Tomiyama Y, Sasaki T, et al.: Quantification of myocardial blood flow using dynamic 320-row multi-detector CT as compared with (1)(5)O-H(2)O PET. Eur Radiol 2014; 24(7): 1547.

[39] Bettencourt N, Chiribiri A, Schuster A, Ferreira N, Sampaio F, Pires-Morais G, et al.: Direct comparison of cardiac magnetic resonance and multidetector computed tomography stress-rest perfusion imaging for detection of coronary artery disease. J Am College Cardiol 2013; 61(10): 1099.

[40] Ko BS, Cameron JD, Meredith IT, Leung M, Antonis PR, Nasis A, et al.: Computed tomography stress myocardial perfusion imaging in patients considered for revascularization: a comparison with fractional flow reserve. Eur Heart J 2012; 33(1): 67.

[41] Tamarappoo BK, Gutstein A, Cheng VY, Nakazato R, Gransar H, Dey D, et al.: Assessment of the relationship between stenosis severity and distribution of coronary artery stenoses on multislice computed tomographic angiography and myocardial ischemia detected by single photon emission computed tomography. J Nucl Cardiol 2010; 17(5): 791.

[42] George RT, Mehra VC, Chen MY, Kitagawa K, Arbab-Zadeh A, Miller JM, et al.: Myocardial CT perfusion imaging and SPECT for the diagnosis of coronary artery disease: a head-to-head comparison from the CORE320 multicenter diagnostic performance study. Radiology 2014; 272(2): 407.

[43] Cury RC, Kitt TM, Feaheny K, Blankstein R, Ghoshhajra BB, Budoff MJ, et al.: A randomized, multicenter, multivendor study of myocardial perfusion imaging with regadenoson CT perfusion vs single photon emission CT. J Cardiovasc Comput Tomogr 2015; 9(2): 103.

[44] Takx RA, Blomberg BA, El Aidi H, Habets J, de Jong PA, Nagel E, et al.: Diagnostic accuracy of stress myocardial perfusion imaging compared to invasive coronary angiography with fractional flow reserve meta-analysis. Circ Cardiovasc Imaging 2015; 8(1).

[45] Sorgaard MH, Kofoed KF, Linde JJ, George RT, Rochitte CE, Feuchtner G, et al.: Diagnostic accuracy of static CT perfusion for the detection of myocardial ischemia. A systematic review and meta-analysis. J Cardiovasc Comput Tomogr 2016; 10(6): 450.

[46] Pontone G, Baggiano A, Andreini D, Guaricci AI, Guglielmo M, Muscogiuri G, et al.: Stress computed tomography perfusion versus fractional flow reserve CT derived in suspected coronary

artery disease: the perfection study. JACC Cardiovasc Imaging 2019; 12(8 Pt 1): 1487.

[47] Baggiano A, Fusini L, Del Torto A, Vivona P, Guglielmo M, Muscogiuri G, et al.: Sequential strategy including FFRCT plus stress-CTP impacts on management of patients with stable chest pain: the stress-CTP RIPCORD study. J Clin Med 2020; 9(7).

[48] Lubbers M, Coenen A, Kofflard M, Bruning T, Kietselaer B, Galema T, et al.: Comprehensive cardiac CT with myocardial perfusion imaging versus functional testing in suspected coronary artery disease: the multicenter, randomized CRESCENT-II trial. JACC Cardiovasc Imaging 2018; 11(11): 1625.

[49] Yu M, Shen C, Dai X, Lu Z, Wang Y, Lu B, et al.: Clinical outcomes of dynamic computed tomography myocardial perfusion imaging combined with coronary computed tomography angiography versus coronary computed tomography angiography-guided strategy. Circ Cardiovasc Imaging 2020; 13(1): e009775.

[50] van Rosendael AR, Dimitriu-Leen AC, de Graaf MA, van Zwet EW, Jukema JW, Bax JJ, et al.: Impact of computed tomography myocardial perfusion following computed tomography coronary angiography on downstream referral for invasive coronary angiography, revascularization and, outcome at 12 months. Eur Heart J Cardiovasc Imaging 2017; 18(9): 969.

[51] Sharma RK, Arbab-Zadeh A, Kishi S, Chen MY, Magalhaes TA, George RT, et al.: Incremental diagnostic accuracy of computed tomography myocardial perfusion imaging over coronary angiography stratified by pre-test probability of coronary artery disease and severity of coronary artery calcification: The CORE320 study. Int J Cardiol 2015; 201: 570.

[52] Nakamura S, Kitagawa K, Goto Y, Omori T, Kurita T, Yamada A, et al.: Incremental prognostic value of myocardial blood flow quantified with stress dynamic computed tomography perfusion imaging. JACC Cardiovasc Imaging 2019; 12(7 Pt 2): 1379.

[53] van Assen M, De Cecco CN, Eid M, von Knebel Doeberitz P, Scarabello M, Lavra F, et al.: Prognostic value of CT myocardial perfusion imaging and CT-derived fractional flow reserve for major adverse cardiac events in patients with coronary artery disease. J Cardiovasc Comput Tomogr 2019; 13(3): 26.

[54] Meinel FG, Pugliese F, Schoepf UJ, Ebersberger U, Wichmann JL, Lo GG, et al.: Prognostic value of stress dynamic myocardial perfusion CT in a multicenter population with known or suspected coronary artery disease. AJR Am J Roentgenol 2017; 208(4): 761.

[55] Pontone G, De Cecco C, Baggiano A, Guaricci AI, Guglielmo M, Leiner T, et al.: Design of CTP-PRO study (impact of stress Cardiac computed Tomography myocardial Perfusion on downstream resources and PROgnosis in patients with suspected or known coronary artery disease: a multicenter international study). Int J Cardiol 2019; 292: 253.

[56] Ho KT, Ong HY, Tan G, Yong QW: Dynamic CT myocardial perfusion measurements of resting and hyperaemic blood flow in low-risk subjects with 128-slice dual-source CT. Eur Heart J Cardiovasc Imaging 2015; 16(3): 300.

[57] Yu M, Chen X, Dai X, Pan J, Wang Y, Lu B, et al.: The value of low-dose dynamic myocardial perfusion CT for accurate evaluation of microvascular obstruction in patients with acute myocardial infarction. AJR Am Journal Roentgenol 2019; 213(4): 798.

[58] Schuijf JD, Matheson MB, Ostovaneh MR, Arbab-Zadeh A, Kofoed KF, Scholte A, et al.: Ischemia and no obstructive stenosis (INOCA) at CT angiography, CT myocardial perfusion, invasive coronary angiography, and SPECT: the CORE320 study. Radiology 2020; 294(1): 61.

[59] Rief M, Zimmermann E, Stenzel F, Martus P, Stangl K, Greupner J, et al.: Computed tomography angiography and myocardial computed tomography perfusion in patients with coronary stents: prospective intraindividual comparison with conventional coronary angiography. J Am College Cardiol 2013; 62(16): 1476.

[60] Linde JJ, Hove JD, Sorgaard M, Kelbaek H, Jensen GB, Kuhl JT, et al.: Long-term clinical impact of coronary CT angiography in patients with recent acute-onset chest pain: the randomized controlled CATCH trial. JACC Cardiovasc Imaging 2015; 8(12): 1404.

[61] Sorgaard MH, Linde JJ, Kuhl JT, Kelbaek H, Hove JD, Fornitz GG, et al.: Value of myocardial perfusion assessment with coronary computed tomography angiography in patients with recent acute-onset chest pain. JACC Cardiovasc Imaging 2018; 11(11): 1611.

[62] Linde JJ, Sorgaard M, Kuhl JT, Hove JD, Kelbaek H, Nielsen WB, et al.: Prediction of clinical outcome by myocardial CT perfusion in patients with low-risk unstable angina pectoris. Int J Cardiovasc Imaging 2017; 33(2): 261.

[63] Han R, Sun K, Lu B, Zhao R, Li K, Yang X: Diagnostic accuracy of coronary CT angiography combined with dual-energy myocardial perfusion imaging for detection of myocardial infarction. Exp Ther Med 2017; 14(1): 207.

[64] Nakauchi Y, Iwanaga Y, Ikuta S, Kudo M, Kobuke K, Murakami T, et al.: Quantitative myocardial perfusion analysis using multi-row detector CT in acute myocardial infarction. Heart 2012; 98(7): 566.

[65] Pan J, Yuan M, Yu M, Gao Y, Shen C, Wang Y, et al.: Myocardial blood flow quantified by low-dose dynamic CT myocardial perfusion imaging is associated with peak troponin level and impaired left ventricle function in patients with ST-elevated myocardial infarction. Korean J Radiol 2019; 20(5): 709.

[66] Meinel FG, Ebersberger U, Schoepf UJ, Lo GG, Choe YH, Wang Y, et al.: Global quantification of left ventricular myocardial perfusion at dynamic CT: feasibility in a multicenter patient population. AJR Am J Roentgenol 2014; 203(2): W174.

[67] Meinel FG, Wichmann JL, Schoepf UJ, Pugliese F, Ebersberger U, Lo GG, et al.: Global quantification of left ventricular myocardial perfusion at dynamic CT imaging: prognostic value. J Cardiovasc Comput Tomogr 2017; 11(1): 16.

[68] Vliegenthart R, De Cecco CN, Wichmann JL, Meinel FG, Pelgrim GJ, Tesche C, et al.: Dynamic CT myocardial perfusion imaging identifies early perfusion abnormalities in diabetes and hypertension: insights from a multicenter registry. J Cardiovasc Comput Tomogr 2016; 10(4): 301.

[69] Tomizawa N, Fujino Y, Kamitani M, Chou S, Yamamoto K, Inoh S, et al.: Longer diabetes duration reduces myocardial blood flow in remote myocardium assessed by dynamic myocardial CT perfusion. J Diabetes Complication 2018; 32(6): 609.

[70] Bettencourt N, Ferreira ND, Leite D, Carvalho M, Ferreira WDS, Schuster A, et al.: CAD detection in patients with intermediate-high pre-test probability: low-dose CT delayed enhancement detects ischemic myocardial scar with moderate accuracy but does not improve performance of a stress-rest CT perfusion protocol. JACC Cardiovasc Imaging 2013; 6(10): 1062.

[71] Rochitte CE, George RT, Chen MY, Arbab-Zadeh A, Dewey M, Miller JM, et al.: Computed tomography angiography and

perfusion to assess coronary artery stenosis causing perfusion defects by single photon emission computed tomography: the CORE320 study. Eur Heart J 2014; 35(17): 1120.

[72] Andreini D, Mushtaq S, Pontone G, Conte E, Collet C, Sonck J, et al.: CT perfusion versus coronary CT angiography in patients with suspected in-stent restenosis or CAD progression. JACC Cardiovasc Imaging 2020; 13(3): 732.

[73] Delgado C, Vazquez M, Oca R, Vilar M, Trinidad C, Sanmartin M: Myocardial ischemia evaluation with dual-source computed tomography: comparison with magnetic resonance imaging. Rev Esp Cardiol (Engl Ed) 2013; 66(11): 864.

[74] Meinel FG, De Cecco CN, Schoepf UJ, Nance JW, , Jr., Silverman JR, Flowers BA, et al.: First-arterial-pass dual-energy CT for assessment of myocardial blood supply: do we need rest, stress, and delayed acquisition? Comparison with SPECT. Radiology 2014; 270(3): 708.

[75] Kim SM, Chang SA, Shin W, Choe YH: Dual-energy CT perfusion during pharmacologic stress for the assessment of myocardial perfusion defects using a second-generation dual-source CT: a comparison with cardiac magnetic resonance imaging. J Comput Assist Tomogr 2014; 38(1): 44.

[76] Ko SM, Park JH, Hwang HK, Song MG: Direct comparison of stress- and rest-dual-energy computed tomography for detection of myocardial perfusion defect. Int J Cardiovasc Imaging 2014; 30(Suppl 1): 41.

[77] Delgado Sanchez-Gracian C, Oca Pernas R, Trinidad Lopez C, Santos Armentia E, Vaamonde Liste A, Vazquez Caamano M, et al.: Quantitative myocardial perfusion with stress dual-energy CT: iodine concentration differences between normal and ischemic or necrotic myocardium. Initial experience. Eur Radiol 2016; 26(9): 3199.

[78] Nishiyama H, Tanabe Y, Kido T, Kurata A, Uetani T, Kido T, et al.: Incremental diagnostic value of whole-heart dynamic computed tomography perfusion imaging for detecting obstructive coronary artery disease. J Cardiol 2019; 73(5): 425.

[79] Yi Y, Xu C, Wu W, Wang Y, Li YM, Shen ZJ, et al.: Myocardial blood flow analysis of stress dynamic myocardial CT perfusion for hemodynamically significant coronary artery disease diagnosis: The clinical value of relative parameter optimization. J Cardiovasc Comput Tomogr 2020; 14(4): 314.

[80] Yang J, Dou G, He B, Jin Q, Chen Z, Jing J, et al.: Stress myocardial blood flow ratio by dynamic CT perfusion identifies hemodynamically significant CAD. JACC Cardiovasc Imaging 2020; 13(4): 966.

[81] Alessio AM, Bindschadler M, Busey JM, Shuman WP, Caldwell JH, Branch KR: Accuracy of myocardial blood flow estimation from dynamic contrast-enhanced cardiac CT compared with PET. Circ Cardiovasc Imaging 2019; 12(6): e008323.

[82] Yi Y, Xu C, Wu W, Wang Y, Li YM, Ge YQ, et al.: Stress dynamic myocardial CT perfusion for symptomatic patients with intermediate- or high-risk of coronary artery disease: optimization and incremental improvement between the absolute and relative myocardial blood flow analysis. J Cardiovasc Comput Tomogr 2020; 14(5): 437.

[83] Li Y, Dai X, Lu Z, Shen C, Zhang J: Diagnostic performance of quantitative, semi-quantitative, and visual analysis of dynamic CT myocardial perfusion imaging: a validation study with invasive fractional flow reserve. Eur Radiol 2020; 31(1): 525–34.